

Characterisation of the influence of cooling rates on structure and properties of dynamic vulcanizates

DISSERTATION



zur Erlangung des akademischen Grades

Doktor-Ingenieur
(Dr.-Ing.)

vorgelegt der

Mathematisch-Naturwissenschaftlich-Technischen Fakultät
- Fachbereich Ingenieurwissenschaften -
Martin-Luther-Universität Halle-Wittenberg

von Frau Diplom-Ingenieur Dörte Scharnowski
geb. am 27. November 1974 in Brandenburg a. d. Havel

Dekan der Fakultät: Prof. Dr.-Ing. habil. H. Altenbach

Gutachter: 1. Prof. Dr.-Ing. habil. H.-J. Radusch (Halle)
2. Ch.mo. Prof. S. Piccarolo (Palermo, Italien)
3. Prof. Dr.-Ing. habil. Schnabel (Halle)

Halle (Saale), 07.03.2005

urn:nbn:de:gbv:3-000008563

[<http://nbn-resolving.de/urn/resolver.pl?urn=nbn%3Ade%3Agbv%3A3-000008563>]

Acknowledgments

On this point I would like to express my deep gratitude towards all the persons who have a direct or indirect share on the completion of this work.

I would like to thank Prof. H.-J. Radusch (MLU Halle-Wittenberg) for his tutorship supporting and helping me always with new ideas in the course of this work.

I would like to thank Prof. S. Piccarolo (University of Palermo) for giving me the chance to use the fast quenching equipment, for his continuous help, fruitful discussions and suggestions during the whole working period.

Several people have supported me in the completion of the experimental work, among those I wish to express my gratitude towards:

- Dr. Z. Kiflie (University of Palermo) for introducing to me the rapid quenching technology and his continuous effort to solve troubleshooters
- Dr. V. La Carruba (University of Palermo) for giving me the chance to apply the fast quenching technique under pressure and numerous discussions regarding the work
- Dr. R. Adhikari (MLU Halle-Wittenberg) for his efforts to help me to receive high quality AFM – pictures
- Dr. T. A. Huy (MLU Halle-Wittenberg) for the rheo-optical FTIR – spectroscopy
- Dr. T. Koch (TU-Wien) for the nanoindentation experiments
- Dr. H. Le Hong (MLU Halle-Wittenberg) for his continuous help, suggestions and discussion regarding the determination of the mechanical properties of the samples
- Dr. A. Wutzler (MLU Halle-Wittenberg) for helping me during the dynamic vulcanization and his continuous suggestions regarding the work
- Dipl.-Ing. Illisch for the suggestions regarding the rubber crosslinking reactions and the numerous helpful discussions
- Dr. Lüpke (MLU Halle-Wittenberg) and Dr. I. Kolesov for the help and suggestions regarding the DMTA measurements
- Dr. R. Androsch (MLU Halle-Wittenberg) for his help on the interpretation of the WAXD spectra
- the technical staff of the working group “Kunststofftechnik” (MLU Halle-Wittenberg)

I would like to thank also several colleagues for the scientific and moral support during the whole work. Among them are S. Frangov and P. Doshev (MLU Halle-Wittenberg) as well as N. Dincheva and M. Botev.

Last but not least I would like to thank my husband P. Bonsignore and my parents for their support and their backhold during the whole period.

Contents

<u>1</u>	<u>Introduction</u>	3
<u>2</u>	<u>Dynamic vulcanizates and dynamic vulcanization</u>	5
2.1	<u>Dynamic vulcanizates as part of TPE</u>	5
2.2	<u>Application trends of dynamic vulcanizates</u>	5
2.3	<u>Dynamic vulcanization</u>	6
2.3.1	<u>Morphology development</u>	7
2.3.2	<u>Curing methods</u>	8
<u>3</u>	<u>Crystallization behavior of dynamic vulcanizates and their components</u>	12
3.1	<u>Crystallization behavior of iPP</u>	12
3.1.1	<u>Isothermal crystallization</u>	13
3.1.2	<u>Nonisothermal crystallization</u>	14
3.1.3	<u>The mesomorphic form of iPP</u>	16
3.2	<u>Crystallization behavior of copolymers</u>	18
3.2.1	<u>EPDM</u>	18
3.2.2	<u>EOC</u>	19
3.3	<u>Crystallization behavior of iPP/copolymer blends</u>	21
3.3.1	<u>Crystallization of the system PP/EPM</u>	22
3.3.1.1	<u>PP/EPM blends</u>	22
3.3.1.2	<u>PP/EPM vulcanized blends</u>	23
3.3.1.3	<u>PP/EPM reactor blends</u>	24
3.3.2	<u>Crystallization of the system PP/EPDM</u>	24
3.3.2.1	<u>PP/EPDM blends</u>	24
3.3.2.2	<u>PP/EPDM vulcanized blends</u>	26
3.3.3	<u>Crystallization of the system PP/EOC</u>	27
3.3.3.1	<u>PP/EOC blends</u>	27
<u>4</u>	<u>Fast cooling - state of the art</u>	29
4.1	<u>Rapid cooling methods with defined cooling rates</u>	29
<u>5</u>	<u>The relationship between cooling conditions and structure/morphology formation in DV processing</u>	32
<u>6</u>	<u>Investigation of the relationship between cooling conditions and structure/morphology</u>	34
6.1	<u>Preparation of the dynamic vulcanizates</u>	34
6.1.1	<u>Materials</u>	34
6.1.2	<u>Dynamic vulcanization technology</u>	34
6.2	<u>Controlled rapid quenching technique</u>	36
6.3	<u>Characterization of morphology</u>	37
6.3.1	<u>Wide angle x-ray diffraction</u>	37
6.3.2	<u>Density</u>	37
6.3.3	<u>Polarized light microscopy</u>	38
6.3.4	<u>Atomic force microscopy</u>	38
6.4	<u>Characterization of thermal behavior</u>	38
6.4.1	<u>Differential Scanning Calorimetry</u>	38
6.4.2	<u>Dynamic mechanical thermal analysis</u>	39
6.5	<u>Characterization of mechanical properties</u>	39
6.5.1	<u>Microhardness</u>	39
6.5.2	<u>Miniature tensile test</u>	40
6.5.3	<u>Rheoptical FTIR - spectroscopy</u>	41
6.6	<u>Influence of cooling conditions on the morphology and the properties of dynamic vulcanizates and their components</u>	42
6.6.1	<u>The morphology of the pure components</u>	42
6.6.1.1	<u>iPP</u>	42

6.6.1.2	<u>EOC and EPDM</u>	47
6.6.2	<u>The morphology of dynamic vulcanizates</u>	49
6.6.2.1	<u>Dynamic vulcanizates based on the system PP/EOC</u>	49
6.6.2.2	<u>PP/EPDM 30/70p and PP/EPDM 30/70r</u>	58
6.6.3	<u>The thermal behavior of the pure components</u>	66
6.6.3.1	<u>iPP</u>	66
6.6.3.2	<u>EOC and EPDM</u>	70
6.6.4	<u>The thermal behavior of dynamic vulcanizates</u>	71
6.6.4.1	<u>PP/EOC 30/70p</u>	71
6.6.4.2	<u>PP/EPDM 30/70p and PP/EPDM 30/70r</u>	73
6.6.5	<u>The mechanical properties of the pure components</u>	80
6.6.5.1	<u>IPP</u>	80
6.6.5.2	<u>EOC</u>	81
6.6.6	<u>The mechanical properties of dynamic vulcanizates</u>	82
6.6.6.1	<u>PP/EOC 30/70p</u>	82
6.6.6.2	<u>PP/EPDM 30/70p and PP/EPDM 30/70r</u>	86
7	<u>Conclusions for the dimensioning of processing techniques of dynamic vulcanizates</u>	93
8	<u>Summary</u>	94
9	<u>Zusammenfassung</u>	97
10	<u>List of symbols</u>	101
11	<u>Literature</u>	105

1 Introduction

Dynamic vulcanizates (DV) belong to the group of thermoplastic elastomers (TPE) which combine rubber-elastic deformation behavior at room temperature with thermoplastic process ability at elevated temperatures. This is possible due to a multiphase structure consistent soft and hard regions being responsible for the rubber elasticity and thermoplastic melting behavior respectively. Generally TPE can be divided into two major groups: block-copolymers and polymer blends. The structure of a DV, being part of the ultimate group, in comparison to the structure of a block-copolymer is shown in figure 1.1. TPE belonging to the group of copolymers are phase-separated systems, consisting of a hard and a soft phase, which are thermodynamically immiscible and present as individual phases /1/. The crystalline or amorphous hard segments work as thermally reversible network points in a soft matrix. They melt or soften at elevated temperatures enabling the TPE to be processed like a thermoplastic material.

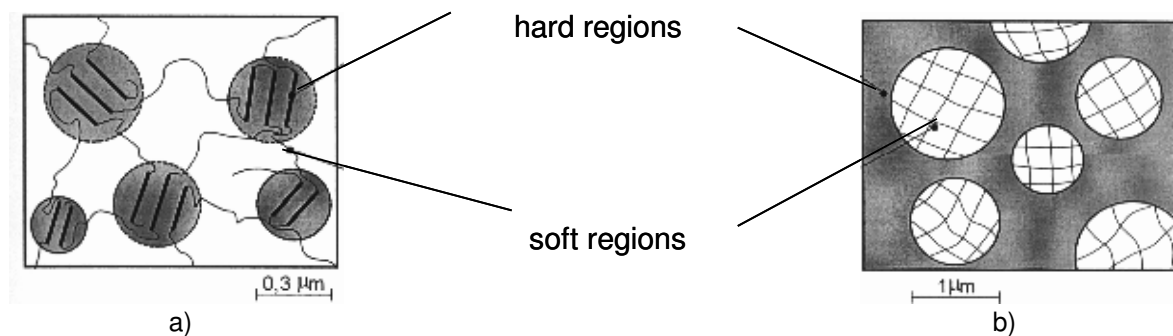


Fig. 1.1 Structure of TPE schematically a) block-copolymer compared to b) dynamic vulcanizates

Dynamic vulcanizates consist of a thermoplastic matrix enclosing finely dispersed crosslinked rubber particles (fig. 1.1b)). The variation of the thermoplastic matrix material and the rubber phase provides for a wide range of physical and chemical properties /2/.

The use of TPE ranges from consumer goods to the automotive industry. The latter shows the highest amount of application. Their great advantage compared to conventional fully crosslinked vulcanizates lays in their ability to be processed more economically and to be recycled easily. In processing the dimensional stability as well as predictable mechanical properties of the final parts are essential. These properties are influenced by several processing parameters. A very important step during thermoplastic processing is the cooling from the hot melt. The cooling process during injection molding for example is taking up the most part of the cycle time. Figure 1.2 shows how warpage takes place after injection molding originated by asymmetric thermal induced residual stressed caused by uneven cooling. Uneven cooling occurs also in parts with large thickness differences due to the poor heat conductivity of polymer materials. In order to increase productivity producers tend to lower cooling times by increasing cooling rates as much as possible.

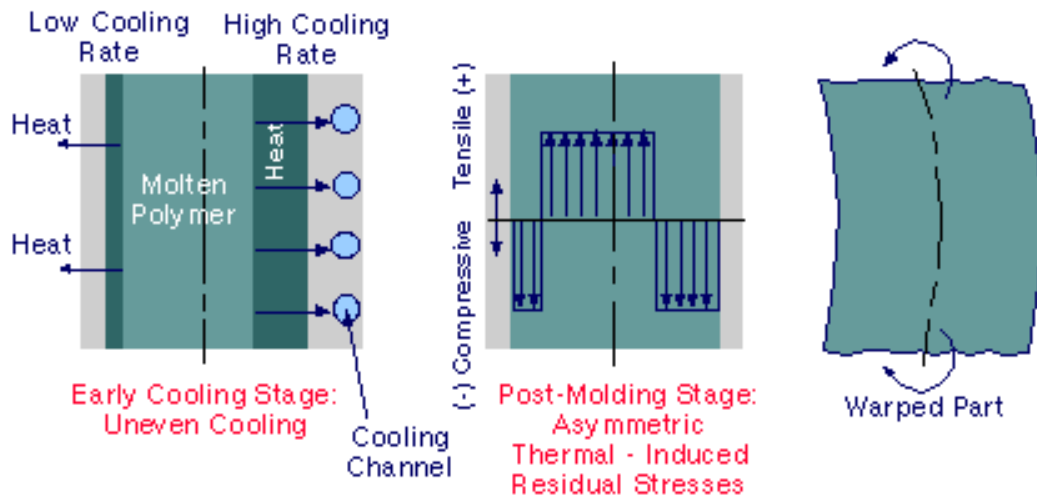


Fig. 1.2 Scheme of the mechanism of warpage caused by uneven cooling rates during injection molding.

The increase of cooling rates however give raise to different problems such as volume shrinkage especially in parts of semi-crystalline materials, suppression of crystallinity and therefore poor mechanical properties, thermal stresses in the part. The investigations of the influence of cooling rates on crystal morphology and properties until now cover only pure thermoplastic materials such as iPP, PA and PET /3/ and to a small extend also filled thermoplastics /128/ and PP/PA blends /142/.

In this work the influence of fast cooling on structure and properties of dynamic vulcanizates as multiphase system of a semicrystalline thermoplastic matrix and a crosslinked elastomeric phase will be investigated. The main issues to study, next to cooling rates, were the influence of the type of elastomer used and the crosslinking agents used for dynamic vulcanization as well as the amount of thermoplast content on morphology, thermal and mechanical behavior. This work should give a contribution to the possibility to predict the final properties of DV during the processing by triggering the cooling rates.

2 Dynamic vulcanizates and dynamic vulcanization

2.1 Dynamic vulcanizates as part of TPE

Thermoplastic Elastomers combine rubber elastic and thermoplastic properties. They can be divided into two groups /4/; multi-block copolymers and blends (fig.2.1). The first group are copolymers consisting of an elastomeric and a hard block. Styrene block copolymers (TPE-S) exhibit a wide range of application resulting from the properties such as hardness, grip and rebound. Polyesterester block copolymers (TPE-E) exhibit good mechanical properties until 160°C, resistance to oil and fat as well as high polarity providing the ability to be glued and varnished. Polyurethane/elastomer block copolymer (TPE-U) is a classical TPE showing very good mechanical properties and high resistance to wear. Polyamide/elastomer blockcopolymers (TPE-A) can be compared to both previous groups with respect to their mechanical properties. Polyethylene/poly (α -olefin) block copolymers exhibit a rather low temperature range of use. TPE blends can be divided in TPE-O with a non-crosslinked rubber phase and TPE-V with a crosslinked rubber phase. Due to their un-crosslinked rubber phase TPE-O are preferably used at lower temperatures without exposition to high mechanical stress. TPE-O are transparent, have a low density and an attractive price. Problematically can be the high shrinking. Partially and fully crosslinked TPE-V are widely used in automotive industry, exhibit low hardness and high application temperature until over 100°C. Dynamic vulcanizates belong to this type of Thermoplastic Elastomers /5/

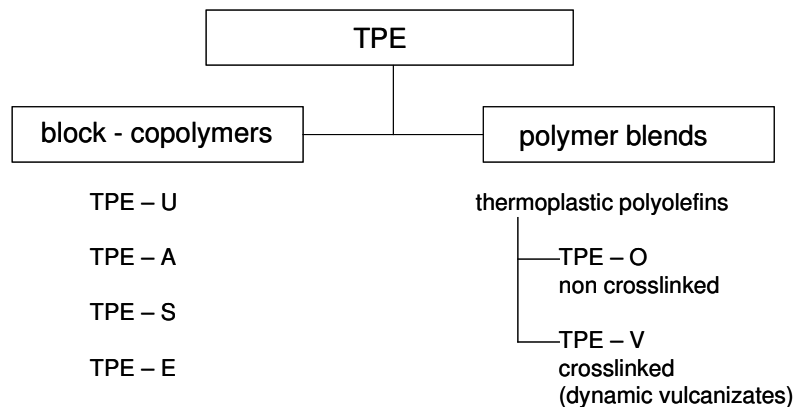


Fig. 2.1 Classification of TPE

2.2 Application trends of dynamic vulcanizates

While at the beginning of the use of TPE-V the aim was to substitute existing applications of elastomers now they are also opening new fields of application. This is explained mainly by their processing potential. The use in automotive industry plays a big role also since lately a lot has been done to improve the thermal reliability and oil resistance as well as to reduce the compression set. Thermoplastic process ability provides more recycling possibilities and their use for fast joints provides an easy way of de-montage. A big advantage is also the possibility to produce parts in one step of extrusion or injection moulding (2-component-injection

moulding) /6/. Major application fields of TPE-V and their development over the years are shown in figure 2.2.

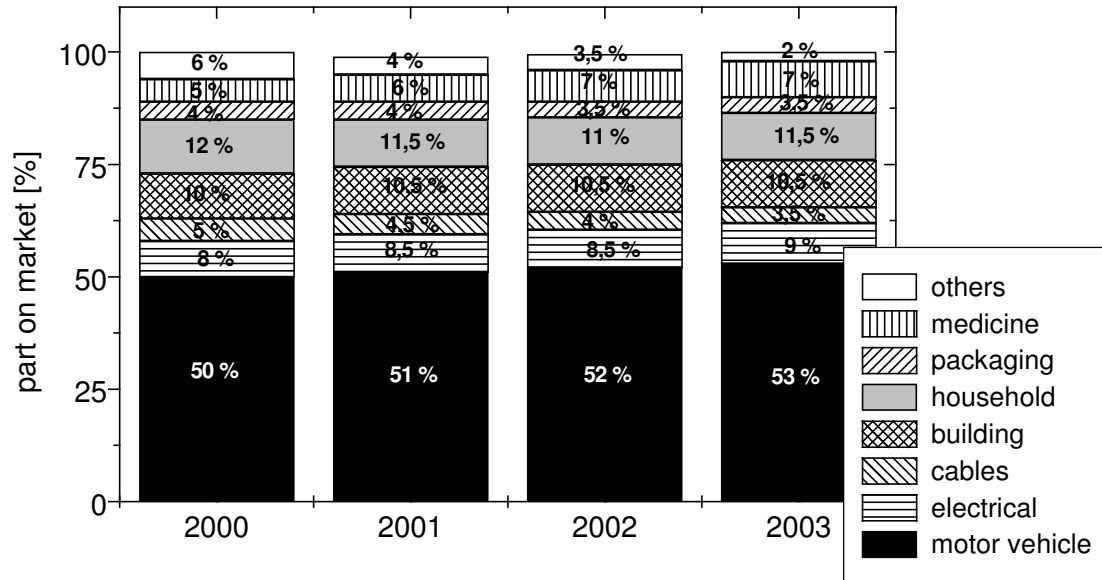


Fig. 2.2 Divisions of application fields for TPE-V in Germany 2000-2003 /6/

2.3 Dynamic vulcanization

The dynamic vulcanization process was first used by Gessler and Haslett /7/ for the preparation of high impact compositions containing different amounts of partially vulcanized elastomer in an iPP/Polyisobutylene blend. The first crosslinked PP/EPDM blend was produced by Holzer and co-workers /8/. The first TPE-V introduced to the market were derived from Fisher's/9,10/ discovery of partially crosslinking of the EPDM phase of EPDM/PP by controlling the degree of vulcanization by limiting the amount of peroxide. Further improvement of the thermoplastic process ability of these blends was reached by Coran, Das and Patel /11/ by fully crosslinking of the rubber phase under dynamic shear. They demonstrated the effect of the size of particles and the degree of cure on the materials properties as shown in figure 2.3. Raetzsch et al. /12/ developed a new type of dynamic vulcanizates by means of peroxidic crosslinking of the copolymer phase providing high strength and elasticity as well as colorability.

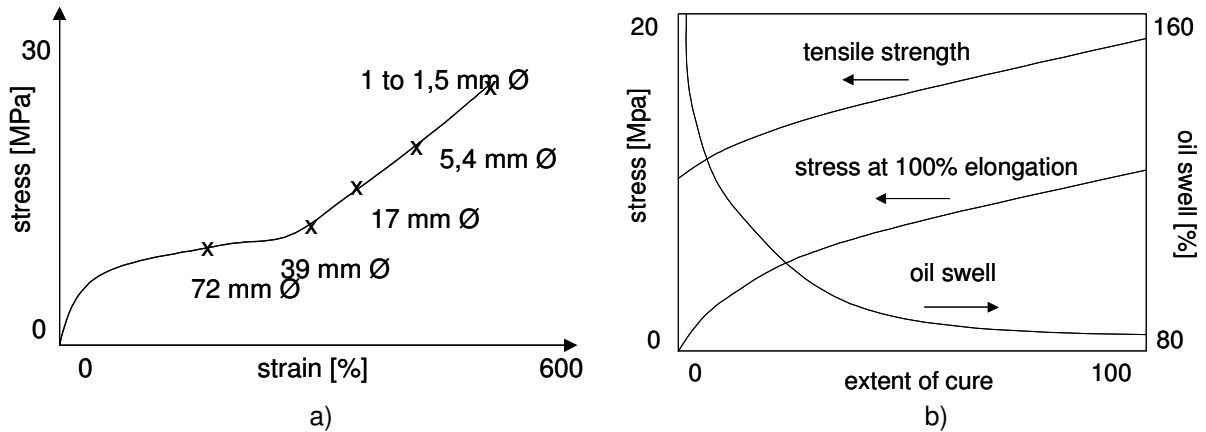


Fig. 2.3 a) Effect of rubber particle size on stress-strain properties of TPE-V b) Effect of curing on mechanical properties and oil swell of TPE-V /14/

2.3.1 Morphology development

During dynamic vulcanization generally thermoplastic matrix material as well as a rubber component are blended in an extruder resulting in a, so-called, co-continuous blend morphology. By means of a second opening a crosslinking agent can be added into the extruder (see fig. 2.4).

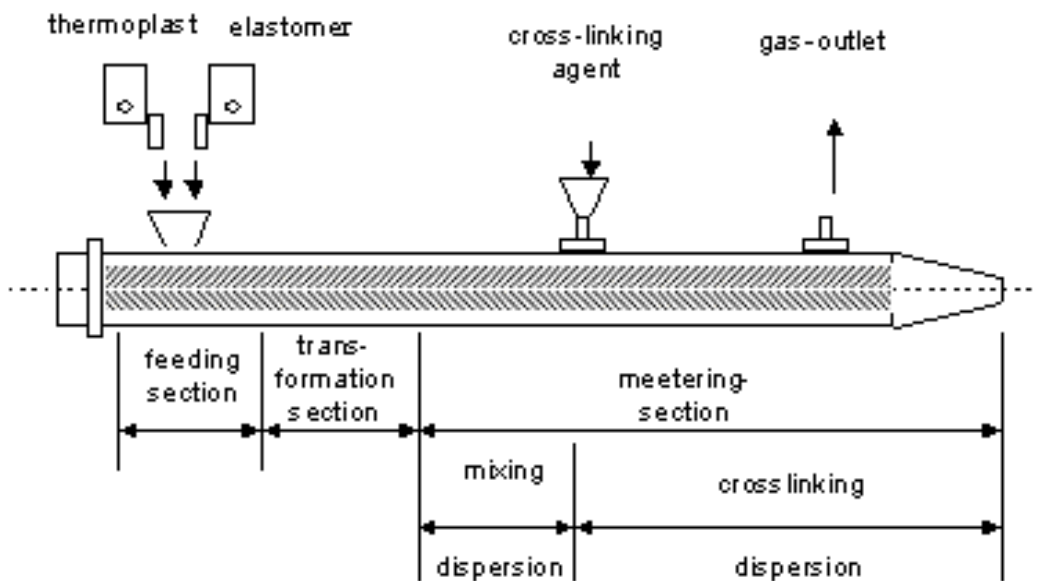


Fig. 2.4 Scheme of extruder profile for dynamic vulcanization

During the crosslinking of the rubber phase the viscosity of the rubber increases causing the blends viscosity ratio to increase, since the viscosity of the thermoplastic matrix remains the same. The shear stress causes rubber phase to fall apart into fine dispersed rubber particles in a thermoplastic matrix. This process is schematically shown in figure 2.5. The formation of the characteristic matrix-particle morphology is essentially influenced by the kinetics of the vulcanization and the resulting crosslinking density of the rubber phase /13,14/.

If the crosslinking density of the elastomeric phase is very poor, the rubber phase will be able to undergo large deformation and remains co-continuous. If on the other hand the crosslinking density is too high the rubber phase can only be deformed under shear stress without ripping apart. Therefore an optimum of crosslinking density of 10 to $20 \times 10^{-5} \text{ mol/cm}^3$ has been suggested /15-17/.

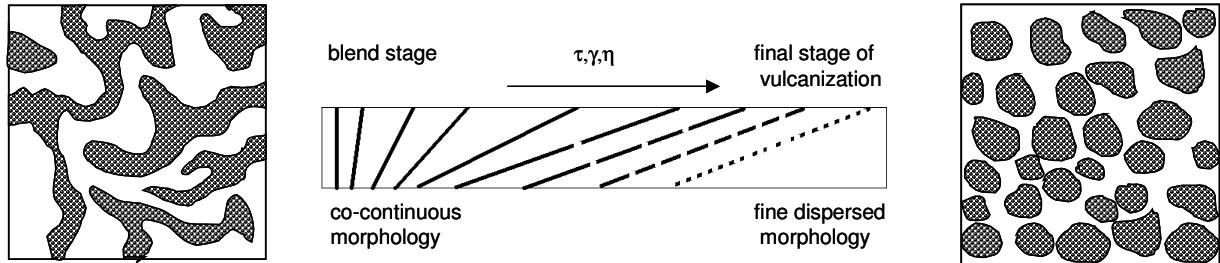


Fig. 2.5 Scheme of morphology development of dynamic vulcanizates during the crosslinking

2.3.2 Curing methods

The crosslinking of the rubber phase in heterogeneous blends consisting of a thermoplastic and a rubber component takes place by introduction of a crosslinking system during the mixing process. During the crosslinking covalent bonds are formed between network points resisting thermal and chemical stresses. Several crosslinking agents are used for rubber vulcanization. Among them are those who require unsaturated double bonds in the molecules to be crosslinked such as:

- sulfur /18,19/
- phenolic resins /25/

In addition to vulcanization agents accelerators, such as sulfenamides or thiuram sulfides, in combination with activators, such as zink oxide or stearic acid, are used to shorten curing times and to prevent thermo-oxidative degradation of the polymer.

A scheme of the vulcanization process by the classical vulcanization agent sulfur is shown in figure 2.6.

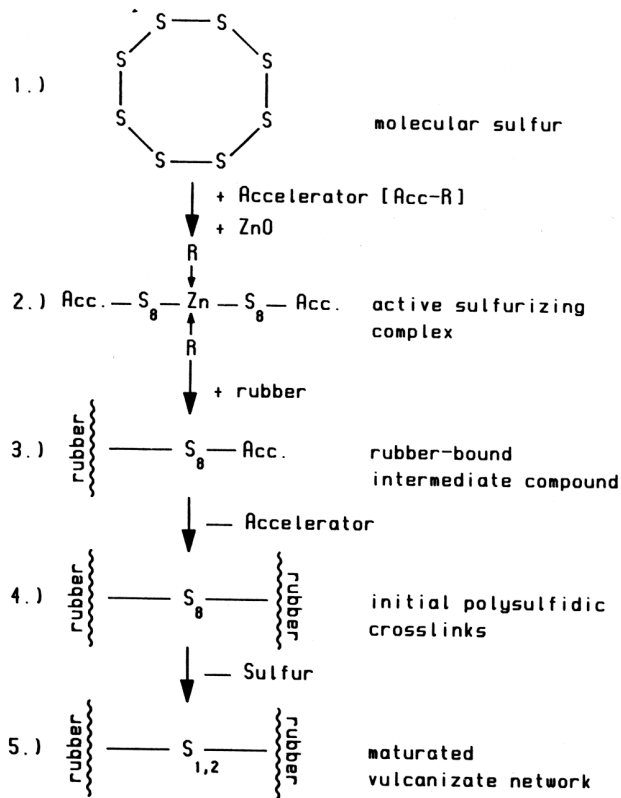


Fig. 2.6 Scheme of crosslinking reaction with sulfur.

By means of accelerators and activators the sulfur cycle opening (1) occurs providing for an active sulfurizing complex (2). The self destruction of this complex results in an active sulfur oligomer (3), which reacts with the rubber molecules crosslinking them (4). Due to the high vulcanization temperatures thermo-oxidative degradation of the rubber molecules as well as the sulfidic bridges can take place. Maturation (5) is the separation of sulfur from the polysulfidic bridges. Reshuffling the crosslinks may form intramolecular bridges (cyclic structures).

Phenol formaldehyde resins are also used to vulcanize diene elastomers in the absence of sulfur (see fig. 2.7). The crosslinking reaction occurs through the free phenol groups in the presence of stannous or iron chloride as catalysts. Vulcanizates with good mechanical properties and enhanced resistance to moisture and heat are obtained.

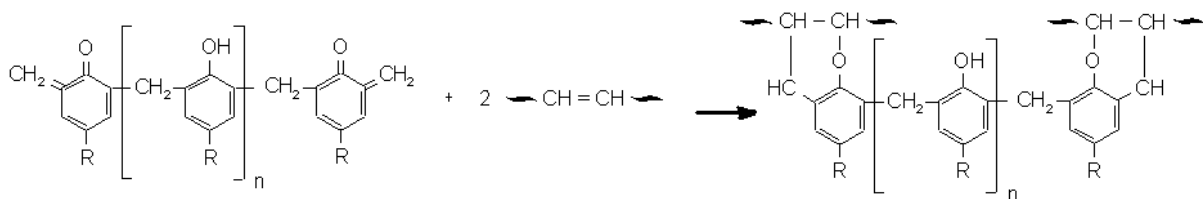


Fig. 2.7 Crosslinking reaction of a diene elastomer with phenolic resin

Saturated as well as unsaturated rubbers or copolymers can generally be crosslinked by free radicals, induced by:

- irradiation /22/.
- silanes /23/
- peroxides /24,25/

For irradiation crosslinking with high-energy radiations, free radicals are formed on the polymer chain, which couple to form carbon - carbon crosslinks. In this case, the elastomer, that does not contain vulcanizing agents, is heated to 100-150°C, pressed and then, irradiated.

During crosslinking with silanes a polyfunctional network structure is formed, in which the polymer chains are crosslinked via siloxan bridges (Si-O-Si). In case of EPDM two steps are necessary. First unsaturated organosilane molecules are grafted onto a polymer chain, which

was first activated with peroxide. Secondly the crosslinking reaction via hydrolysis and kondensation result in Si-O-Si bridges between the polymer chains.

The mechanism of crosslinking using peroxides is a homolytical one. At the beginning of the vulcanization process, the organic peroxide splits into two radicals. The free radicals formed as a consequence of the decomposition of the peroxide, abstract hydrogen atoms from the elastomer macromolecules, converting them into macroradicals. In the case of an ethylene-propylene copolymer, the radical formed by the decomposition of the peroxide attacks the tertiary carbon atom. The resulting macroradicals react with each other forming carbon - carbon intermolecular bridges. The crosslinking reaction of an EPM with peroxide is shown in figure 2.8.

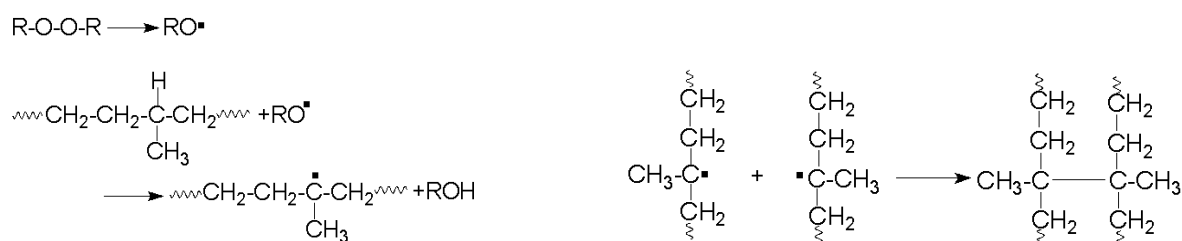


Fig. 2.8 Crosslinking reactions with peroxide

Simultaneously with these crosslinking processes, side reactions occur, which reduce vulcanization. Thus, peroxides can react with the components of the compound, i.e., antioxidants, plasticizers, extenders, etc., and can be deactivated. Other side reactions can take place on the radical centers formed on the elastomer backbone. These radicals can disproportionate leading to a saturated molecule and an unsaturated one.

Type and amount of ter-monomer, ethylene content and degree of branching of an EPDM influence the peroxide crosslinking efficiency and resulting vulcanizate properties. The effect of type and amount of third monomer on crosslinking efficiency was measured by the maximum torque difference in a rheometer and was rated as dicyclopentadiene (DCPD) > ethylidene norbonene (ENB) >> hexadiene (HD). This result was explained by different steric and chemical environment of the free double bond. Nevertheless the effect of type of third monomer on vulcanizate properties as hardness and compression set was low. High ethylene contents promote tensile properties being not only a result of higher crosslinking efficiency, but also of partial crystallinity of the polymer. High ethylene contents cause a high compression set at low temperatures. The branching level not only lowers the crosslinking efficiency, but also the kinetics of the crosslinking process /26/.

A general problem during crosslinking is posed by thermo-oxidative degradation processes. Polypropylene is depolymerised by free radicals in a so-called „chain - scission” process. The reason for this lays in the different reactivity of secondary and tertiary C-atoms in PE and PP /27/. Therefore only EPDMs with an ethylene content above 50 mol% apply for radical crosslinking. During the free radical crosslinking acetophenone is formed providing for a characteristic smell. At elevated temperatures acetophenone is diffusing out of the polymer /28/. When oxygen is present a chain reaction occurs initiated by decomposition of hydroperoxides. However, it was suggested that higher crosslinking levels hinder the penetration of oxygen into the polymer matrix decreasing the oxidation rate protecting the polymer from extended oxidation /29/. The use of coagents such as triallylcyanourate during peroxidic crosslinking in dynamic vulcanization of PP/EPDM systems has proven to be successful preventing β -scission for EPDM with ethylene contents below 50 wt% /30/. Another

method to prevent chain scission is the use of monomers such as styrene, which reacts with the free radicals. The effect is visible on the torque curve in the internal mixer. If chain scission occurs after the adding of the peroxide the torque is not reaching a stable value but gradually sinking. The addition of styrene prevents this decrease.

3 Crystallization behavior of dynamic vulcanizates and their components

During processing, among other parameters, the crystallization behavior during solidification of the thermoplastic materials is of great interest for the process itself but also the determining factor for the final properties of these materials. In this chapter the crystallization behavior of the components of DV used in this study iPP as well as the copolymers EOC and EPDM (EPM) will be described.

3.1 Crystallization behavior of iPP

Isotactic polypropylene is a semicrystalline polymer widely used in industry and stands for excellent mechanical properties up to a melting temperature around 180°C together with a relative low price. Lately new catalysts and production techniques have lead to a great variety of molecular weight and structure, which can be tailored to meet the demands for specific applications.

As a semicrystalline polymer iPP shows a hierarchic morphological ordering (fig. 3.1). The isotactic molecular chain arranges in a helical conformation forming a monoclinic unit cell. The unit cell dimensions for the α -crystalline form are of the size of a few nm and can be observed by wide angle x-ray diffraction (WAXD). These small unit cells form lamellae, which can be observed by small angle x-ray diffraction (SAXD) or high resolution electron microscopy /31/. The next higher morphological step is formed by spherulites consisting of building block of lamellae-shaped crystals. The dimensions are in order of 1 to 50 μ m and can be accessed by polarized optical microscopy (POLMI) and small angle light scattering (SALS). The morphological biggest scale reveals finally visually i.e. skin-core morphology /32,33/.

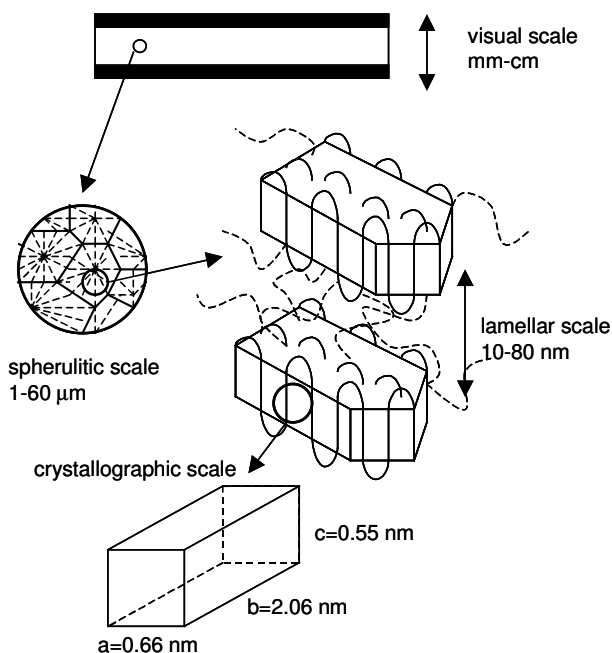


Fig. 3.1 Morphological scales in iPP with indicated size of dimensions for α -crystalline form /34/

3.1.1 Isothermal crystallization

Isothermal crystallization kinetics and resulting morphology has often been described via an Avrami analysis. In the isothermal case, assuming that kinetics are controlled by random nucleation and isotropic growth, the fraction of crystallites $\chi(t)$ transformed between times t and t_0 is given by the Avrami equation:

$$x(t) = 1 - \exp(-K(T)(t - t_0)^n) \quad \text{eq. 3-1}$$

At constant temperature T , χ is the crystalline fraction (dimension less), t is the time (min), K is the crystallization constant (min^{-1}), and n is a constant related to the crystallization mechanism or dimension of growth. This relationship has been proven for iPP by means of different technical methods such as optical microscopy and differential scanning calorimetry (DSC) /35,36/. Sometimes this relationship is also referred to as Kolmogorov-Johnson-Mehl-Avrami (KJMA) approach /37/.

The kinetics of crystallization for the α -form of iPP has also been described by the secondary nucleation theory. Hoffman and co-workers developed the following relation to describe the growth rate G related to changes in nucleation and growth mechanisms with undercooling /38-41/.

$$G = G_0 \exp\left[\frac{-U^*}{R(T_c - T_\infty)}\right] \times \exp\left[\frac{-K_g}{T_c(\Delta T)f}\right] \quad \text{eq. 3-2}$$

G_0 is a pre exponential factor, R is the gas constant, U^* stands for activation energy for the diffusion of the growth front and T_∞ is the temperature at which the crystallization ceases. T_g is glass transition temperature, T_m^0 is the equilibrium melting point and T_c is the crystallization temperature. The crystallization undercooling ΔT is given by $T_m^0 - T_c$. The factor f stands for heat of fusion and the heat of fusion per unit volume Δh_f can be written as $2T_c(T_c + T_m^0)$. K_g depends on the crystallization regime, which relates to the relative rates of surface nucleation and surface spreading. Different kinetic regimes describe the growth rate G by relative rates of surface nucleation and crystalline layer growth at the evolving front (fig. 3.2).

- Regime I: the first crystalline layer is forming after the initial nucleation
- Regime II: multiple nucleation events occur prior to completion of first crystalline layer
- Regime III: nucleation density approaches size of molecular cross-section prior to completion of first molecular layer

K_g is given by:

$$K_g(III) = K_g(I) = 2K_g(II) = \frac{4b_0\sigma\sigma_e T_m^0}{\Delta h_f k} \quad \text{eq. 3-3}$$

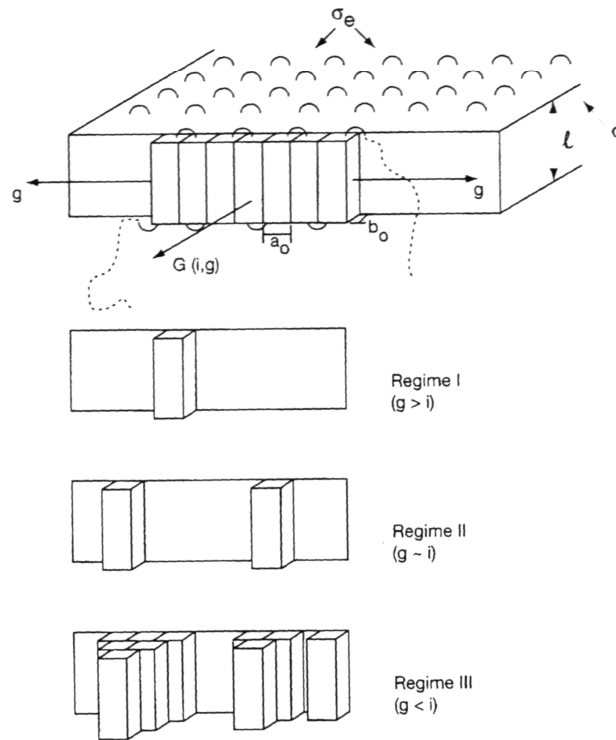


Fig. 3.2 Scheme of crystallization growth rate kinetics according to regime analysis /34/

This theory was used also by Carvalho et al. who found increasing growth rates with decreasing amount of molecular weight, increasing amount of ethene sequences and decreasing amount of grafting in grafted polymers /42/.

The velocity of crystal growth is determined by surface free energy ΔG_b .

$$\Delta G_b = \frac{4b_0\sigma_a\sigma_b}{\Delta\mu_v} \quad \text{eq. 3-4}$$

With μ_v being the difference in bulk free energy per unit volume between liquid and solid, b_0 the thickness of one monolayer of molecules and σ_a and σ_b the interfacial free energies per unit area of the (100) or (110) interface between solid and liquid /43/.

3.1.2 Nonisothermal crystallization

During cooling in injection molding of thermoplastics, crystallization processes take place mostly nonisothermal often with cooling rates higher than 200 K/min. It is quite difficult to reproduce and track such conditions experimentally and various techniques have been used and described in literature (chapter 4.1).

Despite the large number of models developed for the isothermal crystallization only a few exist to explain the crystallization under nonisothermal conditions. Ozawa /47/ developed a model assuming constant cooling conditions, that crystals originate from nuclei expanding as spherulites, and that their radial growth rate is constant at a given temperature. The untransformed volume fraction $1-X(T)$ at a temperature T is related to cooling rate dT/dt by the expression:

$$\ln\{-\ln[1-X(T)]\} = c - m \ln(dT/dt) \quad \text{eq. 3-5}$$

Where c is a constant and m indicates the type of nucleation and morphology. The Ozawa theory cannot be applied in polymers where secondary crystallization occurs /44/. The Nakamura equation /45/ was used by Hieber /46/ to create a direct correlation between the Avrami and Ozawa /47/ crystallization rate constant. The author shows, that in this way it is possible to compare isothermal and constant cooling rate crystallization data. According to this analysis performed on literature data for iPP, the maximum crystallization rate takes place approximately between T_g and T_m around 80°C .

Ziabicki introduced a more generalized model to describe nonisothermal crystallization. His model takes into account both transient and athermal effects. The model is able to predict the crystallization kinetics with temperature, pressure and stress changing with time /48,49/.

Relying on the works of Krüger /50/ and Woldt /51/ studying the nonisothermal crystallization of copper using a modified KJMA-approach Brostow et al. /37/ studied the nonisothermal crystallization of PP and PP/EPDM blends. The transformation of The Avrami equation 3-1 is done by approximation of continuous temperature-time curves by subsequent isothermal steps, with each step obeying the isothermal KJMA kinetics. This results in:

$$X(T) = 1 - \exp\left[\frac{-K_{eff}T \exp(-(\Delta E_a / kT))}{dT / dt'(\Delta E_a kT)}\right]^\alpha \quad \text{eq. 3-6}$$

Where K_{eff} stands for the modified nucleation and growth rate parameter, dT/dt' is the constant rate associated with the nonisothermal experiment and ΔE_a is the change of activation energy associated with the transformation.

Ding and Spruiell /52,53/ observed during nonisothermal experiments a plateau in the temperature vs. time curve, explained by the energy release during crystallization being higher than the energy taken away by the cooling medium. The curve consisted of an isothermal and a nonisothermal part. They adapted the Hoffmann-Lauritzen-Equation (eq. 3-2) to fit the nonisothermal part of the curve by substituting T_c by the temperature at which the plateau was found. Lim et al. /54/ used for the description of nonisothermal crystallization also a modified Hoffmann-Lauritzen-Equation (eq. 3-2) and exchanged T_c with $(T_m - (dT/dt')t)$ with T_m being the temperature at which the first measurable data was recorded and dT/dt' the constant cooling rate. This results in equation 3-7.

$$G_n = G_{0n} \exp\left[\frac{-U^*}{R[(T_m - (dT/dt')t) - T_\infty]}\right] \times \exp\left[\frac{-K_g \{T_m^0 + (T_m - (dT/dt')t)\}}{2(T_m - (dT/dt')t)^2 \{T_m^0 (T_m - (dT/dt')t)\}}\right] \quad \text{eq. 3-7}$$

G_n is the nonisothermal crystallization growth rate and G_{0n} is the pre-exponential factor containing quantities non strongly dependent on temperature. By integration of this modified equation they received the nonisothermal spherulite radius r_{en} as function of time since the nonisothermal growth rate is $G_n = dr_{en}/dt$. Adapting this theory Carvalho et al. /55/ found similar values of isothermal and nonisothermal growth rates for homopolymers.

3.1.3 The mesomorphic form of iPP

Isotactic Polypropylene is polymorph and exhibits as such more than one crystalline form depending on the crystallization conditions /56/:

- α -form, dominant form, isothermal crystallization
- β -form, slow growth rates at high temperature gradients, certain nucleating agents /57/
- γ -form, crystallization of very low molecular weight fractions /58/, crystallization at high pressure /59/
- mesomorphic form, rapid cooling conditions

The mesomorphic (or “smectic”) phase is an intermediate state of order between amorphous and crystalline states and is commonly observed after rapid cooling.

The name “smectic” indicates a degree of order higher than that of an ideal nematic liquid crystalline phase, with the molecular parallelism being the only degree of order. By means of x-ray measurements and IR spectra it was found that in this partially ordered phase the individual chain maintain the helical conformation being parallel. The packing of the chains perpendicular to their axes is more disordered than in direction to the axes. However the relative displacement and orientations of neighbouring chains do not appear to be completely random. Corradini et al. /60/ compared derived models of x-ray patterns from different aggregates of sequences with helical conformation with experimental x-ray patterns. This comparison suggested parallel chain organisation into bundles with correlational order restricted to 3-4nm but could not be described by any type of unit cell.

Miller /61/ suggested a para-crystalline structure, with edges of unit cells being distorted in both directions.

Also Geil and Gezovich /62/ suggested a hexagonal unit cell structure similar to the β -form. They found small “ball-like” structures or nodules being small imperfect hexagonal crystallites.

Allister et al. /63/ proposed the quenched state being composed of 60% amorphous structures and helices arranged in a “square array and a cubic or tetragonal symmetry”. Other works proposed the mesomorphic regions being formed by aggregates of helices lacking three-dimensional order /64,65/.

Caldas et al. /66/ showed by means of TEM dark-field image that the quench cooled morphology consists of three phases:

- microcrystalline regions with sizes ranging from 10 – 20nm with α -form
- regions of lower crystalline order, also consisting of α -monoclinic form, exhibiting less compact helical ordering evidenced by larger unit cell constants
- an amorphous phase exhibiting some periodicity without scattering in the dark field image

The absence of well defined lamellar ordering has been proven by the lack of well-defined SAXD maxima /67,68/.

Alberola et al. /69/ found an increase of T_g of iPP from the quenched to the annealed state by DMTA measurements and explained it by a constraint of the amorphous phase caused by small disordered structures. He also investigated the drawing behavior of quenched and annealed iPP /70/. Wang et al. /71/ observed by means of TEM cluster-like structures of the size of 10nm situated in the amorphous phase.

Regarding the mechanical properties of the monoclinic form in comparison to the mesomorphic form Seguela et al. /72/ found that the latter is more ductile due to reduced intermolecular cohesion. Furthermore, an applied stress induces the transformation of the smectic form into the monoclinic one.

It has also been known that the mesomorphic form is unstable with increasing temperature followed by a mesomorphic to α -form transition on heating. This transition is characterized by an exotherm in DSC scans at temperatures of 65 to 120°C and accompanied by an increase of crystallinity /67-69/.

O'Kane suggested that the mesomorphic to α -form transition is a solid-state transition being followed by an increase in the long range ordering /68/. The crystallinity of the quenched samples lays in the order of 35-40 %. It is also suggested that the small disordered crystals reorganize by helix reversals to larger crystals /73,74/.

Androsch et al. /75/ reported about an increase of the degree of locally reversible crystallization and melting within the metastable structure in quenched iPP in comparison to slowly crystallized samples. The degree of crystallinity based on enthalpy of the quenched materials at room temperature was 36 % with respect to 53 % of the slowly cooled sample. By means of atomic force microscopy AFM after heating and subsequent annealing at 140 °C of quenched iPP small globular structures of crystals of the size of 20-30nm have been observed. The state before annealing was described as consisting of regions with different structural order, small particles within a matrix of mesomorphic or amorphous structures.

The formation of the mesomorphic phase is formed by rapid quenching and can be controlled by the rate of cooling from the melt. Piccarolo et al. /76/ found a continuous decrease of α -form and increase in mesomorphic phase with increasing cooling rates. However above a certain threshold of cooling rate the mesomorphic phase is predominant and reaches a certain equilibrium value. By means of a deconvolution technique applied to the wide angle x-ray diffraction (WAXD) pattern of both iPP it was possible to estimate quantitatively the phase distribution /77,78/. This procedure was described more detailed by Martorana et al. /79/. In the iPP type with narrow molecular weight distribution it was found that α - to meso-phase transition takes place gradually between 10 and 100K/s with an increasing amount of mesomorphic phase to the favor of the decreasing amount of α -phase and reaching an equilibrium value above 100K/s (see fig.3.3a)). In the iPP with broad molecular weight distribution the transition takes place sharply at 140K/s with a sudden fall of the amount of α -monoclinic form and the rising of the amount of mesomorphic form (see fig.3.3b)). This was explained by faster crystallization kinetics in the latter case due to the higher amount of low molecular weight fractions. In both cases however the amorphous form content remained constant until 10 K/s and increased afterwards gradually from 50 to 75%.

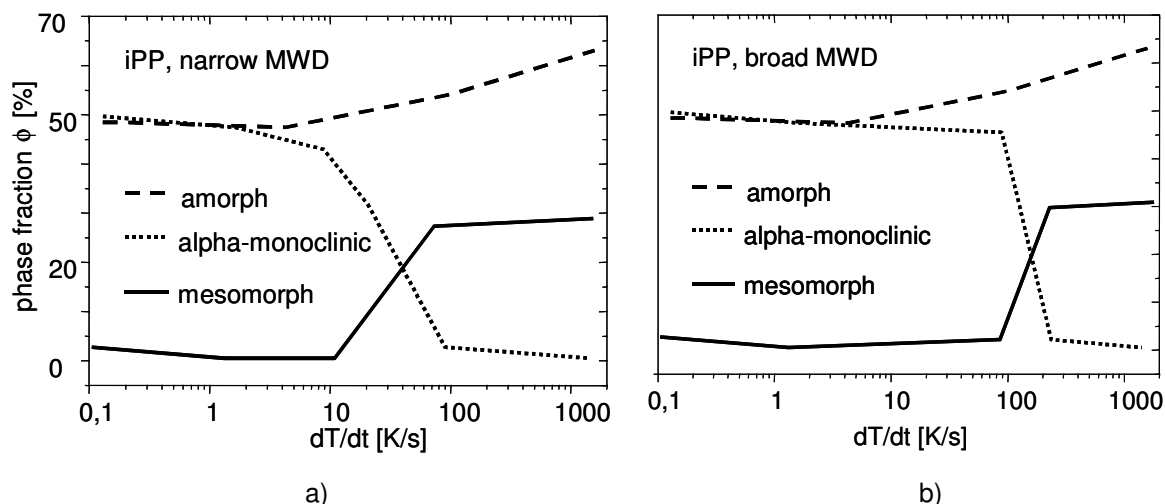


Fig. 3.3 Schematic phase fraction distribution of two types of iPP vs. cooling rates /79/

SAXD and WAXD studies of annealing of originally quenched iPP with defined cooling rates showed the existence of two different long - period values designated to the mesomorphic form at the original quenched state and the α -form forming during annealing /80/. Recently the quantitative analysis of the SAXD and WAXD data revealed that during annealing of originally quenched iPP the structural rearrangement consists of a thickening of already existing α -phase lamellae at the expenses of the amorphous regions as well as the structural rearrangement of the mesophase transforming into the α -monoclinic phase /81/.

The influence of cooling rate on the distribution of the different crystalline forms in PP-copolymers containing different amounts of ethylene content (0 to 3.1 %wt) and nucleating agents has been investigated by Foresta et al. /82/. The formation of γ -phase, indicated by the 2nd WAXD peak being higher than the first one, was found to decrease with increasing cooling rate reaching zero at 10 K/s, but to increase with increasing amounts of nucleating agent. The increasing ethylene content resulted in an increase of γ -phase, which is still enhanced in the presence of nucleating agent. Furthermore, a higher stability of γ -phase with respect to α -phase towards higher cooling rates was observed. This stabilizing effect appeared even more in the copolymer case. This was explained by lowered free energy of the γ -phase with respect to α -phase at high temperatures for homopolymers and lowered temperatures for copolymers.

3.2 Crystallization behavior of copolymers

The copolymers EPDM and EOC can form the elastomeric phase of the DV. In DV the elastomeric phase is the major component although being finely dispersed in the thermoplastic matrix, e.g. iPP. The rubber elastic properties of the DV will be mainly governed by the rubber phase. Therefore the crystallization behavior of the copolymers are of great interest and shall be discussed in the following, focused on the rubber used in this work.

3.2.1 EPDM

Copolymerization of ethylene with propylene forms EPM. Copolymerization with an unsaturated diene-termonomer forms side chains on the EPM-main chain resulting in

ethylene-propylene-diene terpolymer (EPDM) (fig. 3.4a) /83/. The unsaturation employed by diene provides for a greater compounding versatility, since EPDM can be vulcanized using sulfur or peroxide curing agents.

The ethylene-propylene (E/P) ratio ranges from 44/55 to 75/25, and are reported as weight percent in EPM. The content of methyl groups is here referred to as C3-content. Higher ethylene containing EPDM grades possess a small amount of crystallinity /84/. T_m and T_g change with composition. Narrow intermolecular compositional distributions show narrower melting behavior /86/ (fig.3.4b)).

Scholtens, Riande and Mark /85/ investigated the type and degree of crystallinity, the mechanical and thermal behavior of different types of cured and uncured EPDM in the stretched and unstretched state. They found in all EPDM types experimental evidence of, what they called, microparacrystalline structures. The amount increases with increasing ethylene content and degree of stretching. Above 80 mol% of ethylene content they assumed a change from microparacrystallinity to regular crystallinity.

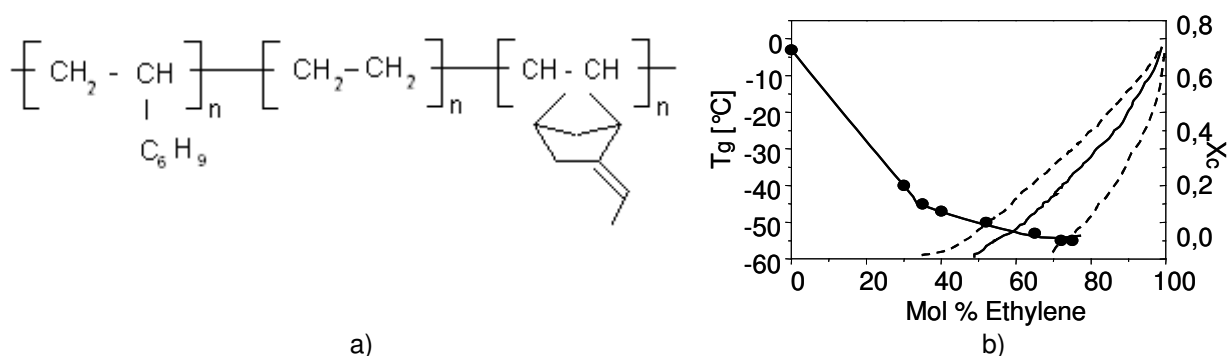


Fig. 3.4 a) EPDM molecular structure b) glass-transition-temperature T_g and degree of crystallinity X_c vs. ethylene content for an EPM schematically /86/

3.2.2 EOC

Ethylene/1-octene copolymer (EOC) is an ethylene copolymer made by copolymerisation of ethylene with octene or hexene comonomer (fig. 3.5a)). The use of metallocene catalysts gave the possibility for the synthesis of those copolymers with structure and properties completely ranging from low density polyethylene like materials to TPE. The ethylene sequences provide the thermoplastic processing /86/. Commercial grades have co-monomer contents ranging from 0.01 to 14.3 mol%, which are responsible for its thermal and mechanical properties. The higher the octene content the more number of branches resulting into more soft rubber-like properties and lower melting temperature /87/. The comonomer content influences significantly the degree of crystallinity /88/ and highly branched chains may lead to molecular segregation /89/ (fig.3.5b)).

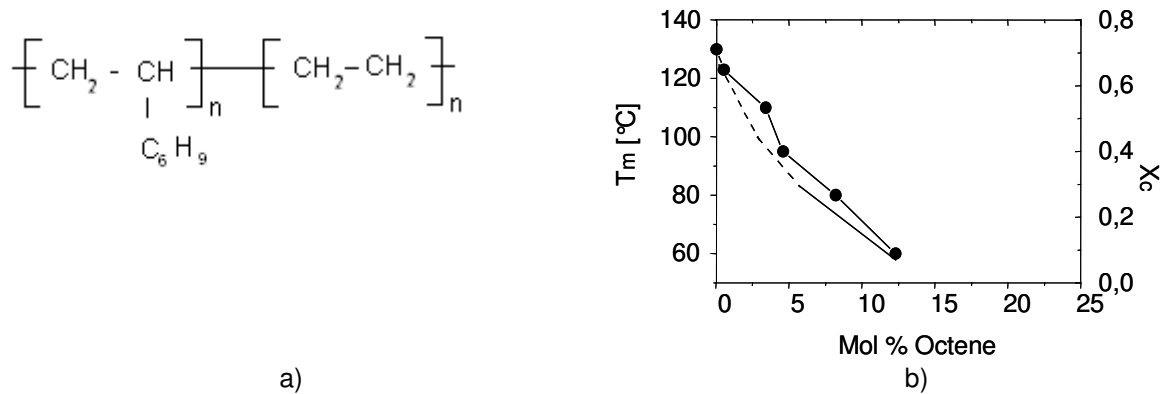


Fig. 3.5 a) EOC molecular structure b) melt- Temperature T_m and degree of crystallinity X_c vs. octene-content schematically /91/.

Bensason et al. /90/ proposed a classification of EOC based on their comonomer content after obtaining morphological data, and data from DSC and DMTA measurements from different EOC types. He divided the EOC in four types with mechanical properties ranging from elastomer-like to HDPE-like (fig. 3.6). The crystal morphology is divided into:

- Type I: bundle like-crystals
- Type II: mix of bundle-like crystals and lamellae
- Type III: lamellae / spherulites
- Type IV: lamellae / spherulites

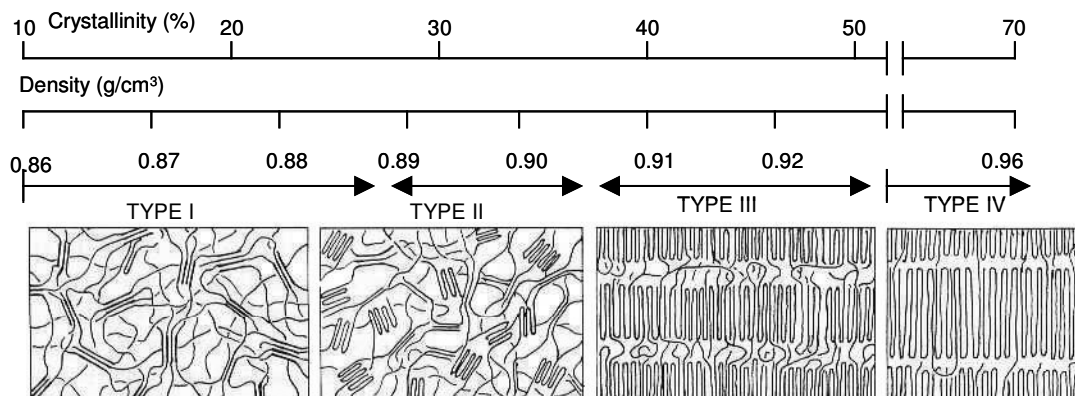


Fig. 3.6 Schematic drawing of crystalline morphology types of EOC with corresponding degree of crystallinity and density according to Bensason et al. /126/

Alizadeh et al. /91/ found for EOC with varying octene content (0 to 12.3 mol%) a characteristic crystallization temperature below which small crystals are forming, which melt just above their formation temperature. Crystallization above this temperature takes place from the free melt and leads to lamellar structures of increasing perfection and size for higher crystallization temperature or higher ethylene content.

Androsch and Wunderlich /92/ found by means of small angle x-ray scattering for EOC with (38 wt%) of comonomer content a distinct three-phase structure, an amorphous and two ordered phases; one orthorhombic and the second presumably hexagonal. The same authors studied the annealing of EOC by means of temperature modulated and standard differential scanning calorimetry /93/. The TMDSC enabled them to quantitatively separate reversing and

nonreversing apparent heat capacities using quasi isothermal measurements; i.e. measurements carried out during annealing by modulation around a fixed base temperature. At least five latent heat contributions to the apparent heat capacities between glass and melting transition; primary and secondary crystallization, reorganization, locally reversible melting, and the gauche trans equilibrium. By means of wide angle x-ray measurements Androsch /94/ found a decreasing peak assigned to the (110) lattice plane of the same EOC type for increasing cooling rates, ranging from 1 to 20 K/min at room temperature. He observed the formation of α -crystalline phase followed by perfection of the grown crystallites and the development of a mesomorphic form, both having different kinetics and thermodynamics.

Vanden Eynde et al. /95/ studied the influence of high pressure on the thermal behavior of linear polyethylene and EOC with different branch content (0 to 8 mol%). Increasing pressure shifts the melting and crystallization regions towards higher temperature due to a decrease in entropy. According to him at high pressure and high temperature the increased chain mobility enables the chains in the case of LPE to organize into extended chain crystals; in the case of EOC into folded chain crystals with stem length corresponding to the ethylene sequence length, called extended ethylene sequence crystals. Increasing the cooling rate for EOC with 2.1 mol% octene content shifts the melting endothermic peak during the subsequent heating towards lower temperature and a broadening of the melting peak. This was interpreted as gradual reorganisation during heating of the small imperfect crystals caused by the fast quenching.

Kolesov et al. /96/ compared plates of EOC with different co-monomer content formed by injection molding with varying processing conditions, such as mold temperature, mass temperature, holding pressure etc.. No significant change of degree of crystallinity and resulting density was observed in dependence of processing conditions. However with lower cooling times and higher injection velocity stress-strain measurements showed a shift of the mechanical behavior toward higher brittleness. This shift was explained by restricted mobility of the amorphous chains due to orientation of the amorphous phase or the raise of the specific crystal surface.

3.3 Crystallization behavior of iPP/copolymer blends

Blends of PP and copolymers such as EPM, EPDM, and later EOC have been used to improve the impact behavior of PP at low temperatures due to their elastomer like behavior. Therefore a lot of studies have been done to reveal the morphology and crystallization behavior of these blends non- or partially crosslinked. Generally more work has been done on non-vulcanized blends mainly with iPP as major component forming the matrix in order to determine the influence of rubber on the crystallization behavior of the iPP. This can be summarized as follows:

- rubber acts as a nucleating agent for iPP, either by providing heterogeneous nuclei by their phase boundary or residuals as additives left in the rubber phase during the processing /97,101,106/
- iPP crystal growth is hindered by the rubber phase, less perfect crystals are formed which influence the thermal parameters, T_m is lowered, T_c influenced /97,98,100,106,113,120/

- C3 content in the EPM and EPDM rubber types influence the overall crystallinity of the blends, some authors suggest partial dilution of C3 chains and less perfect iPP chains leaving the perfect crystals /97/

Very few investigations have been performed on vulcanized blends with iPP being the minor component mainly blended in internal mixers with low shear rates resulting in less dispersion of rubber particles. Therefore the application of these results to explain the influence of the morphology on the crystallization behavior in DV must be done carefully. The influence of crosslinking on crystallization behavior can be summarized as follows.

- vulcanized blends contain less perfect iPP crystals even though it remained unclear whether this was an effect of the hindrance due to the rubber phase being major component or iPP chain scission occurring during peroxidic curing /103,116/
- size, neatness, and regularity decreased in crystallized samples similar to the uncured blends /116/
- no clear long spacing value could be determined which was explained by either very large values or a broad dispersion of the lamellar thickness /103/

3.3.1 Crystallization of the system PP/EPM

3.3.1.1 PP/EPM blends

EPM is a copolymer similar to EPDM except for the lack of the diene monomer. On the background of this similarity the investigation of the crystallization behavior of blends of iPP and EPM found in literature shall be discussed in the following. PP/EPM blends with the weight ratios 100/0, 90/10, 85/15 and 80/20 and EPM with different ethylene/propylene ratios and therefore varying degrees of crystallinity have been studied by Greco et al./97/. Investigations by means of optical and scanning electron microscopy, DSC, WAXD on the 80/20 blend revealed that EPM-copolymer act as nucleating agents for iPP spherulites. For given crystallization conditions the morphology, i.e. mode and dispersion of the EPM-component, as well as thermal and mechanical behavior depend on the C3 content of the copolymer. The higher the C3 level the stronger is the nucleating effect on the iPP matrix, resulting in a larger number of smaller spherulites. As revealed by etching tests, with increasing polypropylene content the compatibility between EPM and iPP enhances, which was explained by amorphous C3 regions of the copolymer being incorporated into the intraspherulitic regions of the matrix. Increasing T_m and peak narrowing in the DSC scans have been explained by the ability of the C3 regions of the copolymer to extract less perfect molecules with low molecular weight from the iPP matrix. Increasing C3 content also increases the stiffness and yield stress of the iPP.

Further /98/ studies of the same group on a similar materials system polymerized under different conditions showed that with increasing EPM content the thickness of the crystalline lamellae decreased while the amorphous interlamellar layer increased. This was explained by the diffusion of EPM molecules with low molecular mass into the amorphous interspherulitic regions of the iPP matrix forming domains more or less connected with the amorphous layer; thus increasing its thickness resulting in hindering the spherulitic growth. However the molecular structure and composition of the EPM were found to have no significant influence on the crystallization of the blend. This contrary finding to the first work was explained by the use of a different catalyst-system used for iPP and EPM resulting in higher isotacticity of iPP

and a lower amount of irregularities and heterogeneities in the EPM. It was stated that EPM does not show any nucleating effect on the iPP matrix and that no diffusion of iPP molecules diffuse into the EPM phase.

Investigations on the influence of surface tension of melts of different EPM types on blend morphology and resulting mechanical properties in PP/EPM 80/20 blends revealed a decrease of E-Moduli with increasing EPM co-monomer contents. Surface tensions of melts of EPM decrease with increasing co-monomer content, reaching the values of the iPP melt /99/.

The miscibility of a PP/EPM 50/50 blend, obtained by melt extrusion, has been studied by time resolved-light scattering, small angle x-ray diffraction, and optical microscopy /100/. In contrary to the statements before /101/ regarding immiscibility of PP and rubber at all temperatures, these authors found a liquid-liquid phase separation at high temperatures similar to the spinodal decomposition (SD). It was shown that the amount of EPM in the PP rich phases formed by SD is related to the crystallization rate and the crystalline morphology and decreasing with increased phase separation time. This decrease induced the lower crystallization rate and a smaller long period.

3.3.1.2 PP/EPM vulcanized blends

The effect of viscosity ratio, C3 content and peroxide treatment on PP/EPM 80/20 blends has been studied by Kim et al./102/. Spherulite size of iPP was found to decrease with decreasing viscosity ratio as observed by polarized light microscopy and explained by nucleating activity of the EPM phase. Increasing the viscosity ratio the EPM particles increased in size while the interfacial area decreased. Crystallization temperature was lowered with increasing viscosity ratio being also an effect of the increased particle size. Peroxide treatment raised the viscosity ratio and influenced the crystallization behavior therefore indirectly. C3 content was not found to have an influence on particle size. High C3 EPM grades caused T_m , T_c , X_c to increase

Dynamically vulcanized PP/EPM blends with a weight ratio of 30/70 have been investigated by Martuscelli /103/ by means of DSC, optical and electron scanning as well as SAXD and WAXD and compared to its uncured blend and iPP. In the vulcanized blend the minor phase iPP became matrix surrounding the vulcanized EPM particles crystallizing in a so called cobweb-structure which appeared to be constituted of row structures of stacked lamellae. Lower iPP melting temperatures were explained by more defective and thinner iPP crystals due to the presence of the cured EPM phase or chain scission of iPP molecules as result of the peroxidic crosslinking. After isothermal crystallization the cured blend showed a lower degree of crystallinity compared to that of pure iPP and the iPP/EPM blend uncured. It was suggested that due to possible branching of iPP molecules as result of the peroxide a different molecular structure of iPP is forming. Regardless of the curing polarized optical microscopy showed microspherulitic structures in the blend, similar in shape to those of neat iPP. In both cured and uncured blends, size, neatness, and regularity of the spherulites of iPP, were found to strongly decrease during isothermal crystallization with decreasing T_c . The crystal growth in the blends seems to be lower than in iPP and its uncured blend. No long spacing thickness could be obtained from SAXD measurements for the cured blend. It was suggested that possibly the layer thickness is significantly larger than those of iPP and the uncured blend or characterized by a wide distribution of the long period. The mechanism of elastic recovery of the cured blend was explained by a so-called "leaf-spring" model, making the connected crystalline iPP lamellae ordered in row structures responsible for the elastic behavior.

However, the change from co-continuous to fine dispersed rubber particles is not complete since dynamic vulcanization in an internal mixer does not provide high shear stress during mixing like an extruder.

3.3.1.3 PP/EPM reactor blends

Different to the melt blending technology the reactor blending takes place during polymerization of both components in a reactor. With this technology even more than 50% rubber can be introduced in the blend still being dispersed in the PP-matrix. Yokohama et al. /104/ studied the crystallization and morphology of two PP/EPM reactor blends, one containing 60 and the other 70 wt% of EPM component. The EPM particles in the 70 wt% blend appeared finer and more dispersed than in the 60 wt% blend which still contains some co-continuous portions. Polarized light microscopy of crystallized samples revealed that the spherulite growth rate is slower for both with respect to neat PP. In the blend with the more dispersed particles the growth rate is faster than in the less dispersed blend. This was explained by steric hindrances, causing more time to the PP chains to fill the space by growing crystals. Inclusions of elastomer in the spherulites appear also finer in the more dispersed sample. Addition of EPM also causes positive birefringence of the spherulites with respect to negative birefringence of homo PP in the same range of crystallization temperatures. Nevertheless the crystallization of PP is hindered by EPM both in nucleation and growth of spherulites.

Carvalho et al. /105/ studied the nonisothermal crystallization of heterophasic PP-EPM copolymers different ethylene contents (6.8 to 13 wt%) and grafted iPP by means of the same technique as described above /55/. By means of polarized optical light microscopy the velocity of spherulite growth was determined and fitted with the modified Hoffmann and Lauritzen equation. The fitting worked well for heterophasic copolymers with ethylene contents of 9 to 10 wt%. The non-isothermal growth rate of heterophasic copolymers and grafted iPP was found to be higher than for homopolymers. This was explained by EPM particles and monomers introduced by maleic anhydride grafting reacting as nucleating agents during nonisothermal crystallization.

3.3.2 Crystallization of the system PP/EPDM

3.3.2.1 PP/EPDM blends

Martuscelli /106/ and coworkers created thin films of PP/EPDM-blends with EPDM-contents ranging from 10 to 40 wt% by compression molding of powder. He found the elastomer separated in droplet like domains dispersed in the intraspherulitic regions, aligned in radial directions. The number of nuclei per unit area increases with percentage of rubber. At a given T_c the addition of EPDM caused only a small depression of the radial growth rate of spherulites. The growth-rate plotted vs. different rubber content at a certain undercooling shows a maximum at 20 %, more pronounced for higher undercooling. The free energy of formation of critical nuclei, the free energy of folding were calculated and showed a minimum between 10 and 20 % EPDM content, whereas in earlier studies with EPM /107/ the contrary was found. The minimum of the melting temperature at constant T_c plotted over the rubber content was found around 10 wt% EPDM-content and explained by phase separation, followed by molecular fractionation and preferential dissolution of smaller more defect molecules of crystallizable component into the domains of the uncrystallized polymer. At

higher EPDM contents (above 20 %) the iPP matrix consists therefore of more perfect crystals causing the increase in T_m .

Wenig et al. /108/ studied the morphology, interaction of blend components and crystallization kinetics of PP/EPDM (amorphous) blends with elastomer contents of 5 to 30 wt% by DSC, DMTA, WAXD, SAXD and polarizing microscopy. It was found that the dispersion of EPDM depends on the blend composition and has a maximum at 10 % EPDM content. An interface layer between both components is suggested, formed by migration of iPP molecules into the EPDM phase. Furthermore it was stated that specific interactions between the components are causing the glass transition of EPDM in the blend to be higher than pure EPDM. In later works /109/ the effect of adding a slightly crystalline EPDM to iPP was compared to the blend with an amorphous EPDM with respect to nucleation and crystallization kinetics. It was found that the dispersion of semicrystalline EPDM is different from that of amorphous EPDM causing different effects on nucleation and crystal growth. It is believed that the composition of the interface layer between iPP and EPDM depends on the crystallinity of the EPDM. Both EPDM types are incorporated in the iPP spherulites causing a decrease in maximum growth rate of the latter. The decreased surface free energy of the iPP crystals causes secondary crystallization.

Wenig /110/ studied the crystallization of PP/EPDM blends (elastomer content 5-20 wt%) during isothermal crystallization by means of WAXD and optical microscope. Avrami exponents were determined, showing that secondary crystallization takes place within the already formed spherulites and increases the crystallinity of the sample. The spherulitic radius is not influenced by the elastomer. Both Avrami exponent and interlamellar distance show a minimum and maximum respectively around 10 % confirming the findings of Martuscelli. It was stated that the EPDM affects both primary and secondary crystallization.

Dharmarajan et al. /111/ studied the influence of ethylene content of the EPDM phase in PP/EPDM 70/30 and viscosity ratio on blend morphology and impact strength. It was reported that for a given PP MFR value, less ethylene content or more amorphous type EPDM resulted in higher impact strength. Lower viscosity difference gave finer dispersion.

PP/EPDM blends showed with increasing elastomer content decreasing Young's modulus and stress at maximum load. Strain at break and impact strength increased /112/. As for the blends of PP with EOC, Da Silva /122/ found for PP/EPDM blends of different compositions the same crystallization kinetics behavior. Low elastomer content (until 20 wt%) caused an increase in spherulite size and subsequent increments of EPDM (E/P ratio 75/25, 5 wt% ENB) provoked a decrease in crystal size. Spherulitic growth rates increase above 20 wt% of elastomer.

Zysk et al. /113/ found for PP/EPDM blends with different EPDM content (25 und 60 %wt) and different types, smaller spherulite radii but a higher number of spherulites with respect to iPP crystallized at the same condition. It was stated that the EPDM particles play an important role as nuclei for the formation of the spherulites resulting in a higher degree of crystallinity. They are also hindering the spherulite formation, especially in the 40/60 blend with co-continuous blend morphology, resulting in a lower growth rate and less perfect crystalline structures which lack well defined boundaries. Therefore the melting temperature appears decreased. The elastomer particles are moving along the growing crystallization and agglomerate to bigger particles. Above a certain size they are embedded in the spherulites /114/.

Brostow et al. /37/ studied the nonisothermal melting and recrystallization behavior of a PP/EPDM 70/30 blend by means of DSC. In the isothermal case it was found that in the blend recrystallization occurred faster, resulting however in a lower degree of crystallinity than in iPP. No change in melting temperature was observed at low rates. During heating with 20 K/s T_m of the blend is higher than for iPP. T_c in all cases appears higher in blends with respect to iPP. The degree of crystallinity in blends is lower than in iPP for slow heating and the same in the fast heating case. The isothermal and nonisothermal crystallization, with cooling rates at 10, 15 and 20 K/min, was studied by means of the KJMA approach. He found for the isothermal crystallization Avrami exponents around 4 and for nonisothermal cases around 2 indicating the difference in the modes of nucleation and growth. At 10 K/s two slopes are apparent while at 15 and 20K/min the slopes appear linear. This indicates that rapid recrystallization leads to the growth of different crystal morphologies than obtained from constant rates cooling. At slow cooling rates two crystalline structures are obtained.

3.3.2.2 PP/EPDM vulcanized blends

Slusarski et al. /115/ generated iPP/EPDM vulcanizates of different contents of amorphous EPDM ranging from 5/95 to 40/60 wt% by means of mixing on a two mill roll and subsequent vulcanizing with dicumylperoxide under internal conditions. In the blends a higher degree of crystallinity was found with respect to the calculated one by additional rule. With increasing iPP content the iPP long period first increased until 33/67 and then decreased again at 40/60. It was explained by the authors that iPP acts as nuclei for the propylene monomer units in the EPDM resulting in increased crystallinity. However the morphology of the system has not very clearly been reported as microheterogeneous morphology. Very likely the blend morphology consisted of a vulcanized EPDM matrix with dispersed iPP particles. It was not stated that iPP was matrix as it is the case for dynamic vulcanization in the extruder where high shear stresses cause the so-called island-matrix morphology.

Later studies of this group /116/ on the same system by means of DMTA showed a peak sharpening of the iPP relaxation $\tan \delta$ maxima which was related to an increased phase separation. A shift of these maxima to lower temperatures was explained by the formation of a thin diffusion layer on the interface. DSC and WAXD studies it was observed that with decreasing iPP content the crystalline phase results more defect. Crystal size and lamella thickness decrease with increasing EPDM content. Heterogeneous nucleation occurs in the blend. The structure, imperfect recrystallization, observed below PP/EPDM 15/85 differs from the structure, diffusion layer on the interphase, of the blends with higher iPP content. For nonisothermal crystallization Avrami coefficients values were found between 3 and 4, increasing with increasing iPP content in the blend.

Ludwig and Moore /117/ found an increased dispersion of EPDM in PP/EPDM 80/20 blends vulcanized with peroxide and a hexafunctional coupling agent. The crystallization temperature of PP in the blend was found to increase. This was explained by reduced mobility of the iPP chains due to crosslinking resulting in lower crystallization kinetics.

In order to explain the elastic recovery of PP/EPDM dynamically vulcanized commercial blend Yang /118/ and co-workers applied the theory of partially miscibility at elevated temperatures and lowered LCST induced by high shear rates during blend mixing. The partially mixed state would be frozen in by vulcanization of the rubber. According to the authors rubber impurities occluded in the iPP matrix causes the formation of fragmented crystallites. The same group /119/ investigated the strain recovery of iPP/hSBR 50/50 blends,

which consist of an iPP matrix with embedded hSBR particles in order to get an idea about the reversibility of this type of thermoplastic elastomer. The blends have been quenched cooled in different media, e.g. water or dry ice, reaching different crystalline sizes. They found however lower crystalline sizes of the iPP matrix in the blends compared to the neat iPP prepared with the same treatment. They found a local minimum of residual strain, i.e. best strain recovery, for crystal sizes between 10 and 1 nm.

3.3.3 Crystallization of the system PP/EOC

3.3.3.1 PP/EOC blends

Early work of Da Silva /120/ with iPP blended with 30%wt EOC (24 wt% octene content) suggested immiscibility. The iPP melting peak broadening was subscribed to changes in the crystal morphology of iPP. The glass transition temperature was found shifted to lower temperature (from -47 to -54 °C), which was explained by thermal tensions forming in the EOC domains due to the higher thermal extension coefficient with respect to iPP resulting in an negative hydrostatic pressure within the domains.

Later /121/ the rheological behavior and the blend morphologies of iPP blended with different weight percentages of EOC (24 wt% octene content) were studied. It was found that the EOC is located within the iPP matrix in small spherical shaped domains, with increasing size as the EOC content increases. Above 50 wt% of EOC co-continuous phase morphology is observed. DSC scans and tan delta curves from DMTA measurements show partial miscibility for 5 and 20 wt% EOC. The degree of crystallinity decreases with growing EOC content from 44 to 6 % for iPP and iPP/EOC 20/80 respectively. It was found that at least for the immiscible iPP/EOC blends the crystallization behavior of iPP remains unchanged by EOC.

By means of polarized optical light microscopy /122/ it was found that at 5 wt% EOC content the PP spherulite size reaches a maximum and decreases at higher elastomer content, indicating phase separation. However spherulithic growth rates of iPP were observed to first decrease until 20 wt% EOC and then to increase again with increasing EOC content until phase inversion takes place.

McNally /123/ studied thermal and mechanical properties of PP/EOC blends with EOC contents below 30 wt%. DSC scans revealed for pure EOC (25 wt% octene content) a glass transition temperature around 50 °C and a broad crystalline melting endotherm around 36°C. The iPP crystalline melting took place at 168 °C regardless of the amount of EOC in the blend. However the blends with increasing EOC content showed an iPP melting peak broadening suggesting a disruption of PP crystals with resulting distribution of PP crystallite size. With an EOC content of 30 wt% in the blend the crystalline content changed from 39 to 34 wt%. For pure EOC the tan d curves showed a glass transition at -20 °C. The blends up to 5 wt% EOC showed no EOC glass transition. With rising EOC contents the EOC glass transition temperature peak grew more intense but remained lower than for neat EOC, starting around -40 and rising to -30 °C. This was explained by the author by miscibility but could also be explained by with hindrance of the amorphous parts of EOC due to iPP. This hindrance decreases with increasing EOC phase content. The glass transition of neat iPP takes place at 15 °C and decreases slightly in blends with increasing EOC content to 10 °C. This could again be explained by the hindrance of the movement of the amorphous iPP phase with

increasing EOC contents. So the tendency of the glass transition temperatures to move towards the other blend component is explained by interactions on the molecular level.

The influence of content, molecular weight and comonomer contents of EOC in blends with up to 30 % EOC content was studied by Premphet et al. /124/. Tensile strength was found to increase with decreasing EOC content and for a given blend with decreasing comonomer content and increasing molecular weight. Impact strength was found suddenly to increase at 10 % EOC content. The authors calculated a corresponding ligament thickness of matrix between the rubber particles and compared the value with experimental values from microscopy. The critical ligament thickness of 0.3 to 0.4 μm was determined. The EOC particles exhibited a bimodal size distribution of 0.1 and 0.3 μm , the latter being more present at high comonomer contents.

Mäder et al. /125/ observed also a EOC T_g depression from -42 to -60 $^{\circ}\text{C}$ from bulk to PP/EOC 60/40 blends and explained it by volume dilatation of the immersed elastomer phase due to the higher shrinkage coefficient of the EOC phase with respect to the iPP matrix.

Blends of two EOC copolymers were studied by Bensason /126/ by means of DSC, one component having a high branch content of 14 mol% octene and the other component varying from 3.3 to 8.5 mol%. For blends 50 %wt of both components having high branch contents he suggested a morphology with separate crystalline regions interconnected by a miscible non crystalline phase. For the combination with 80 wt% high and 20 % low branch content it was believed that a continuous network was formed by the high branch content EOC and phase separated domains of the EOC with low branch content.

4 Fast cooling - state of the art

Since solidification during thermoplastic processing very often involves high velocity gradients, high thermal gradients and high pressures, the development of a model able to describe polymer behavior turns out to be really complex. Due to the experimental difficulties, the study of polymer structure developed under processing conditions has been mainly performed using conventional techniques such as dilatometry and DSC. The investigations possible using these techniques normally involve experiments under isothermal conditions or non-isothermal conditions but at cooling rates several orders of magnitude lower than those experienced in industrial processes, often leading to quite different structures and properties /3/.

4.1 Rapid cooling methods with defined cooling rates

Spherulitic growth rates were studied by Ding and Spruiell /52,53/ based on light depolarizing microscopy at different cooling rates up to 100 K/s. The Polymer between two thin glass plates is cooled down on the microscope sample stage by a gaseous liquid supplied at constant temperature. The temperature of the polymer is measured by a thermocouple embedded directly in the sample. The sample geometry was chosen by heat transfer analysis in order to neglect a temperature distribution across the sample. The light scattering effect occurring when crystallization takes place was observed and the corrected depolarized light intensity was measured in order to study crystallization kinetics.

Malkin et al. /127/ observed the crystallization kinetics of 2-3 cm thick Polyamid 6 (PA6) plates, which were cooled from 205 to 120 °C in 80 min, reaching only a cooling rate of 0.05 K/s. They determined the temperature along the thickness of the sample by means of three thermocouples.

Piccarolo et al. /78/ developed a new experimental set up in order to study nonisothermal crystallization at high cooling rates. A schematic drawing of the apparatus and the samples in the samples holder is shown in figure 4.1. The sample is wrapped in aluminium film to prevent leakage of the hot melt and placed between two metal slabs and heated to the desired temperature by means of an electric heater. After the necessary holding time the sample is placed in the lower part of the box and water is sprayed onto the sample holder in order to cool the sample to below room temperature. The temperature is measured by a fast response thermocouple embedded in one of the metal slabs made of a copper-beryllium-alloy. The slabs are slightly pressed onto the sample by means of metal springs in order to compensate the shrinkage during solidification and to guarantee thermal conductivity. Cooling rates can be varied by changing the cooling medium, its temperature and its flow rate (pressure and spray nozzle geometry) as well as by choosing thicker metals slabs i.e. by acting on the removed heat flux or on the thermal capacity of the sample assembly. The exact cooling rates are determined after the cooling from the temperature-time curves by taking the first derivation at a temperature, which shows the maximum of crystallization rate.

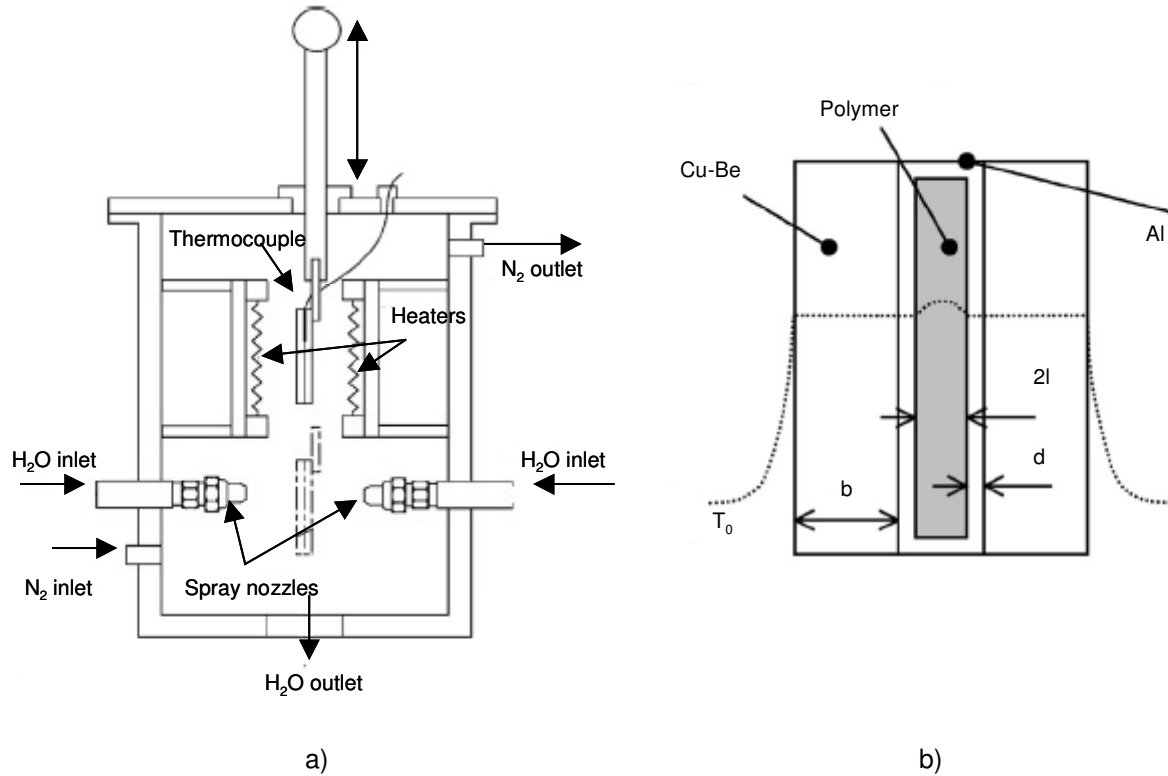


Fig. 4.1 (a) Scheme of the experimental set-up for quenching experiments; (b) sample assembly and temperature profiles. $b = 1\text{--}2\text{ mm}$; $l = 50\text{--}100\text{ }\mu\text{m}$; $d = 10\text{ }\mu\text{m}$ /3/.

Moneke /128/ developed an apparatus for rapid cooling of disc-shaped polymer samples of different thickness in a cylinder made by a special isolating material. The sample is heated and cooled by two different pistons subsequently reaching cooling rates of 200 K/s at a pressure of 30 bar. The temperature-time curves are obtained by a thermocouple embedded between two polymer discs at varying distance from 0.01 to 1 mm from the cooling surface. Volume changes have been determined separately by means of standard dilatometers and temperature conduction was measured. Materials studied were PP, PET homo-polymers and with varying glass fiber content. However the pressure in the cooling experiments was not varied. Also an influence of the thermocouple itself on the crystallization behavior is notable caused by nucleation processes on the surface boundary.

Brucato, La Carruba, et al. /129,130/ designed a new equipment in order to approach typical pressure as used in injection molding and measuring the temperature in the cavity during polymer solidification at the same time. They used a modified injection molding machine in order to supply a pre-determinable and maintainable pressure. The mould consists of two parts; the fixed part with a preheated cavity and a pressure sensor in order to measure the pressure during filling and the movable part containing the cooling liquid system. The cavity is closed towards the spray side with a copper-beryllium diaphragm containing a thermocouple allowing the temperature to be tracked during the cooling process. It is worth noticing that in order to avoid the influence of the temperature of the mould on the temperature measurement during cooling, an insulating ring of a special ceramic material is placed between diaphragm and mould. Finally the hot melt is filled into the cavity. The cooling liquid is sprayed on the diaphragm and the polymer solidifies only in one direction from diaphragm to the sprue. The cooling rate measured at the diaphragm and can be changed either by increasing the thermal mass of the diaphragm (higher thickness) or increasing the heat flux of the spray liquid. Two cooling rates taken at 70 °C, 100 and 20 K/s, at different

pressures (0, 1, 8, 24, 40 MPa) have been reported. The experimental scheme of the mould is shown in figure 4.2.

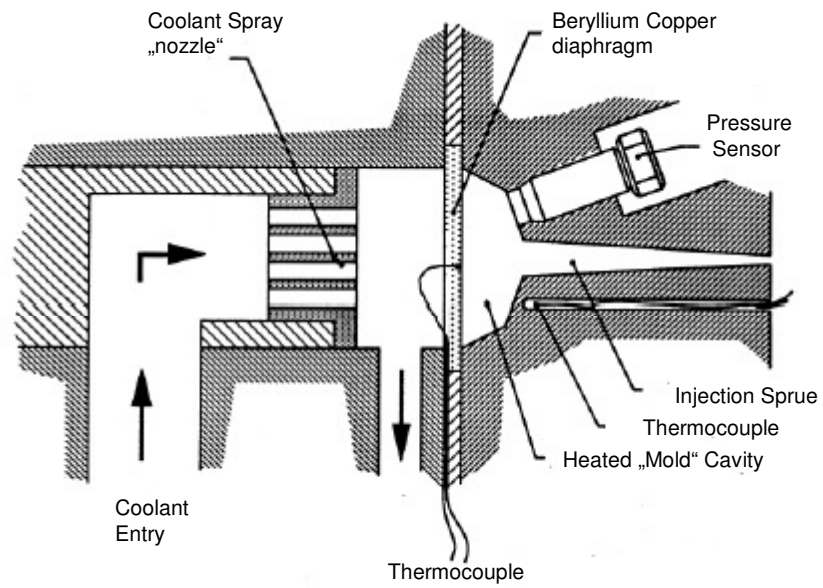


Fig. 4.2 Modified injection mould for defined cooling under pressure used by La Carruba /130/

5 The relationship between cooling conditions and structure/morphology formation in DV processing

The solidification behavior and its relation with final structure and properties of thermoplastic/rubber systems is a complex topic with several influencing factors, such as type and amount of the components as well as the chemical state of the components, i.e. crosslinked or uncrosslinked, and the existence of fillers. Several investigations on the influence of these factors on crystallization behavior under mainly isothermal conditions have been performed as described in chapter 3.3. In polymer processing however mainly nonisothermal conditions for polymer solidifications are found with large cooling rates up to 1000 K/s. The cooling device developed by Piccarolo [3] proved to be successful to simulate these conditions and was used until now mainly to determine the crystallization behavior of homopolymers under high cooling rates. This device is used in this work to investigate the solidification behavior under processing conditions of DV and its homopolymers. Next to cooling rates, the influence of type and amount of the rubber component and the crosslinking agent on the final structure and properties is determined.

As shown in the scheme in figure 5.1 first DV will be prepared varying the elastomer type and the crosslinking agent. Secondly the obtained DV and the basic components are cooled with defined cooling rates. Dynamic vulcanizates will be prepared for this study based on iPP, EOC and EPDM. These pure components are the first objects of investigation in order to compare them subsequently with the DV. It can be assumed that with rising cooling rates there will be a change in the crystalline structure in the semicrystalline iPP matrix, from α -crystalline to smectic. Due to the semicrystallinity of the copolymers forming the rubber phase it must be cleared also, if it will be affected by cooling rates. Methods such as wide angle x-ray diffraction (WAXD), optical microscopy under polarized light, and atomic force microscopy can be used to determine the type of crystalline structure, e.g. amorphous, α -crystalline or mesomorph, which develops under the cooling rates as well as the amount of each phase. Since there is also an influence of the existing crystalline formation on the remelting behavior DSC and DMTA measurements will be performed as well. There is a proportional relationship between degree of crystallinity, density, elastic modulus, and hardness. Therefore also density and microhardness measurements as well as tensile testing can be used to determine indirectly the effect of cooling rates on crystalline structure. This gives also the possibility to predict, the way such bulk properties are influenced by processing. Finally the obtained relationships should be used to predict the influence of the processing parameter cooling rate on the final part properties and to optimize the processing parameter set under the point of high productivity and maximized application properties.

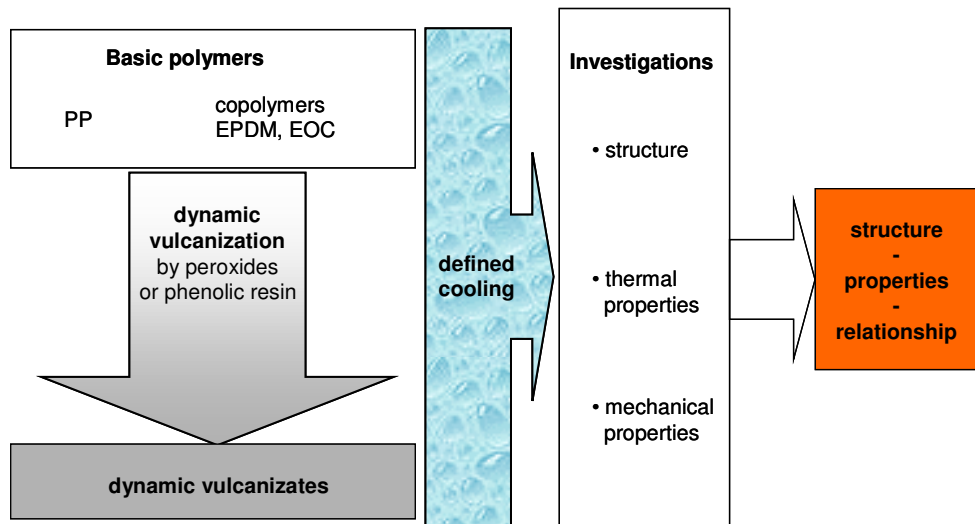


Fig. 5.1 Plan of experimental work to determine the influence of cooling process on the structure-properties relationship of DV.

6 Investigation of the relationship between cooling conditions and structure/morphology

6.1 Preparation of the dynamic vulcanizates

6.1.1 Materials

For dynamic vulcanization the following basic components were chosen. As matrix material served isotactic polypropylene iPP (Stamylan 14E10, DSM Germany) with an MFR (230 °C and 21.6 N) of 3 dg/min (corresponding to 14 Mooney viscosity), an Izod Impact (at 23 °C) strength of 3.4 kJ/m², flexural modulus of 1400 N/mm² and a Vicat softening temperature of 151 °C at 10 N and 83 °C at 50 N. In order to guarantee no side effects of additives on the crystallization behavior this type is free of additives.

For the rubber part in DV two different copolymers were chosen and used alternatively. The first one ethylene-octene copolymer EOC (Engage 8180, DuPont Dow Elastomers) with 42 %wt octene content, a melt flow index of 0.5 dg/min, a Shore A hardness of 66, a tensile strength of 7.2 MPa, a 100 % tensile modulus of 1.7 MPa, an ultimate elongation of >800%, and a brittle to tough temperature of -76 °C /131/.

Furthermore, especially to compare DV made from different rubber types, an ethylene-propylene-diene terpolymer EPDM (Nordel IP 4725P, DuPont Dow Elastomers) with 70 wt% ethylene, 25 wt% propylene, 5 wt% ENB (E/P ratio 2.8/1, dien/olefin ratio 1/19), with a broad molecular weight distribution (MWD) was chosen as second rubber type. Compared with the other EPDM types of this Nordel series this semicrystalline type had a high level nonsaturated bonds guaranteeing fast curing /132/.

In order to obtain a good dispersion during melt mixing similar viscosities of PP and the copolymers had to be chosen. The Mooney viscosity of EOC was 35 and of EPDM 25. In order to receive rubber-like DV and also to avoid the overlapping effects of both rubber and matrix crystallization the rubber components were chosen to contain low degrees of crystallinity. This was however limited in case of the EPDM with a crystallinity of 12 wt% /133/. In order to guarantee free flowing pellets for extrusion only EPDM grades with a minimum degree of crystallinity of 12 wt% were available. The crystallinity of EOC with this comonomer content was stated to be 10 wt% /90,91/.

6.1.2 Dynamic vulcanization technology

The DV were prepared by means of a twin screw extruder ZSK25 (Werner&Pfleiderer) using either a peroxydic crosslinking system or a phenolic resin crosslinking system:

- a): peroxydic crosslinking system (nomenclature letter: p)
 - peroxide for crosslinking, Dialkylperoxide, 2,5-Dimethyl-2,5-di (tert-butylperoxy)-hexane (Luperox 101, AtoFina)
 - styrene for inhibition of PP chain scission
 - acetone as transport media
- b): phenolic resin crosslinking system (nomenclature letter: r)

phenolic resin for curing, (Vulcaresen 510PA)
SnCl₂ as initiator

The exact compositions of the curing systems for each DV are indicated in table 6.1.

For the system a) the polymers were added by a rotating metering system providing a throughput of 87 g/min. The extruder was equipped with a second opening, where the liquid crosslinking system was introduced into the barrel. The liquid was fed with a flexible tube pump. The output of the pump was set to the calculated value corresponding to the curing system composition. The extruder worked with a screw speed of 350 rpm and a temperature profile for the zones I to IX of 190/190/200/200/200/210/220/220/220 °C. The extruded double strand was led into a water bath and cut in a strand granulator.

In order to receive a row of PP/EOC and PP/EPDM DV with varying iPP contents the latter were blended with iPP in the single screw extruder PL2100 (Brabender) with an L/D 19/26. For all zones I to IV the temperature was chosen as 200°C and a screw speed of 500 rpm. The DV with 30/70 blend compositions were homogenized also in this extruder in order to guarantee the same processing history with respect to the blended compositions.

For the system b) the use of the liquid metering pump was not appropriate since both crosslinking components were solid powders. Therefore the DV PP/EPDM 30/70r was prepared in a two - step process. The polymers were first blended by means of the twin screw extruder and granulated. The conditions were chosen as above. Afterwards this granulate was mixed with the powder-like crosslinking system. This mixture was dynamically vulcanized in the extruder. Since the resulting product was not very homogeneous the PP/EPDMr was homogenized again in a single screw extruder PL2100 (Brabender) L/D 19/25. For all zones I to IV the temperature was chosen as 200°C, a screw speed of 500 rpm and the screw with mixing elements.

The nomenclature, chosen for the samples prepared in the extruder, is explained on the following example.

PP/EOC thermoplast part/rubber part
30/70 wt% of thermoplast/wt% of rubber part
p letter indicates the type of crosslinking system (p peroxide; r phenolic resin)

Table 6.1 Material, curing system and processing history of blend series made by extrusion

Material	crosslinked with	Processing
PP/EOC 30/70p	3 phr Peroxide 1,5 phr Styrene 4,5 phr Acetone	dynamic vulcanization by use of twin screw extruder, ZSK 25, Werner&Pfleiderer
PP/EOC 40/60p	3 phr Peroxide	addition of iPP by use of Single Screw Extruder, PL2100, Brabender
PP/EOC 50/50p	1,5 phr Styrene	
PP/EOC 60/40p	4,5 phr Acetone	
PP/EOC 70/30p	blended with PP	
PP/EPDM 30/70p	1,5 phr Luperox 3 phr Styrene 4,5 phr Acetone	
PP/EPDM 40/60p	1,5 phr Luperox	
PP/EPDM 50/50p	3 phr Styrene	
PP/EPDM 60/40p	4,5 phr Acetone	
PP/EPDM 70/30p	blended with PP	
PP/EPDM 30/70r	5 phr Vulcaresen PA510 0,5 phr SnCl ₂	

In order to determine the influence of the amount of curing agent and the amount of rubber on mechanical properties another series of resin cured PP/EPDM has been prepared by means of the internal mixer, chamber volume 55 cm³ (W50 HT, PL 2100 Brabender). The curing system for all blends and DV made by internal mixing are described in table 6.2. The temperature was set to 200 °C and the speed to 65 rpm.

The nomenclature, chosen for the samples prepared in the internal mixer, is explained on the following example:

PP/EPDM thermoplast part/rubber part
 30/70 wt% of thermoplast/wt% of rubber part
 r letter indicates the type of crosslinking system (p peroxide; r phenolic resin)
 k internal mixer
 5 number indicates the amount in the unit phr of phenolic resin used for crosslinking

Table 6.2 Material, curing system and processing history of blend series made by internal mixing

material	crosslinked with	Processing
PP/EPDM 30/70rk5	5 phr Vulcaresen	internal mixer, W50HT, Brabender
PP/EPDM 40/60rk5	PA510	
PP/EPDM 50/50rk5	0,5 phr SnCl ₂	
PP/EPDM 30/70rk3	3 phr Vulcaresen PA510 0,5 phr SnCl ₂	
PP/EPDM 30/70rk1	1 phr Vulcaresen PA510 0,5 phr SnCl ₂	
PP/EPDM 30/70rkb	blend non cured	
PP/EPDM 40/60rkb		
PP/EPDM 50/50rkb		

6.2 Controlled rapid quenching technique

The melting and subsequent solidification of the samples at distinct cooling rates was done using the apparatus of Piccarolo et al. /76/ as described in chapter 4.1. The samples were prepared by pressing thin sheets of 200 µm at 220 °C, a holding time of 10 min, and a pressure of 10 MPa. From these sheets the samples with dimensions of approx. 20 x 20 mm were cut and wrapped carefully in small envelopes of aluminum foil. By means of thickness measurements and visual control it was made sure that only homogeneous samples were cut.

The samples were placed in the sample holder and fixed to the assembly by screws and metal springs. In order to insulate the sample holder slabs from the mounting assembly two small stripes of mica have been placed in between. The whole assembly was then carefully introduced in the heating/cooling box and all thermocouples connected. The sample was heated to a desired temperature and hold for a definite time. The exact data is indicated in table 6.3.

By means of the pressure regulation of the cooling liquid and the choice of the nozzle diameter the cooling rate could be predetermined. The highest cooling rates of 1000 K/s were received with 1mm thin Cu-Be plates, nozzle with a diameter of approx. 1 mm, cooling medium water and $p_{\text{cooling medium}} = 0.6$ MPa. The slowest cooling rates of 0.01 K/s were received with 4 mm thick Cu plates and cooling with air.

After cooling the sample was taken out of the sample holder assembly, placed into small plastic bags, and stored at $-10\text{ }^{\circ}\text{C}$ to prevent thermodynamically caused phase changes. The cooling rate was determined by the software by means of first derivation of the temperature-time-curve at an indicated temperature.

Table 6.3 Heating and cooling parameters for the different sample materials

Material	heating to temperature [°C]	holding time [min]	cooling rate taken at temperature [°C]
PP	200	10	70
EOC	100	10	50
EPDM	100	10	50
all DV	180	5	70

6.3 Characterization of morphology

6.3.1 Wide angle x-ray diffraction

Wide angle x-ray diffraction measurements were performed using the diffractometer D8 Advance (Bruker) with Cu - anode at a voltage of 40 kV in reflection mode. Reflection mode was chosen in order to increase the signal by doubling the sample thickness of 200 μm . The powder patterns were received from 2Θ 6 to 35° with a step size of 2Θ 0.1° and a step time of 2 s. Before measuring the samples were placed on the sample holder (glass plate) and fixed by steel clamps, positioned outside of the area touched by the beam. From the received patterns the background was subtracted, which had been taken for each series of samples.

6.3.2 Density

Density and its reciprocal specific volume are sensitive to the state of aggregation of a material; i.e. density increases and specific volume decreases from polymer melt to the solid state. In the solid state the specific volume changes also if the polymer is in the amorphous state or if it is showing a certain type of crystalline phase, e.g. α -crystalline or smectic. The specific volume can be measured by dilatometric methods or in a density gradient column. The dilatometer shows the advantage of measuring the density in course of a temperature and pressure in a range covering the melt and the solid state. The dilatometer however can not realize high rates during cooling of the sample due to its large thermal mass. In the density gradient column the samples can not be measured “in situ”. However samples, which have been quenched from the melt with high cooling rates under atmospheric pressure in the quenching apparatus can be measured. It can be assumed that at low cooling rates the amount of α -crystalline phase is higher than at high cooling rates resulting in a higher density. The density measurement in the gradient column has been proven very useful to determine the crystalline state of iPP together with other methods /78/.

Density measurements were carried out with a gradient column filled with a mixture of ethanol and distilled water according to the ASTM D1505-85 standard test method. The samples were cut into small pieces not larger than 3 x 3 mm. For each cooling rate at least three samples were introduced into the column. Before placing the samples in the column the samples were put in a small container, which was evacuated with a vacuum pump and then filled with the light liquid of the column in order to avoid the formation of air bubbles on the

samples. The temperature was 20 °C. For each material a new column was filled according to the desired density range. The gradient column of iPP had a resolution of 0.001 cm/g³. The very small density differences, which had to be measured in case of the DV due to the small iPP content required a very high resolution. The gradient column for the copolymers and the DV had a resolution of approx. 0.0001 cm/g³.

6.3.3 Polarized light microscopy

The cooled samples with a thickness of 200 µm permitted the observation of state of crystallinity by means of polarized light microscopy. The microscope RM-DX (Leica) was set in transmission mode with crossed polarizers. Micrographs were taken at 5 and 10 X magnifications. The samples were placed onto a glass slide and observed. The microscope was connected with a CCD camera, which transmitted the picture to the computer.

6.3.4 Atomic force microscopy

The samples were prepared by melting on a hot stage being covered on both sides with thin glass plates. Afterwards they were quenched in water or solidified on air. The originally cooled samples could not be taken for AFM measurements due to their roughness, since they were solidified on Al - foil. The samples were measured under tapping mode using the atomic force microscope from Digital Instruments Santa Barbara equipped with a Si cantilever with a spring constant of approx. 20 N/m and a radius of 10 nm. The height and the phase signal have been obtained parallel. In this work only the phase signal was discussed.

6.4 Characterization of thermal behavior

6.4.1 Differential Scanning Calorimetry

The heat flux calorimeter DSC 820 (Mettler Toledo) equipped with a liquid nitrogen cooling assembly served for the determination of the X_c , T_m and T_c of the cooled samples. The first heat run revealed the structure initiated by cooling of the sample. The cooling run and the second heat run showed the crystallization temperature and melting temperature of the sample cooled and reheated in the DSC. The measuring parameters are indicated in table 6.4. The heating velocity was 20 K/min. Faster heating provided a higher melting peak area. In order to receive maximum contact with the aluminium pan without melting (normally data after the first heating run is more reliable due to the enhanced contact of the molten sample) and in order to increase the sample/pan volume ratio, the 20 µl pan was used.

Table 6.4. Measuring parameters used for DSC measurements

	T range [°C]	dT/dt [K/min]	t hold [min]
1. heat run	-80 to 190	20	5
1. cool run	190 to -80	10	5
2. heat run	-80 to 190	20	5

The degree of crystallinity of iPP in DV was determined according to equation 5-1.

$$X_c = \frac{\Delta H_f^{PP}}{\Delta H_f^{PP0} + \Delta H_f^R / \Delta H_f^{R0}} \quad \text{eq. 6-1}$$

ΔH_f^{PP} is the melting enthalpy, determined from the area of the melting peak. ΔH_f^{PP0} is the melting enthalpy at 100 % crystallinity of iPP ($\Delta H_f^0=209$ J/g for iPP /134/). The area of the melting peak and therefore the melting enthalpy of the rubber phase was very low due to the originally low degree of crystallinity in the rubber (in EPDM only 12 wt%). Therefore the rubber enthalpy part has been neglected.

6.4.2 Dynamic mechanical thermal analysis

The dynamic mechanical thermal analyzer DMTA MARK 3E (Rheometric Scientific) has viscoelastic behavior. The samples 0.2 x 2 x 20 mm were cut from the samples. In the dynamic temperature ramp test the samples were characterized in tensile mode at a frequency of 10 Hz, strain of 0.2 % and at temperatures from -80 to 150 °C with 2 K/min heating rate. (The original gap was 7 mm.)

In the frequency-temperature-sweep-test the samples were heated from -60 to 150°C with a rate of 0.5 K/min. At every temperature a tensile strain of 0.2 % was applied with a frequency of 0.01 to 50 Hz. By this way it was possible to characterize the temperature- and frequency-dependent behavior of the material. The activation energy E_a of a relaxation process can be determined by the following equation:

$$\ln f = a + E_a (1/RT) \quad \text{eq. 6-2}$$

with f being the frequency of the test, a being the shifting factor, R the gas constant and T the temperature. The activation energy was determined by determination of the shift factor a by means of the time-temperature-superposition of the storage moduli as well as by plotting $\ln f$ over the reciprocal of the temperature of the individual transitions. The best results also with respect to literature data was given by plotting of f over the reciprocal individual transition temperatures taken from the $\tan \delta$ plots of different frequencies. Every transition in a polymeric material, e.g. the β -transition indicating the starting movement of the amorphous, phase, shows a characteristic activation energy E_a . The question was, if the movement of the mesomorphic phase shows such a characteristic E_a as well. The activation energies have been determined for the α -, meso-, and β -transitions taking place in pure iPP only since in DV the meso- and α -transitions of iPP are not clearly visible due to the softening of the rubber phase around 40 °C.

6.5 Characterization of mechanical properties

6.5.1 Microhardness

The microhardness is an important mechanical property which has been show to cross the gap between bulk properties, e.g. elastic modulus, and microstructure, e.g. crystal thickness /130,151/. It can be assumed that with increasing cooling rates and decreasing amount of α -crystalline phase resulting in lowered crystal thickness also microhardness will decrease. The microhardness was measured by means of a Vickers indenter from the microhardness measuring advice (Anton Paar). At least 5 data points have been taken for each loading force. The forces are indicated in table 6.5. After application of the force F for 6 s the length of the

diagonals d of the indentation was measured and the average value was calculated. The microhardness MH was calculated according to equation 6-3.

$$MH = d(F)/d(d^2) * 1.854 \quad \text{eq. 6-3}$$

In order to guarantee that the indentation deepness was less than 0.1 of the total sample thickness the diagonals length had to be less than 140 μm . In case of the DV the measured diagonals showed values between 50 and 100 μm representing therefore an area of the sample larger than the elastomer particles and being therefore representative for both phases.

The measurement of MH of EOC was rather difficult. Although the applied forces were the lowest possible in this test the diagonals were reaching values around 120 μm , being therefore on the edge of applicability of this test.

Table 6.5 Forces applied in microhardness tests

Material	F [cN]
PP	7; 10; 20; 30
PP/EOC 30/70 p	0.5; 1; 1.5; 2
EOC	0.5; 0.7, 1

Furthermore it must be stated that this test neglects the amount of reversible deformation of elastomers. Normally the hardness of elastomers is measured by Shore hardness measurements or microtests of rubber /135/ which was not applicable here due to the small sample dimensions. However, MH tests have been performed by Balta Calleja et al. /151/ on a PP/EPM blend using also 6s of holding time to minimize creep of the sample.

6.5.2 Miniature tensile test

The miniature tensile test was applied in order to verify the findings from the microhardness measurements since this parameter is directly related to the elastic modulus. It can therefore be assumed that the form of the stress-strain-curves indicates the effect of the cooling rate on the DV.

Due to the small sample dimensions to provide equal cooling throughout the sample it was impossible to apply a tensile test standard method. The System MiniMat 200 (Rheometric Scientific) served for determination of the stress-strain-behavior. 3 to 5 samples with dimensions of 0.2 x 2 x 20 mm were cut from each cooled sheet. The force measuring device was chosen with a maximum force of 20 N for the DV and 200N for iPP. (The initial gap was 7 mm). The measuring temperature was room temperature and the traverse speed 5 mm/min.

The residual elongation or strain as indication of the rubber-elastic behavior of the material was determined using the same measuring device applying a hysteresis run. The force was loaded until 300 % elongation and afterwards de-loaded with the same velocity of 5 mm/min. The residual elongation ε_r was calculated by the following equation:

$$\varepsilon_r = \varepsilon_{\text{end}}/\varepsilon_{\text{start}} * 100 \quad \text{eq. 6-4}$$

The total energy of deformation was calculated by integration of the area below the loading stress curve (fig. 6.1). The reversible part of work of deformation W_{rev} , which gives an idea about the amount of elastic deformation, was calculated by integration of the area of the

deloading stress data over strain. The irreversible work W_{irrev} of deformation, which stands for the plastic part of deformation, was determined by subtracting the reversible work from the total work. This method is described more precisely in the literature /136/.

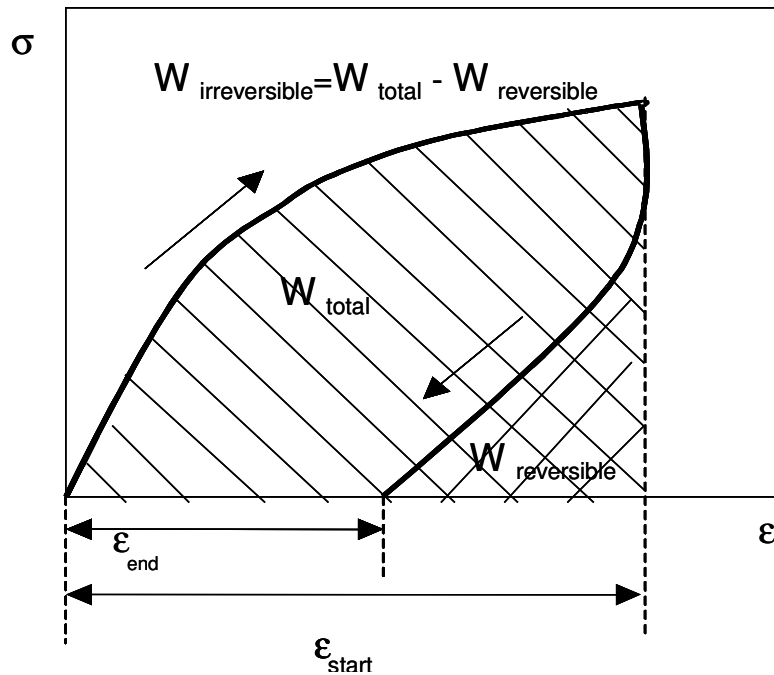


Fig. 6.1 Scheme of hysteresis cycle in order to determine the residual elongation ϵ_r

6.5.3 Rheoptical FTIR - spectroscopy

For the investigation of the orientation behavior of the different phases in DV the spectrometer S2000 (Perkin Elmer) was used in the wavelength range between 700 and 3500 cm^{-1} . A resolution of 2 cm^{-1} at 25 scans was applied. The tests have been performed without polarizer and with polarizer in 0° (parallel do drawing direction) and 90° (vertical to drawing direction). The absorption was measured of the samples showing dimensions of 10 x 20 x 0.1 mm. The deformation was applied in steps of 50 %. The degree of orientation O was determined by equations 6-5 and 6-6:

$$O = \frac{(D-1)}{(D+2)} \times \frac{(D_0+2)}{(D_0-1)} \quad \text{eq. 6-5}$$

The dichroidic ratio D can be determined by:

$$D = A_{\parallel} / A_{\perp} \quad \text{eq. 6-6}$$

with A_{\parallel} and A_{\perp} as absorption for parallel and vertical oriented radiation. D_0 is the dichroidic ratio at perfect order, i.e. in case of all chain segments being oriented parallel to drawing direction. For the orientation of the crystalline phase of iPP the 841 band and for the EPDM phase the 722 band were used according to Huy /139/.

6.6 Influence of cooling conditions on the morphology and the properties of dynamic vulcanizates and their components

6.6.1 The morphology of the pure components

6.6.1.1 iPP

WAXD

The influence of thermal history on crystalline phase development has been investigated by wide angle x-ray diffraction (WAXD). The WAXD pattern of neat iPP shows at low cooling rates the typical α -monoclinic peaks (fig. 6.2), indicating the existence of the α -monoclinic crystalline form which has been described in chapter 3.1. At very low cooling rate of 0.12 K/s the distinct split of the reflection of (111) and (131), (041) indicates a higher crystalline perfection presumably due to secondary crystallization. For the sample quenched at 30 K/s the first smectic peak appears as shoulder at $2\Theta = 21.1^\circ$. The smectic peaks indicate the existence of the smectic or mesomorphic phase, which has been described in chapter 3.1.3. Above 70 K/s only two broad smectic peaks at $2\Theta = 14.7^\circ$ and 21.1° are observed.

Similar pattern have been observed by Piccarolo et al. /76,77/ and a deconvolution technique has been applied by the same group in order to study the phase distribution /79/. This technique was applied here in a similar way. The WAXD cumulative pattern of iPP was divided into 10 different peaks indicated in the table 6.6. The fitting was done by means of the Origin Microcal program using the peak fitting modul. The best fitting of the peaks was obtained by the Pearson VII function, which depends on four parameter: the angular position, the width, the height and the shape parameters, which ranges in the $(1,\infty)$ interval, the lower bound corresponding to a Lorentzian peak shape and the upper one to a Gaussian. The asymmetric shape of the amorphous halo instead was described by an Asymmetric II Sigmoidal function. The results from each fitting of the WAXD-pattern from each sample cooled at a certain cooling rate are enclosed in the appendix. The amount of each phase has been calculated from the area of the peaks belonging to a certain phase.

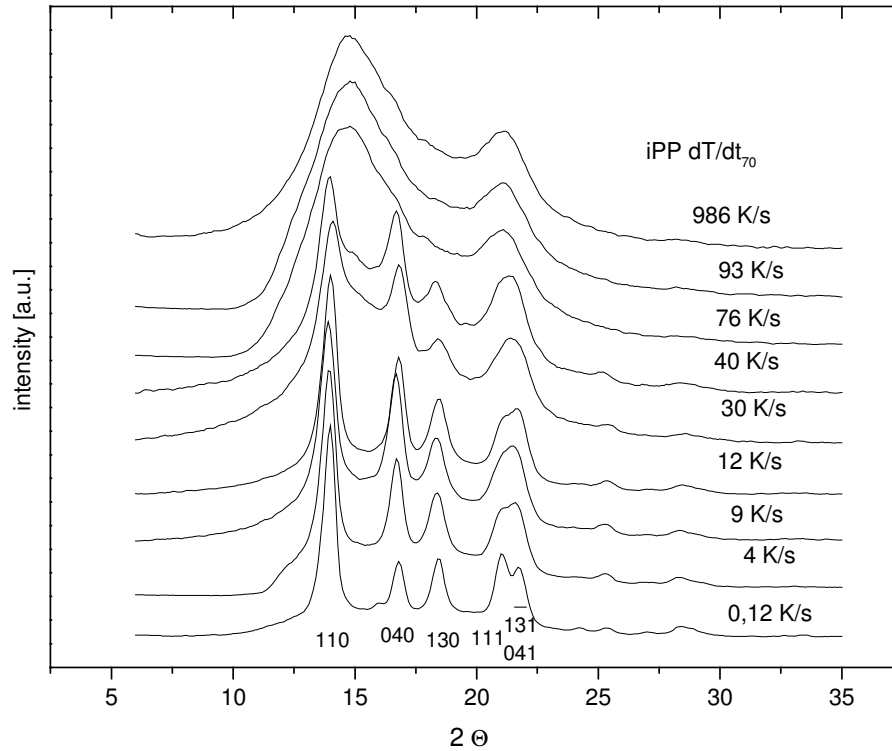


Fig. 6.2 WAXD cumulative patterns of iPP quenched at indicated cooling rates.

Table 6.6 Indication of the peak fitting functions and corresponding phases

number	phase type	lattice plane	angular position 2Θ [°]	type fit function
1	α -monocline	110	13,95	Pearson VII
2	α -monocline	040	16,79	Pearson VII
3	α -monocline	130	18,44	Pearson VII
4	α -monocline	131	21,04	Pearson VII
5	α -monocline	041	21,77	Pearson VII
6	α -monocline	060	25,27	Pearson VII
7	α -monocline	-	28,52	Pearson VII
8	amorphous	-	16,3	Asymmetric II Sigmoidal
9	mesomorphic	-	14,79	Pearson VII
10	mesomorphic	-	21,21	Pearson VII

A typical peak fit of the cumulative pattern of iPP solidified with 9 K/s is shown in figure 6.3.

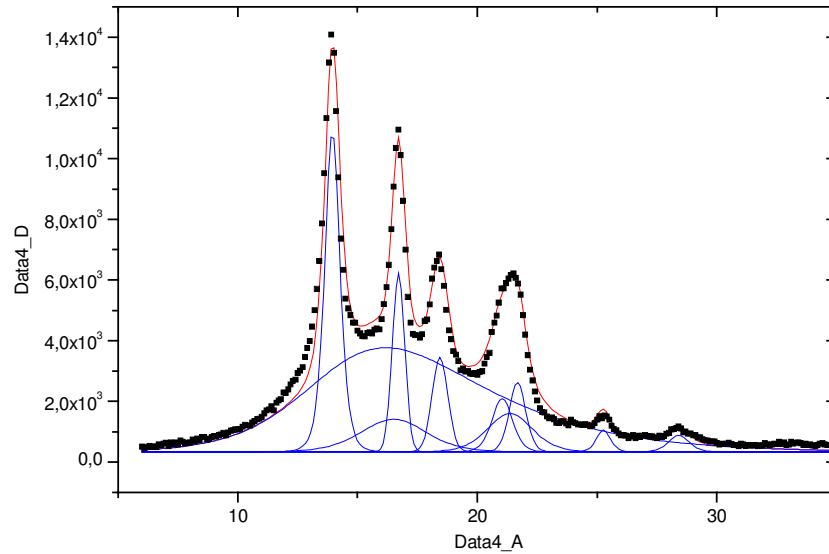


Fig. 6.3 Results from the peak fit of iPP solidified with 9 K/s

The phase distribution of the polymorphic phases vs. cooling rate is shown below in figure 6.4. The fraction of the amorphous phase is slightly increasing from 50 to 60 % with increasing cooling rate. The α -monoclinic phase decreases first to a little extend. Between 20 and 80 K/s there is a drop from 40 % down to almost 0 %. Above this cooling rate the value remains unchanged. The mesomorphic phase increases from 0% at 0.1 K/s to about 35% at 100 K/s and remains constant thereafter.

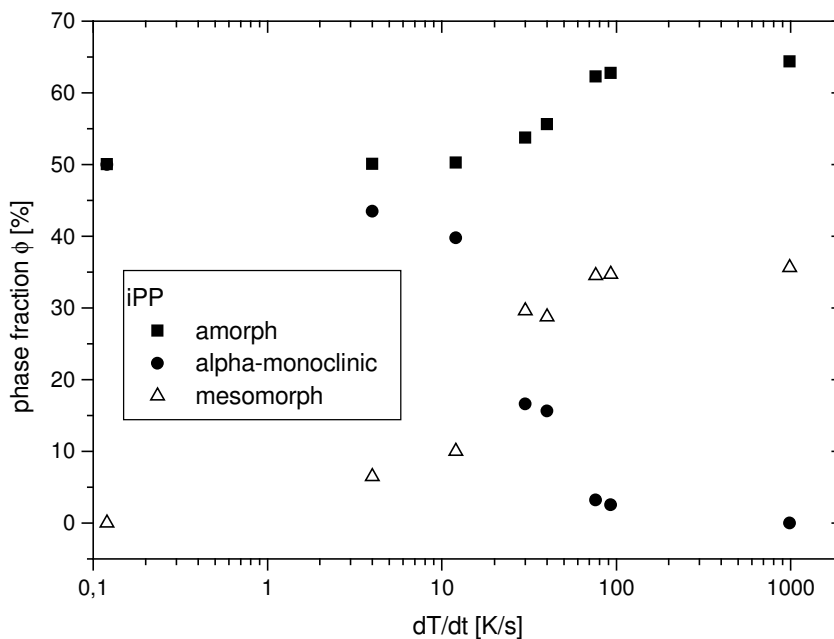


Fig. 6.4 Phase distribution vs. cooling rates of the amorphous, α -monoclinic and mesomorphic phases in iPP.

The mesomorphic phase replaces the α -monoclinic phase almost completely, first increasing slightly and then until 80 K/s suddenly to 40%. The same phase fraction development has been observed by Martorana et al. /79/ for an iPP with a high molecular weight and a narrow molecular weight distribution.

Density and Polarized Light Microscopy

The observed crystalline structures have been verified by polarized light microscopy and density measurements. The density measurements were used to indicate more precisely the change of structure at certain cooling rates. The density vs. cooling rate curve of iPP can be divided in three zones according to the major crystalline phase content. At slow cooling rates from 2 to 20 K/s the α -crystalline form is present as shown above and described in different papers by Piccarolo et al. [76-81]. The density value decreases slightly from 0.898 to 0.896 g/cm³. The micrograph obtained under polarized light reveals small spherulitic structures with the typical Maltese cross pattern (fig. 6.5a).

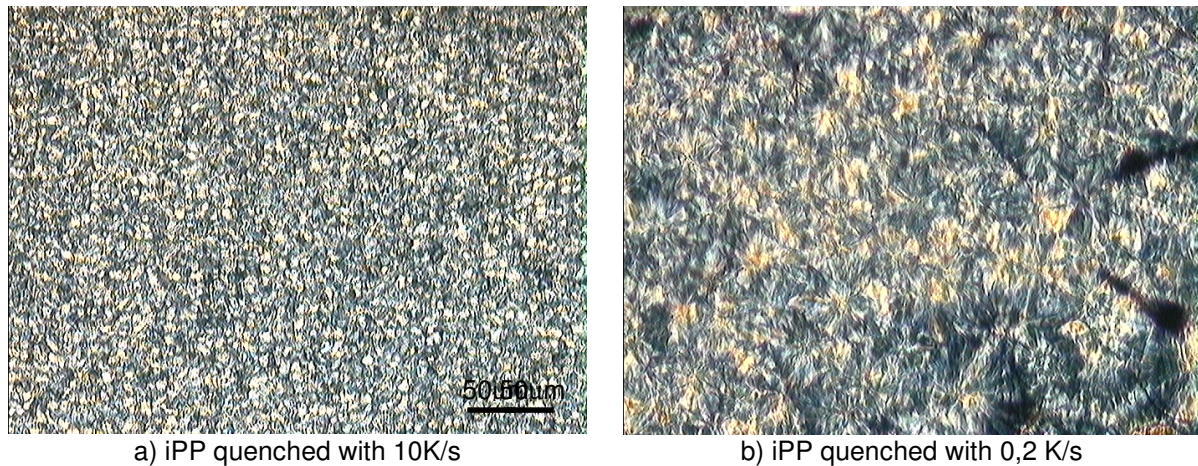


Fig. 6.5: Micrographs from iPP solidified at a) 10/s and b) 0.2 K/s. Optical microscopy, polarized light.

At very slow cooling rates below 2 K/s the solidification takes place at such a low rate that low temperature crystallization, i.e. secondary crystallization can take place parallel to primary crystallization. The density value indicates this by an increased value of 0.903 g/cm³. Enhanced birefringence can be seen on the micrograph and larger spherulites with the size ranging between 50 to 200 μm (fig.6.5b)). This behavior was observed for iPP by La Carruba [130,137] and a model was proposed taking into account both processes. His model was based on the assumptions, that secondary crystallization is a process leading to α -phase with a higher degree of perfection and that the latter grow only on the formed α -phase from primary crystallization substituting the amorphous phase. The driving force of the secondary crystallization is the difference between the primary α -phase fraction and the actual secondary α -phase fraction.

At cooling rates from 20 to 50 K/s a sharp density drop from 0.896 to 0.886 g/cm³ occurs which is a result of the transition towards to the mesomorphic form. The higher the amount of low molecular weight content the faster the crystallization kinetics and the “later” the transition takes place i.e. at higher cooling rates. The lower the molecular weight distribution the slower the crystallization kinetics takes place. Therefore this iPP type shows the transition already at low cooling rates between 20 and 50 K/s. This threshold depends at least on molecular weight and nucleating agents.

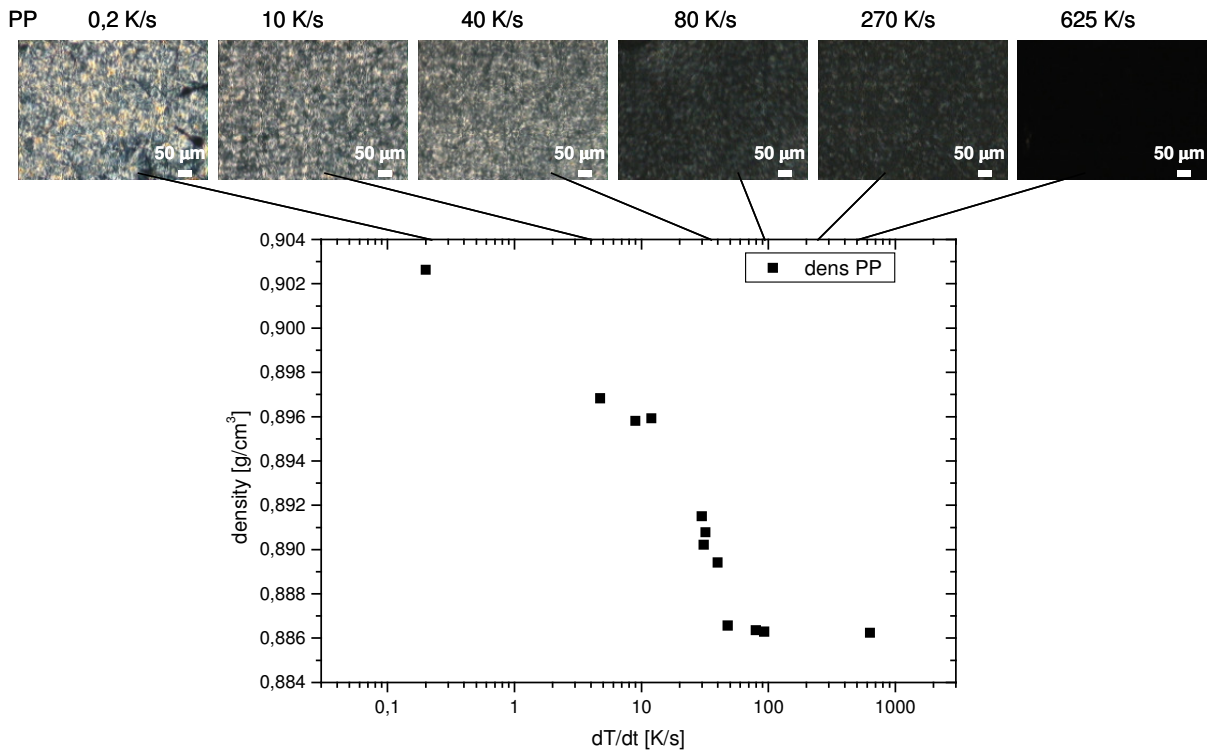


Fig. 6.6 Density (at 20 °C) vs. cooling rate plot with corresponding micrographs (obtained under crossed polarizers) of PP quenched with indicated cooling rates

Above 50 K/s the density values of iPP remain stable around 0.886 g/cm³ and do not depend on cooling rates. Only the mesomorphic phase and the amorphous phase are present at these cooling rates. The overall density changes observed between 0.1 to 1000 K/s was 0.017 g/cm³. The density change of the transition drop was 0.01 g/cm³.

In order to receive an idea about the trustworthiness of the phase contents derived from WAXD deconvolution, the total density ρ was calculated according to equation 6-7.

$$\rho = \varphi^{\alpha}(\rho^{\alpha}) + \varphi^a(\rho^a) + \varphi^m(\rho^m) \quad \text{eq. 6-7}$$

with φ being the phase fraction of the indicated phases; i.e. α for the α -crystalline phase, a for the amorphous phase and m for the mesomorphic phase. The density values $\rho^{\alpha}=0.94$ g/cm³ and $\rho^a=0.85$ g/cm³ have been found in literature [138]. These density values calculated with these literature data did not correspond to the total density found here. Therefore new values have been calculated according to the iPP polymorphic phase fraction values at 0.12 K/s assuming however the ratio of the literature values to be constant.

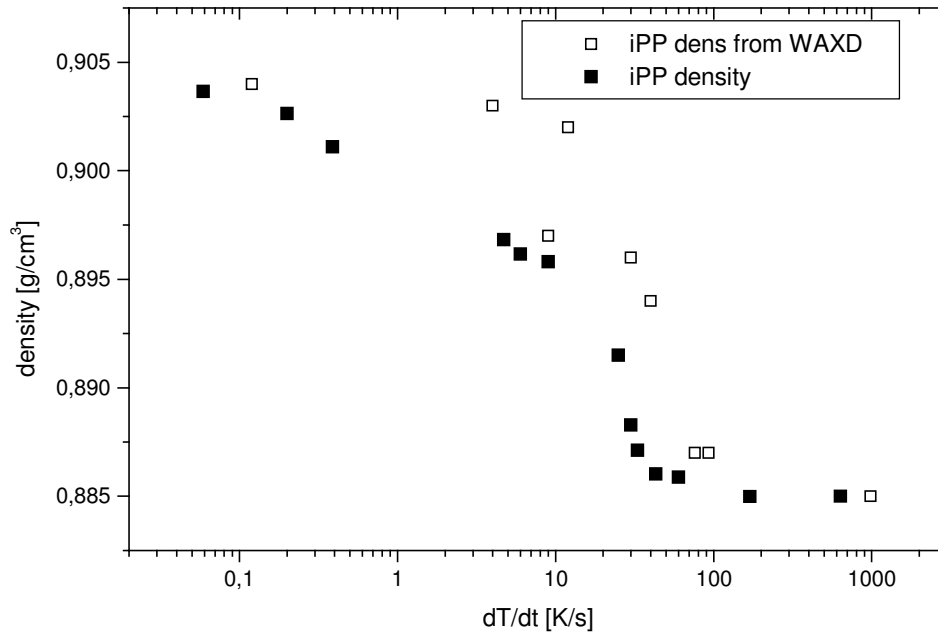


Fig. 6.7 Comparison of the measured density values and density values calculated from phase fractions derived from WAXD deconvolution vs. cooling rate

The same procedure was repeated for iPP cooled with 986 K/s to receive the mesomorphic value, which was not found in literature. The density values for the different phases finally used for the calculation were $\rho^{\alpha}=0.951 \text{ g/cm}^3$, $\rho^{\beta}=0.857 \text{ g/cm}^3$ and $\rho^m=0.936 \text{ g/cm}^3$. The results for iPP (fig. 6.7) confirm very nicely the actual density data and can be taken as prove that the phase fractions received from WAXD deconvolution are correct for iPP.

6.6.1.2 EOC and EPDM

WAXD

The pattern of EOC (fig. 6.8a)) shows a single reflection at $2\Theta = 19.3^\circ$. Although Androsch et al. /94/ reported the decrease of a second peak around $2\Theta = 21^\circ$ assigned to the 110 lattice plane for EOC with 38 wt% of co-octene with increasing cooling rate at 20 K/min, no such evidence was found in this case. The high cooling rates realized in this work do not influence the crystalline structure of EOC.

EPDM shows a single reflection around $2\Theta = 19.5^\circ$ (fig 6.8b)) with a broader maximum when compared to that of EOC. Similar pattern have been reported by Scholtens et al. /85/ with an ethylene content of 78 mol%.

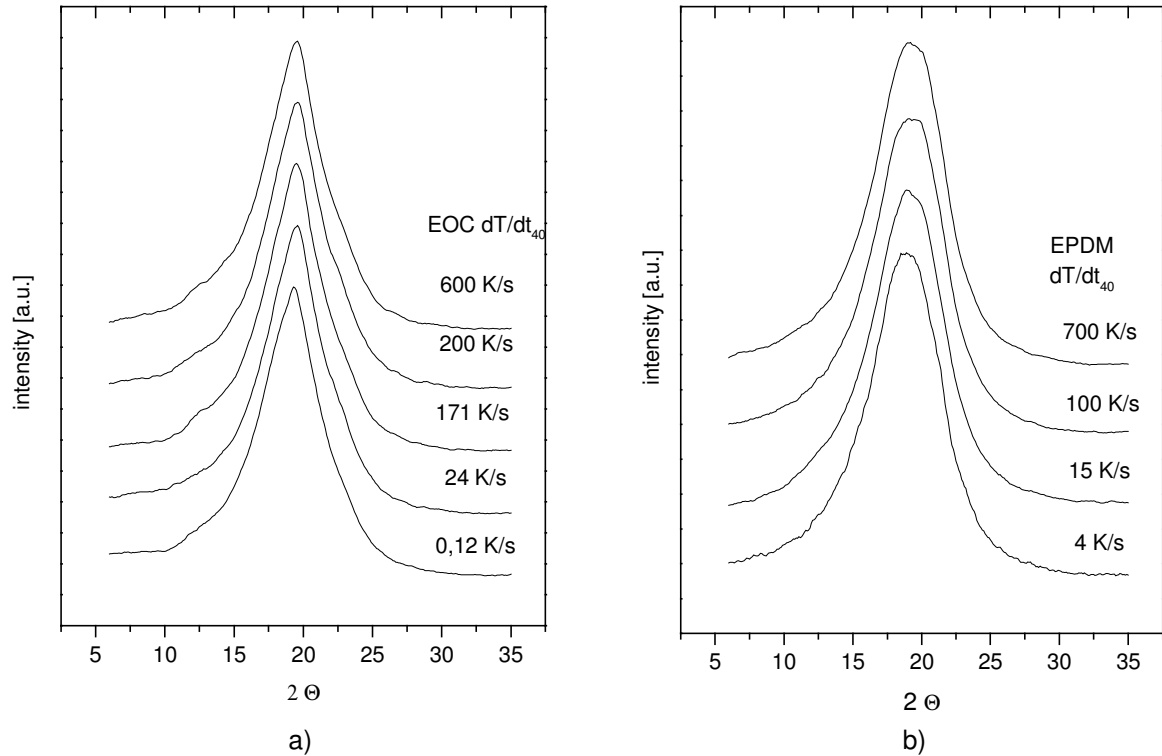


Fig. 6.8 WAXD cumulative pattern of a) EOC and b) EPDM quenched at indicated cooling rates.

Density

Cooling rates do not influence the density values of both copolymers EOC and EPDM (see fig.6.9). EOC shows a density of approximately 0.871 g/cm^3 and EPDM a slightly higher density of 0.877 g/cm^3 . The EOC density value lays slightly above the value measured by Bensason et al. /90/ for the same EOC type. The comonomer content is 42 wt% corresponding to 13 mol%. A crystallinity content of 10 % for this EOC type is stated elsewhere /90,91/. According to the classification of Bensason et al. /90/ this EOC type belongs to type I with so called fringed micelles exhibiting a low melting temperature and the absence of cooling rate effects. EPDM with an E/P ratio of 70/25 exhibits only a small amount of crystallinity (12 wt%, /133/). There was no birefringence detected by polarized microscopy.

Since both copolymers do not exhibit any dependence of cooling rates it can be assumed that changes of density values of the DV can be ascribed to changes in the iPP matrix material. The density values of crosslinked EOC and EPDM have not been obtained because it was impossible to apply the same crosslinking procedure as with respect to the DV in the extruder. Therefore the density values which depend to a great extent on the crosslinking parameters cannot be shown. However a higher density value can be expected due to the chemical network points formed by the crosslinking. Since no evidence of effect of cooling rate on density values of the pure copolymers could be found, also effects on the crosslinked rubber phase can be excluded.

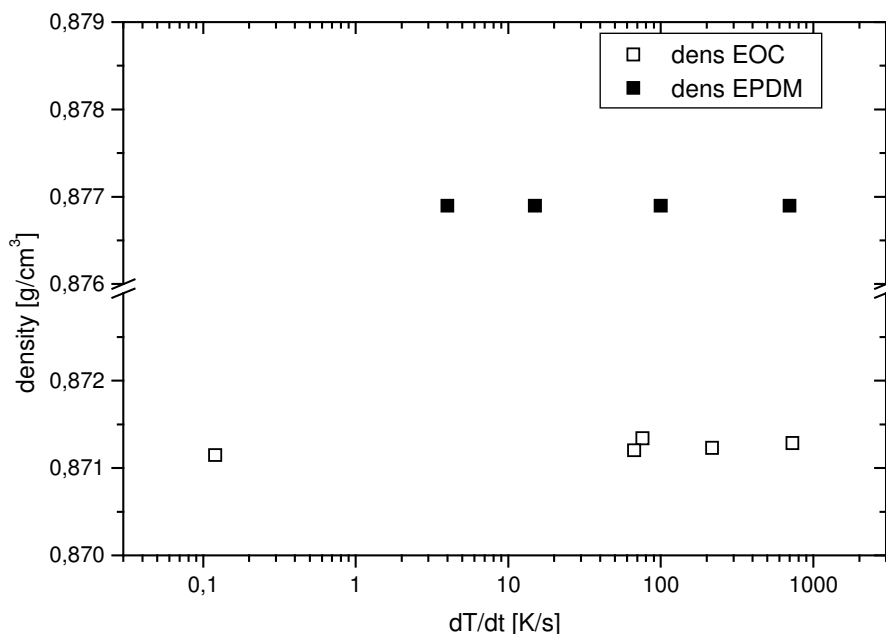


Fig. 6.9 Density (at 20 °C) vs. cooling rate plot of EOC and EPDM quenched with indicated cooling rates

6.6.2 The morphology of dynamic vulcanizates

After discussing the morphology changes with cooling rates of the pure components, the DV as well as their diluted versions shall be discussed in this chapter, comparing these results with the ones from the pure components. Since from the pure components only the iPP morphology changed with the cooling rate, it is expected that the change of morphology in DV takes place only in the matrix or as result from interactions taking place on the rubber - matrix interface.

6.6.2.1 Dynamic vulcanizates based on the system PP/EOC

WAXD – PP/EOC 30/70p and 70/30p

The WAXD pattern of the DV PP/EOC 30/70p and its iPP rich version PP/EOC 70/30p are shown in fig. 6.10a) and b), respectively. The pattern appears as an superposition of pattern from iPP and EOC. For PP/EOC 30/70p (see fig 6.10a)) the EOC reflection at $2\Theta = 19.5^\circ$ is clearly visible at higher cooling rates since it is the only contribution of organized crystalline structure. At smaller cooling rates superposition with iPP peaks partially hinders the relevance of EOC reflection, much broader due to the high level of disorder of their crystals. The peaks indicating the α -monoclinic crystalline form of iPP at $2\Theta = 14; 16.8; 18.5; \text{ and } 20.8^\circ$ are visible even until 192 K/s. Only at 860 K/s the (110) reflection at $2\Theta = 13.98^\circ$ disappears and the maximum at $2\Theta = 14.8^\circ$, indicating the mesomorphic phase, appears instead. It is worth noticing that in neat iPP (fig. 6.2) already above 70 K/s the reflections of the mesomorphic phase can be seen only.

When looking at the WAXD pattern of the iPP rich DV PP/EOC 70/30p the peaks indicating the α -monoclinic phase especially the one at $2\Theta = 16.8^\circ$ standing for the (040) lattice plane

can be recognized even at the sample quenched at 123 K/s, although the “smectic” peaks are already present at $2\Theta = 14.8^\circ$ and 21.1° . The EOC peak remains unchanged at $2\Theta = 19.5^\circ$ for all cooling rates.

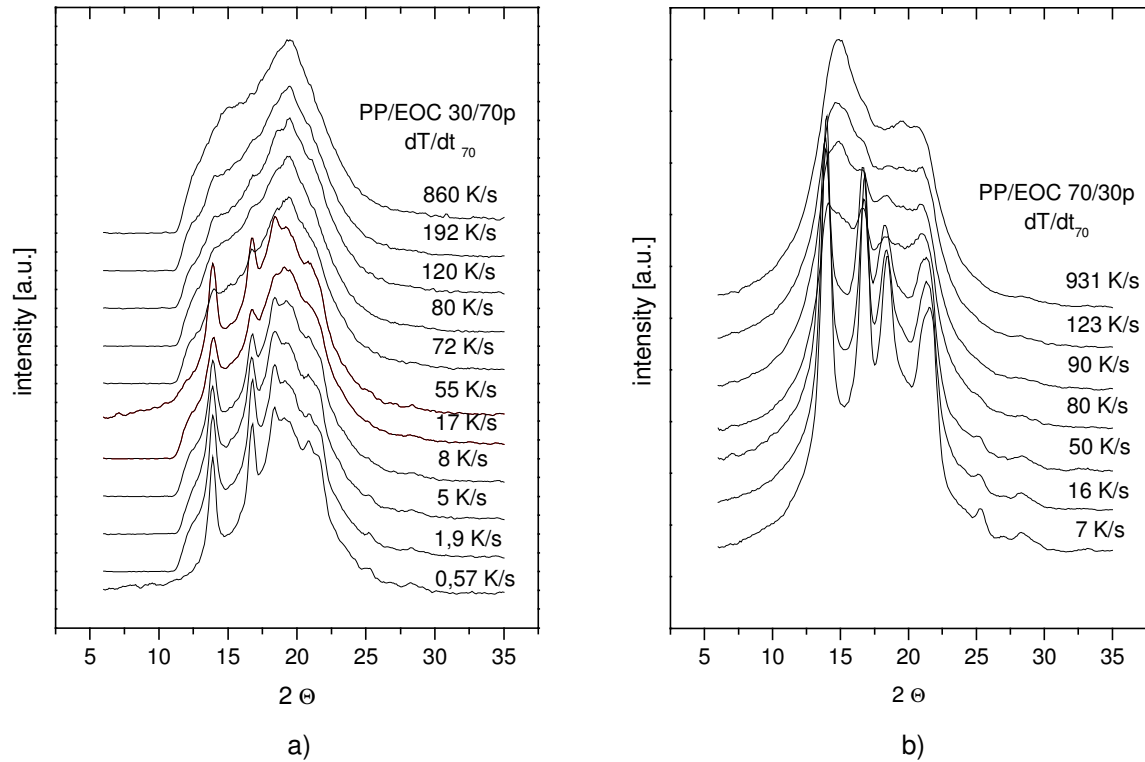


Fig. 6.10 WAXD cumulative pattern of a) the DV PP/EOC 30/70p and its iPP rich version b) PP/EOC 70/30p quenched at indicated cooling rates.

In order to determine the phase fractions at different cooling rates the same deconvolution technique as described above was applied here. However, additionally to the phases of the iPP (amorphous, α -monoclinic, mesomorphic), the maximum of the EOC had to be considered which, in case of PP/EOC 30/70p, area takes up to approx. 70 % of the total powder pattern area. The shape of the bulk EOC powder pattern was fitted best with a Pearson Voigt II function (see table 6.7). The difficulty of the superposition of the phases especially of the amorphous iPP and the EOC was eliminated by controlling the amount of phases; i.e. 30 % iPP and 70 % EOC, or in case of the PP/EOC 70/30 70 % and 30 %, respectively.

Table 6.7 Indication of the peak fitting function and the corresponding phase EOC.

number	phase type	angular position 2Θ [°]	type fit function
11	EOC	19.13	Pearson Voigt II

An example of a fitting of a PP/EOC 30/70p solidified at 8 K/s is shown in figure 6.11.

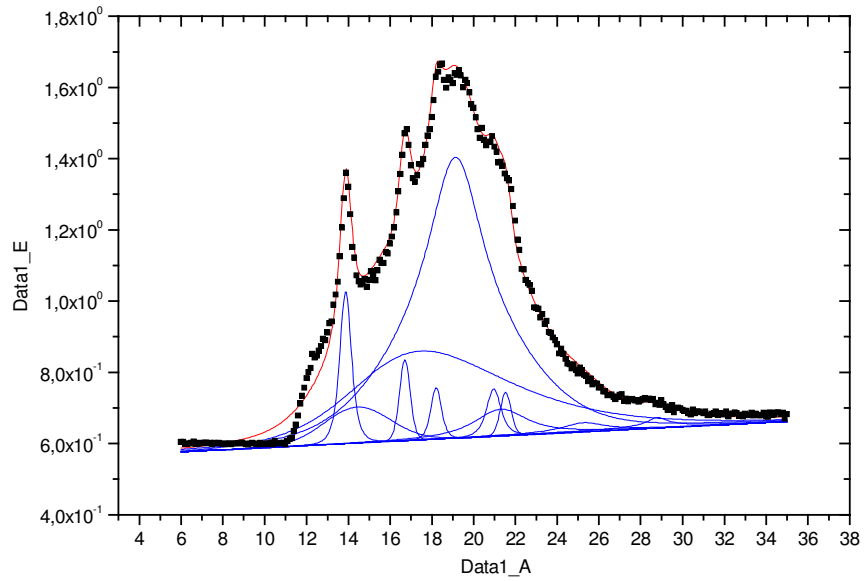


Fig. 6.11 Results from the peak fit of PP/EOC 30/70p solidified with 8 K/s

In order to compare the results to the bulk iPP the phase fractions of the iPP matrix of PP/EOC 30/70p were calculated from the fitting and are shown in figure 6.12. The amorphous phase remains almost constant around 60 %. The α -monoclinic phase decreases gradually from 45 to 25 % until 50 K/s, then exhibiting a drop from 20 to 10 % between 50 and 100 K/s and then decreasing gradually until 0 % at 1000 K/s. The mesomorphic phase is steadily increasing from 0 to 45 %.

It is important to note that the drop of the α -monoclinic phase content, transition zone, takes place later with respect to bulk iPP. This may be because of enhanced crystallization due to heterogeneous crystallization on the phase boundaries between iPP and EOC.

Another difference to the bulk iPP is the higher total amount of mesomorphic phase reached at high cooling rates: 45 % with respect to 35 % of the bulk iPP. This means that the mesomorphic phase replaced totally the α -monoclinic phase, unlike in iPP, where the amorphous phase grows in favor of the mesomorphic phase at high cooling rates.

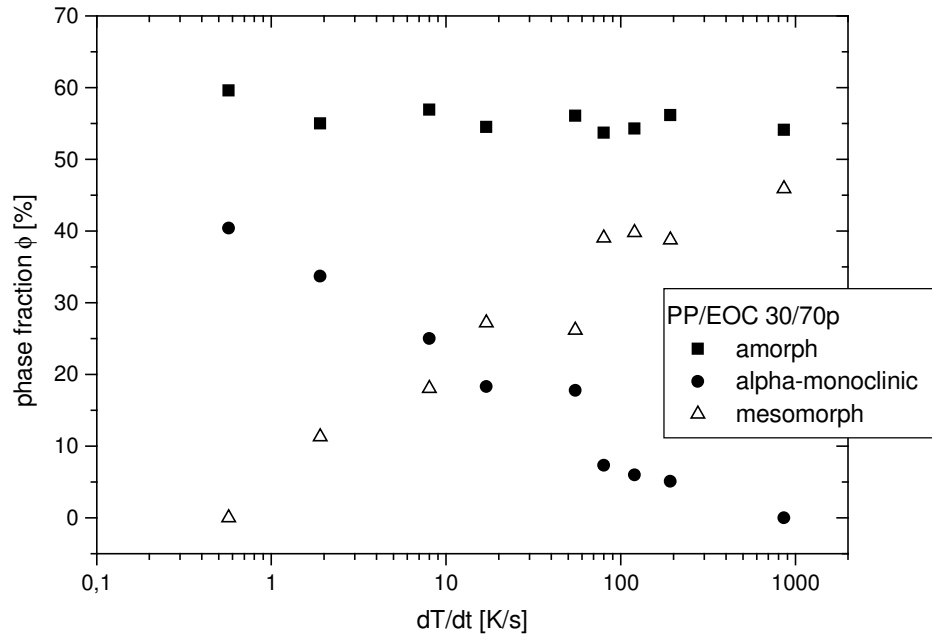


Fig. 6.12 Phase distribution vs. cooling rates of the amorphous, α -monoclinic, and mesomorphic phases in the iPP matrix of PP/EOC 30/70p.

The phase fraction development of the iPP matrix of the iPP rich PP/EOC 70/30p (see fig. 6.13) is similar to the one from PP/EOC 30/70p (see fig. 6.12). The phase transition is shifted to higher cooling rates with respect to bulk iPP. This confirms the role of boundary layers for enhanced crystallization, since both iPP poor and iPP rich versions of DV exhibit this behavior.

The value of the α -monoclinic phase at low cooling rates of the iPP rich version is found similar to the values for pure iPP and the PP/EOC 30/70p around 40 – 50 %. Also in this case the α -monoclinic phase is completely replaced by the mesomorphic phase at high cooling rates reaching values around 45 %. The amorphous phase content remains stable. This means also a certain preference towards the growth of the mesomorphic phase in the rubber environment.

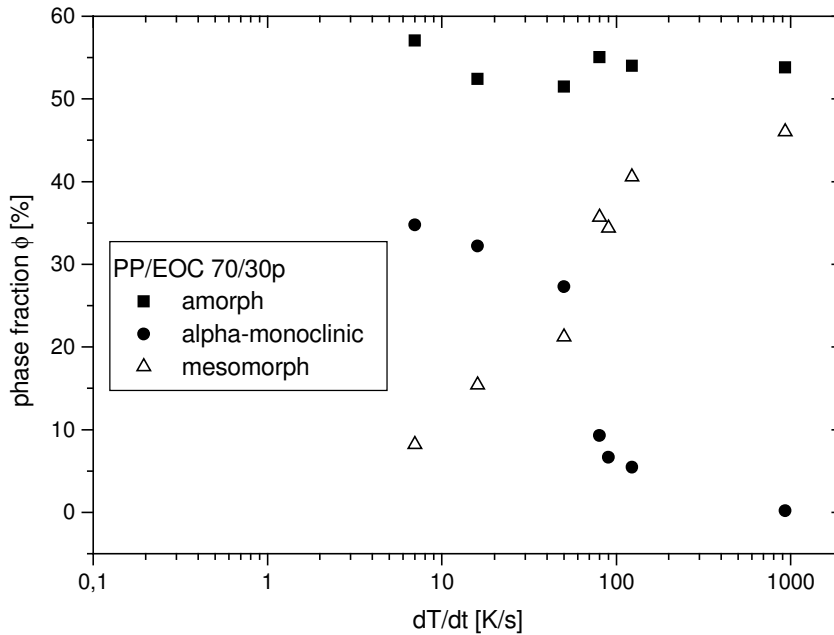


Fig. 6.13 Phase distribution vs. cooling rates of the amorphous, α -monoclinic and mesomorphic phases in the iPP-matrix of PP/EOC 70/30p

Density and optical microscopy under polarized light - PP/EOC 30/70p

The density vs. cooling rate curve of the DV resembles the form of the data for pure iPP (see fig. 6.14). Due to the low polypropylene content in the DV the values are lower as well as the overall density change. Below 2 K/s secondary crystallization occurs in the iPP and causes a higher density value around 0.883 g/cm^3 . At low cooling rates below 50 K/s the cooling rate affects the amount of the α -crystalline part of iPP. Increasing cooling rates from 2 to 60 K/s causes the density to decrease from 0.882 to 0.879 g/cm^3 . This density change however is larger than the one of pure iPP, when calculated according to blend content. This means that the contribution of secondary crystallization is more significant with respect to pure iPP. The reason for this behavior could be chemical, due to the peroxidic crosslinking, as well as physical interaction on the interphase between rubber and iPP. However since also the resin crosslinked DV (see fig. 6.25) shows this large secondary crystallization chemical influence due to chain scission caused by peroxidic curing can be excluded. Secondary crystallization in DV is probably more enhanced due to the larger specific interfacial area and enhanced nucleation. Another explanation could be that decreased chain mobility due to the rubber phase causes increased secondary crystallization because the primary crystallization is more incomplete. The model proposed for secondary crystallization by La Carruba /130/ (discussed in chapter 6.6.1.1) is also valid. It stated that the α - phase is forming in secondary crystallization from the amorphous phase, which exhibits also a higher fraction in DV when compared with bulk iPP.

The transition zone containing both, alpha-crystalline and mesomorphic structures, is indicated by a sharp density drop between 60 and 110 K/s from 0.879 to 0.877 g/cm^3 . Above these cooling rates the density values decrease only slightly from 0.877 to 0.876 g/cm^3 . From 0.1 to 1000 K/s a total density change of 0.007 g/cm^3 can be observed.

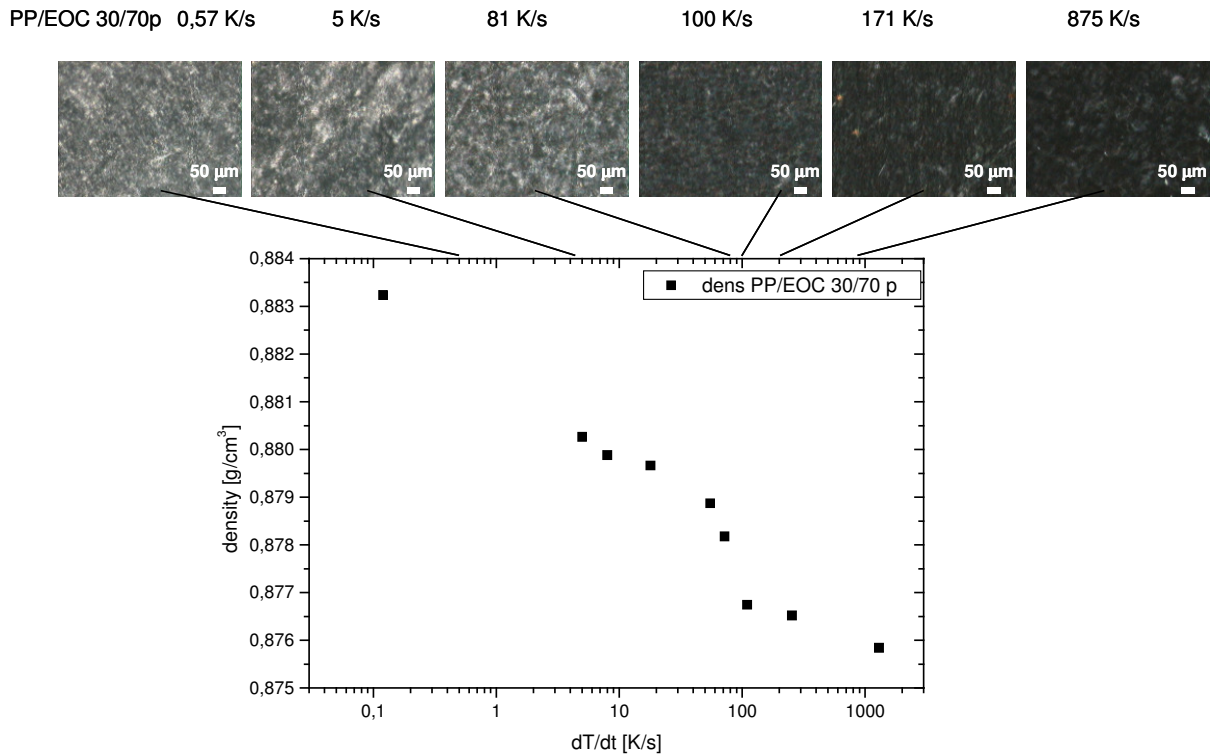


Fig. 6.14 Density (at 20°C) vs. cooling rate plot with corresponding micrographs (obtained under crossed polarizers) of PP/EOC 30/70 quenched with indicated cooling rates

The polarized micrographs show birefringence of the iPP matrix. However no spherulites can be observed. The growth of spherulitic structures in the iPP matrix is hindered by the rubber phase, with a content of 70 wt%. Similar micrographs have been reported for PP/EPDM DV with a rubber content of 30/70 wt% [139]. It was stated that the supermolecular structure of the PP matrix of DV with rubber content above 50 wt% cannot be compared to bulk polypropylene. Da Silva et al. [122] observed in polarized micrographs of PP/EOC and PP/EPDM blends with a rubber content of 60 wt% only “points” of crystallization. Therefore it can be concluded that the ability of polypropylene to form large supermolecular structures is hindered in case of the rubber phase being the major blend component. This fact is independent from the polypropylene forming the matrix, as in DV, or being dispersed in the rubber, as in the blend.

In order to check the reliability of the phase distribution data retrieved from WAXD deconvolution the total density was calculated according to equation 6-7 and the additional calculation taking into account the density from the EOC phase 0,871 g/cm³, which remained unchanged by cooling rate. The calculated and the experimental density values shown in figure 6.15 correspond very well. Even though the total values differ to some extent, the trend remains the same, confirming the WAXD data.

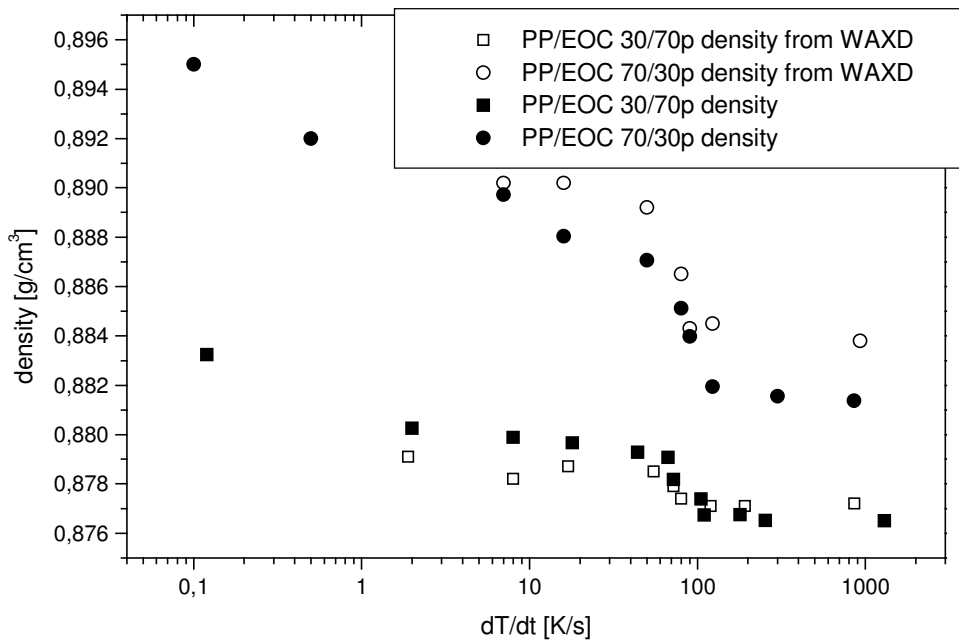


Fig. 6.15 Comparison of experimental density values and density values calculated from phase fractions derived from WAXD deconvolution vs. cooling rate.

Density of dynamic vulcanizates with different iPP/EOC ratios

In order to see the influence of the PP/rubber ratio of a DV on its crystallization behavior with respect to cooling rates the DV PP/EOC 30/70p has been compounded with different percentages of iPP in order to receive a blend row with different PP/EOC ratios. In these blends iPP still forms the matrix with embedded crosslinked rubber particles with a different particle - matrix ratio.

The density of these DV with varying thermoplastic content was measured and shown in figure 6.16. The values show an influence of cooling rates on density values due to their influence on the crystallization behavior of iPP or iPP matrix. The total density seems to depend roughly on the amount of iPP. It is however important to notice that also in the blend series the transition zone from α -crystalline to mesomorphic has been shifted to higher cooling rates already at the presence of only 30 wt% of rubber in the diluted DV.

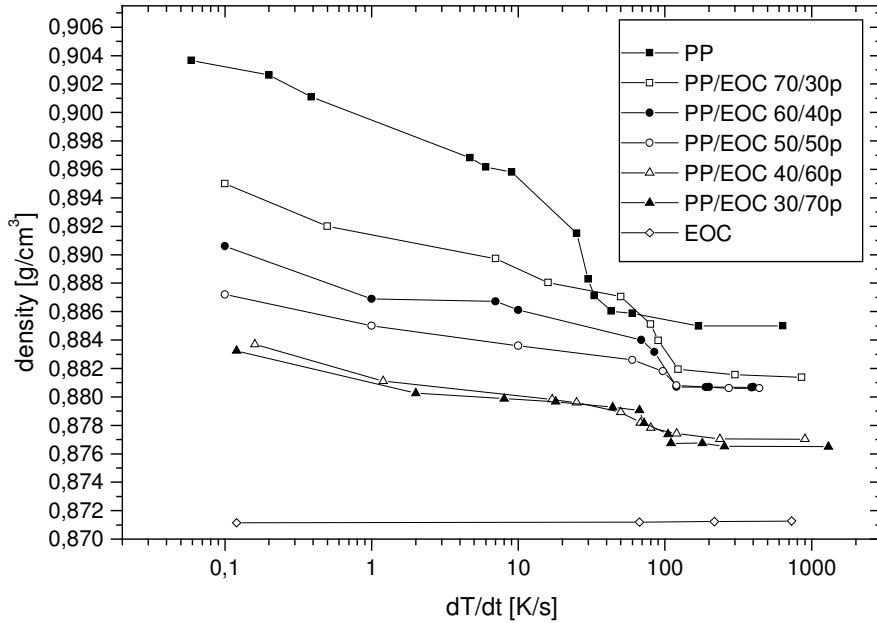


Fig. 6.16 Density vs. cooling rate plots of PP, EOC and its DV with compositions of 70/30, 60/40, 50/50, 40/60, 30/70 peroxidic crosslinked and quenched with indicated cooling rates.

In order to compare the density vs. cooling rates data from the different diluted DV the lowest density values at the highest cooling rates have been subtracted from the other values. The total changes of densities are listed in table 6.8. Then these values have been normalized to their iPP content in the DV and are also listed in table 6.8. The normalized total density change of the diluted DV differs from the values of the bulk iPP. That means that they do not correspond to the additive volume contribution law, i.e. the amount of density change does not depend directly on the amount of iPP. However the normalized density change of the transition zone is lower with respect to iPP.

Table 6.8 Total density change and density change of transition drop of iPP and DV.

material	$\Delta\rho_{\text{total}}$ [g/cm ³]	$\Delta\rho_{\text{total}}$ normalized to iPP [g/cm ³]	$\Delta\rho_{\text{transition}}$ [g/cm ³]	$\Delta\rho_{\text{transition}}$ normalized to iPP [g/cm ³]	dT/dt [K/s] range of transition
iPP	0.017		0.01		20-50
PP/EOC 70/30p	0.0136	0.0194	0.0051	0.0073	60-120
PP/EOC 60/40p	0.001	0.017	0.0032	0.0053	60-120
PP/EOC 50/50p	0.0066	0.0138	0.0019	0.0038	60-120
PP/EOC 40/60p	0.0067	0.0168	0.0016	0.004	60-120
PP/EOC 30/70p	0.0074	0.0247	0.0021	0.0070	60-120

Density vs. cooling rate data of PP and the DV has been fitted linear by dividing the curve into four sections:

- alpha – secondary crystalline: from 0.1 to 2 K/s
- alpha – crystalline: iPP 2 to 20 K/s, DV 2 to 50 K/s
- transition: iPP 20 to 50 K/s, DV 50 to 100 K/s
- mesomorphic: iPP 50 to 1000 K/s, DV 100 to 1000 K/s

For EOC the no regions have been distinguished. Therefore only one fit from 0 to 100 K/s was necessary.

The application of linear curve fitting using the equation

$$\rho_{\text{fit}} = I + S * dT/dt \quad \text{eq. 6-8}$$

in the indicated regions resulted in values which are in good agreement with the original curve (see fig. 6.17 and 6.18). In order to see if slope and intercept in the different regions depend directly on the blend compositions these values were calculated also according to weight ratio of PP and EOC.

$$I = \varphi_w^{\text{iPP}} * I^{\text{iPP}} + \varphi_w^{\text{EOC}} * I^{\text{EOC}} \quad \text{eq. 6-9}$$

$$S = \varphi_w^{\text{iPP}} * S^{\text{iPP}} + \varphi_w^{\text{EOC}} * S^{\text{EOC}} \quad \text{eq. 6-10}$$

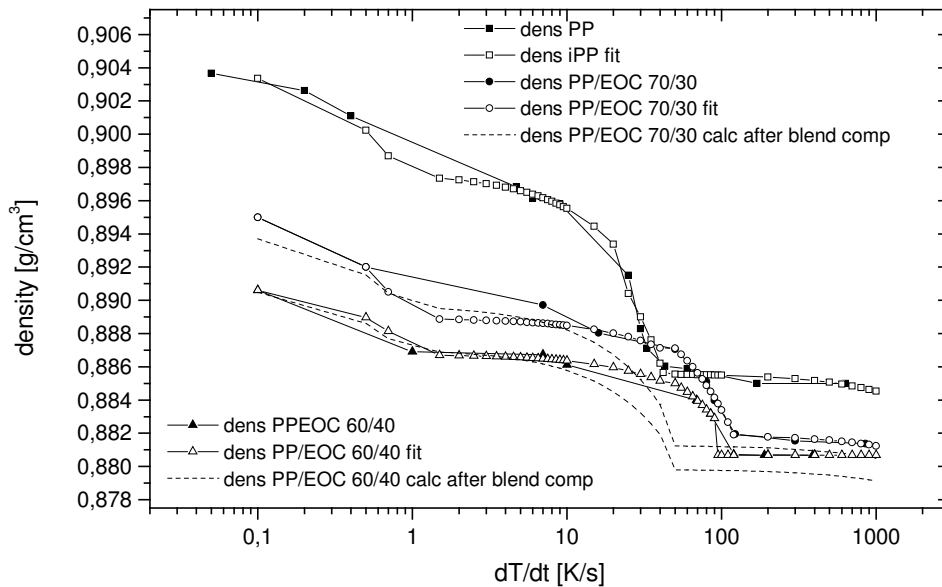


Fig. 6.17 Density vs. cooling rate plots of PP and its DV with compositions of 70/30, 60/40 peroxidic crosslinked and quenched with indicated cooling rates, fitted curve and curve calculated according to blend compositions

As seen in the figures 6.17 and 6.18 the calculated density values correspond to the real values only in the first part of the curve, at low cooling rates. At high cooling rates, in the zone with the iPP containing a mesomorphic structure, the calculated values appear all lower than the actual density values. This trend becomes more evident the higher the amount of rubber. The measured density values of the PP/EOC 30/70p are found above the calculated values (see fig. 6.18). This could be caused by a different amorphous/mesomorphic phase ratio in the iPP matrix of the quenched diluted DV. The higher the rubber content the higher the steric hindrances of the iPP molecular chains but also the higher the surface of phase boundary which have both an effect on crystallization.

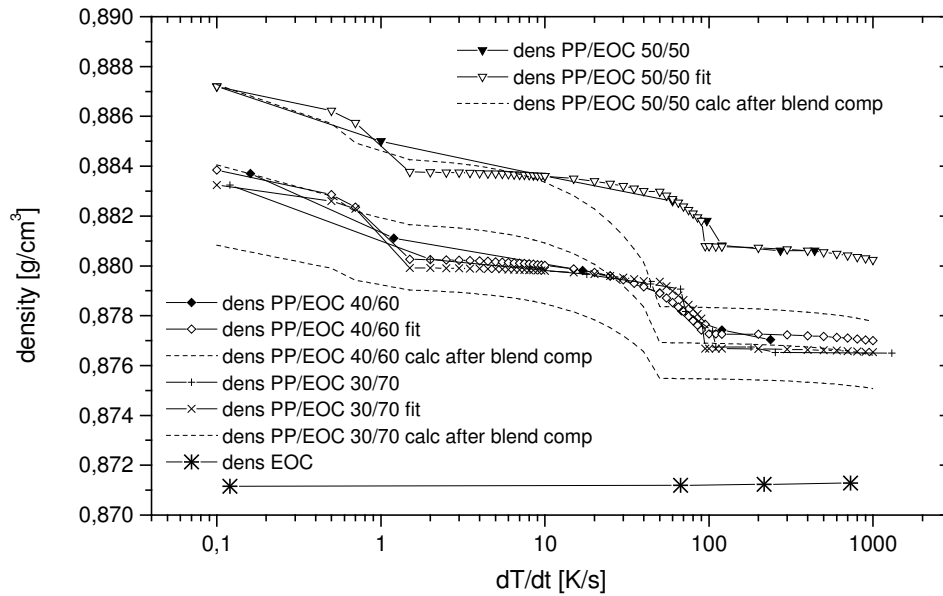


Fig. 6.18 Density vs. cooling rate plots of DV with compositions of 50/50, 40/60, 30/70 and EOC peroxidic crosslinked and quenched with indicated cooling rates, fit of density and density calculated according to blend compositions

6.6.2.2 PP/EPDM 30/70p and PP/EPDM 30/70r

WAXD – PP/EPDM 30/70p and PP/EPDM 30/70r

The cumulative patterns of PP/EPDM 30/70 peroxidic and resin crosslinked are shown in figure 6.19 a) and b)). As before the patterns appear as superposition of the EPDM deflection with its maximum around $2\Theta = 19^\circ$ and the pattern of iPP. The α -monoclinic reflections of the (110), (040) and (130) lattice planes are clearly visible until 98 K/s in case of the peroxidic crosslinked PP/EPDM 30/70p and even until 134 K/s in case of the PP/EPDM 30/70r crosslinked by phenolic resin. In the latter case the peaks also appear sharper and more pronounced than for the peroxidic crosslinked version. It must be stated that no evidence of γ -phase formation was found in our case although it was found by Foresta et al. /82/ as a result of nucleating agents in iPP. However the enhanced stability of the α -phase towards high cooling rates seems to exist in this case.

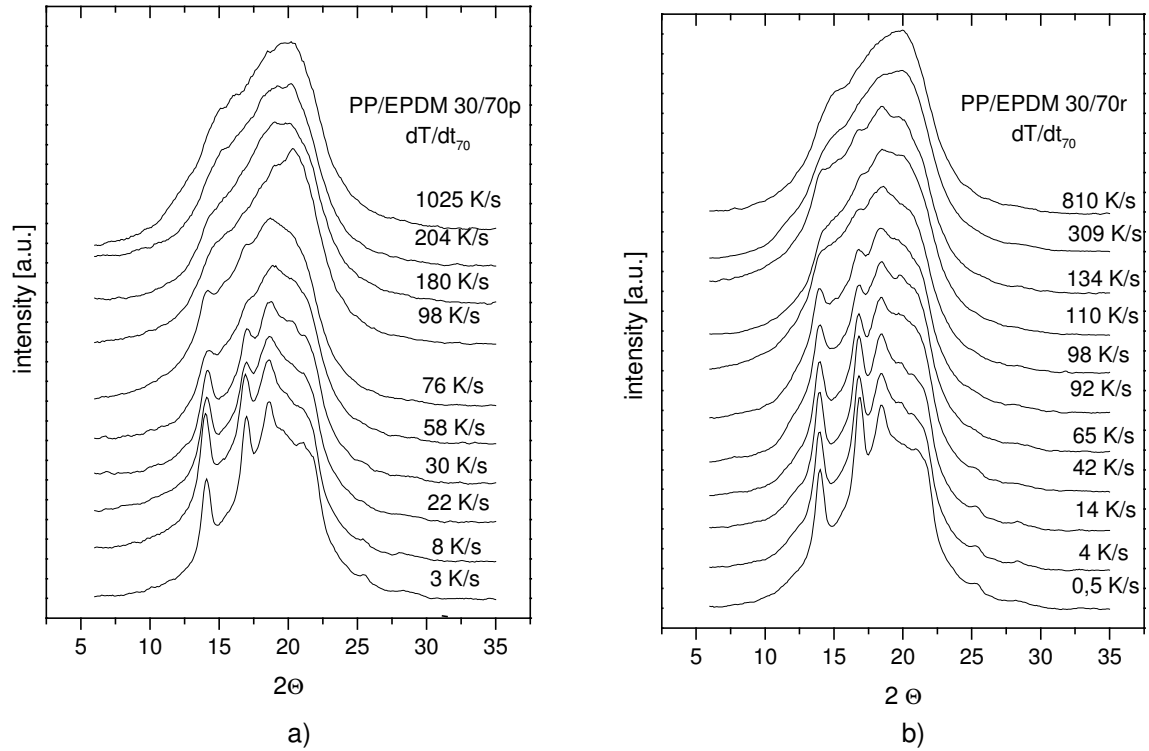


Fig. 6.19 WAXD cumulative pattern of a) the DV PP/EPDM 30/70p and b) PP/EPDM 70/30r quenched at indicated cooling rates

The same deconvolution technique as above was applied here, by replacing the EOC reflection with the EPDM reflection for the fitting. The whole pattern was considered an overlay of the amorphous, α -monoclinic and mesomorphic reflections of iPP (see table 6.1), which had to take up a total area of around 30 % and the reflection of EPDM, best fitted by a PearsonVII function taking up approx. 70 % of the area (see table 6.9).

Table 6.9 Indication of the peak fitting function and the corresponding phase EPDM.

Number	phase type	angular position 2Θ [°]	type fit function
11	EPDM	18.83	Pearson VII

An example of the fitting of a PP/EPDM 30/70p solidified at 30 K/s is shown in figure 6.20.

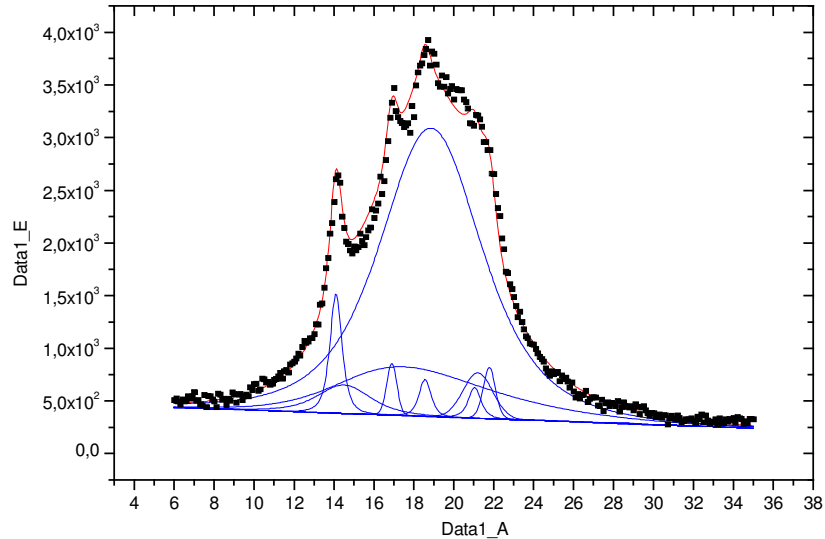


Fig. 6.20 Results from the peak fit of PP/EPDM 30/70p solidified with 30 K/s

The phase distribution of the iPP matrix of PP/EPDM 30/70p (see fig. 6.21) shows a similar dependence on the cooling rates as the PP/EOC 30/70p (see fig. 6.12). The α -monoclinic phase decreases first slowly from 40 to 30 % until 50 K/s. The transition zone is found between 50 and 110 K/s. The mesomorphic phase increases gradually until 110 K/s and remains stable at higher cooling rates around 55 %, at a higher level than the amorphous phase. The amorphous phase remains around 50 % with increasing cooling rates, which is 10 % lower than in iPP and in the iPP matrix of the PP/EOC 30/70p (fig. 6.12). This means that the rubber type has an influence on the amount of amorphous phase of the iPP matrix of the DV. D’Orazio et al. /107/ found a preferential dissolution of smaller more defect molecules of crystallizable component iPP into the domains of the uncrystallized polymer EPDM. According to them, at higher EPDM contents (above 20 %) the iPP matrix would consist therefore of more perfect crystals. This could be an explanation of the lower amorphous content in the iPP matrix of the PP/EPDM 30/70p assuming that these dissolution processes takes place also into the crosslinked rubber phase.

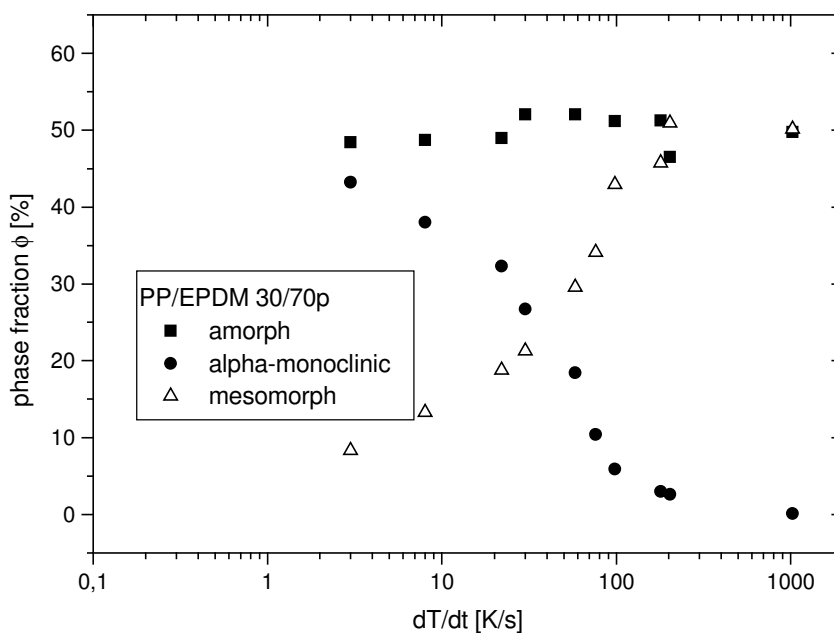


Fig. 6.21 Phase distribution vs. cooling rates of the amorphous, α -monoclinic and mesomorphic phases in the iPP-matrix of PP/EPDM 30/70p

In case of the PP/EPDM 30/70 crosslinked by phenolic resin the amorphous zone stays around 55 %, being at slow cooling rates slightly lower than the α -monoclinic phase (see fig. 6.22). The α -monoclinic phase fraction remains around 55 % and drops between 100 and 300 K/s reaching 0 at 100 K/s. The mesomorphic phase increases steady until 110 K/s and increases afterwards slowly replacing the α -monoclinic phase and, to a certain extend, also the amorphous phase reaching up to approx. 60 % of phase fraction.

The shift of transition zone to higher cooling rates seems to be more pronounced than the one in DV crosslinked by phenolic resin. This could be explained by the existence of SnCl_2 as initiator for the crosslinking reaction, which is still present as powder in the final DV and act presumably as nucleating agent, enhancing the crystallization. This explains also the high level of α -monoclinic phase with respect to amorphous phase at low cooling rates. The crosslinking reaction by phenolic resin does not cause chain scission in the iPP matrix. This disapproves the idea mentioned above of low molecular weight fractions formed during peroxidic crosslinking by being responsible for the shift of the transition zone.

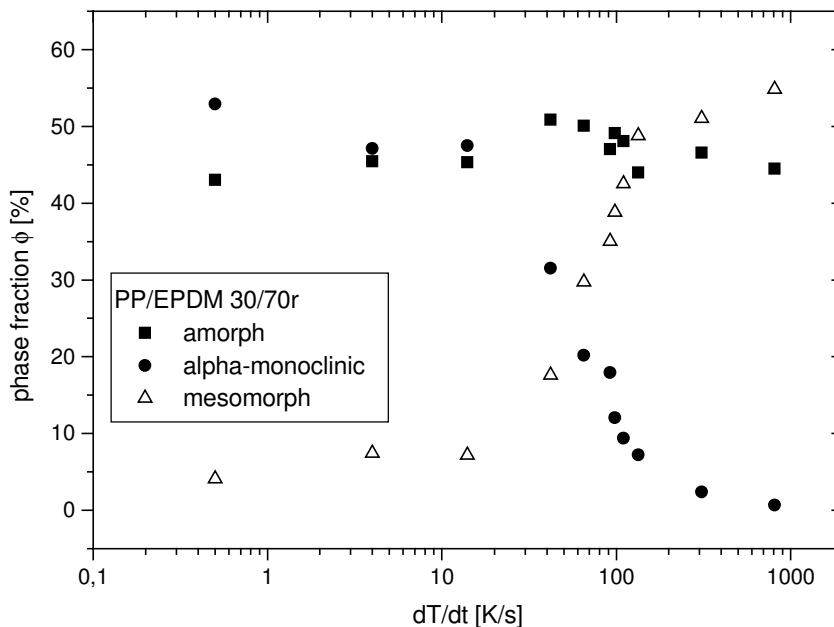


Fig. 6.22 Phase distribution vs. cooling rates of the amorphous, α -monoclinic and mesomorphic phases in the iPP - matrix of PP/EPDM 30/70r

Both PP/EPDM 30/70 p and r exhibit low values of α -monoclinic phase fraction around 30 % at low cooling rates, confirming the assumption of growth suppression due to the hindering of the rubber phase. D'Orazio et al. /103/ reported also a decrease of the degree of crystallinity and crystal size for PP/EPM 30/70 peroxidic crosslinked with respect to pure iPP for a given T_c . The evaluation of the half width of reflections of the α -monoclinic phase in this work gave no distinct results, due to the different fitting functions with respect to literature. In both PP/EPDM 30/70p and r at high cooling rates, above 100 K/s, the mesomorphic phase formation seems to be favored replacing the amorphous phase. Since this is not the case for the PP/EOC types, only the EPDM can be responsible for this behavior.

Density and optical microscopy under polarized light - PP/EPDM 30/70p and PP/EPDM 30/70r

The polarized light micrographs show birefringence at low cooling rates. However no spherulithic superstructures have been observed. D'Orazio et al. /103/ reported microspherulithic superstructures in the iPP matrix of PP/EPM 30/70 peroxidic crosslinked crystallized at 124 °C., which was not the case here. Figure 6.23 shows the birefringence of the iPP matrix forming a white contrast to the black EPDM phase in a slowly solidified PP/EPDM 30/70r. The island matrix structure of the DV is visible with rubber particles of 2-5 μm .

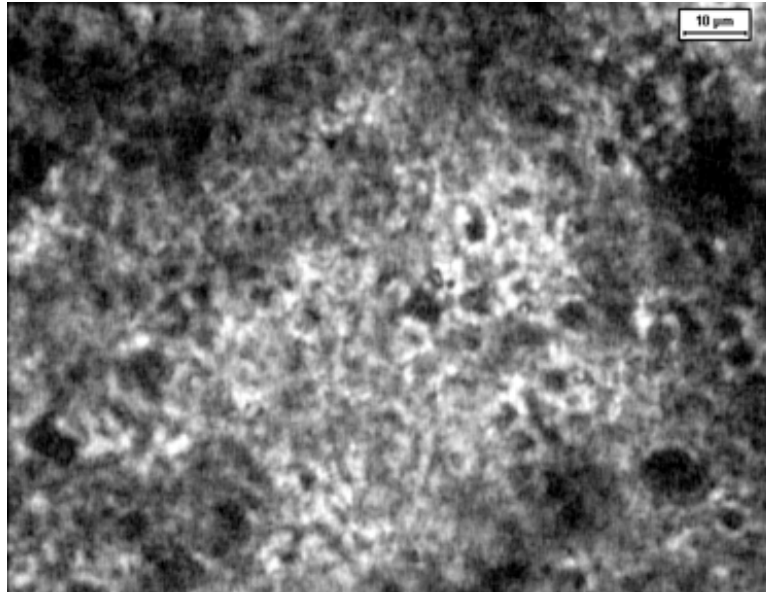


Fig. 6.23 Optical micrograph of PP/EPDM 30/70r solidified at 0,5 K/s, polarized light.

The form of the density vs. cooling rate curve of PP/EPDM 30/70p in fig. 6.24 appears similar to the DV based on EOC. Below 2 K/s there is a zone of higher density values around 0.889 g/cm^3 due to secondary crystallization of the iPP phase. With increasing cooling rate the density decreases to 0.886 g/cm^3 . The transition takes place between 60 and 110K/s with a density drop from 0.886 to 0.884 g/cm^3 . Above 110 K/s the density value decreases only slightly to 0.883 g/cm^3 .

The density values of PP/EPDM 30/70r crosslinked by phenolic resin (see fig. 6.25) depend on the cooling rate in a similar manner as the other DV described above. Nevertheless, the overall level of density of the resin crosslinked DV is higher than the level of the peroxide crosslinked DV. This could simply be caused by the presence of the SnCl_2 acting as filler with a higher density (2.7 g/cm^3). Another explanation could be, that the macroscopically measured density of crosslinked elastomers is direct proportional to chemical network density according to the rubber network theory /140/; except for very high levels of crosslinking density. This would mean that the EPDM phase in the DV crosslinked by resin shows a higher crosslinking density than the peroxide crosslinked DV. Finally also the distance between the dispersed rubber particles, i.e. the bridge width of the iPP, influences the macroscopic density /141/.

However, the zone at which secondary crystallization takes place in PP/EPDM 30/70r (see fig. 6.25), indicated by a higher level of density values around 0.8895 K/s, seems to be extended to 10 K/s when compared to PP/EPDM 30/70p (see fig. 6.24). The cooling rate area

with a major α -crystalline phase content in the iPP matrix stretches to 60 K/s. The following transition zone is much larger compared to the peroxidic crosslinked DV and extends to approx. 150 K/s. The reason for the presence of the α -crystalline form at these high cooling rates can be caused by nucleation by the activator SnCl_2 used for the crosslinking with phenolic resin. However there was not SnCl_2 nucleating activity reported in literature.

Above this cooling rate the density values remain stable around 0.885 g/cm^3 . These values, which can be connected to the mesomorphic phase of the iPP, are higher than the density values of the peroxidic crosslinked DV PP/EPDM 30/70p. The difference between both curves (peroxidic to resin) varies from 0.0013 to 0.002 g/cm^3 from low to high cooling rates. The upward shift can be explained again by the presence of the activator SnCl_2 .

The polarized micrographs in figure 6.25 appear lighter with respect to the peroxidic crosslinked DV. This can be an indication of a higher degree of crystallinity. Even at high cooling rates above 150 K/s the existence of light structures can be seen. These structures, slightly visibly also for PP/EPDM 30/70p might be ascribed to the ability of EPDM to form supermolecular crystalline structures even at higher cooling rates.

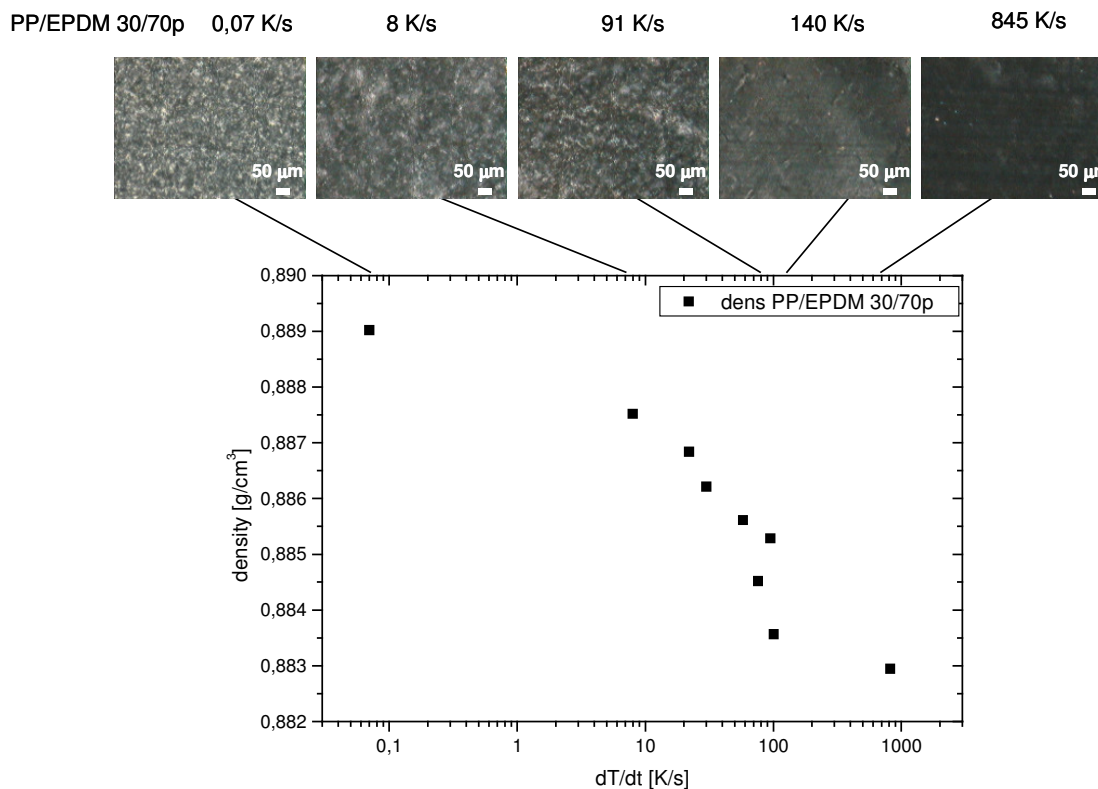


Fig. 6.24 Density (at 20°C) vs. cooling rate plot with corresponding micrographs (obtained under crossed polarizers) of PP/EPDM 30/70p quenched with indicated cooling rates

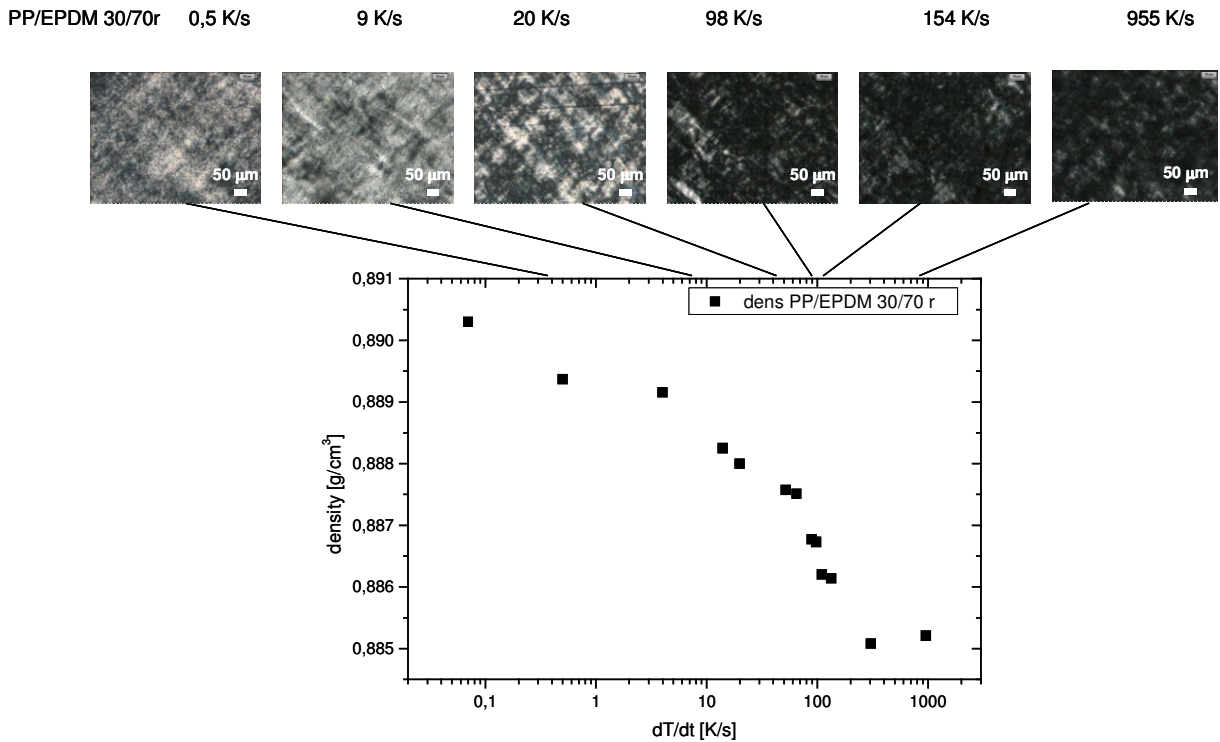


Fig. 6.25 Density (at 20°C) vs. cooling rate plot with corresponding micrographs (obtained under crossed polarizers) of PP/EPDM 30/70r quenched with indicated cooling rates

As for PP/EOC 30/70p also here the density values have been calculated from phase distribution data retrieved from WAXD deconvolution according to equation 6-7. A comparison of both datasets is shown in figure 6.26. The measured values of density lay above the calculated density values but the shape of the curve resembles the measured density dependence of cooling rates.

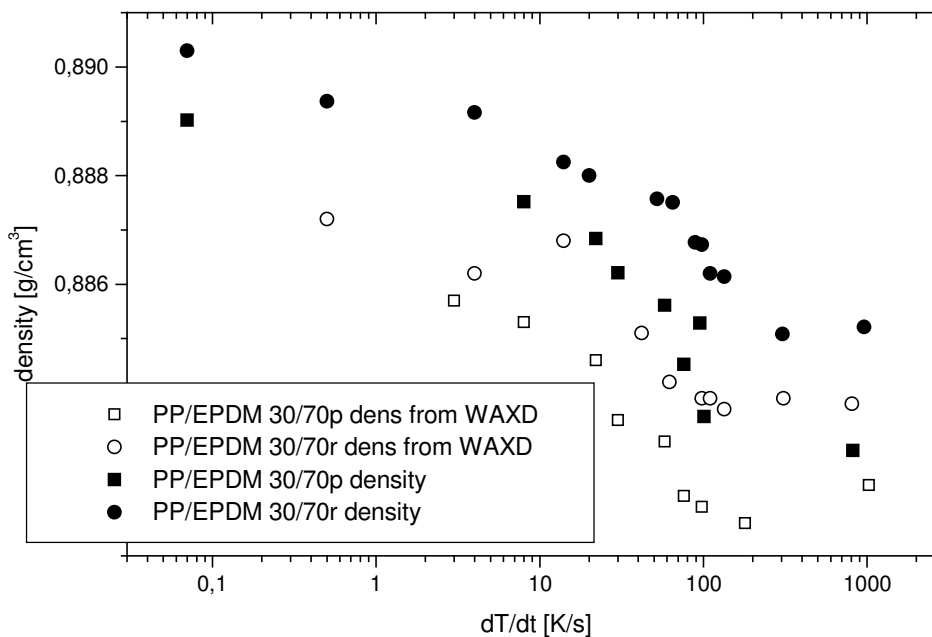


Fig. 6.26 Comparison of the measured density values and density values calculated from phase contents derived from WAXD deconvolution vs. cooling rate

Comparison of density dependence on cooling rates between iPP and dynamic vulcanizates

The total changes of densities between low and high cooling rates are listed in table 6.10. Then these values have been normalized to their iPP content in the DV, also listed in table 6.10. The normalized values of the total change of density of the peroxidic crosslinked DV appear a little bit higher than the total density change of iPP. The normalized density value of the DV cured with phenolic resin is equal to the value of iPP. The density drop taking place during the transition zone is slightly below the normalized value of iPP.

The most striking difference however is found in the cooling rates ranges. The transition zone of all DV starts at 60 K/s, while the transition from α -crystalline to mesomorphic phase in iPP takes place between 20 and 50 K/s. In other words, the iPP matrix of DV solidified at a cooling rate of 50 K/s appears still α -crystalline while the bulk iPP solidified at the same cooling rate has already formed the mesomorphic phase. This implies the presence of a more stable α -crystalline form in DV. Even though the formation of perfect crystals is hindered by the rubber phase more stable crystals are formed due to enhanced heterogeneous crystallization on the phase boundaries between rubber and iPP. The same effect has been observed by Colletti et al. /142/ for PP/PA blends. The paper described a shift of α -crystalline to mesomorphic transition zone of iPP to higher cooling rates for both PP rich and poor blends with respect to their bulk iPP. This was explained by faster crystallization due to enhanced crystallization at the interface. This fact was underlined by transcristalline morphology found at the interface by means of WAXD.

Table 6.10 Total density change and density change of transition drop of iPP and DV.

	$\Delta\rho_{\text{total}}$ [g/cm ³]	$\Delta\rho_{\text{total}}$ normalized to iPP [g/cm ³]	$\Delta\rho_{\text{transition}}$ [g/cm ³]	$\Delta\rho_{\text{transition}}$ normalized to iPP [g/cm ³]	dT/dt [K/s] range of transition
iPP	0.017		0.01		20-50
PP/EOC 30/70p	0.008	0.0267	0.0021	0.0070	60-120
PP/EPDM 30/70p	0.0059	0.0197	0.0021	0.0070	60-120
PP/EPDM 30/70r	0.0051	0.0170	0.0024	0.0080	60-150

In case of the peroxidic crosslinked DV one could also ascribe this effect to chain scission taking place in iPP during the dynamic vulcanization. In fact lowering the molecular weight and increasing the molecular weight distribution could also shift the transition of iPP to higher cooling rates /78/. However this effect has been observed also for blends and for the DV crosslinked by phenolic resin, which reacts only with the double bonds provided by the diene terpolymer. Therefore an influence of chain scission or curing effects on the shift of the transition zone to higher cooling rates can be excluded. The DV crosslinked by phenolic resin shows an even larger transition zone. This difference can be caused by the SnCl₂ used as activator for crosslinking, which act as nuclei during crystallization. This explains the existence of α -crystalline form at high cooling rates.

Atomic force microscopy PP/EPDM 30/70p

Atomic force microscopy (AFM) has been used to verify the island-matrix phase morphology been formed by dynamic vulcanization and to reveal eventually existing superstructures in the iPP matrix of the DV. In figure 6.27a) the AFM image of a slowly cooled PP/EPDM 30/70p is shown. The black areas represent the rubber phase, being softer than the iPP matrix (grey to white). The size of the rubber particles seems to be divided into larger and smaller particles.

An island-matrix morphology can be seen. The reason for the amount of EPDM phase appearing to be less than 70% is the melting of the sample against the surface. Already elsewhere /143/ it was shown by AFM for PP/EPM blends, that the less viscous phase tends to go to the surface. The iPP matrix appears much brighter than the rubber phase and can be distinguished very well, due to the strong contrast. Cross - hatched lamellae are shown surrounding the rubber particles, with a thickness of 6-10nm and a length until 500nm.

The AFM image of the quenched sample shows a lower phase contrast (see fig. 6.27b)). Again the island matrix morphology can be seen, with rubber particles of larger and smaller size. The iPP phase appears grey, with very few lamellar structures of smaller dimensions, which could however be assigned to the α -crystalline phase, which can still be present also when quenching in water. The dimensions of these fine filament like structures in figure 6.27b) are approximately one half of the cross - hatched structures in figure 6.27a) lateral and longitudinal. Androsch et al. /75/ observed immediately after quenching of iPP no ordered structures and after annealing small globular structures of crystals of the size of 20-30 nm with a tendency of lateral aggregation. Those structures have not been observed here. The very bright structures surrounding some of the rubber particles are artifacts on the surface.

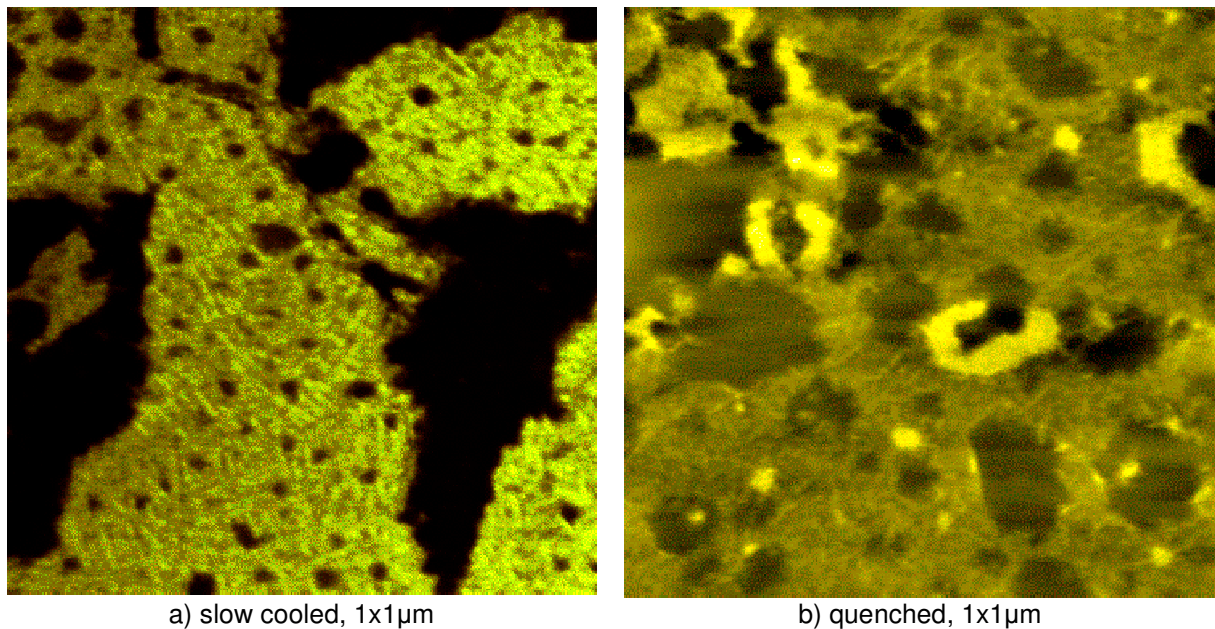


Fig. 6.27 AFM phase images of PP/EPDM 30/70p, a) solidified on air and b) quenched in water

6.6.3 The thermal behavior of the pure components

6.6.3.1 iPP

DSC

The DSC 1st heating scans of pure iPP are shown below in figure 6.28. Caldas et al. /66/ reported the existence of a small endotherm between 30 and 75 °C corresponding to 4.4 J/g ascribed to the melting of small crystals formed during annealing at room temperature. Grebowicz /144/ instead reported this zone to small crystals also formed for quenched samples without annealing. T_{onset} of this endotherm in the thermographs reported in this work

was impossible to determine graphically in an exact way because of the overlapping of the glass transition. Therefore the area of this endotherm, which belongs to the melting of the mesomorphic phase could not be determined. However the local maximum of this endotherm lays around 45 °C and does not show a significant dependence on cooling rate. Only at very low cooling rates of 0.3 K/s no such endotherm can be found.

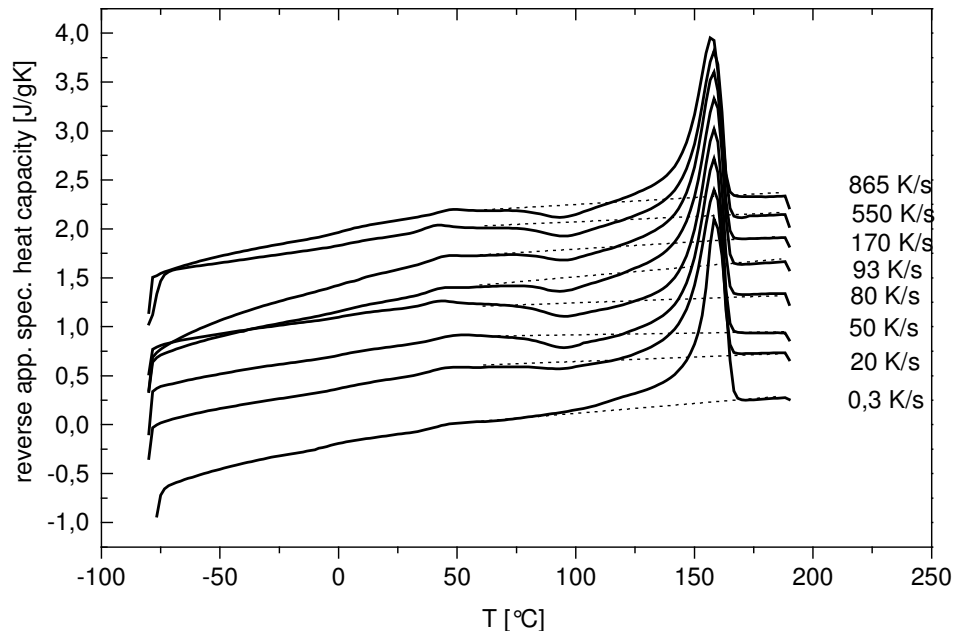


Fig. 6.28 DSC first heating run of iPP solidified at indicated cooling rates

As stated in other studies /66,75/ the metastable phase of iPP quenched at high cooling rates undergoes a recrystallization leading to an exothermic local maximum. T_{onset} of this area lays around 75 °C and T_{max} around 95 °C (exact temperatures in table 6.11). The integrated area of this maximum is zero at low cooling rates, rises between 10 and 70 K/s up to approx. 8 J/g and remains at this value at higher cooling rates (see fig. 6.28). This end value corresponds to the value 8.8 J/g found in literature by Caldas et al. /66/ for quenched iPP.

The large endotherm between approx. 127 and 175 °C belongs to the melting of the developed crystalline morphology. T_{max} of this second endotherm or T_{m} is 158°C. This value is not changed with increasing cooling rates and remains the same also during the second heating run. The cooling and second heating runs are shown in the appendix. T_{c} and T_{m} are shown in table 6.11. T_{c} lays around 111°C and does not change significantly with increasing cooling rate. As expected the second heating run does not show an evidence of melting and recrystallization zones of the mesomorphic phase as in the first heating run since all samples have been slowly cooled with 10 K/min during the previous cooling run. T_{m} of the second heating run is 158 °C, the same as in the first heating run.

In order to determine the degree of crystallinity X_{c} of the quenched sample influenced by the cooling rates the calculation has been done according to eq. 6-1 of the reorganization and melting enthalpy between 75 and 175 °C. The degree of crystallinity of iPP is shown in figure 6.37 and decreases from 45 to 35 % in the transition zone between 30 and 50 K/s. The latter value is the same as reported by Androsch et al. /75/ The first one is different since the exact rate of solidification was not reported.

Table 6.11 The onset temperature T_{onset} of the 1st exotherm and the 2nd endotherm and the maximum temperature T_{max} of the 1st endotherm, the exotherm and the 2nd endotherm. The melting temperature T_m of the 1st heating run. The crystallization temperature T_c of the cooling and the melting temperature T_m of the 2nd heating run.

dT/dt [K/s] iPP	T_{max} 1st Endo	T_{onset} Exo	T_{max} Exo	T_{onset} 2nd Endo	T_m (T_{max} 2nd Endo)	T_c	T_m
		1st heat run [°C]		cool run [°C]		2nd heat run [°C]	
0.3	-	-	-	-	158	111	158
20	47	75	95	129	158	111	158
50	50	76	95	125	158	111	158
80	43	76	95	130	158	112	158
93	46	76	95	126	158	113	158
170	45	75	95	126	158	113	158
550	42	75	95	128	158	111	158
865	46	76	94	128	157	111	157

DMTA

The storage modulus E' and the loss modulus E'' of iPP are shown in fig. 6.29 a). The storage moduli below glass transition lay at around 4000 MPa for slowly cooled samples and only 2200 MPa for the fast cooled samples. After the β -transition (glass transition) at around 15 °C the storage modulus shows a drop appearing to be more severe for the fast cooled samples. At 25 °C the storage modulus of the iPP cooled slowly with 0.3 K/s is 1400 MPa. The value of the fast cooled iPP is only 720 MPa, approx. one half of the slowly cooled value. The drop of storage modulus of the fast cooled samples is steeper, but the slope changes again around 50 °C. This is presumably due to reorganisation processes, approx. at the same point where the 1st endothermal maximum was found in the DSC scans, which was assigned to the melting of the mesomorphic phase. However, around 110 °C where this process seems to be finished different values are reached than in the slowly cooled samples, 80 MPa compared to 280 MPa. This means that annealing of the mesophase does not result in the same structure as the original α -monoclinic phase, which was already stated by Androsch et al. /75/.

The loss modulus shows a maximum around 15 °C indicating the β -transition, i.e. the glass-transition where the amorphous segments start to move. This transition shows much better in the course of the tan delta values (fig.6.29b)). It is very clear that the β -transition temperature (T_g) depends strongly on cooling rates. The iPP cooled with 0.3 K/s shows a β -transition at 14 °C whereas the sample cooled with 1160 K/s shows a β -transition at 26 °C. The dependence on cooling rates is shown in figure 6.29b). T_g grows continuously until it reaches a stable value at 26 °C above 100 K/s. The shift to higher temperatures could be explained by a hindered movement of the amorphous phase in the presence of the immersed mesomorphic phase, i.e. small crystalline forms with less order. Whereas slowly crystallized iPP contains distinct crystalline phases well separated from the amorphous regions. Alberola et al. /69/ have found the inverse effect for quenched and annealed PP explaining the downwards shifting of T_g from 17 to 10 °C after annealing by what he called decrease of physical crosslinking degree of the amorphous phase, i.e. an amorphous phase in the quenched state strongly crosslinked by microcrystallites exhibiting small size and a very low degree of perfection.

In the region between 40 and 150 °C at low cooling rates the α -transition can be noted with a broad maximum around 75 °C indicating reorganization processes in the crystalline phase due to flipflop mechanism and screw motion of methylene group in the crystal lattice (see fig. 6.29b)). Rault /145/ called this α_c transition and stated that it takes place between 50 and 170

°C depending on the crystalline thickness. At higher cooling rates above 20 K/s instead a second and more pronounced peak at 57 °C can be seen, ranging from 40 to 80 °C, which can be assigned to the movement and reorganisation of the mesomorphic phase, further referred to as “meso”-transition. The start of this reorganisation process determined by DMTA, i.e. the local minimum after the β -transition around 43 °C, lays near the maximum of the 1st endothermal area in DSC, which was assigned to the melting of the mesophase. The reason why the DSC maximum of reorganization is found later around 75 °C is due to the higher frequency applied in DMTA. At cooling rates above 20 K/s the α -transition takes place after the “meso” transition, shown in a broad shoulder in the tan delta curve between 100 and 150 °C.

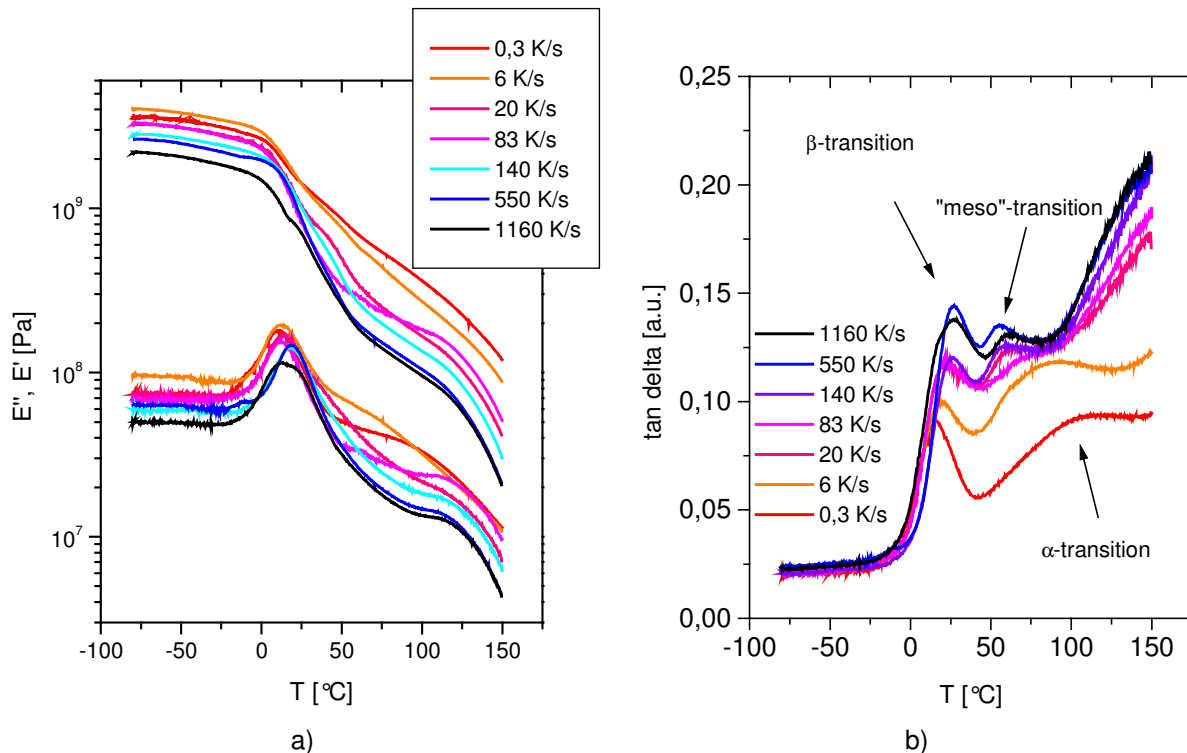


Fig. 6.29 Storage modulus E' , loss modulus E'' (a) and tan delta (b) of iPP solidified at indicated cooling rates.

The difference of the “meso”-transition and the α -transition can be noted also in the values of activation energy E_a shown in figure 6.30, which was determined from the tan delta values by means of equation 6-2 (see chapter 6.4.2). The E_a of the β -transition lays around 300 kJ/mol for all cooling rates, which agrees well with the value $E_a=328$ KJ/mol found for the β -transition by Porzucek /146/. Alberola et al. /69/ reported a decrease of activation energy ranging from 470 kJ/mol of the quenched to 300 kJ/mol of the annealed sample. A slight increase from 300 to 400 kJ/mol can be found only in the E_a values of β -transition determined from E'' .

The E_a of the α -transition starts at 125 kJ/mol and grows slowly with increasing cooling rates to 525 kJ/mol. Similar starting values, 107-170 kJ/mol /147/ and 98 kJ/mol /148/, have been found in literature. The rise of the activation energy of α -transition with increasing cooling rate indicates the changes in the crystalline phase of iPP. The E_a of the “meso”-transition lays with 4000 kJ/mol remarkably higher than the α -transition confirming the fact that it is not only a shifted α -transition.

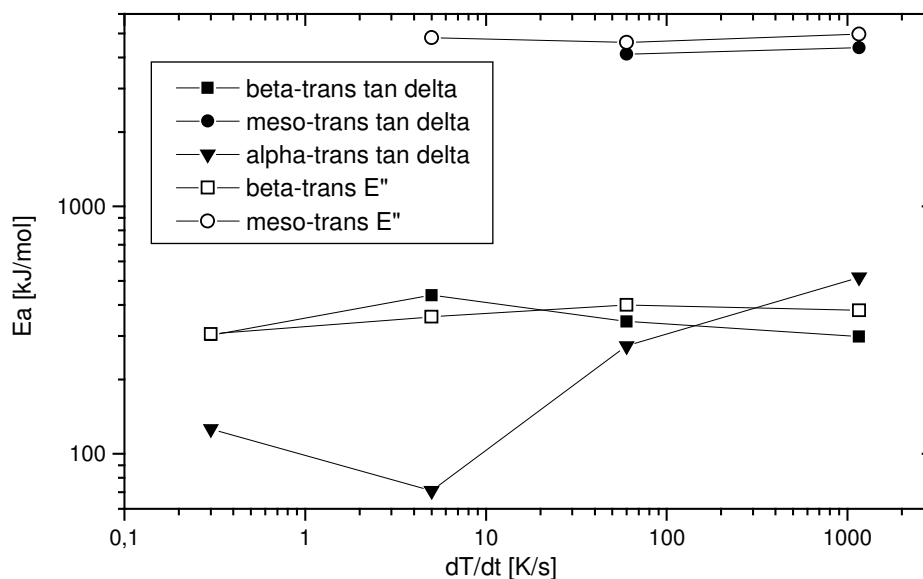


Fig. 6.30 Activation energies E_a of β -, meso- and α -transitions of iPP determined by tan delta and E'' data

6.6.3.2 EOC and EPDM

DSC 2nd heating and cooling scans of the uncrosslinked rubber components of the DV used in this study EOC and EPDM are shown in figure 6.31a) and b), respectively. EOC shows a lower T_g than EPDM, which depends in both cases on the comonomer content octene and propylene respectively. T_m of EOC is higher than for EPDM. T_c of 20°C of the EPDM used in this study is similar to the T_c found for an EPDM with 78 mol% studied by Scholtens et al. /85/. They also stated that the degree of crosslinking does not influence significantly the DSC thermograms.

Between 18 and 70 °C the melting endotherm of the EOC phase is found for all cooling rates exhibiting two peaks; the first sharp peak at 35 °C and the second peak at 50 °C (see fig. 6.32b)). Androsch et al. /93/ studied the annealing of EOC (38 wt%) by means of TMDSC. Processes such as primary and secondary crystallization, reorganization, locally reversible melting, and the gauche trans equilibrium are responsible for the first sharp endotherm and take place also in this case during annealing even below 0 °C, since the sample have been stored at these temperatures. The second heating run shows only the second peak, which indicates the melting of the bundle like crystals, which existence was suggested by Bensason et al. /90/ for EOC with this comonomer content. The first peak does not appear because the time between solidification and melting was not sufficient to allow further organization processes. T_c of EOC in the cooling run is 33 °C, slightly below the first "annealing" endotherm as stated by Alidazeh et al. /91/, and does not depend on cooling rate.

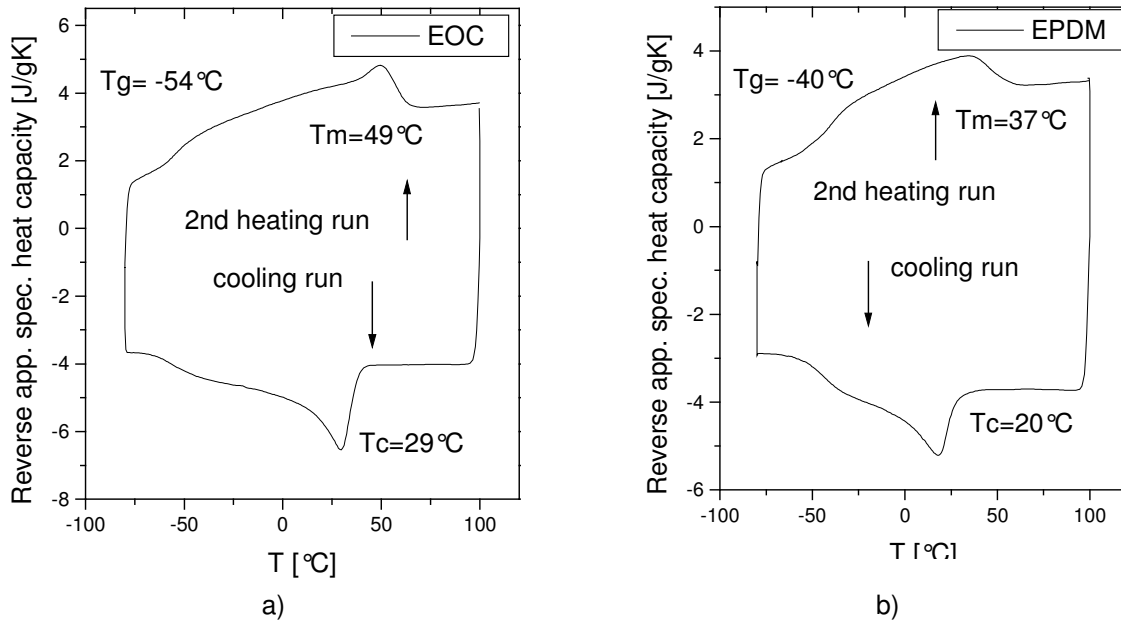


Fig. 6.31 DSC heating and cooling scans from a) EOC and b) EPDM

6.6.4 The thermal behavior of dynamic vulcanizates

6.6.4.1 PP/EOC 30/70p

DSC

The DSC 1st heating scans of PP/EOC 30/70p are shown in figure 6.32a). The first endotherm of quenched iPP, found between 35 and 75 °C, is partly overlaid by the melting endotherm of EOC and cannot clearly be distinguished.

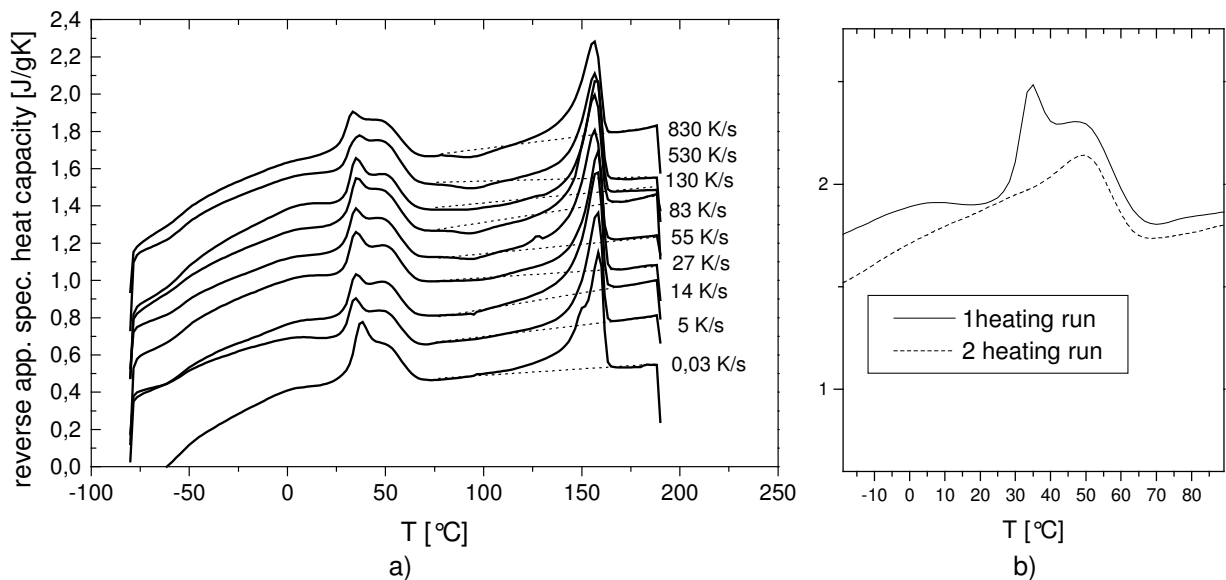


Fig. 6.32 a) DSC first heating run of PP/EOC 30/70p solidified at indicated cooling rates and b) the melting zone of the EOC phase of the 1st and 2nd heat run of PP/EOC 30/70p cooled with 5K/s

Therefore in table 6.12 the maximum (T_{max}) of the 1st endotherm and the onset (T_{onset}) of the exotherm are not shown. The values of the T_{onset} (95°C) and T_{max} (126°C) of the exotherm and the T_m (158°C) of the iPP matrix of the DV are the same as of pure iPP (table 6.11). T_c of the iPP matrix in the DV in the cooling run is with 114 °C slightly higher than in pure iPP (111°C). Also T_c of EOC is with 33°C higher than in the pure EOC (29°C). In contrary to pure iPP the T_m of the second heating run here is 5 degrees lower (153°C) than in the first heating run, being the same for all cooling rates. Da Silva et al. reported for blends of PP with 5 to 60 % of EOC (38 wt% octene content) partial miscibility of the blend components and multiple iPP melting endotherms, which were assigned to inhomogeneity of the crystal size. However, it remains unclear why this happens only during the second heating run.

Between 20 and 110 K/s the integrated area of the exotherm for the melting and reorganization of the mesomorphic phase grows from 0 to 7 J/g, reaching a stable value afterwards (see fig. 6.36) while the corrected value of the crystallinity (see fig. 6.37) decreases in this zone from 35 to 25 %.

Table 6.12 The onset temperature T_{onset} of the 1st exotherm and the 2nd endotherm and the maximum temperature T_{max} of the exotherm and the 2nd endotherm of iPP. The melting temperature T_m of the 1st heating run of EOC and iPP. The crystallization temperature T_c of the cooling and the melting temperature T_m of the 2nd heating run of EOC and iPP.

dT/dt [K/s]	T_{m1}	T_{m2}	T_{onset} Exo	T_{max} Exo	T_{onset} 2nd Endo	T_m	T_c		T_m	
PP/EOC 30/70p	EOC		iPP				EOC	iPP	EOC	iPP
	1st heat run [°C]						cool run [°C]		2nd heat run [°C]	
0,03	38	50	-	-	-	158	33	111	50	153
5	35	50	-	-	125	158	33	113	50	154
14	35	49	-	95	125	158	33	114	49	153
55	35	48	-	95	126	156	33	114	48	153
83	35	49	-	93	123	157	33	113	49	153
130	35	48	-	93	125	157	32	113	48	153
530	36	48	-	94	126	156	33	113	48	153
830	33	48	-	93	125	157	33	113	48	153

DMTA

The storage modulus E' and the loss modulus E'' of PP/EOC 30/70p are shown in figure 6.33. At -80 °C, below the glass transition of the rubber phase, the storage modulus lays between 600 and 900 MPa appearing without a clear dependence on cooling rate. After the glass transition of EOC around -50°C the storage modulus decreases showing already here a strong difference between the fast and the slowly cooled samples. The slope of decrease of the samples cooled with 0.03 K/s is less intense than the slope of the fast cooled samples. The slope of the slow cooled sample (0.03 K/s) changes again at -20, 40 and 80 °C. The slope of the fast cooled sample (786 K/s) changes at -30, 50 and 75 °C, while the intermediate cooling rates lay somewhere in between. At 25°C the storage modulus of the fast cooled sample is with 35 MPa only half of the storage modulus of the slowly cooled sample 66 MPa. This emphasizes again the importance of cooling rate on properties at room temperature even if the DV contains only 30 %wt of iPP.

The glass transition of the EOC can be seen very distinct in the tan delta maximum between -37 and -45 °C (see fig. 6.33). The scatter does however not depend on cooling rate and is caused by varying crosslinking density; higher crosslinking degrees shifts the T_g to higher temperatures, due to hindered segmental mobility [149]. This is responsible also for the

difference in storage modulus below glass transition of the EOC phase. Between 13 and 25 °C the T_g of the iPP is found, less distinct than in the case of pure iPP. However also here the shift of T_g with increasing cooling rates can be noted as in pure iPP (see also fig. 6.40). Above 100 °C the sample softens due to the high amount of EOC in the DV causing the scatter in tan delta values.

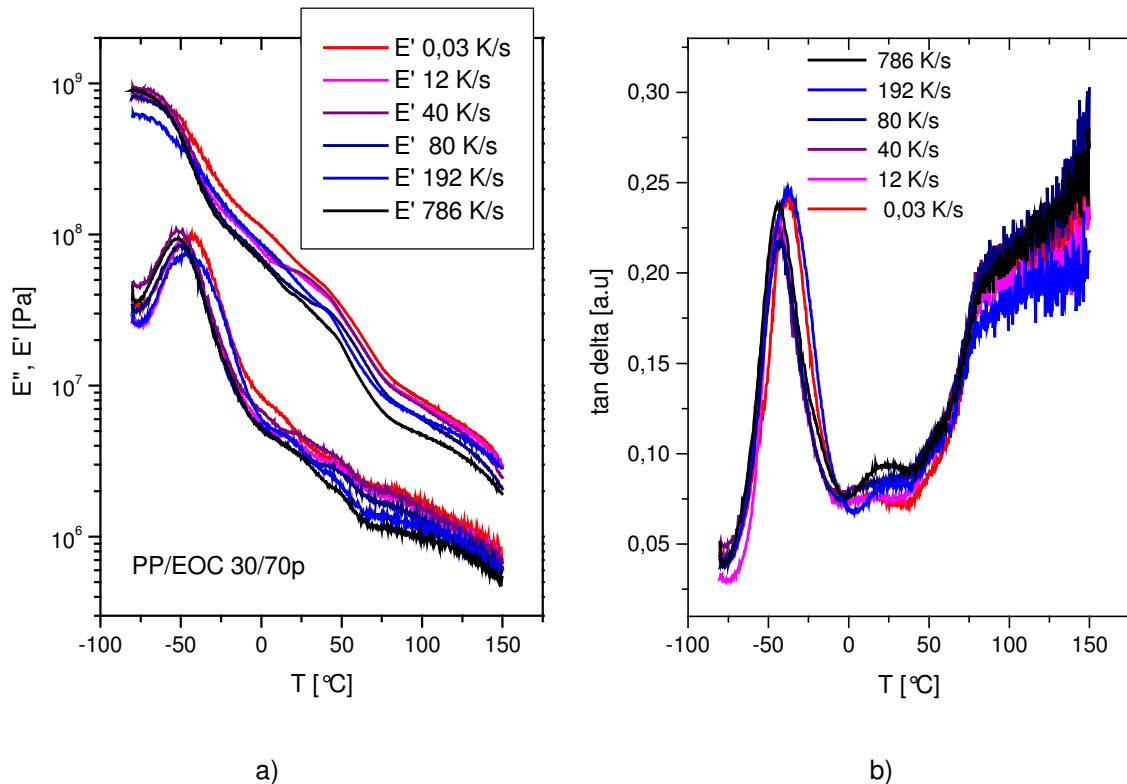


Fig. 6.33 Storage modulus E' , loss modulus E'' (a) and $\tan \delta$ (b) of PP/EOC 30/70p solidified at indicated cooling rates.

6.6.4.2 PP/EPDM 30/70p and PP/EPDM 30/70r

DSC

The melting behavior of PP/EPDM 30/70 peroxidic and resin crosslinked is shown in figures 8.34 and 8.35, respectively. T_g of EPDM appears around -40 °C, the same as in pure EPDM. Transition temperatures are shown in table 6.8 and 6.9 for peroxidic and resin crosslinked PP/EPDM 30/70, respectively. In the first heating run EPDM exhibits a sharp endothermic melting peak around 37 °C after a local maximum around 5 °C. In the 2nd heating run this melting peak appears less distinct (see fig.6.34b). Responsible for this behavior are, like in EOC, reorganization processes of the crystalline phase of EPDM taking place during annealing in the time period between the fast cooling and the DSC measurement. Before the second heating run time is not sufficient enough to allow these processes. There is no temperature shift of this melting peak between first and second heating run, no dependence on cooling rate as well as no difference to pure EPDM.

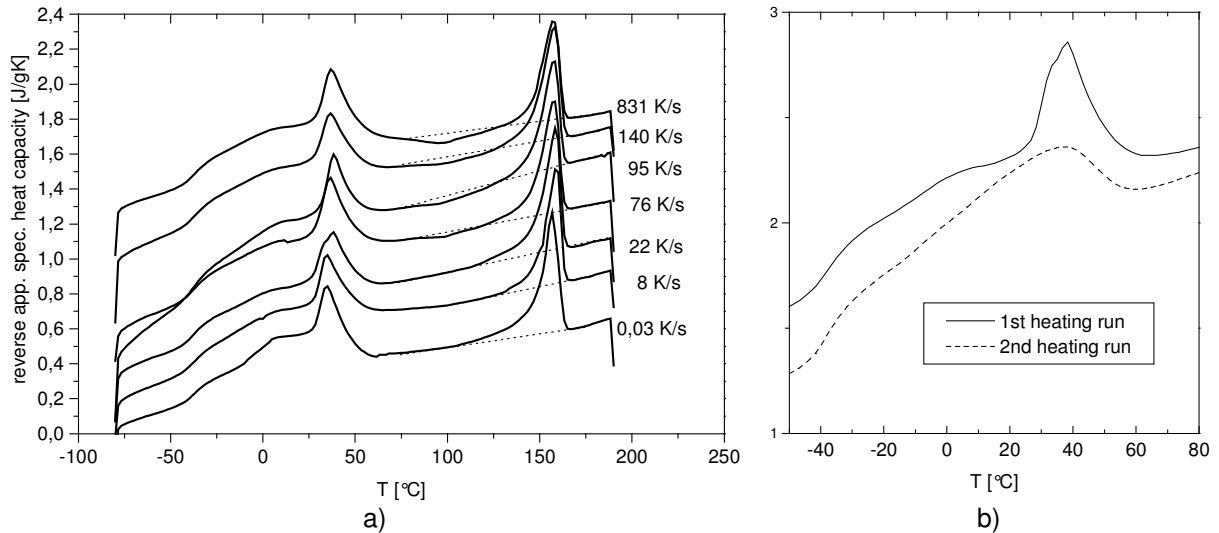


Fig. 6.34 a) DSC first heating run of PP/EPDM 30/70p solidified at indicated cooling rates and b) the melting zone of the EPDM phase of the 1st and 2nd heat run of PP/EPDM 30/70p quenched with 22K/s

During the first heating scan above cooling rates of 76 K/s an exothermal area can be distinguished with a local maximum at 95 °C, which onset is overlapped by the melting of the EPDM phase, the same as in the DV. The lack of effect of EPDM incorporation to iPP on its melting point has been found also by Brostow et al. /37/ for an EPDM content of 30 %wt (E/P ratio not indicated) and Wenig et al. /109/. Bielinski et al /116/ reported only a slight decrease of T_m from 163 to 161 °C respectively from pure to the iPP phase in a DV PP/EPDM 33/67 crosslinked by DCP. They reported however for lower amounts of iPP a significant change of T_m resulting from less perfect and thinner crystals of iPP at very high amounts of EPDM. The following iPP melting endotherm has a maximum around 158 °C, the same as in the second heating run and in pure iPP, unchanged by cooling rate. The melting temperatures and crystallization temperatures of PP/EPDM 30/70p of the first, the second heat and the cooling run are shown in table 6.13.

Table 6.13 PP/EPDM 30/70p - The onset temperature T_{onset} of the 1st exotherm and the 2nd endotherm and the maximum temperature T_{max} of the exotherm and the 2nd endotherm of iPP. The melting temperature T_m of the 1st heating run of EPDM and iPP. The crystallization temperature T_c of the cooling and the melting temperature T_m of the 2nd heating run of EPDM and iPP.

dT/dt [K/s] PP/EPDM 30/70p	T_g	T_{m1}	T_{m2}	T_{max} Exo	T_{onset} 2nd Endo	T_m	T_c		T_m	
	EPDM			iPP			EPDM	iPP	EPDM	iPP
	1st heat run [°C]						cool run [°C]		2nd heat run [°C]	
0,03	-40	5	35	-	-	157	23	116	36	157
8	-38	6	36	-	-	158	23	116	36	156
22	-38	6	38	-	-	158	23	116	37	156
76	-38	7	36	98	120	158	-	116	37	158
95	-37	12	38	93	117	156	23	116	38	157
140	-37	9	37	94	123	158	25	116	39	157
831	-38	5	37	96	148	157	24	116	37	156

During the cooling run T_c of the iPP matrix of the peroxidic crosslinked DV appears around 116 °C (see table 6.13) and in some cases for the resin crosslinked PP/EPDM even at 127°C (see table 6.14), which is higher than T_c of the pure iPP (111°C). This T_c shift of approx. 5° C is a sign of nucleation effects induced by the rubber phase. It was also found by Brostow et al.

/37/ for PP/EPDM 70/30 and also by D’Orazio et al. /103/ for PP/EPM 30/70 dynamically vulcanized with peroxide. Responsible for the very strong shift in some cases of PP/EPDM 30/70r is the presence of the powderlike SnCl_2 activator, which enhances the nucleating effect already existing due to the rubber particles.

The first heating runs of PP/EPDM 30/70r quenched with different cooling rates are shown in figure 6.35.

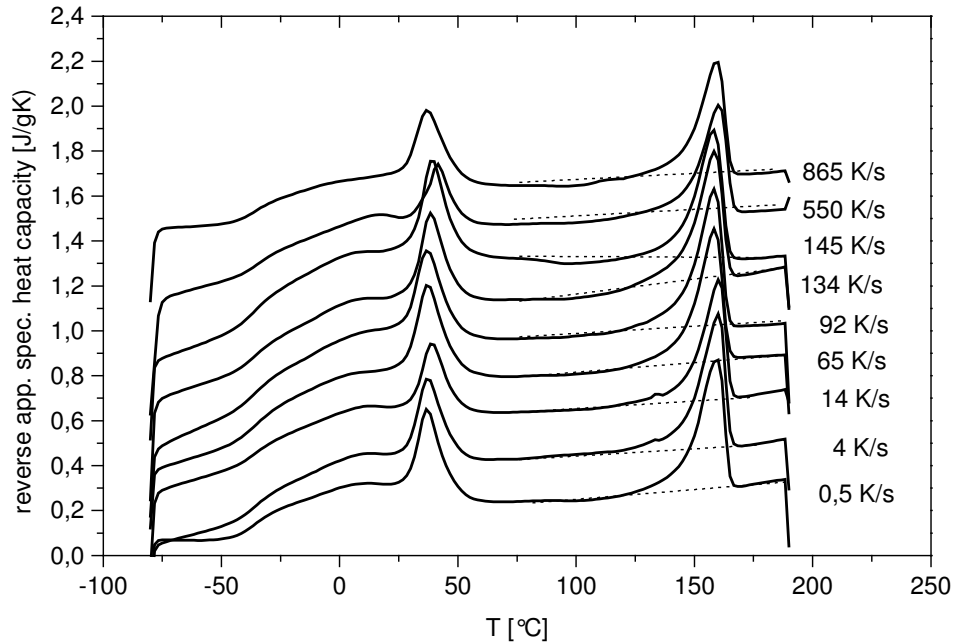


Fig. 6.35 First heating run of PP/EPDM 30/70r solidified at indicated cooling rates.

Table 6.14 PP/EPDMr - The onset temperature T_{onset} of the 1st exotherm and the 2nd endotherm and the maximum temperature T_{max} of the exotherm and the 2nd endotherm of iPP. The melting temperature T_m of the 1st heating run of EPDM and iPP. The crystallization temperature T_c of the cooling and the melting temperature T_m of the 2nd heating run of EPDM and iPP.

dT/dt [K/s]	T_g	T_{m1}	T_{m2}	T_{max} Exo	T_{onset} 2nd Endo	T_m	T_c		T_m	
PP/EPDM 30/70r	EPDM			iPP			EPDM	iPP	EPDM	iPP
	1st heat run [°C]						cool run [°C]		2nd heat run [°C]	
0,5	-34	11	37	-	144	160	25	117	38	158
4	-36	13	38	-	148	160	26	118	38	160
14	-36	13	38	-	147	160	25	121	38	160
65	-37	7	37	-	150	158	26	115	39	158
92	-37	12	37	95	144	158	25	116	37	158
134	-36	7	38	95	143	158	25	115	38	158
145	-35	8	39	95	147	158	25	117	37	158
550	-35	16	41	97	148	158	25	127	38	160
865	-35	-	37	95	146	160	26	127	39	160

As stated in chapter 6.6.3 the mesomorphic phase received after fast cooling undergoes recrystallization, indicated by an exothermic local maximum between 75 and 125 °C. The integrated values of this exothermal maximum have been discussed for iPP in chapter 6.6.3 and are shown in figure 6.36. The integrated area of the DV shows the same behavior in dependence on cooling rates. However, they reach constant higher levels at higher cooling rates 100K/s compared to 70K/s of iPP. This shift is even more apparent for the phenolic resin

crosslinked DV of PP/EPDM 30/70r, which is consistent with the results from density measurements and the alpha phase content derived from WAXD deconvolution (see chapters 6.6.1 and 6.6.2). It was attributed to the enhanced nucleation effect due to the presence of the SnCl_2 . The total end values of the heat of recrystallization of DV are lower than the values from iPP. This is contrary to the calculated mesomorphic phase content from WAXD deconvolution (see chapters 6.6.1 and 6.6.2). The lower values could also derive from a superposition of the EOC and EPDM melting with the exothermal area of the mesomorphic phase of the iPP matrix.

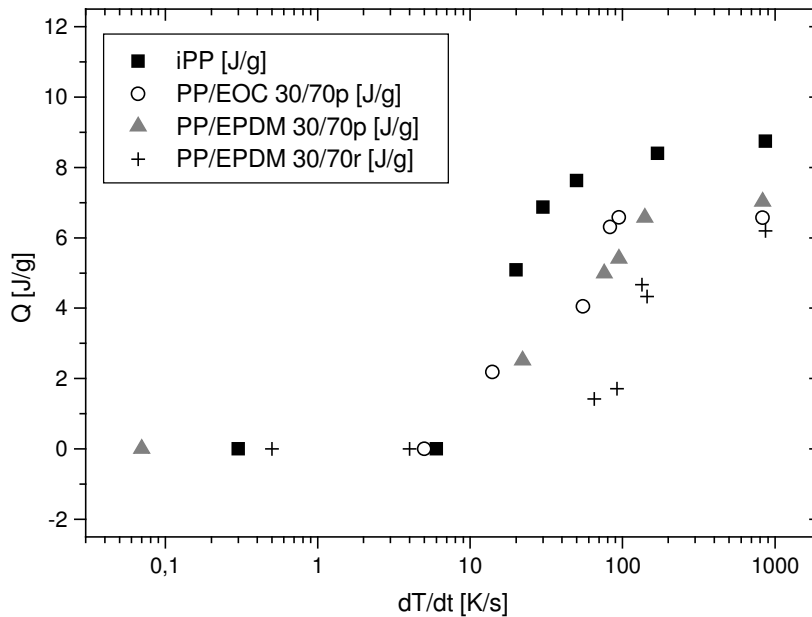


Fig. 6.36 Calculated heat Q of exothermic transition from the heat flux of the 1st DSC heating run in the interval between 75 and 125 °C of iPP and the DV quenched at indicated cooling rates.

The degrees of crystallinity X_c as calculated by equation 6-1 for iPP and the dynamic vulcanizates are shown in figure 6.37. The values of the iPP matrix of both the PP/EPDMp and r are slightly below the value for neat iPP (47 %) for low cooling rates. D'Orazio /98,103/ found different values of 36 % for iPP and 32 % for PP/EPM 30/70 cured by peroxide explained this by the presence of the rubber phase. After the drop between 30 and 150 K/s the total value of PP/EPDMp is very low, approx. 15 %, compared to that of the resin crosslinked DV, which exhibits with 35 % almost the same degree of crystallinity like iPP at high cooling rates. It is worth noticing that the drop of degree of crystallinity of PP/EPDM 30/70 crosslinked by phenolic resin appears above 100 K/s, later than the peroxidic crosslinked DV. The same shift of drop, assigned to the transition between α -crystalline and mesomorphic iPP phase, was found in density and the α -phase content derived from WAXD deconvolution (see chapter 6.6.2). Like PP/EPDM 30/70p, also the peroxidic crosslinked PP/EOC 30/70p shows with approx. 20 % very low degrees of crystallinity at high cooling rates. However the total degrees of crystallinity at high cooling rates are not consistent with the findings of the deconvolution of the WAXD patterns in chapter 6.6.2, where the alpha crystalline phase content at high cooling rate is reduced below 10 % for iPP as well as all DV. The difference of the total results of both methods derives from the different evaluation methods and measured sample area. Therefore the differences in total values of the degree of crystallinity at high cooling rates calculated from DSC measurements will be neglected.

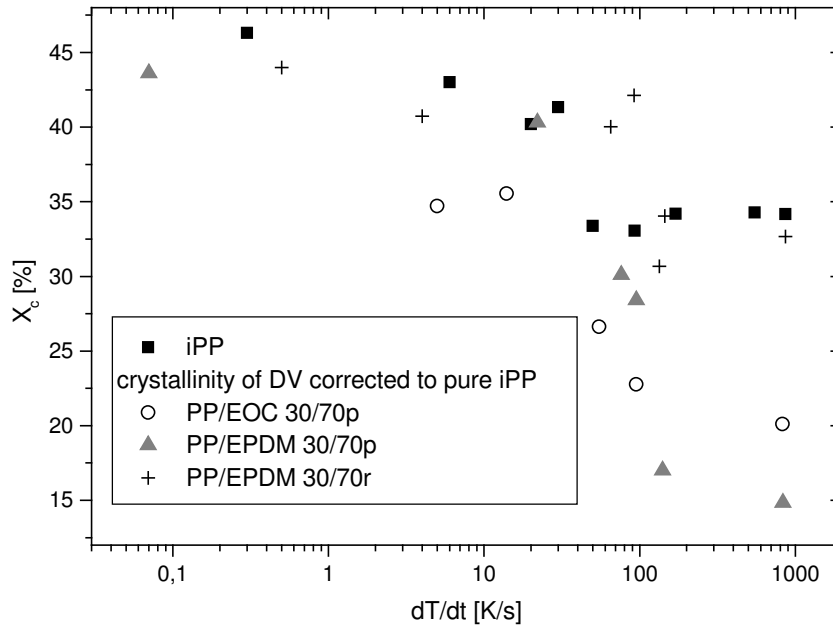


Fig. 6.37 Degrees of crystallinity X_c of iPP and the DV quenched at indicated cooling rates calculated according to eq. 6-1.

DMTA

The results of the DMTA measurements of PP/EPDM_p and r, peroxidic and resin crosslinked, are shown in the figures 6.38 and 6.39. The storage moduli of PP/EPDM 30/70p and r below the EPDM glass transition lay between 500 and 1000 MPa and do not depend on cooling rate (see figures 6.38a) and 6.39a)). After the glass transition of EPDM the storage modulus decreases with increasing temperature. The slope of the PP/EPDM 30/70p crosslinked by peroxide cooled with 845 K/s changes several times at -11 , 16 , 41 and 62 °C and the slope of the slowly cooled sample changes at -13 , 15 and 75 °C. The level of storage modulus does not depend on cooling rate until 40 °C.

The tan delta (see fig. 6.38b)) show a T_g of the EPDM phase between -28 and -33 °C. A similar value has been found in literature /150/. The variation can be explained again due to different crosslinking degrees. The T_g of the iPP matrix increases with increasing cooling rates from 14 to 26 °C as in pure iPP.

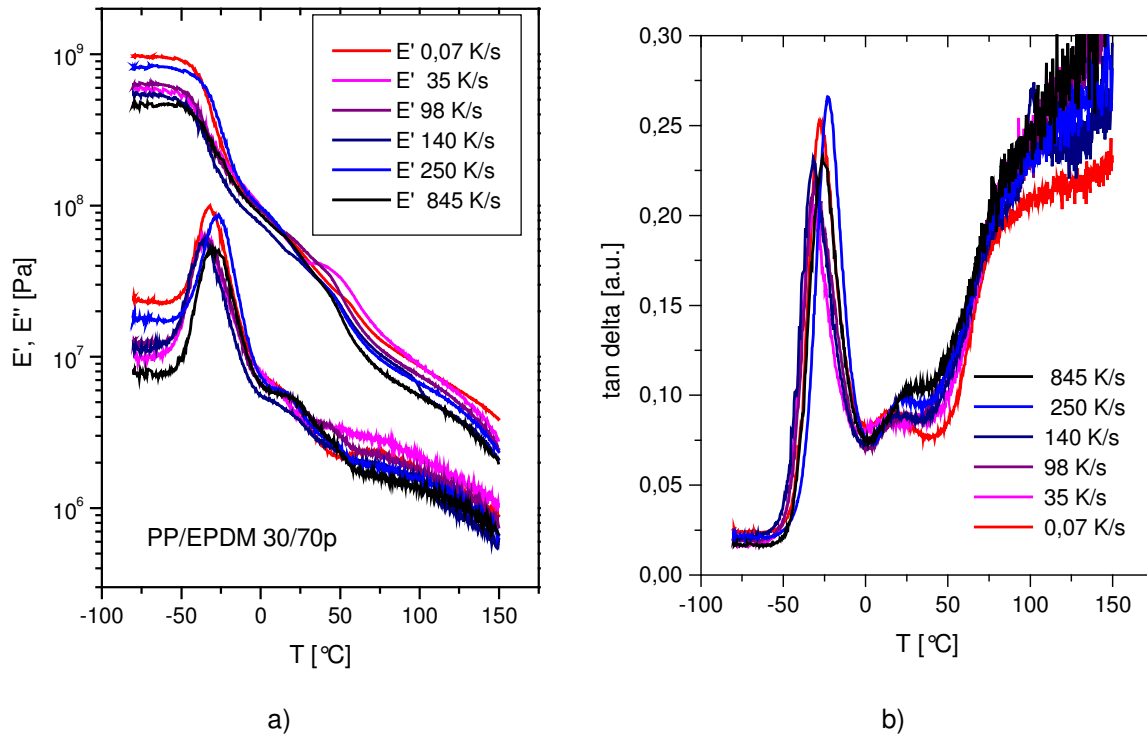


Fig. 6.38 Storage modulus E' , loss modulus E'' (a) and tan delta (b) of PP/EPDM 30/70p solidified at indicated cooling rates.

The storage modulus of PP/EPDM 30/70r crosslinked by phenolic resin decreases after the glass transition of the EPDM phase changing its slope several times, at -2 , 44 and 67 °C in the fast cooled case and -11 and 41 °C in the slow cooled case. The level of storage modulus does not depend very much on cooling rate until above approx. 50 °C, even higher than in the peroxidic crosslinked case. The storage moduli of different DV fast and slowly cooled are shown in table 6.15. In fact the difference between fast and slowly cooled values of PP/EPDM30/70 p and r is lower than in the case of PP/EOC 30/70p. This is not easy to explain. A first reason could be the melting area of EPDM finishing at 50 °C, above that the iPP matrix would have more influence on the mechanical properties. But the melting area of EOC is completed even higher around 75 °C and here the dependence on cooling rate shows up already above 15 °C, the glass transition of iPP. Strangely also the T_m of EPDM measured by DSC do not depend on the type of crosslinking, but are both found around 37 °C. The reason for this must be therefore the increased crosslinking density of the EPDM phase, which does not melt completely and still influences total E' above the melting of the rubber phase. The reason for the higher crosslinking degree could be the existence of unsaturated bonds in the EPDM with respect to the EOC. This would mean that the higher the crosslinking degree of rubber phase of DV, the less the effect of cooling rate on room temperature.

Table 6.15 Storage modulus values at room temperature of DV solidified at fast and slow cooling rate.

cooled	E' [MPa] at $T=25$ °C		
	PP/EOC 30/70p	PP/EPDM 30/70p	PP/EPDM 30/70r
slow	35	40	48
fast	60	50	56

The tan delta values of the PP/EPDM 30/70r exhibit an overall lower level (see fig. 6.39b)). T_g of the resin crosslinked EPDM phase lays between -28 and -30 °C, like in the peroxidic case. The scatter is lower which indicates a more homogeneous degree of crosslinking. Since crosslinking density is direct proportional to storage modulus, and therefore indirect

proportional to $\tan \delta / 149$, it is obvious that vulcanization with phenolic resin reaches higher crosslinking degrees in the rubber phase than peroxidic crosslinking. Another confirmation of this are the lower $\tan \delta$ values above 100 °C indicating that the softening of the rubber phase is less intense than in the peroxidic crosslinked case.

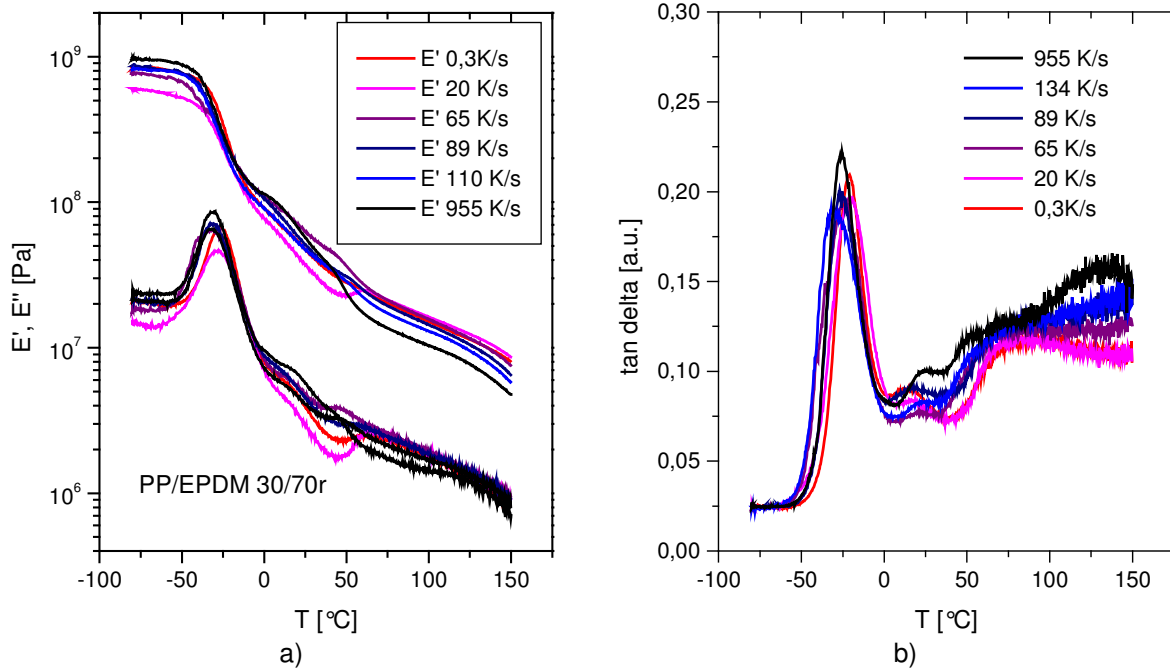


Fig. 6.39 Storage modulus E' , loss modulus E'' (a) and $\tan \delta$ (b) of PP/EPDM 30/70r solidified at indicated cooling rates.

Like in the other DV the T_g of the iPP-matrix in the PP/EPDM 30/70r shifts with cooling rate to higher temperatures as shown in figure 6.39. T_g vs. cooling rate of iPP and the iPP matrix of all DV are shown in figure 6.40. The shift of T_g of the iPP-matrix of the DV seems to start above 30 K/s, whereas the pure iPP shift of T_g starts already at lower cooling rates. The shift of the β -transition temperature is direct proportional to the mesophase content and confirms the results derived from the WAXD data.

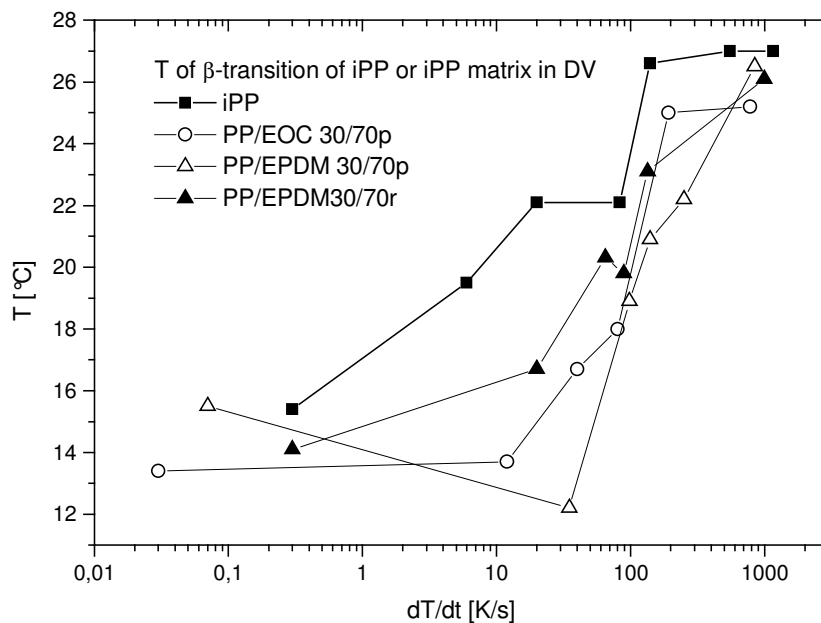


Fig. 6.40 β -transition temperatures (T_g) vs. cooling rates of iPP and iPP-matrix in the DV.

6.6.5 The mechanical properties of the pure components

As seen in the storage moduli, there is a great influence of cooling rates on structure and properties. The effect of cooling rates on mechanical behavior like microhardness, tensile deformation and reversibility of deformation is subject of this chapter.

6.6.5.1 IPP

The microhardness

The microhardness MH was measured according to the method described in chapter 6.5.1. The results are shown in figure 6.41. The values until 100 K/s resemble the values found by La Carruba /130/ for iPP solidified at ambient pressure.

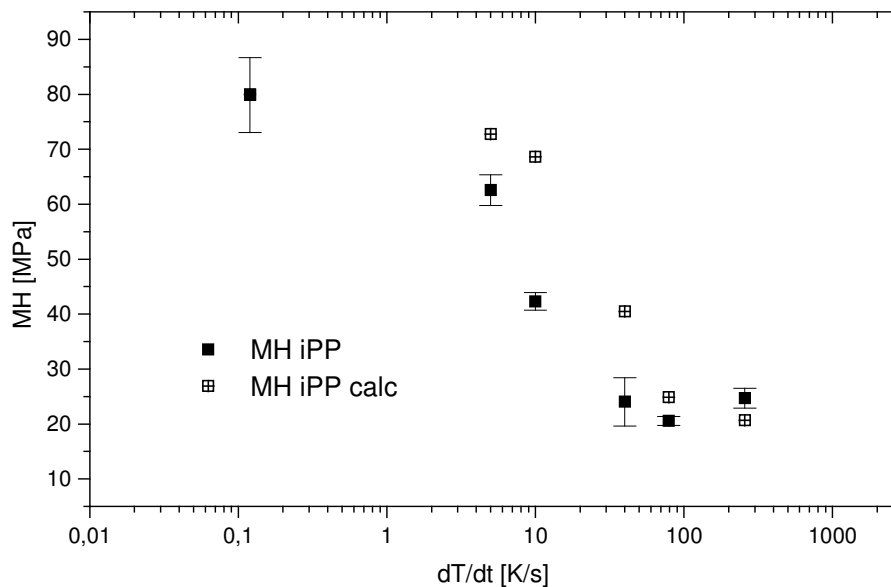


Fig. 6.41 Measured and calculated microhardness values MH of iPP solidified at indicated cooling rates. The calculation was performed according to eq. 6-11.

The theoretical microhardness MH of iPP was calculated by the following equation

$$MH = \varphi^{\alpha}(MH^{\alpha}) + \varphi^a(MH^a) + \varphi^m(MH^m) \quad \text{eq. 6-11}$$

with φ being the phase fraction of the α -monoclinic phase, the amorphous phase and mesomorphous phase indicated by the indices α , a and m respectively derived from WAXD. Flores et al. /151/ measured higher values for MH of quenched iPP around 100 MPa and annealed 110 MPa. However this quenching technique was not comparable to the one used in this work and only lower cooling rates could have been obtained. They calculated MH from an additive calculation of $MH^a = 30$ MPa of the amorphous phase content and $MH^c = 210$ MPa of the crystalline phase content and suggested $MH^c = 230$ MPa for a infinitely thick α -monoclinic crystal. A calculation of MH by placing these values and the phase contents derived from WAXD data in eq. 6-11 did not match the MH value measured here. The MH values of each phase have therefore been fitted to the measured values results by using $MH^a =$

10 MPa for the amorphous phase, $MH^m = 40$ MPa for the mesomorphic phase and $MH^\alpha = 150$ MPa for the α -monoclinic phase. The results indicated by MH iPP calc are shown above in figure 6.41.

The stress – strain - behavior

The stress – strain - behavior has been investigated by means of the Minimat tensile tester as described in chapter 6.5.2. Due to the small sample size the values shown here are not to be seen as characteristic values as obtained from DIN specifications. However, the value of the yield strength of iPP at low cooling rate 29.5 MPa corresponds to the values and the stress - strain curve pattern found elsewhere [152,153]. With increasing cooling rate this value decreases in the same manner as density and microhardness reaching a value of 5 MPa (see figure 6.42a)). This means that fast cooled iPP exhibits only 0.2 % of yield stress of the slowly cooled samples. Alberola et al. [70] reported a tensile strength value of quenched iPP of 28 MPa and 30 MPa of iPP annealed at 70 °C. However they did not report the exact quenching procedure, therefore these values should not be compared with the ones found here.

The tensile diagrams in figure 6.41a) show the influence of cooling rates on stress – strain - behavior. The yield point indicating the plastic deformation is lower with increasing cooling rates. The slope of the curve until 5 % strain decreases with increasing cooling rates. At the low drawing ratios used no destruction of the samples was noticed.

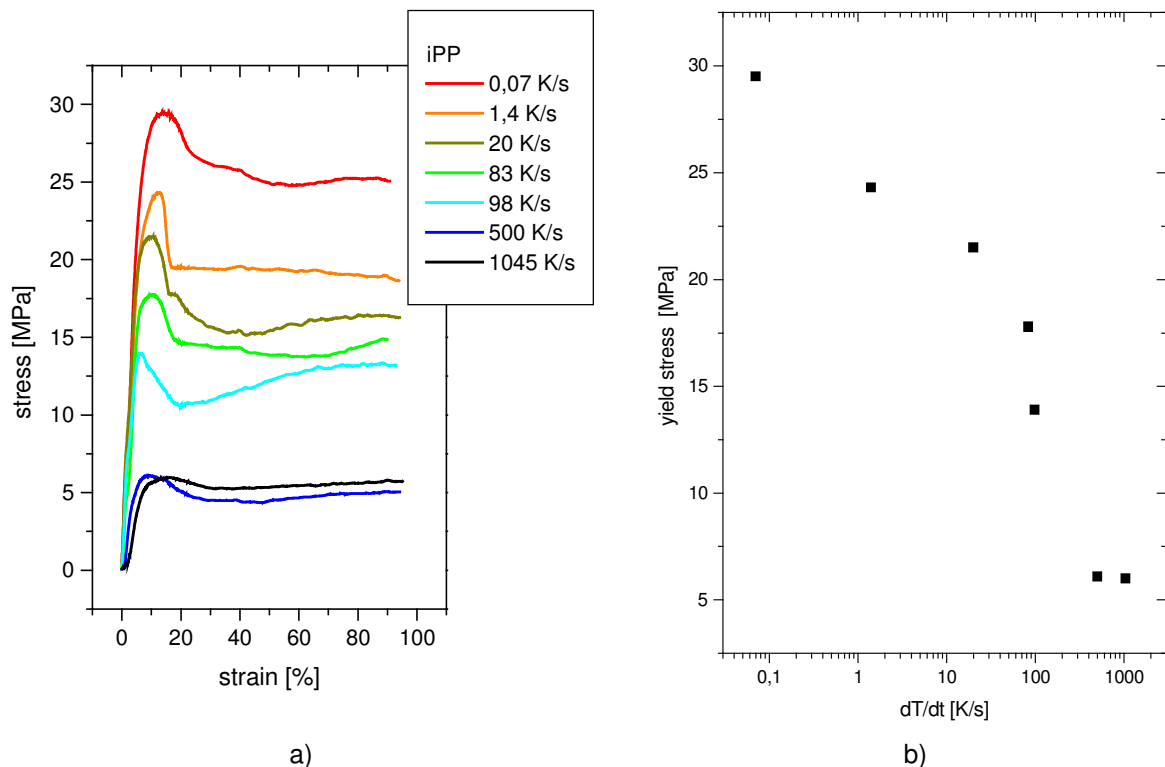


Fig. 6.42 a) Stress-strain diagrams of iPP solidified at indicated cooling rates; b) yield tensile strength vs. cooling rates of iPP.

6.6.5.2 EOC

The microhardness

Due to the softness of the EOC the use of microhardness measurement proved to be not very applicable. The large imprint at the lowest force possible indicated that this type of hardness determination is limited in case of elastomers as already discussed in chapter 6.5.1. Nevertheless values of 1.3 MPa and 1.3 MPa have been obtained for slow and fast cooled EOC confirming the fact that EOC MH does not change with the cooling rate. The values are shown in figure 6.43.

6.6.6 The mechanical properties of dynamic vulcanizates

6.6.6.1 PP/EOC 30/70p

The microhardness

The microhardness values MH of PP/EOC 30/70p vs. cooling rate are shown in figure 6.43 together with the MH values of EOC and iPP. At cooling rates until 40 K/s stable values are found around 5 MPa and decreasing around 100 K/s to a value of 2 MPa. Equation 6-11 has been used to calculate the theoretical MH of the iPP - matrix of the DV MH^{iPP} by means of the data derived from WAXD of the amorphous, α -monoclinic and mesomorphic phase fractions (see fig. 6.12). The microhardness of the DV MH^{DV} was then determined by the following equation:

$$MH^{DV} = \varphi_w^{EOC} * MH^{EOC} + \varphi_w^{iPP} * MH^{iPP} \quad \text{eq. 6-12}$$

φ_w^{EOC} and φ_w^{iPP} are the phase fractions by weight of the EOC and the iPP phase respectively. MH^{EOC} has the value 1.3 MPa. The results of MH^{DV} are shown in figure 6.43 being referred to as MH PP/EOC 30/70p calc. Comparing these values to the measured value it is obvious that equation 6-12 cannot be used here to calculate the total MH value. Already Flores et al. /151/ found that there is no linear dependency between rubber content and MH for PP/EPM reactive blends with an iPP - matrix.

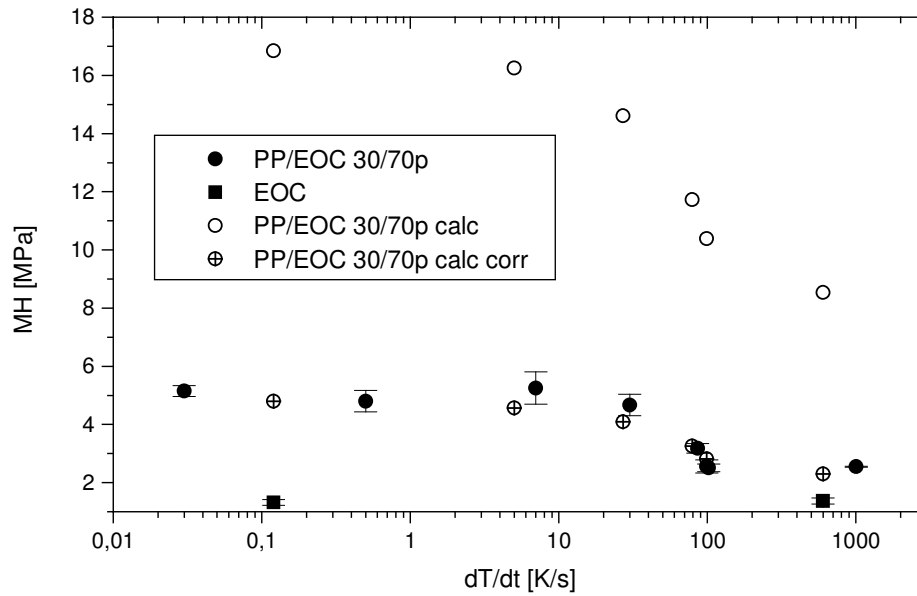


Fig. 6.43 Measured and calculated microhardness values MH of PP/EOC 30/70p and EOC solidified at indicated cooling rates.

In order to receive information about the influence of EOC content on the MH values of the DV, the microhardness was measured from pressed samples of iPP, EOC, and DV based on PP/EOC p with different thermoplast / rubber ratios. The results are shown in figure 6.44 (solid squares). These values have been fitted by the exponential equation 6-13 (see thin line in fig. 6.44):

$$MH^{DV} = MH^{iPP} * \exp(-\phi_w^{EOC}/29) \quad \text{eq. 6-13}$$

MH^{iPP} is the microhardness of the iPP - matrix in the DV calculated from the phase fraction data obtained from WAXD deconvolution (see fig. 6.12). Equation 6-13 was used to recalculate the microhardness data of the DV. The results are shown above in figure 6.43 indicated with MH PP/EOC 30/70 calc corr and match perfectly the real measured MH values of PP/EOC 30/70p. This can be seen as prove of the data derived from WAXD (see fig. 6.12).

Using the measured data of MH^{iPP} vs. cooling rate in equation 6.13 the dependence of MH values of the DV with different rubber / thermoplast ratio on cooling rate can be predicted. See open symbols in figure 6.44.

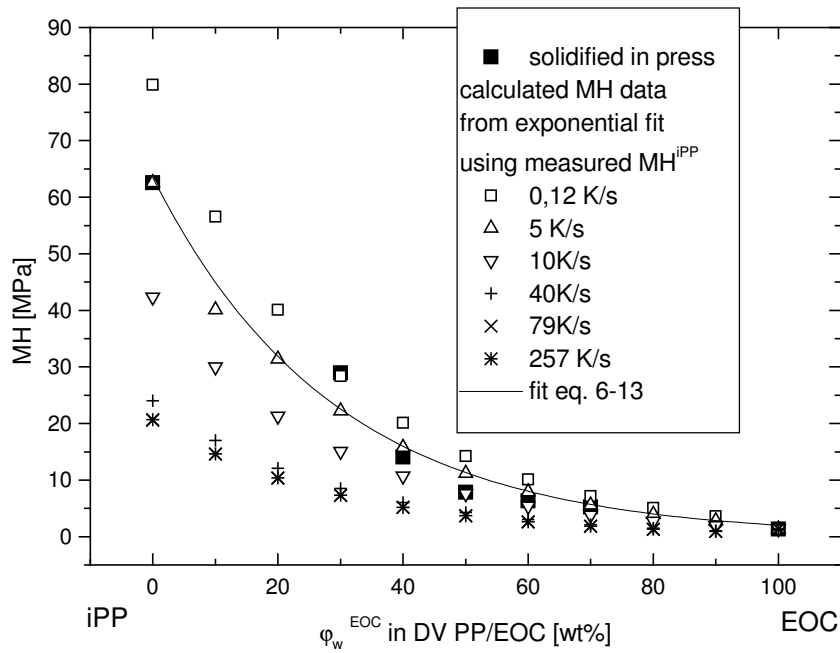


Fig. 6.44 Microhardness vs. content of EOC, solid squares: measured values from pressed samples; open symbols: iPP and EOC measured at indicated cooling rates, the other points are calculated by the exponential equation 6-7.

It shows that in PP/EOC 30/70p the change of hardness values due to cooling rate is much lower than in original iPP due to this exponential law. The change of macroscopic mechanical properties in DV is connected with structural parameters such as degree of crystallinity and network density. With increasing degree of iPP the degree of crystallinity increases linearly while the network density increases exponentially [139]. Therefore, the exponential decrease of microhardness with increasing amount of rubber is caused by the total network density in DV.

The stress – strain - behavior

The stress strain diagram of PP/EOC 30/70p is shown in figure 6.45. The shape of the curve is more of elastomeric type as expected. However the drawing of the films was done only until 200 %, until that no rupture of the DV is noted. At higher drawing ratios a strain hardening is typical for DV. The stress value of the slowly cooled DV at 50 % elongation is 4.3 MPa and for the slowly cooled sample 2.9 MPa. The measured values are compared to the other DV in figure 6.48.

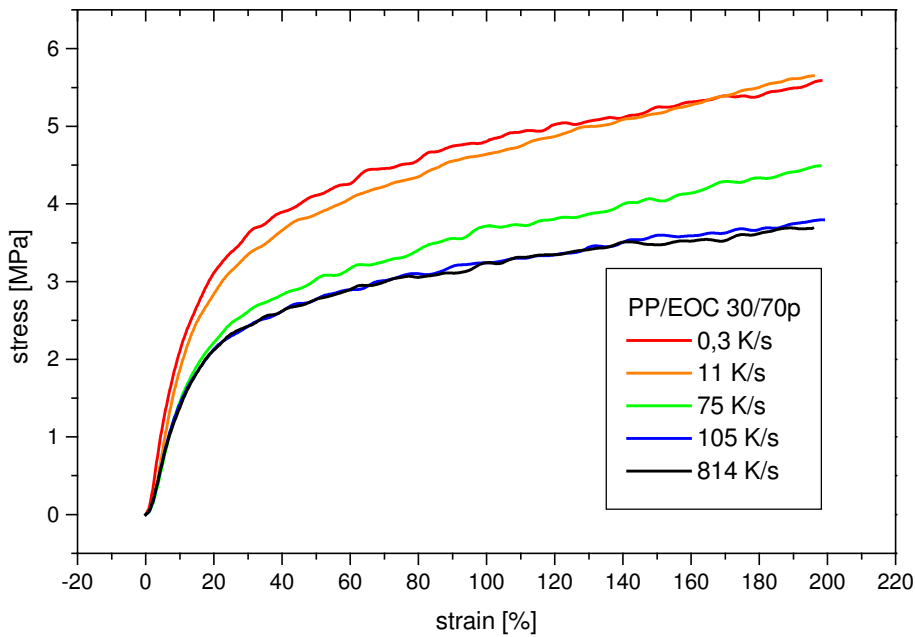


Fig. 6.45 Stress-strain diagrams of PP/EOC 30/70p solidified at indicated cooling rates.

The irreversible deformation behavior

The residual deformation gives information about the irreversibility of the deformation behavior of a DV and was determined as described in chapter 6.5.2. The residual strain of the DV PP/EOC 30/70p vs. cooling rate is shown below in figure 6.46a). The values at low cooling rates lay around 50 % and increase with increasing cooling rates to 60 %. At high deformations the nonreversibility is mainly determined by the thermoplastic phase /152/. Therefore a dependence on cooling rate was expected. The higher values at high cooling rates imply a higher amount of plastic deformation of the iPP matrix due to the increased amount of mesomorphic phase. When looking at the content of reversible and irreversible work of deformation (see fig. 6.46b)) it is clear that the work of plastic deformation is lower at high cooling rates. This means that the work necessary to deform the mesomorphic phase plastically is lower than for the α -monoclinic phase. The reversible or elastic work of deformation does not depend on cooling rate but it is influenced by the type and the chemical crosslinking density of the elastomer phase.

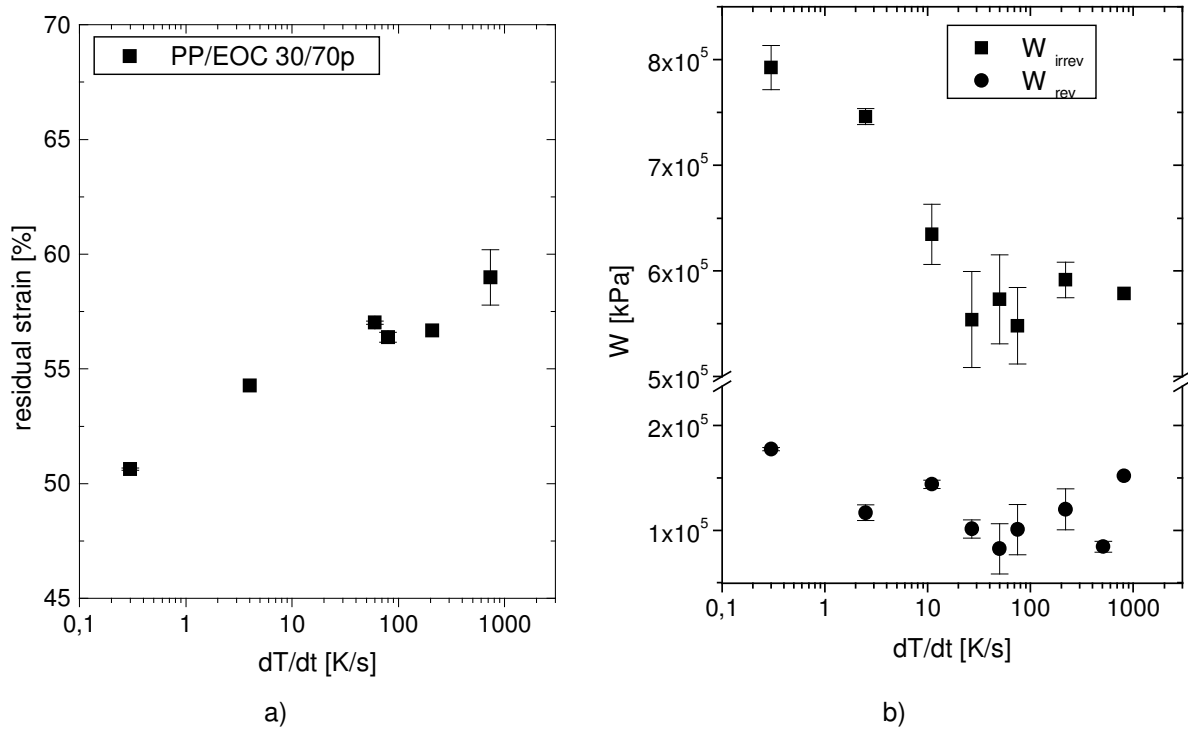


Fig. 6.46 PP/EOC 30/70p solidified at indicated cooling rates a) residual strain after deloading b) reversible and irreversible work of deformation during load and deload cycle

6.6.6.2 PP/EPDM 30/70p and PP/EPDM 30/70r

The stress – strain behavior

The stress-strain diagrams of the DV based on PP/EPDM cooled with different cooling rates are shown in figure 6.47. The values of the tensile stress at 50% elongation are shown in figure 6.48. These values and also the stress strain diagrams show that the resin crosslinked DV exhibits a higher tensile strength compared to the peroxidic crosslinked version, presumably due to different crosslinking densities. The PP/EPDM 30/70r slowly cooled shows similar values as the same DV found in literature [152].

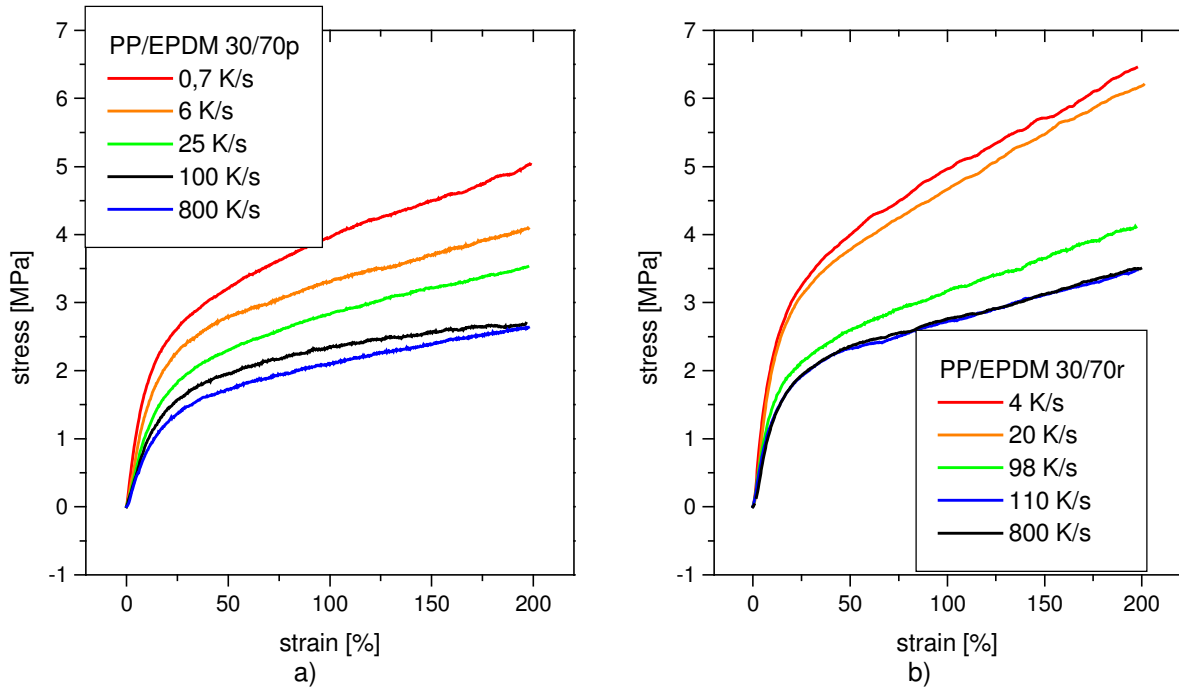


Fig. 6.47 Stress-strain diagrams of a) PP/EPDM 30/70p and b) PP/EPDM 30/70r solidified at indicated cooling rates, measured at room temperature.

The stress values at 50 % elongation (see fig. 6.48) of all DV show the same dependence on cooling rates as the values of microhardness, density and degree of crystallinity. This shows that the mechanical properties of the DV depend not only on the amount of thermoplast fraction but also the degree of crystallinity in the iPP matrix.

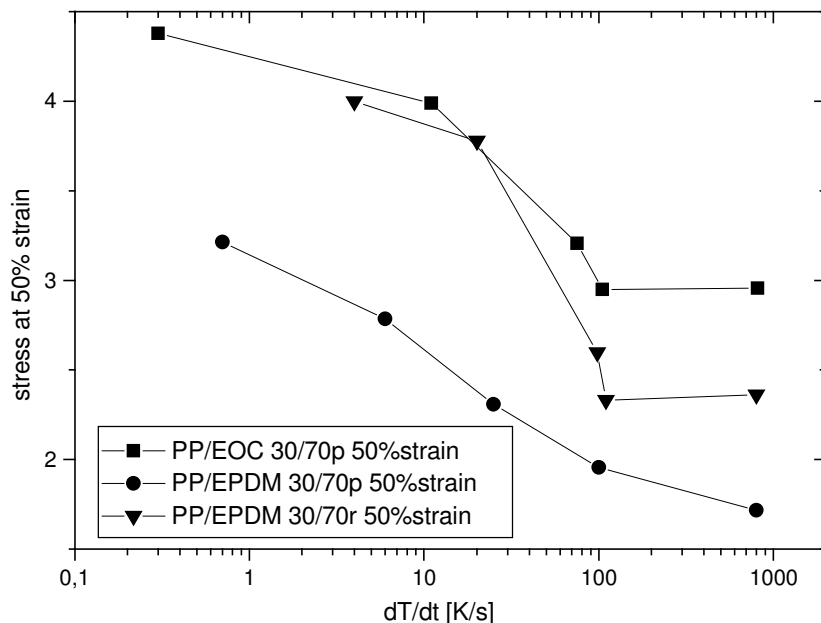


Fig. 6.48 Comparison of tensile stress values at 50% strain of the DV PP/EOC 30/70p, PP/EPDM 30/70p and PP/EPDM 30/70r solidified at indicated cooling rates.

Rheoptical investigations by Huy /139/ of the deformation behavior of DV showed that the orientation of the EPDM phase is higher than the iPP phase resulting from a heterogeneous orientation distribution due to stress concentration in the matrix. It was observed that the

orientation of the rubber phase increases continuously while the orientation of the iPP phase undergoes a local minimum due to the change of deformation mechanisms at low drawing rates.

In order to see the influence of cooling rate on the orientation behavior of the different phases in the DV the same measurements have been performed here on two fast cooled DV (see figure 6.49)). The orientation of the iPP phase (see fig. 6.48a)) takes place more gradually compared to the orientation of the EPDM phase (see fig. 6.48b)) in case of the fast cooled samples. In the latter case the final degrees of orientation are higher than the slowly cooled samples measured in literature /139/. The slope of orientation of the fast cooled iPP phase starts to increase at 100 % strain compared to the slow cooled iPP phase, which can be an indication that the critical shear stress of the deformation of the mesomorphic phase entities is lower than the α -monoclinic phase. Therefore with a lower degree of crystallinity higher degrees of orientation can be obtained (0.35 and 0.3 for the peroxidic and resin crosslinked DV).

The EPDM phase of the fast cooled DV shows low degrees of orientation at low strain rate. The orientation increases suddenly above 50 % strain with a much higher slope compared to the slow cooled sample, which grows gradually reaching a final value of 0.3 (see fig. 6.49b)). The final orientations of the fast cooled EPDM phase amount to 0.4. This and the starting point of orientation support the theory of heterogeneous deformation in the thermoplastic phase where the local stress overcomes the critical shear stress. Since the critical shear stress of the deformation of the mesomorphic iPP is much lower than the crystalline one the plastic flow takes place more enhanced allowing also the orientation of the distributed elastomer phase.

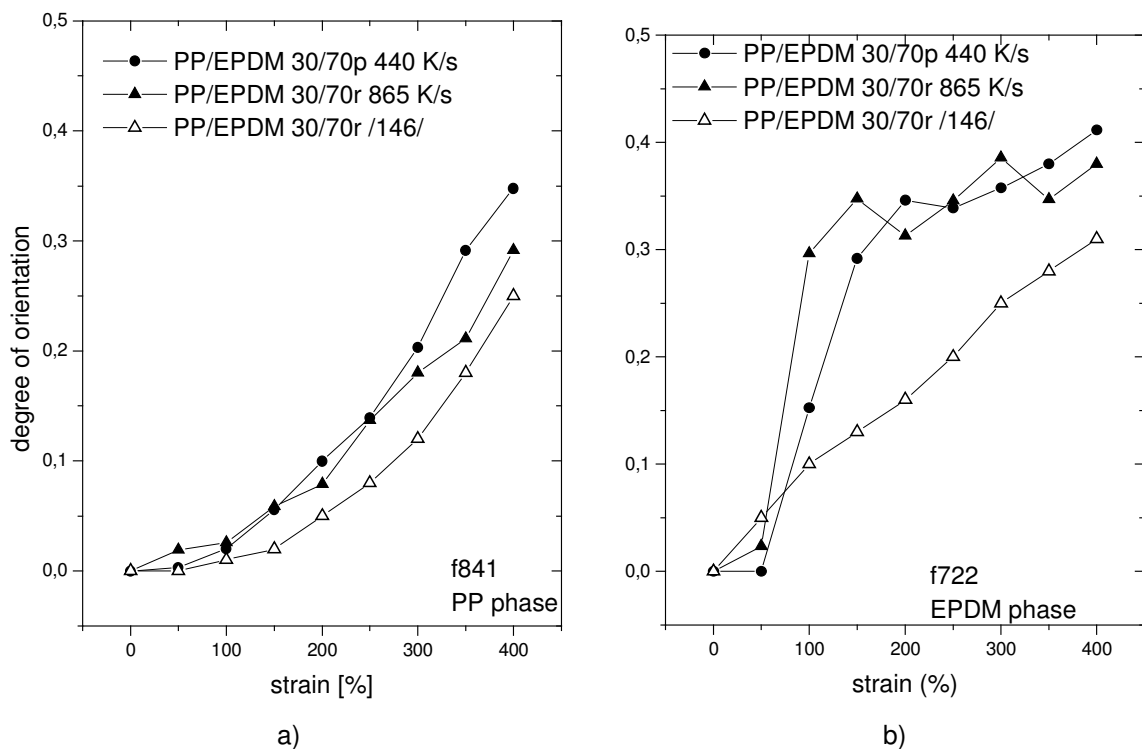


Fig. 6.49 Degree of orientation measured by FTIR rheoptical analysis of dynamic vulcanizates PP/EPDM 30/70p and r of a) the iPP matrix and b) the EPDM phase at indicated cooling rates.

The stress – strain behavior of DV with different iPP/EPDM ratios and amount of crosslinking agent

The tensile strength values of the DV differ depending on their components as well as on the crosslinking agent. In order to study this influence together with different cooling rates on tensile behavior series of DV based on PP/EPDM with varying EPDM content and amount of crosslinking agent phenolic resin have been prepared.

The stress-strain diagrams of the DV based on PP/EPDM crosslinked with 5 phr and varying PP/EPDM ratio are shown in figure 6.50. The test was performed only until 200 % strain because it was assumed that the stress – strain behavior is influenced more significant by cooling rates at low strain ratios. Strain hardening can be expected at higher strain ratio as it is typical for DV. With increasing EPDM content decreasing tensile strength can be noted. Similar findings for DV have been reported in literature [150,152] and were explained with the decreasing amount of iPP matrix and a connected lower degree of crystallinity. The fast cooled samples exhibit all lower tensile strength than the slowly cooled samples.

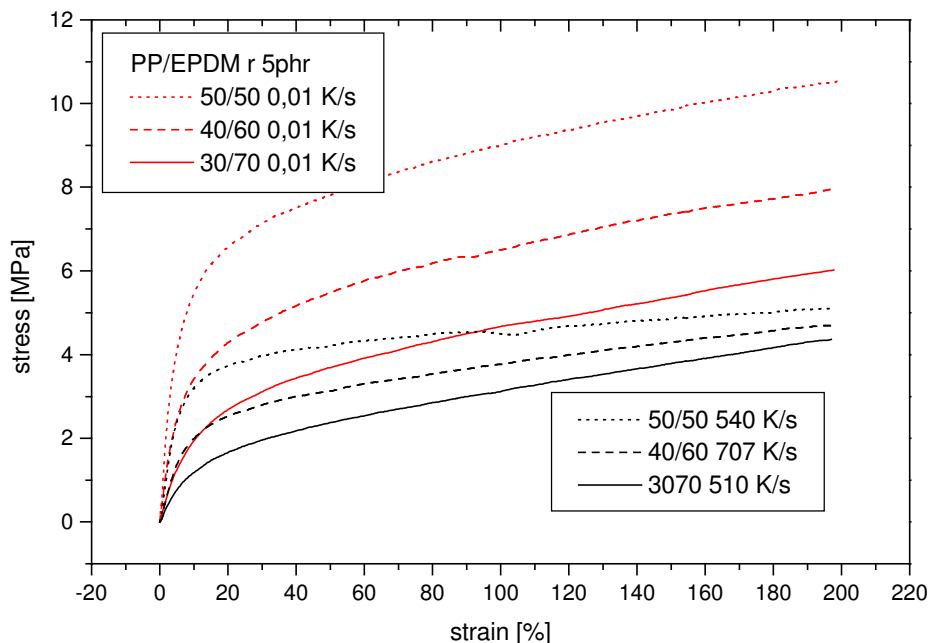


Fig. 6.50 Stress-strain diagrams of PP/EPDM r with different elastomer contents solidified at indicated cooling rates

The slope of stress values until 10 % strain, i.e. the elastic modulus at 10% strain, further referred to as $E_{10\%}$, and the stress values at indicated strains have been extracted from the stress - strain diagrams (fig. 6.50). These values are shown versus EPDM content in figure 6.51. The $E_{10\%}$ of the slow and fast cooled samples (fig. 6.51a)) show the same relationship with EPDM content as the microhardness in figure 6.44. The stress values until 50 % strain of the slowly cooled DV show a similar relationship. The fast cooled samples exhibit at strains of 200 % a different relationship; i.e. the change of stress with EPDM content is much lower than for the stress values of the slowly cooled samples (fig. 6.51b)). It is possible that due to the higher plastic deformability of the mesomorphic phase, as described above, the deformation of the enclosed rubber particles is less hindered. From rheoptical FTIR measurements it was shown that the ratio of α -monoclinic to mesomorphic phase is influencing the overall deformation behavior, i.e. also that of the rubber phase. Although these

measurements have not been performed for different amounts of elastomer content with varying cooling rates, it can be assumed that the deformation of the rubber phase is less hindered in the fast cooled case, which would explain the difference in slope at high strains.

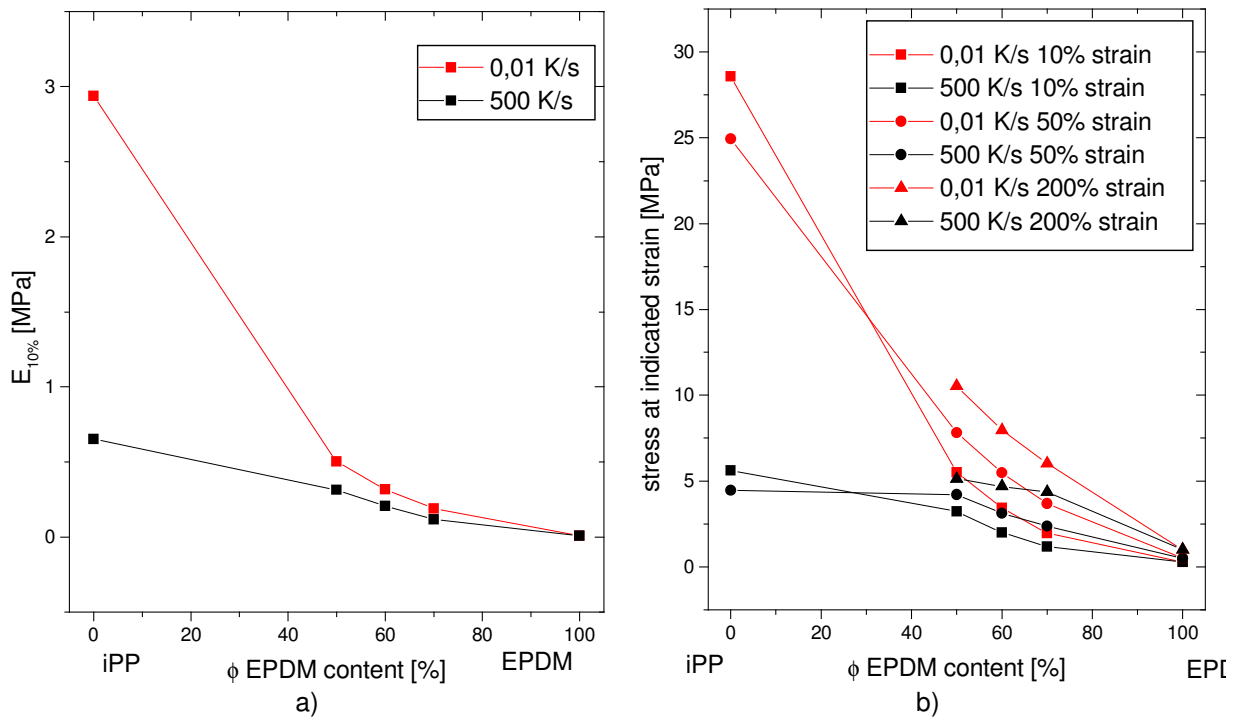


Fig. 6.51 Comparison between fast and slowly cooled DV: a) $E_{10\%}$ and b) stress at different strain vs. content of EPDM. The value of EPDM was taken from /152/.

The stress-strain diagrams of the DV based on PP/EPDM 30/70 crosslinked with varying amounts of phenolic resin as well as the blend are shown in figure 6.52. As observed by Huy /139/ the tensile strength and the elastic modulus increase with increasing amounts of crosslinking agents due to a higher chemical network density and the smaller particle size reached during dynamic vulcanization. Huy observed a higher degree of orientation in both iPP and EPDM phase with increasing amount of crosslinking agent. This was explained by higher stress on the local deformation unit in the iPP matrix caused by the higher stiffness of the rubber phase. Above approx. 30 % strain the stress values of the fast cooled samples increase with a similar slope than the slowly cooled samples starting from a lower point due to the lower starting moduli. The influence of cooling rate on the stress - strain behavior is not as intense as by changing the thermoplast content (fig. 6.50). Here the deformation of the DV takes place as a result of increasing chemical crosslinking density, whereas the physical crosslinking density remains as defined by cooling rates.

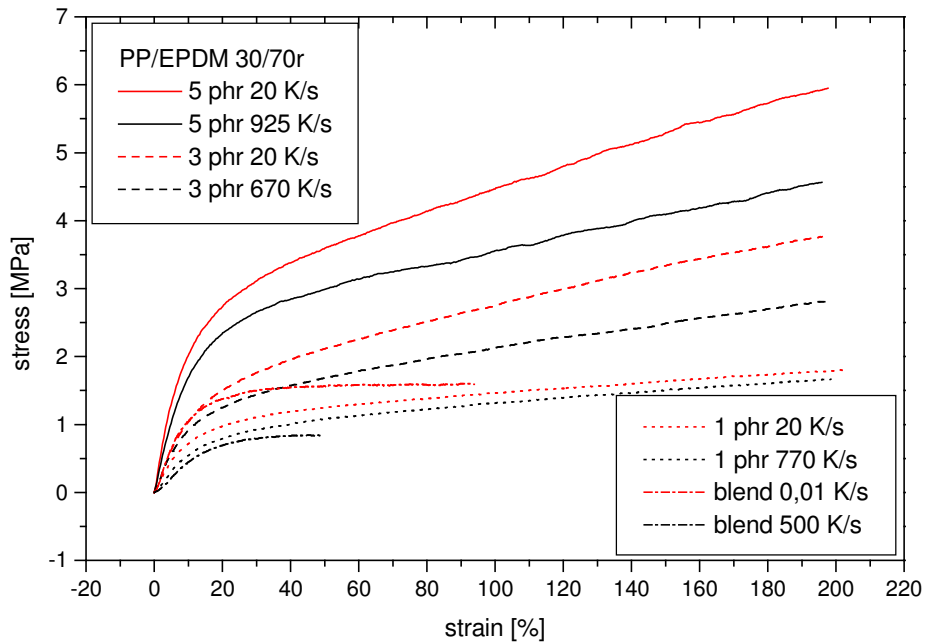


Fig. 6.52 Stress-strain diagrams of PP/EPDM 30/70r with different amount of crosslinking agent and the blend solidified at indicated cooling rates

However a significant change of curve shape between blend and crosslinked rubber phase can be noted. The influence of cooling rate on the stress - strain behavior of the blend with a co-continuous morphology is much higher than on the DV with an island-matrix-morphology. In the first case only the physical network points attribute to the deformation behavior. In the second case both, the chemical (crosslinking density in EPDM phase) and the physical network points (crystalline lamellae in the iPP matrix), influence the deformation behavior. Furthermore, the co-continuous blend morphology allows only maximum strains of break of 100 % in the slow and 40 % in the fast cooled state.

The irreversible deformation behavior

In order to determine the influence of the amount of thermoplastic content, the amount of crosslinking agent, and cooling rates on the irreversible deformation behavior of DV residual strain measurements have been performed as described in chapter 6.5.2. The residual strains vs. cooling rate for DV with different iPP content are shown in figure 6.53a). At low cooling rates the PP/EPDM 30/70p shows the lowest value of 35 % residual strain. The values increase with increasing amount of iPP. Similar values have been measured for the same DV by Le and Huy /148,152/. The residual strain values increase with increasing cooling rates approx. 10 %. This increase appears even stronger with increasing thermoplast content. This confirms that the reversibility of DV at high strains is determined mainly by the thermoplastic phase. The higher the amount of mesophase in the iPP matrix the lower the critical shear stress for deformation, as proven by rheoptical measurements, and the lower the work necessary for plastic deformation, as shown for PP/EOC30/70p (see chapter 6.6.6.1). Yang et al. /119/ determined the residual strain of PP/hSBR 50/50 blend quenched in different media reaching various crystal sizes in the iPP matrix. After passing a maximum of residual strain values of 60 % at low lamellae sizes the residual strain decreased reaching a local minimum

around 25 % at higher crystalline sizes between 10 and 15 nm. This means that the lamellae size influences the strain recovery.

The amount of crosslinking agent does not influence the amount of residual strain as much as the thermoplast content (see figure 6.53b)). The residual strain of the DV crosslinked by only 1 phr crosslinking agent is higher due to the very low degree crosslinking received. It has been observed by Huy /139/ that an increase of degree of chemical crosslinking increases the reversibility of a DV only until a certain amount reaching a plateau afterwards.

Various authors have proposed a so called two-network-theory to explain the influence of morphology of DV on the deformation behavior /103,148/. They proposed a thermally reversible network of crystall lamellae of the thermoplastic matrix, which exists parallel to the thermally stable chemical network of the rubber phase. Also Yang et al. /119/ proposed a network in the iPP matrix of a thermoplastic elastomer consisting of fragmented lamellae which would react as tie points to provide high strain recovery. The smaller and more disturbed are these crystallites, the easier they can be destroyed by bulk deformation rendering poor strain recovery.

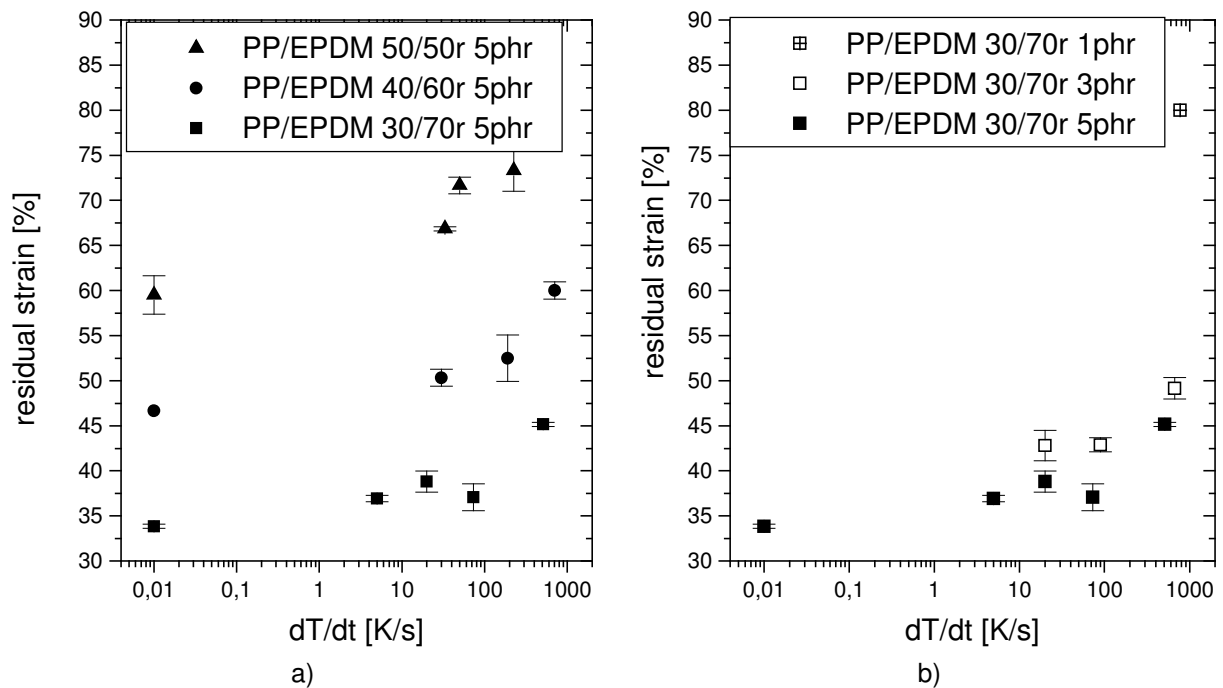


Fig. 6.53 Residual strain after deloading of PP/EPDM crosslinked by phenolic resin vs. indicated cooling rates depending on a) different amount of iPP content and b) different amount of crosslinking agent

7 Conclusions for the dimensioning of processing techniques of dynamic vulcanizates

Dynamic vulcanizates have shown in this work, that their structure and therefore their properties react less sensible to the processing parameter cooling rate. This is caused by the following reasons:

- 1.) Only the thermoplastic matrix iPP is affected by DV, while the rubber phase, forming the major phase fraction, remains unchanged due to its low degree of crystallinity.
- 2.) The formation metastable mesophase in favor of the stable α -phase occurs at higher cooling rates when compared to pure iPP.

The last fact plays a role in processing, e.g. an injection molding process, where cooling rates of approx. 100 K/s are reached on the outer wall of the molded part. At these cooling rates only a small fraction of metastable mesomorphic phase would be formed in the iPP matrix of the DV, whereas in pure iPP the stable α -phase would be replaced completely by the mesomorphic phase. When producing very thin parts applying cooling rates above 100 K/s the change in mechanical properties should not be neglected, which are lowered elastic moduli, consequently lower hardness values, and even more important, the less rubber-elastic behavior (which was shown in increasing residual strain values with increasing cooling rates). Positively, the specific volume change with cooling rates is for DV much lower with respect to pure iPP. Therefore DV provide less shrinking during cooling and less morphological gradients, which can cause internal stresses. The low change of specific volume with increasing cooling rates also widens the spectrum of mold design.

However, this positive conclusion for injection molding of pure DV must be reconceived in case of the multi-component injection molding. Multi-component injection molding, as special field of the injecting molding, is receiving more and more significance because elaborate stick, join, and mounting steps may be saved at the construction of multi-functional devices. Hard – soft - combinations are favored in industrial use. The injection molding of iPP combined with DV, with iPP as matrix-material, provides for a good bonding in this hard-soft combination. An example of this combination in a mold is shown in figure 7.1. In this example the iPP component and the DV component are shown on the left and the right side, respectively. The vertical black line in the middle indicates the bond between both materials. The thin curves represent the cooling rate vs. sample depth at 18°C mold temperature and the thick line at 80°C mold temperature.

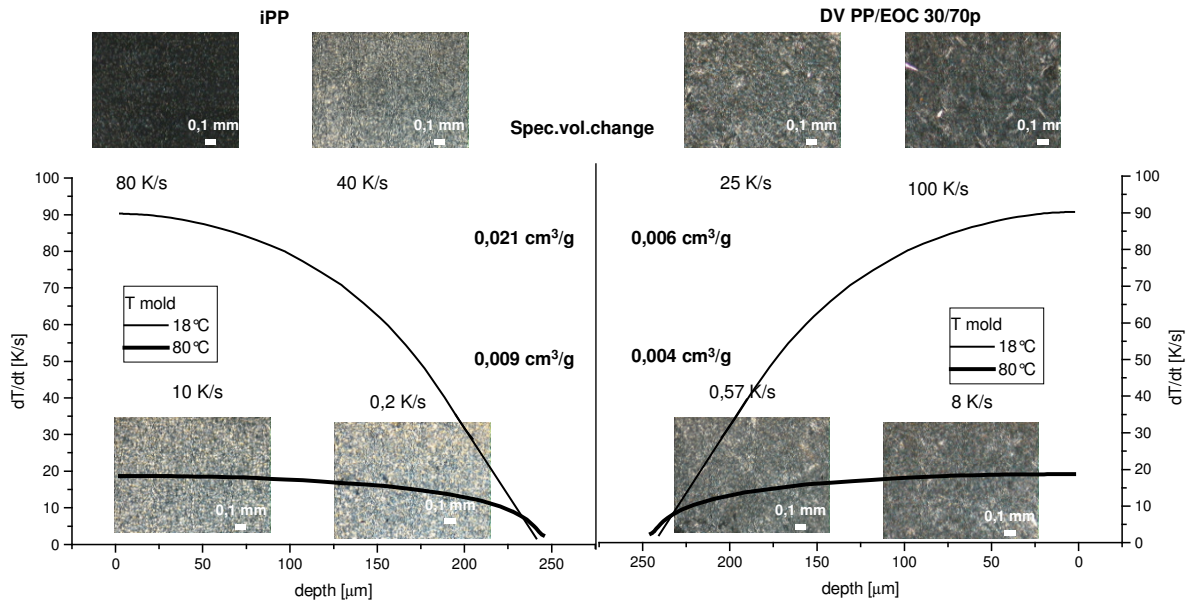


Fig. 7.1 Cooling rates vs. sample depth for two-component injection molded part consisting of iPP and PP/EOC 30/70p with different mold temperatures, showing micrographs obtained at indicated cooling rates and specific volume changes of each material.

The corresponding pictures show exemplarily the morphology of the two materials quenched at two different cooling rates corresponding to each curve; i.e. outside and inside of the part. It can be seen that with a mold temperature of 18°C in iPP an outer layer of mesomorphic phase appears whereas on the inside the α -crystalline phase has been formed. The results are mechanical property gradients and internal stresses. The DV side on the other hand shows similar morphologies on the outside and the inside providing more homogeneous properties. This can be reached for iPP only when a higher mold temperature is applied. Next to inhomogeneous morphology also the specific volume change can be a troubleshooter regarding shrinking. The specific volume change has been calculated from the density values of the materials at the cooling rates between outer and inner layer of the part. The specific volume change of the iPP part at the low mold temperature is 0.021 g/cm³ and of the DV only 0.006 g/cm³; i.e. the shrinkage due to cooling rates of the DV is approx. one third of the shrinkage in iPP causing internal stresses. In order to receive theoretically a similar shrinkage the mold part touching the iPP side should be cooled slower, for example at 80 °C than the DV side. However, this is true only neglecting the pressure dependence of the specific volume change and neglecting other processing parameters influencing the sample crystallinity as for example the injection speed. Another role, which is neglected here, plays the flow induced crystallization (FIC). Flow will enhance the kinetics of crystallization producing highly oriented phases, very often referred to as skin layer. This will counterbalance the effect of cooling on crystalline morphology resulting more in a more stable crystalline phase with respect to the mesophase decreasing the volume change. Due to its higher degree of crystallinity iPP will be influenced more by FIC when compared to DV.

8 Summary

The thermoplastic processability as one of the main advantages of DV when compared to conventional rubber requires a prediction of the effect of cooling rate as one major processing parameter on the final structure and properties of the part. This is important especially for the production of thin walled parts and profiles as used in automotive industry especially when

combined with other thermoplastic materials in multi – component injection molding where high temperature gradients are applied during processing.

The aim of this work was the description of the cooling process during DV processing, the structure formation in dependence on cooling rate, and finally the relationship between technological process conditions and the structure and properties of DV. An intensive cooling method where distinct cooling rates can be applied during the solidification of the material has been developed by Piccarolo et al. /3/. This method was already used to study the influence of fast cooling on the crystallization behavior of different semicrystalline polymers and was applied in this work on DV. The experimental investigations were performed on three DV prepared by dynamic vulcanization in a twin screw extruder, changing the type of elastomer, the type of crosslinking agent, and the amount of thermoplast content in order to observe their role in the development of structure and properties parallel influenced by cooling rates.

Morphological investigations of the pure components showed, that only iPP was influenced by cooling rates whereas the morphology of the copolymers EOC and EPDM showed to be uninfluenced by this processing parameter. The WAXD pattern of EOC and EPDM showed only a single reflection remaining the same for the samples solidified with different cooling rates. The WAXD pattern of iPP showed for slow cooling rates the typical α – monoclinic pattern, which was replaced by the mesomorphic pattern when going to higher cooling rates. In order to receive a numerical value of the amount of phases present in the material when cooled with different cooling rates a deconvolution technique has been applied as used by Martorana /79/. The phase content distribution of pure iPP vs. cooling rates diagrams showed at low cooling rates an equal amount of amorphous and α – monoclinic phase, both around 50%. Between 20 and 80 K/s the amount of α – monoclinic phase dropped to almost zero being at the same time replaced by the mesomorphic phase. This zone was named transition zone. At high cooling rates the values of all phase contents remained at stable levels with the amorphous phase taking up slightly more content than the mesomorphic phase.

The WAXD pattern of DV appeared as superposition of the copolymer and the iPP patterns. A visible change in the pattern with cooling rates was assigned only to the iPP pattern. The phase fractions vs. cooling rates of the iPP matrix of the DV showed a similar dependence on cooling rates in comparison to pure iPP. The mesomorphic phase replaced the α – monoclinic phase completely and the amorphous phase remained stable implying that the formation of mesomorphic phase at high cooling rates is favored with respect to the amorphous phase possibly do to the presence of the rubber phase. The drop of α – monoclinic phase in the iPP matrix of a DV is shifted to higher cooling rates, which was explained by the presence of crosslinked copolymer forming boundary layers giving rise to heterogeneous crystallization.

The density values of iPP and the DV depended on cooling rates in almost the same manner. Three zones (alpha, transition and mesomorphic zone) were indicated. In comparison to the density change of the bulk iPP the density change of the iPP matrix in DV it was found that the transition zone is shifted to higher cooling rates and wider. In other words, the iPP matrix of a DV which has been solidified at a cooling rate of 50 K/s appeared still α -crystalline while the bulk iPP solidified at the same cooling rate had already formed the mesomorphic phase. This implied the presence of a more stable α -crystalline form in DV. Even though the formation of perfect crystals was hindered by the rubber phase more stable crystals were formed due to enhanced heterogeneous crystallization on the phase boundaries between rubber and iPP. In the presence of additionally nucleating structures, as SnCl₂ in the PP/EPDM 30/70r, the transition zone extended even further to higher cooling rates.

AFM micrographs showed for PP/EPDM 30/70p the typical particle-matrix-morphology of DV. The size of the rubber particles seemed to be divided into larger particles of approx. $1\mu\text{m}$ and smaller particles of approx. $0.05\mu\text{m}$. The matrix of the slowly cooled samples showed cross-hatched lamellae surrounding the rubber particles. The phase image of the fast cooled sample showed a much lower contrast between the iPP matrix and the EPDM rubber phase indicating a lower hardness. In fact no crosshatched lamella were observed only very few lamellar structures of smaller dimensions.

Investigations of the thermal behavior of iPP and the DV showed a strong influence of the changed morphology due to cooling rate on thermal transitions. DSC scans of iPP showed with increasing cooling rates the formation of an exothermal area starting before the onset of endothermal melting. This small exothermal local maximum was assigned to reorganization processes of the mesomorphic phase taking place at elevated temperature. A peak of tan delta values from DMTA measurements of the fast cooled iPP samples, named meso-transition, different from the α -transition peak observed for the slowly cooled samples, supported this interpretation of melting of the mesomorphic phase and subsequent recrystallization. Similar results have been found for the DV although this reorganization peak in the DMTA data was partly superimposed by the softening of the copolymer phase. Tan delta peaks obtained by DMTA measurements of the DV showed a glass transition of EPDM around $-30\text{ }^{\circ}\text{C}$ and $-40\text{ }^{\circ}\text{C}$ in case of the EOC, being independent of cooling rates. As observed by DMTA measurements the β -transition or glass transition of the pure iPP as well as of the iPP matrix of the DV increased with growing cooling rates from $15\text{ }^{\circ}\text{C}$ to $25\text{ }^{\circ}\text{C}$. This was explained by a hindered segmental movement of the amorphous phase in the presence of immersed mesomorphic phase consistent of small, organized forms with low order. The slowly crystallized iPP instead contained distinct crystalline phases well separated from the amorphous regions allowing the movement of the amorphous phase to a greater extend.

DMTA measurements showed a strong dependence of storage modulus and cooling rates. The storage modulus of fast cooled iPP at room temperature was only half of the value of the slowly cooled sample. The storage moduli of the DV at room temperature appeared at a much lower level of only 3 % of the value measured for the pure iPP due to their morphology. Nevertheless, the storage moduli of the fast cooled DV amounted only to values of approx. 65 % of the storage moduli of the slowly cooled samples.

The dependence of storage moduli on cooling rates implied a strong connection between the thermal history and the mechanical behavior of the DV. Miniature tensile test showed an influence of cooling rates on the stress-strain behavior of iPP and DV. Generally lower stress values were reached at high cooling rates. The DV showed a more elastomeric behavior exhibiting lower tensile strength values than iPP. The addition of thermoplast to the DV resulted in higher tensile strength values, especially for the samples cooled at slow cooling rates. This supported the assumption that the tensile strength values depend directly on the amount of crystallinity. The stress values of samples solidified at high cooling rates did not show such a high influence of thermoplast content and reached the same level of stress at higher strain rates. Enhancing the chemical network density of the rubber phase by means of a higher amount of crosslinking agent increased the tensile strength values equally, i.e. also the fast cooled samples reached higher values except the blends, where only co-continuous morphology is present.

Rheoptical measurements on PP/EPDM 30/70r revealed that the iPP matrix showed a higher degree of orientation when solidified at higher cooling rates than at low cooling rates. This

was explained by heterogeneous deformation in the thermoplastic matrix where the local shear stress overcome a critical values being lower for the mesomorphic phase than for the α -monoclinic phase. Also the EPDM phase of the fast cooled samples was oriented to a much higher degree than the slowly cooled sample. The critical shear stress of the deformation of the mesomorphic phase of iPP is much lower than of the α -phase. The plastic flow is more enhanced allowing also the orientation of the distributed elastomer phase.

DV showed less reversibility when solidified at high cooling rates. The higher values at high cooling rates implied a higher amount of plastic deformation of the iPP matrix due to the increased amount of mesomorphic phase. The work of irreversible deformation was lower at high cooling rates, which means the work necessary to deform the mesomorphic phase plastically is lower than for the α -monoclinic phase. The reversible work of deformation did not depend on cooling but was influenced by the chemical crosslinking density of the elastomer phase. These observations were supported by the rheoptical measurements of the orientation of the individual phases. A two - network-model was used to explain the deformation behavior of DV. One network consists of physical network points in shape of crystalline structures, being therefore dependent on the type and amount of crystalline form. The second network is formed by chemical stable network points. Both networks contribute to the deformation and reversibility of a DV.

The microhardness dependence on cooling rates was similar to the dependence of density vs. cooling rate. The microhardness of DV showed a negative exponential dependence on amount of thermoplast content. Based on the data of polymorphic phase content from WAXD microhardness values have been determined for each phase and subsequently summed up to obtain the total microhardness values. These values placed in the exponential equation to describe the influence of thermoplast content gave the possibility to predict microhardness values for a range of cooling rates for different amounts of rubber.

The method of intensive cooling from the melt as developed by Piccarolo et al. /3/ proved to be applicable also for DV in order to determine the influence of cooling rate as one parameter of thermoplastic processing on the crystallization behavior and subsequent morphology development. The rubber phase of the DV used in this study was not influenced by the cooling rate. Nevertheless this cannot be excluded for different rubbers with a higher degree of crystallinity. Further investigations must be performed to clear this aspect. The effect of cooling rates on DV was originated in the iPP matrix and its interaction with the rubber phase. The total changes of properties with cooling rate were much lower in DV than in pure iPP due to the small thermoplast content. However, there is a considerable influence of cooling rate on the mechanical properties. This study gives the possibility to predict property changes in DV according to the applied cooling rates during processing, as shown for a example of bi-component molding of iPP and DV. In order to receive similar specific volume changes in order to lower warpage, lower cooling rates should be applied on the iPP cavity wall with respect to the DV cavity wall. Finally it must be made clear that cooling rates are one of several parameters influencing the final part structure and properties, such as pressure and flow rate. The influence of these parameters in connection with cooling rates on structure and properties of a DV must be investigated in the future.

9 Zusammenfassung

Die thermoplastische Verarbeitbarkeit ist einer der Vorteile von Dynamischen Vulkanisaten (DV) gegenüber herkömmlichen vollvernetzten Gummis. Die Vorhersage über den Einfluss

der Kühlrate aus der Schmelze auf die finale Struktur und Eigenschaften des herzustellenden Teils ist daher von großer Bedeutung. Dies ist wichtig bei der Produktion von dünnwandigen Teilen und Profilen, die in der Automobilindustrie Anwendung finden, vor allem in Kombination mit anderen Thermoplasten im Multi – Komponenten – Spritzguss, wo hohe Temperaturgradienten zwischen Kavitätswand und –innerem auftreten.

Das Ziel dieser Arbeit bestand in der Beschreibung des Ablaufes von Kühlvorgängen während der Verarbeitung von DV, der Strukturbildung in Abhängigkeit von der Kühlrate und abschließend der Beziehung zwischen technologischen Prozessgrößen und den Struktur – Eigenschafts - Beziehungen der DV. Eine Intensivkühlmethode wurde von Piccarolo et al. /3/ entwickelt, bei der Polymerproben mit definierten Abkühlraten aus dem Schmelze- in den festen Zustand überführt werden können. Diese Methode wurde bereits erfolgreich angewandt, um den Einfluss der Intensivkühlung auf das Kristallisationsverhalten verschiedener teilkristalliner Kunststoffe zu untersuchen und wurde hier nun für dynamische Vulkanisate verwendet. Die experimentellen Untersuchungen wurden an verschiedenen DV durchgeführt, die durch dynamische Vulkanisation in einem Doppelschneckenextruder hergestellt wurden. Dabei wurden das iPP/Elast – Verhältnis, sowie die Art der Elastomerkomponente (EOC und EPDM) und des Vernetzersystems variiert, um ihren Einfluss zusammen mit dem Einfluss der Kühlrate auf die Strukturbildung und die Eigenschaften zu untersuchen.

Morphologieuntersuchungen der Ausgangskomponenten zeigten, dass ausschließlich das iPP durch Kühlraten beeinflusst wird, während die Morphologie der Copolymere EOC und EPDM unverändert blieb. Die WAXD – Beugungsdiagramme von EOC und EPDM zeigten ein Maximum gleichbleibend bei allen Kühlraten. Die Röntgenbeugungsdiagramme des iPP zeigten bei niedrigen Kühlraten das für die α – monokline Phase typische Beugungsmuster, welches bei höheren Kühlraten von dem für die mesomorphe Phase typischen Beugungsmuster abgelöst wurde. Um eine quantitative Aussage über die polymorphen Phasenanteile in Abhängigkeit von der Kühlrate zu erhalten, wurde eine Deconvolutionstechnik angewandt in Anlehnung an Martorana /79/. Die Phasenverteilung in iPP zeigte bei niedrigen Kühlraten das Vorhandensein von gleichen Teilen amorpher zu α – monokliner Phase, beide um ca. 50%. Zwischen 20 und 80 K/s fällt der Anteil der α – monoklinen Phase auf null und wird gleichzeitig von der mesomorphen Phase ersetzt. Diese Zone wurde als Übergangszone bezeichnet. Bei höheren Kühlraten veränderten sich die Phasenanteile kaum noch. Nur der Anteil der amorphen Phase nahm noch gering zu.

Die Röntgenbeugungsdiagramme der DV zeigten eine Überlagerung der Beugungsmuster der Copolymere und des iPP. Eine sichtbare Änderung der Beugungsdiagramme mit der Kühlrate wurde ausschließlich durch die iPP Phase hervorgerufen. Die Phasenanteile der iPP – Matrix der DV zeigten eine ähnliche Abhängigkeit von der Kühlrate wie das reine iPP. Die mesomorphe Phase ersetzte die α – monokline Phase vollständig, während die amorphe Phase gleich blieb. Dies implizierte, dass sich die mesomorphe Phase, verglichen mit der amorphen Phase, in der iPP – Matrix der DV bei hohen Kühlraten bevorzugt bildet, vermutlich verursacht durch das Vorhandensein der Elastphase. Der Übergang von α – monokliner Phase zur mesomorphen Phase in der iPP – Matrix von DV zeigte sich zu höheren Kühlraten verschoben. Dafür verantwortlich ist heterogene Kristallisation durch Keimbildung an den Grenzflächen der vernetzten Copolymerphase.

Die Dichten des iPP und der DV zeigen eine ähnliche Kühlratenabhängigkeit, die in drei Abschnitte (Zone der α -Phase, Übergangszone, Zone der mesomorphen Phase) eingeteilt werden konnte. Im Vergleich zum Dichteverlauf des reinen iPP ist im Dichteverlauf des DV

die Übergangszone breiter und zu höheren Kühlraten verschoben, verursacht durch die Bildung einer stabileren Kristallstruktur aufgrund von Phasengrenzen. Mit anderen Worten, die iPP – Matrix des DV, die mit 50 K/s abgekühlt wurde, zeigte noch die α – kristalline Phase, während im reinen iPP, mit gleicher Kühlrate gekühlt, bereits die mesomorphe Phase vorhanden war. Daraus abgeleitet wurde das Vorhandensein einer stabileren α – kristallinen Phase im DV. Obwohl die Bildung von perfekten Kristallen durch die Elastphase behindert wurde, bildeten sich stabilere Kristalle aufgrund von heterogener Kristallisation an den Phasengrenzen. Das Vorhandensein von zusätzlich als Nukleierungsmittel wirkenden Substanzen, wie das SnCl_2 im PP/EPDM 30/70r, bewirkte eine Verbreiterung des Übergangsbereiches hin zu noch höheren Kühlraten.

AFM – Aufnahmen zeigten für PP/EPDM 30/70p die für DV typische Insel – Matrix – Morphologie. Die Größe der Elastpartikel konnte in zwei Bereiche geteilt werden, in größere um 1 μm und kleinere um 0,05 μm . Die iPP - Matrix der langsam gekühlten Probe zeigte „cross - hatched“ Lamellen, welche die Elastpartikel umschlossen. Das Phasenbild der schnell gekühlten Probe zeigte einen geringeren Kontrast zwischen der iPP - und der EPDM – Phase, was auf eine geringere Härte der iPP – Matrix hindeutete. Es konnten auch keine „cross - hatched“ Lamellen festgestellt werden, lediglich eine kleine Anzahl von Lamellen mit geringeren Ausmaßen.

Die Untersuchungen des thermischen Verhaltens des iPP und der DV zeigten einen großen Einfluss der durch Kühlraten geänderten Morphologie auf die thermischen Umwandlungspunkte. Der erste DSC – Heizlauf des gekühlten iPP zeigte mit steigender Kühlrate die Herausbildung einer exothermen Zone, vor Beginn der endothermen Schmelzzone. Dieses schmale exotherme Maximum konnte den Umordnungsprozessen der mesomorphen Phase zugeordnet werden, die bei höheren Temperaturen stattfanden. Ein Peak der $\text{Tan } \delta$ - Temperatur - Kurve aus den DMTA Untersuchungen des schnell gekühlten iPP wurde als meso – Umwandlung bezeichnet und zeigte eine andere Temperaturlage als die α – Umwandlung, die bei langsam gekühlten iPP festgestellt wurde. Dies unterstützt die Interpretation vom Schmelzen der mesomorphen Phase mit anschließender Reorganisation. Ähnliche Ergebnisse wurden auch bei DV festgestellt. Dabei wurde jedoch der Reorganisationspeak im DMTA durch das Erweichen der Copolymerphase überlagert. $\text{Tan } \delta$ - Temperatur - Kurven aus den DMTA Untersuchungen der DV zeigten einen Glasübergang von EPDM bei $-30\text{ }^\circ\text{C}$ und von EOC bei $-40\text{ }^\circ\text{C}$, unabhängig von der Kühlrate. DMTA Untersuchungen zeigten, dass der Glasübergang von reinem iPP sowie der iPP – Matrix des DV mit steigenden Kühlraten von $15\text{ }^\circ\text{C}$ zu $25\text{ }^\circ\text{C}$ verschoben wird. Der Grund dafür liegt in einer Behinderung der Segmentbewegungen der amorphen Phase durch die darin verteilte mesomorphe Phase, die einen geringen Ordnungsgrad zeigt. Das langsam kristallisierte iPP hingegen besteht aus ausgeprägten kristallinen Phasen, die besser von der amorphen Phase getrennt sind und dadurch deren Bewegung weniger einschränken.

DMTA Untersuchungen zeigten eine starke Abhängigkeit der Speichermoduln von der Kühlrate. Der Speichermodul des schnell gekühlten iPP war bei Raumtemperatur nur halb so groß, wie der des langsam gekühlten iPP. Die Speichermoduln des DV lagen aufgrund ihrer Morphologie bei Raumtemperatur deutlich niedriger, bei nur 3% des Wertes des reinen iPP. Die Speichermoduln der schnell gekühlten DV betragen nur 65 % des Wertes der langsam gekühlten DV.

Die hohe Kühlratenabhängigkeit der Speichermoduln ließ eine starke Verbindung zwischen der thermischen Geschichte und des mechanischen Verhaltens des DV erwarten. Die Miniaturzugprüfung ergab einen Einfluss der Kühlrate auf das Spannungs –

Dehnungsverhalten des iPP und des DV. Generell wurden bei höheren Kühlraten geringere Zugspannungen erreicht. Die DV zeigten ein eher gummiartiges Verhalten mit geringeren Zugfestigkeiten als das reine iPP. Die Erhöhung des Thermoplastanteils im DV ergab höhere Zugfestigkeitswerte, speziell für langsam gekühlte Proben. Dies unterstützte die Annahme, dass die Zugfestigkeit direkt vom Kristallinitätsgrad abhängig ist. Die Zugfestigkeit der schnell gekühlten Proben zeigte eine geringere Beeinflussung durch den Thermoplastanteil und erreichte die gleichen Spannungen bei höheren Dehnungsraten. Eine Erhöhung der chemischen Netzwerkdichte der Elastphase durch Erhöhung des Vernetzungsmittels bewirkte eine gleichwertige Erhöhung der Zugfestigkeit; d. h. auch die schnell gekühlten Proben erreichten höhere Werte.

Rheooptische Untersuchungen von PP/EPDM 30/70r zeigten, dass die iPP – Matrix bei hohen Kühlraten einen höheren Orientierungsgrad aufwies als bei langsameren Kühlraten. Dies wurde erklärt durch eine heterogene Deformation der thermoplastischen Matrix, bei welcher die lokalen Spannungen die kritischen Spannungen überschreiten, die bei der mesomorphen Phase niedriger sind als bei der α – kristallinen Phase. Auch die EPDM – Phase der schnell gekühlten Probe erreichte höhere Orientierungsgrade als die der langsam gekühlten Probe. Die für die Deformation benötigte kritische Schubspannung der mesomorphen Phase des iPP war viel geringer als die der α – kristallinen Phase. Das plastische Fließen wurde verstärkt und erlaubte damit ebenfalls die Orientierung der darin eingebetteten Elastomerteilchen.

Die DV zeigten bei höheren Kühlraten eine geringere Reversibilität. Dies ließ bei höheren Kühlraten einen höheren plastische Deformationsanteil der iPP – Matrix erwarten, verursacht durch den höheren Anteil an mesomorpher Phase. Die irreversible Verformungsarbeit war geringer bei höheren Kühlraten, d. h. die für die Deformation der mesomorphen Phase benötigte Arbeit war geringer als für die α – kristalline Phase. Die reversible Arbeit der Deformation zeigte sich nicht von der Kühlrate abhängig, jedoch abhängig von der chemischen Vernetzungsdichte der Elastphase. Dies wurde unterstützt durch die Ergebnisse der rheooptischen Messungen zur Orientierung der einzelnen Phasen. Ein Zwei – Netzwerk – Modell wurde verwendet, um das Deformationsverhalten der DV zu erklären. Ein Netzwerk besteht aus den physikalischen Netzwerkknoten in Form von kristallinen Strukturen und hängt demnach vom Typ und Anteil der kristallinen Phase ab. Das zweite Netzwerk besteht aus chemischen Netzknoten. Beide Netzwerke sind am Deformationsverhalten und der Reversibilität der DV beteiligt.

Die Abhängigkeit der Mikrohärtigkeit des PP/EOC 30/70p von den Kühlraten war der Kühlratenabhängigkeit der Dichte ähnlich. Die Mikrohärtigkeit des DV zeigte eine negative exponentielle Abhängigkeit vom Thermoplastanteil in DV. Basierend auf den Daten der polymorphen Phasenanteile aus den WAXD Messungen konnten Mikrohärtewerte für jede Phase bestimmt und anschließend addiert werden, um die absoluten theoretischen Mikrohärtewerte bei bestimmten Kühlraten zu berechnen.

Die Methode des intensiven Kühlens aus der Schmelze, die von Piccarolo et al. /3/ entwickelt wurde, zeigte sich anwendbar für DV, um den Einfluss der Kühlrate, als wichtigen Verarbeitungsparameter, auf das Kristallisationsverhalten und damit die Morphologiebildung zu bestimmen. Die Elastphase der in dieser Arbeit verwendeten DV wurde nicht von der Kühlrate beeinflusst. Dies kann jedoch nicht für andere Elastomere mit höherem Kristallinitätsgrad ausgeschlossen werden. Hier sind weitere Untersuchungen nötig. Der Einfluss der Kühlrate auf DV beschränkte sich auf die iPP – Matrix, sowie deren Zusammenwirken mit der Elastphase. Die absoluten Änderungen der Eigenschaften mit der Kühlrate sind aufgrund des geringen Thermoplastanteils wesentlich geringer in DV als in

reinem iPP. Es besteht jedoch ein nicht zu vernachlässigender Einfluss der Kühlrate auf die mechanischen Eigenschaften. Diese Arbeit gibt die Möglichkeit, die Eigenschaftsänderungen in DV vorherzusagen, die durch die bei der Verarbeitung angewandten Kühlraten hervorgerufen werden, wie am Beispiel eines Zwei – Komponenten – Spritzgussteils, bestehend aus iPP und DV, gezeigt wurde. Um ähnliche spezifische Volumenänderungen zu erreichen, um heterogenes Schwinden zu verhindern, sollten in diesem Fall an der iPP - Kavitätswand geringere Kühlraten verwendet werden als an der DV – Kavitätswand. Abschließend muss jedoch gesagt werden, dass Kühlraten nur einer von verschiedenen Parametern ist, welche die finalen Eigenschaften des Produkts beeinflussen. Der Einfluss dieser Parameter wie z. B. der Druck und die Fließgeschwindigkeit in Zusammenhang mit der Kühlrate auf die Struktur und die Eigenschaften von DV sollte Gegenstand zukünftiger Untersuchungen sein.

10 List of symbols

Abbreviations

AFM	atomic force microscopy
ASTM	american standard test method
C	carbon
C3	methyl group
DCP	dicumylperoxyde
DCPD	dicyclopentadiene
DMTA	dynamic mechanical thermal analysis
DSC	differential scanning calorimetry
DV	dynamic vulcanizate
E/P-ratio	ethylene/propylene ratio
ENB	ethylidene norbonene
ENDO	endothermal region in DSC thermogram
EOC	ethylene-octene copolymer
EPDM	ethylene-propylene-diene terpolymer
EPM	ethylene-propylene rubber
EPR	ethylene-propylene rubber
EXO	exothermal region in DSC thermogram
FIC	flow induced crystallization
FTIR	fourier transformed infrared spectroscopy
HD	hexadiene
HDPE	high density polyethylene
hSBR	hydrogenated styrene-butadiene rubber
iPP	isotactic polypropylene
IR	infrared spectroscopy
KJMA	Kolmogorov-Johnson-Mehl-Avrami
L/D	length/diameter ratio
LCST	lower critical solution temperature
LPE	linear polyethylene
MFR	melt flow ratio

MH	microhardness
p	peroxidic crosslinked
PA	polyamide
PA6	polyamide 6
PE	polyethylene
PET	polyethyleneterephthalate
POLMI	polarized optical light microscopy
PP	polypropylene
r	resin crosslinked
SALS	small angle light scattering
SAXD	small angle x-ray diffraction
SD	spinodal decomposition
TEM	transmission electron microscopy
TMDSC	temperature modulated differential scanning calorimetry
TPE	thermoplastic elastomer
TPE-A	TPE based on polyether(ester)-polyamide
TPE-E	TPE based on copolyester
TPE-O	TPE based on a blend with a non-crosslinked rubber phase
TPE-S	TPE based on styrene-block copolymers
TPE-U	TPE based on polyurethane
TPE-V	TPE based on a blend with a crosslinked rubber phase
WAXD	wide angle x-ray diffraction

Indices

a	amorphous phase
α	alpha-monoclinic phase
c	crystalline phase
DV	dynamic vulcanizate
EOC	ethylene-octene copolymer phase
iPP	isotactic polypropylene phase
m	mesomorphic phase
PP	polypropylene phase

Symbols

2Θ	Braggs angle
a	shift factor
A_{\parallel}	absorption of parallel oriented radiation
A_{\perp}	absorption of vertical oriented radiation
b_0	thickness of one monolayer of molecules
χ	crystalline fraction
c	constant
d	diagonal of indentation
D	dichroic ratio

D_0	dichroic ratio at perfect order
dT/dt	cooling rate
E''	loss modulus
E'	storage modulus
$E_{10\%}$	elastic modulus at 10% strain
E_a	activation energy
f	frequency
F	force
f	heat of fusion per unit volume
γ	shear velocity
G	growth rate
G_0	pre exponential growth rate
G_{0n}	pre exponential nonisothermal growth rate
G_n	nonisothermal growth rate
η	viscosity
I	intercept
k	crystallization constant
K	constant
K_{eff}	parameter of modified nucleation and growth
K_g	constant of crystallization regime
m	constant of nucleation and morphology
MH	microhardness
MWD	molecular weight distribution
n	constant of dimension of growth
O	degree of orientation
p	pressure
phr	per hundred rubber
Q	heat of exothermic transition
ρ	density
R	gas constant
r_{en}	nonisothermal spherulite radius
ρ_{fit}	fit of density
S	slope
τ	shear stress
t	time
T'	constant cooling rate
t_0	start time
T_m^0	equilibrium melting temperature
T_∞	temperature of crystallization finish
$\tan \delta$	loss factor
T_c	crystallization temperature
T_g	glass transition temperature

T_m	melting temperature
T_{max}	maximum temperature of a certain transition region
T_{onset}	start temperature of a certain transition region
U^*	activation energy of diffusion of growth front
W_{irrev}	irreversible work of deformation
W_{rev}	reversible work of deformation
W_{total}	total work of deformation
$X(T)$	transformed volume section at a temperature
X_c	degree of crystallinity
ΔE_a	change of activation energy
ΔG_b	surface free energy
Δh_f	heat of fusion
ΔH_f^{PP}	melting enthalpy of iPP
ΔH_f^{PP0}	melting enthalpy of iPP of 100 % crystallinity
ΔH_f^R	melting enthalpy of rubber phase
ΔH_f^{R0}	melting enthalpy of rubber phase of 100 % crystallinity
$\Delta \rho_{total}$	total change of density
$\Delta \rho_{transition}$	total change of density during transition
ΔT	undercooling
ϵ_{end}	elongation at start of deloading
ϵ_r	residual elongation
ϵ_{start}	elongation at end of deloading
μ_v	difference in bulk free energy
σ_a	interfacial free energy per unit area of the (110)
σ_b	interfacial free energy per unit area of the (100)
φ	phase fraction
φ_w	phase fraction by weight

11 Literature

- 1 Thermoplastische Elastomere – Herausforderung an die Elastverarbeiter, VDI-Gesellschaft Kunststofftechnik, Düsseldorf, 1997
- 2 A.Y. Coran, R.P. Patel, Thermoplastic Elastomers based on dynamically vulcanized elastomer-thermoplastic blends. in: Thermoplastic Elastomers, G. Holden, N.R. Legge, R. Quirk und H.E. Schroeder, Hanser/Gardner, New York, 1996
- 3 V. Brucato, S. Piccarolo, V. La Carruba, An experimental methodology to study polymer crystallization under processing conditions. The influence of high cooling rates, Chemical Engineering Science, 57 (2002), 4129-4143
- 4 G. Holden, Understanding thermoplastic elastomers, Hanser, Munich, 2000
- 5 K. Gebert, TPE-Einsatz in der Automobilindustrie: Gestern, heute, morgen. in TPE in der Prozesskette, VDI-Gesellschaft Kunststofftechnik, VDI-Verlag, Düsseldorf, 2002
- 6 K. Jürdens; The pan-European strategic market study TPE 2000. in:TPE in der Prozesskette, VDI-Gesellschaft Kunststofftechnik, VDI-Verlag, Düsseldorf, 2002
- 7 A.M. Gessler, W.H. Haslett, (to Esso Research and Engineering Co.) US Patent 3,037,954, June 5, 1962
- 8 R. Holzer, O. Taunus, K. Mehnert (to Hercules Inc.) US Patent 3,262,992, Juli 21, 1966
- 9 W.K. Fischer (to Uniroyal,Inc.) US Patent 3,758,643, September 11, 1973
- 10 W.K. Fischer (to Uniroyal,Inc.) US Patent 3,806,558, September 11, 1973
- 11 A.Y. Coran, B. Das, R.P. Patel, (to Monsanto Co.), US Patent January 19, 1982
- 12 M. Raetzsch, A. Hesse, N. Reichelt, H. Bucka, H. Heinemann, M. Stolp, H.-J. Radusch, (to Borealis), Patent AT000000265495E, November 03, 1998
- 13 H.-J. Radusch, T. Pham, Morphologiebildung in dynamisch vulkanisierten PP/EPDM-Blends, Kautschuk Gummi Kunststoffe, 49 (1996) 249-257
- 14 S. Abdou-Sabet, R.C. Puydak, C.P. Rader, Dynamically Vulcanized Thermoplastic Elastomers, Rubber Chemistry and Technology, 69 (1996) 476-494
- 15 E. Lämmer, Morphologiebildung und Eigenschaften dynamischer Vulkanisate auf Basis von Kautschuk-Propylen-Blends, Dissertation, Martin-Luther-Universität Halle-Wittenberg, 1993
- 16 T. Marinovic, Z. Susteric, I. Dimitrievski, Z. Vekšli, Dynamic Vulcanization of PP-EPDM blends – Effect of crosslinking degree on properties of TPV, Kautschuk Gummi Kunststoffe, 51 (1998) 189-193
- 17 H.-J. Radusch, Th. Lüpke, St. Poltersdorf, E. Lämmer, Dynamic Vulcanizates on the Basis of Polypropylene/Rubber Mixtures, Kautschuk Gummi Kunststoffe, 43 (1990) 767-769
- 18 M. Fedke, Reaktionen an Polymeren, VEB Dt. Verlag für Grundstoffindustrie, Leipzig, 1985
- 19 A. Sengupta, B.B. Konar, Cure Characteristics of Ethylene Propylene Diene Rubber-Polypropylene Blends. I. Calculation of State of Cure in Blends Containing Conventional Sulfur Curing System Under Variable Time-Temperature Conditions, Journal of Applied Polymer Science, 66 (1997) 1231-1236
- 20 A. Chapiro, Radiation Chemistry of Polymeric Systems, Interscience Publisher, New York, 1962
- 21 R.O. Bolt, J.G. Carroll, Radiation Effects on Organic Materials, Academic Press, London, 1963
- 22 T. Zaharescu, R. Setnescu, S. Jipa, T. Setnescu, Radiation Processing of Polyolefin Blends.I. Crosslinking of EPDM-PP blends, Journal of Applied Polymer Science, 77 (2000) 982-987

- 23 H.G. Fritz, Q. Cai, U. Bölz, Zweiphasige thermoplastischer Elastomere, *Kautsch. Gummi Kunststoffe*, 52 (1999) 4, 272-281
- 24 W. Hofmann, *Vulkanisation und Vulkanisationshilfsmittel*, Verlag Berliner Union, Stuttgart, 1965
- 25 T. Kempermann, Schwefelfreie Vulkanisationssysteme für Dienkautschuke, *Kautschuk Gummi Kunststoffe*, 40 (1987) 741-751
- 26 H.G. Dikland, Influence of chemical composition and molecular structure of EPDM on peroxide crosslinking efficiency, *Kautschuk Gummi Kunststoffe*, 49 (1996) 413-417
- 27 W. Hoffman, Vernetzungsmittel in Ethylene-Propylene-Kautschuk, *Kautschuk Gummi Kunststoffe*, 40 (1987) 308-332
- 28 M. Reuter, G. Streit, EPDM-Werkstoffe – ein Vergleich herkömmlicher und neuer Polymerisationstechnik, *Gummi Fasern Kunststoffe*, 50 (1997) 201-209
- 29 M.Baba, J.-L. Gardette, J. Lacoste, Crosslinking on aging of elastomers: I. Photoageing of EPDM monitored by gel, swelling and DSC measurements, *Polymer Degradation and Stability*, 63 (1999) 1, 121-126
- 30 D. Bacci, R. Marchini, M.T. Scrivani, Peroxide Crosslinking of Ziegler-Natta Thermoplastic Polyolefins, *Polymer Engineering and Science*, 44 (2004) 131-140
- 31 D.C.V. Bassett, R.H. Olley, On the lamellar morphology of isotactic polypropylene spherulites, *Polymer* 25 (1984) 935-943
- 32 M. Fujiyama, T. Wakino, Distribution of higher-ordered structures in injection mouldings of particulate-filled polypropylene, *Journal of Applied Polymer Science*, 43 (1991) 97-128
- 33 R. Phillips, G. Herbert, J. News, M. Wolkowicz, High modulus polypropylene: Effect of polymer and processing variables on morphology and properties, *Polymer Engineering and Science*, 34 (1994) 1731-1743
- 34 R.A. Phillips, M.D. Wolkowitz, Structure and Morphology. in: *Polypropylene Handbook*, Ed. E.P. Moore Jr., Hanser, München, 1996
- 35 J.J. Janimak, S.Z.D. Cheng, A. Zhang, E.T. Hsieh, Isotacticity effect on crystallization and melting in polypropylene fractions: 3. Overall crystallization and melting behaviour, *Polymer*, 33 (1992) 728-735
- 36 C.A. Hieber, Correlations for the quiescent crystallization kinetics of isotactic polypropylene and poly(ethylene)terephthalate, *Polymer*, 36 (1995) 1455-1468
- 37 W. Brostow, N. D'Souza, H. Galina, A.C. Ramamurthy, Nonisothermal Thermophysical Evaluation of a Polypropylene + Ethylene Propylene Diene (EPDM) blend, *Polymer Engineering and Science*, 36 (1996) 1101-1106
- 38 J.D. Hoffmann, G.T. Davis, J.I. Lauritzen, *Tratis on solid state chemistry*, Ed. N.B. Hannay, Plenum Press, New York (1976)
- 39 J.D. Hoffmann, Role of reptation in the rate of crystallization of polyethylene fractions from the melt. *Polymer*, 23 (1982) 656-670
- 40 J.D. Hoffmann, Regime III crystallization in melt-crystallized polymers: The variable cluster model of chain folding, *Polymer*, 24 (1983) 3-26
- 41 J.D. Hoffmann, R.L. Miller, Test of reptation concept: crystal growth rate as function of molecular weight in polyethylene crystallized from the melt. *Macromolecules*, 21 (1988) 3038-3051

- 42 B. De Carvalho, R.E.S. Bretas, Quiescent Crystallization Kinetics and Morphology of Isotactic Polypropylene Resins for Injection Moulding. I. Isothermal Crystallization. *Journal of Applied Polymer Science*, 68 (1998) 1159-1176
- 43 F.L. Binsbergen, B.G.M. De Lange, Morphology of Polypropylene Crystallized from the Melt, *Polymer*, 9 (1968) 23-40
- 44 M. Eder, A. Wlochowicz, Kinetics of non-isothermal crystallization of polyethylene and polypropylene, *Polymer*, 24 (1983) 1593-1595
- 45 K. Nakamura, T. Watanabe, K. Katayama, T. Amano, Some aspects of nonisothermal crystallization of polymers. I. Relationship between crystallization temperature, crystallinity, and cooling conditions, *Journal of Applied Polymer Science*, 16 (1972) 1077-1091
- 46 C.A. Hieber, Correlations for the quiescent crystallization kinetics of isotactic polypropylene and poly(ethyleneterephthalate), *Polymer*, 36 (1995) 1455-1467
- 47 T. Ozawa, Kinetics of non-isothermal crystallization, *Polymer*, 12 (1971) 150-158
- 48 A. Ziabicki, Crystallization of polymers in variable external conditions. 1. General equations, *Colloid Polymer Science*, 274 (1996) 209-217
- 49 A. Ziabicki, Crystallization of polymers in variably external conditions. 2. Effects of cooling in the absence of stress and orientation, *Colloid Polymer Science*, 274 (1996) 705-719
- 50 P. Krüger, On the relation between non-isothermal and isothermal Kolmogorov-Jonson-Mehl-Avrami crystallization kinetics, *J. Phys. Chem. Solids*, 54, (1993) 1549-1556
- 51 E. Woldt, The relationship between isothermal and non-isothermal description of Johnson-Mehl-Avrami-Kolmogorov kinetics, *J. Phys. Chem. Solids*, 53 (1992) 521-527
- 52 Z. Ding, J.E. Spruiell, An Experimental Method for Studying Nonisothermal Crystallization of Polymers at Very High Cooling Rates, *Journal of Polymer Science, Part B: Polymer Physics*, 34 (1996) 2783-2804
- 53 Z. Ding, J.E. Spruiell, Interpretation of the nonisothermal crystallization kinetics of polypropylene using a power law nucleation rate function, *Journal of Polymer Science, Part B: Polymer Physics*, 35 (1997) 1077-1094
- 54 G.B.A. Lim, K.S. McGuire, Non-Isothermal crystallization of Isotactic Polypropylene in Dotriacontane. II: Effects of Dilution, Cooling Rate and Nucleating Agent Addition on Growth rate, *Polymer Engineering Science*, 33 (1993) 9, 537-542
- 55 B. De Carvalho, R.E.S. Bretas, Quiescent Crystallization Kinetics and Morphology of i-PP Resins for Injection Moulding. II. Nonisothermal Crystallization as a Function of Molecular Weight, *Journal of Applied Polymer Science*, 72 (1999) 1733-1740
- 56 F.J. Padden Jr., H.D. Keith, Mechanism for lamellar branching in isotactic polypropylene, *Journal of Applied Physics*, 44 (1973) 1217-1223
- 57 A.J. Lovinger, J.O. Chua, C.C. Gryte, Studies on the α and β forms of isotactic polypropylene by crystallization in a temperature gradient, *Journal of Polymer Science, Polymer Physics*, 15 (1977) 641-656
- 58 B. Lotz, S. Graff, J.C. Wittmann, Crystal morphology of the γ - triclinic phase of isotactic polypropylene and its relation to the α phase, *Journal of Polymer Science Polymer Physics*, 24 (1986) 2017-2032
- 59 R. Cambell, Anderson, P.J. Phillips, J.S. Lin, The gamma phase of high-molecular-weight polypropylene: 1. Morphological aspects, *Polymer*, 34 (1993) 4809-4816

- 60 P. Corradini, V. Petraccone, C. DeRosa, G. Guerra, On the Structure of the Quenched Mesomorphic Phase of Isotactic Polypropylene, *Macromolecules*, 19 (1986) 2699-2703
- 61 R.L. Miller, On the existence of near-range order in isotactic polypropylene, *Polymer*, 1 (1960) 135-143
- 62 D.M. Gezovich, P.H. Geil, Morphology of quenched polypropylene, *Polymer Engineering Science*, 8 (1968) 202-209
- 63 P.B. Allister, T.J. Carter, R.M. Hinde, Structure of quenched form of polypropylene, *Journal of Polymer Science, Polymer Physics Ed.*, 16 (1978) 49-57
- 64 Y. Cohen, R.F. Saraf, A direct correlation function for mesomorphic polymers and its application to the smectic phase of isotactic polypropylene, *Polymer*, 42 (2001) 5865-5870
- 65 M. Glotin, R.R. Rahalkar, Some crystallization kinetics of isotactic polypropylene, P.J. Hendra, M.E.A. Cudby, *Polymer*, 22 (1981) 731-735
- 66 V. Caldas, G.R. Brown, R.S. Nohr, J.G. Mac Donalt, L.E. Raboin, The structure of the mesomorphic phase of quenched isotactic polypropylene, *Polymer*, 35 (1994) 5, 899-907
- 67 C.C.Hsu, P.H.Geil, H. Miyaji, K. Asai,. Structure and properties of polypropylene crystallized from the glassy state, *Journal of Polymer Science Physics*, 24 (1986) 2379-2401
- 68 W.J. O'Kane, R.J.Young, A.J. Ryan, Simultaneous SAXS-WAXS and d.s.c. analysis of the melting and recrystallization behaviour of quenched polypropylene, *Polymer*, 35 (1994) 1352-1358
- 69 N. Alberola, M. Fugier, D. Petit, B. Fillon, Microstructure of quenched and annealed films of isotactic polypropylene – Part I, *Journal of Materials Science*, 30 (1995) 1187-1195
- 70 N. Alberola, M. Fugier, D. Petit, B. Fillon, Tensile mechanical behaviour of quenched and annealed isotactic polypropylene films over a wide range of strain rates – Part II, *Journal of Materials Science*, 30 (1995) 860-868
- 71 Z.-G. Wang, B.B. Hsiao, S.Srinivas, G.M.Brown, A.H. Tsou, S.Z.D. Cheng, S.S. Stein, Phase Transformation in quenched mesomorphic isotactic polypropylene, *Polymer*, 42 (2001) 7561-7566
- 72 R. Seguela, E. Staniek, B. Escaig, B. Fillon, Plastic Deformation of Polypropylene in Relation to Crystalline Structure, *Journal of Applied Polymer Science*, 71 (1999) 1873-1885
- 73 B. Wunderlich, M. Möller, J. Grebowicz, H. Baur, Conformational Motion and Disorder in Low and High Molar Mass Crystals in *Advanced Polymer Science*, Vol. 87, Springer Verlag, Berlin, 1988
- 74 R.J.Yan, W. Li, G. Li, B. Jiang, Structure of Mesomorphic Form of Isotactic Polypropylene, *Journal of Macromolecular Science Physics*, 32 (1993) 15-32
- 75 R. Androsch, B. Wunderlich, Reversibly Crystallization and Melting at the Lateral Surface of Isotactic Polypropylene Crystals, *Macromolecules*, 34 (2001) 5950 - 5960
- 76 S. Piccarolo, M.Saiu, Crystallization of polymer melts under fast cooling. II. High-purity iPP, *Journal of Applied Polymer Science*, 46 (1992) 625-634
- 77 V. Brucato, S. Piccarolo, G. Titomanlio, Crystallization kinetics in relation to polymer processing, *Macromolecular Symposia*, 68 (1993) 245-256
- 78 S. Piccarolo, S. Alessi, V. Brucato, G. Titomanlio, *Crystallization of Polymers*, Ed. M. Dosiere, Kluwer Academic Publishers, Dordrecht, 1993

- 79 A. Martorana, S. Piccarolo, F. Scichilone, The X-Ray determination of the amounts of the phases in samples of isotactic poly(propylene) quenched from the melt at different cooling rates, *Macromolecules Chemistry Physics*, 198 (1997) 597-604
- 80 F. Gerardi, S. Piccarolo, A. Martorana, D. Sapoundieva, Study of the long-period changes in samples of isotactic polypropylene) obtained by quenching from the melt and subsequent annealing at different temperatures, *Macromolecules Chemistry Physics*, 198 (1997) 3979-3986
- 81 A. Martorana, S. Piccarolo, D. Sapoundieva, SAXS/WAXS study of the annealing process in quenched samples of isotactic poly(propylene), *Macromolecules Chemistry Physics*, 200 (1999) 531-540
- 82 T. Foresta, S. Piccarolo, G. Goldbeck-Wood, Competition between α and γ phases in isotactic polypropylene: effects of ethylene content and nucleating agents at different cooling rates, *Polymer*, 42 (2001) 1167-1176
- 83 R.T. Sylvest, J.A. Riedel, J.R. Pillow, Bessere Gummiartikel durch INSITE-EPDM Polymere, *Gumi Fasern Kunststoffe*, 50 (1997), 6, 478-483
- 84 D.J. Synnott, D.F. Sheridan, E.G. Kontos, EPDM-polypropylene blends. in: *Thermoplastic Elastomers from rubber-plastic blends*, Ed. S. K. De; Anil K. Bhowmick, Ellis Horwood, New York, 1990
- 85 B.J.R. Scholtens, E. Riande, J.E. Mark, Crystallization in stretched and unstretched EPDM elastomers, *Journal of Polymer Science, Polymer Physics*, 22 (1984) 1223-1238
- 86 E.N. Kresge, Polyolefin based Thermoplastic Elastomers. in: *Thermoplastic Elastomers*, Ed. G. Golden, N.R. Legge, 2nd Edition, Hanser, Munich, 1996
- 87 A.G. Simanke, G.B. Galland, L. Freitas, J.A. H. da Jornada, R. Quijada, R.S. Mauler, Influence of the comonomer content on the thermal and dynamic mechanical properties of metallocene ethylene/1-octene copolymers, *Polymer*, 40 (1999) 5489-5496
- 88 R. Quijada, J. Dupont, M.S.L. Miranda, R.B. Scipioni, G.B. Galland, Copolymerization of ethylene with 1-hexene and 1-octene: Correlation between type of catalyst and comonomer incorporated, *Macromolecules Chemistry Physics*, 196 (1995) 3991-4000
- 89 J. M. Rego, J.A. Gonzalez Oronzco, I. Katime, Determination of the influence of structure and thermal history on the dynamic mechanical properties of high density polyethylenes *Journal of Applied Polymer Science*, 40 (1990) 1453-1472
- 90 S. Bensason, J. Minick, A. Moet, S. Chum, A. Hiltner, E. Baer, Classification of homogeneous Ethylene-Octene Copolymers based on Short-Chain Branch Content, *Journal of Polymer Science B Polymer Physics*, 34 (1996), 1301-1316
- 91 A. Alizadeh, L. Richardson, J. Xu, S. McCarney, H. Marand, Influence of Structural and Topological Constraints on the Crystallization and Melting Behaviour of Polymers, *Macromolecules*, 32 (1999) 6221-6235
- 92 R. Androsch, J. Blackwell, S.N. Chvalun, B. Wunderlich, Wide and Small-Angle X-Ray Analysis of Poly(ethylene-co-octene), *Macromolecules*, 32 (1999) 3735-3740
- 93 R. Androsch, B. Wunderlich, A Study of Annealing of Poly(ethylene-co-octene) by Temperature-Modulated and Standart Differential Scanning Calorimetry, *Macromolecules*, 32 (1999) 7238-7247
- 94 R. Androsch, Melting and crystallization of poly(ethylene-co-octene) measured by modulated d.s.c. and temperature-resolved X-Ray diffraction, *Macromolecules*, 32 (1999) 2805-2812

- 95 S. Vanden Eynde, V.B.F. Method, G.W.H. Höhne, J.W.K. Schawe, H. Reynaers, Thermal behaviour of homogeneous ethylene-1-octene copolymers and linear polyethylene at high pressures, *Polymer*, 41 (2000) 3411-3423
- 96 I.S. Kolesov, H.-J. Radusch, R. Androsch, Einfluss der Verarbeitungsbedingungen im Spritzgussverfahren auf das thermophysikalische und mechanische Verhalten von Ethylen-1-Okten-Copolymeren, Conference Proceedings of P2002, Halle (Saale), 2002
- 97 R. Greco, C. Mancarella, E. Martuscelli, G. Ragosta, Y. Jinghua, Polyolefin blends: 2. Effect of EPM composition on structure, morphology and mechanical properties of iPP/EPR alloys, *Polymer*, 28 (1987) 1929-1936
- 98 L. D'Orazio, C. Mancarella, E. Martuscelli, G. Sticotti, Polypropylene/ethylene-co-propylene blends: Influence of molecular structure of EPR and composition on phase structure of isothermally crystallized samples, *Journal of Materials Science*, 26 (1991) 4033-4047
- 99 T.J. Menke, Maßschneidern der Eigenschaften von Polypropylen Mischungen und Olefincopolymeren, Dissertation, Martin-Luther-Universität Halle-Wittenberg, 2001
- 100 S. W. Lim, K.H. Lee, C.H. Lee, Liquid-liquid phase separation and its effect on crystallization in the extruded polypropylene/ethylene-propylene-rubber blend, *Polymer*, 40 (1999) 2837-2844
- 101 S. M. Dwyer, O.M. Boutni, C. Shu, Compounded Polypropylene Products in Polypropylene Handbook, E.P. Moore Jr, Hanser, Munich, (1996) 212-235
- 102 B.K. Kim, I.H. Do, Effect of Viscosity Ratio, Rubber Composition, and Peroxide/Coagent Treatment in PP/EPR Blends, *Journal of Applied Polymer Science*, 61 (1996) 439-447
- 103 L. D'Orazio, C. Mancarella, E. Martuscelli, G. Sticotti, R. Ghisellini, Thermoplastic Elastomers from iPP/EPR Blends: Crystallization and Phase Structure Development, *Journal of Applied Polymer Science*, 53 (1994) 387-404
- 104 Y. Yokohama, T. Ricco, Crystallization and Morphology of Reactor -Made Blends of Isotactic Polypropylene and Ethylene-Propylene Rubber, *Journal of Applied Polymer Science*, 66 (1997) 1007-1014
- 105 B. De Carvalho, R.E.S. Bretas, Quiescent Crystallization Kinetics and Morphology of i-PP Resins for Injection Moulding. III. Nonisothermal Crystallization of the Heterophasic and Grafted Polymers, *Journal of Applied Polymer Science*, 72 (1999), 1741-1753
- 106 E. Martuscelli, C. Silvestre, L. Bianchi, Properties of thin films of isotactic polypropylene blended with polyisobutylene and ethylene-propylene-diene terpolymer rubbers, *Polymer*, 24 (1983), 1458-1467
- 107 E. Martuscelli, C. Silvestre, G. Abate, Morphology, crystallization and melting behaviour of films of isotactic polypropylene blended with ethylene-propylene copolymers and polyisobutylene, *Polymer*, 23 (1982), 229-237
- 108 W. Wenig, A. Wasiak, Interactions between the components in isotactic polypropylene blended with EPDM, *Colloid and Polymer Science*, 271 (1993) 824-883
- 109 W. Wenig, M. Asresahegn, The Influence of Rubber-Matrix Interfaces on the Crystallization Kinetics of Isotactic Polypropylene blended with Ethylene-Propylene-Diene Terpolymer (EPDM), *Polymer and Engineering Science*, 33 (1993) 14, 877-888

- 110 W. Wenig, Ageing effects during isothermal crystallization of polypropylene blended with elastomers, *Journal of Materials Science*, 29 (1994), 4708-4712
- 111 N. Dharmarajan, L.G. Kaufman, The effect of EPDM and Polypropylene molecular properties on Thermoplastic Polyolefin Compounds, Conference Proceedings ANTEC San Francisco 1994, 3402-3407
- 112 A.L.N. Da Silva, F.M.B. Coutinho, Some Properties of Polymer Blends Based on EPDM/PP, *Polymer Testing*, 15 (1996) 45-52
- 113 Th. Zysk, S.G. Zhao, G.W. Ehrenstein, Struktur und Eigenschaften von Elastomermodifizierten Thermoplasten, *Kautschuk Gummi Kunststoffe*, 45 (1992) 943-950
- 114 J. Nordmeier, Schlagzähmodifizierung von Polypropylene auf einem Zweischichtknetter, Dissertation, TH Aachen, 1986
- 115 L. Slusarski, D. Bielinski, A. Wlochowicz, C. Slusarczyk, Structure and Properties of Polyolefin Blends, *Polymer International*, 36, (1995) 261-268
- 116 D.M. Bielinski, L. Slusarski, A. Wlochowicz, C. Slusarczyk, Some Aspects of Isotactic Polypropylene Crystallization in an Ethylene-Propylene-Diene Rubber Matrix, *Polymer International*, 44, (1997) 161-173
- 117 K.N. Ludwig, R.B. Moore, Compatibilization of PP/EPDM blends via a Hexafunctional Coupling Agent and Peroxide During Reactive Extrusion, *Journal of Elastomers and Plastic*, 34 (2002), 171-183
- 118 Y. Yang, T. Chiba, H. Saito, T. Inoue, Physical characterization of a polyolefinic thermoplastic elastomer, *Polymer*, 39 (1998) 3365-3372
- 119 Y. Yang, N. Otsuka, H. Saito, T. Inoue, Y. Takemura, Morphology and elastomeric properties of isotactic polypropylene/hydrogenated poly(styrene-co-butadiene) blends : a potential for a new thermoplastic elastomer, *Polymer*, 40 (1999) 559-564
- 120 A.L.N. Da Silva, M.I.B. Tavares, D.P. Politano, F.M.B. Coutinho, M. C. G. Rocha, Polymer Blends Based on Polyolefin Elastomer and Polypropylene, *Journal of Applied Polymer Science*, 66 (1997) 2005-2014
- 121 A.L.N. Da Silva, M. C. G. Rocha, F.M.B. Coutinho, R. Bretas, C. Scuracchio, Rheological, Mechanical, Thermal, and Morphological Properties of Polypropylene/Ethylene-Octene Copolymer Blends, *Journal of Applied Polymer Science*, 75 (2000) 692-704
- 122 A.L.N. Da Silva, M. C. G. Rocha, L. Lopes, B. S. Chagas, F.M.B. Coutinho, The Effect of Addition of Different Elastomers upon the Crystalline Nature of PP, *Journal of Applied Polymer Science*, 81 (2001) 3530-3537
- 123 T. McNally, P. McShane, G.M. Nally, W.R. Muroh, M. Cook, A. Miller, Rheology, phase morphology, mechanical, impact and thermal properties of polypropylene/metallocene catalysed ethylene 1-octene copolymer blends, *Polymer* 43 (2002), 3785-3793
- 124 K. Premphat, W. Paecharoenchai, Polypropylene/Metallocene Ethylene-Octene Copolymer Blends with a Bimodal Particle Size Distribution: Mechanical Properties and Their Controlling Factors, *Journal of Applied Polymer Science*, 85 (2002), 2412-2418
- 125 D. Mäder, M. Bruch, R.D. Maier, F. Stricker, R. Mühlhaupt, Glass Transition Temperature Depression of Elastomers Blended with Polypropylenes of Different Stereoregularities, *Macromolecules*, 1999, 32, 1252-1259
- 126 S. Bensason, S. Nazarenko, S. Chum, A. Hiltner, E. Baer, Elastomeric blends of homogeneous ethylene-octene copolymers, *Polymer*, 38 (1997) 15, 3913-3919

- 127 A.Y. Malkin, V.P. Beghishev, I.A. Keapin, Z.S. Adrianova, *Polymer Engineering Science*, 24 (1984), 1402
- 128 M. Moneke, *Die Kristallisation von verstärkten Thermoplasten während der schnellen Abkühlung unter Druck*, Dissertation, TU Darmstadt 2001
- 129 V. Brucato, V. La Carruba, S. Piccarolo, G. Titomanlio, *Polymer Solidification under Pressure and High Cooling Rates*, *International Polymer Processing*, 15 (2000) 1, 86-94
- 130 V. La Carruba, *Polymer Solidification under Pressure and High Cooling Rate*, Dissertation, University of Palermo 1999
- 131 Engage Product Information, DuPontDow Elastomers, <http://www.dupontdow.de>
- 132 Nordel Technical Information, DuPontDow Elastomers, <http://www.dupontdow.de>
- 133 Nordel Grade Selection Guide, DuPontDow Elastomers, <http://www.dupontdow.de>
- 134 Advanced Thermal Analysis System. <http://web.utk.edu/~athas>
- 135 R. P. Brown, *Physical testing of rubber*, 3. Ed., Chapman & Hall, London 1996
- 136 T. Lüpke, *Experimentelle Bestimmung thermisch aktivierbarer und athermischer Spannungsnateile am Polyethylen*, Martin-Luther-Universität Halle-Wittenberg, Dissertation
- 137 V. La Carruba, V. Brucato, S. Piccarolo, Phenomenological approach to compare the crystallization kinetics of iPP and PA6 under pressure, *J. Polymer Sci. Polym. Phys.*, 40 (2002) 1, 153-175
- 138 <http://www.polymerdoctor.com>
- 139 T. A. Huy, *Rheo-optische Charakterisierung des Deformationsverhaltens dynamischer Vulkanisate*, Dissertation, Martin-Luther-Universität Halle-Wittenberg, 1999
- 140 C.R.G. Treloar, *The physics of rubber elasticity*, Clarendon Press, Oxford 1975
- 141 S. Ilisch, H. Menge, H.-J. Radosch, Vernetzungsausbeute an konventionellen und dynamischen Vulkanisaten, *Kautschuk Gummi Kunststoffe*, 43 (2000) 206-212
- 142 C. Colletti, S. Piccarolo, A. Valenza, Solidification behaviour of PA6/iPP blends at high cooling rates, *Intern. Polymer Processing*, 15 (2001) 1, 46-52
- 143 B. Nysten, E. Tomasetti, Polypropylene/(ethylene-propylene) copolymer blends: surface morphology and elasticity as measured by AFM and FMM, *Polymer preprints*, 39 (1998) 1167-1168
- 144 J. Grebowicz, S.-F. Lau, B. Wunderlich, The thermal properties of Polypropylene, *Journal of Polymer Science, Polym. Symp.*, 1984, 71, 19-37
- 145 J. Rault, The α Transition in Semicrystalline Polymers: A new look at crystallization Deformation and Aging Process, *Journal of Macromolecular Science, C* 37 (1997) 335-387
- 146 K. Pozucek, G. Coulon, J.M. Lefebvre, B. Escaig, Plastic flow of PP and a PP-based blend, Part I, experimental determination of thermal activation parameters, *Journal of Materials Science*, 24 (1989) 2533-2540
- 147 J. Brandrup, E.H. Immergut, *Polymer Handbook*, Wiley and Sons, New York, 1989
- 148 H. H. Le, *Spannungsrelaxationsuntersuchungen zur Charakterisierung des zeitabhängigen Deformationsverhaltens thermoplastischer Elastomere*, Dissertation, Martin-Luther-Universität Halle-Wittenberg, 2002
- 149 A.K. Bhowmick, D. Mangaraj, *Vulcanization and Curing Techniques*, ed. A.K. Bhowmick, H.A. Benary and M.M. Hall, *Rubber Products Manufacturing Technology*, Marcel Dekker, New York, 1994

- 150 A.A. Katbab, H. Nazockdast, S. Bazgir, Carbon black-reinforced dynamically cured epdm/pp thermoplastic elastomers. I. morphology, rheology and dynamic mechanical properties, *Journal of Applied Polymer Science*, 75, (1999),. 1127-1137
- 151 A. Flores, J. Aurrekoetxea, R. Gensler, H.H. Kausch, F.J. Balta´ Calleja, Microhardness-structure correlation of iPP/EPR blends: influence of molecular weight and EPR particle content, *Colloid Polymer Science*, 276 (1998) 786–793
- 152 T.A. Huy, T. Lübke, H.-J. Radusch, Hysteresis- und Relaxationsverhalten dynamischer Vulkanisate auf Basis von PP/EPDM, *KGK*, 53 (2000) 11, 656-662
- 153 K. Premphet, W. Paecharoenchai, Polypropylene/Metallocene Ethylene-Octene Copolymer Blends with bimodal Particle Size Distribution: Mechanical Properties and their controlling factors, *Journal of Applied Polymer Science*, 85 (2002) 2412-2418

1. Appendix

WAXD fittings iPP

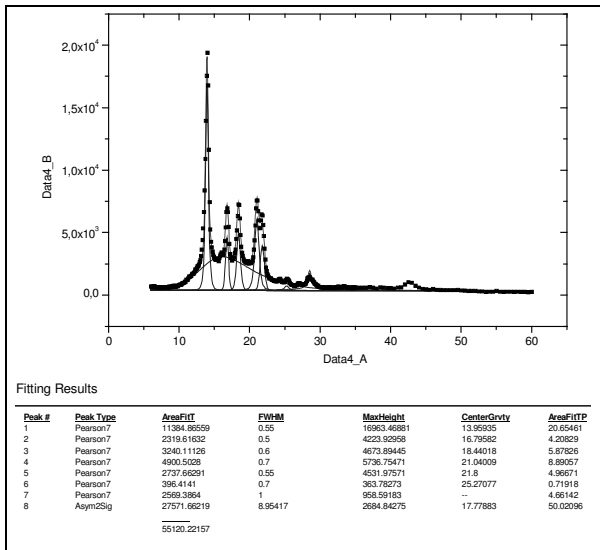


Fig. A1: iPP 1.12 K/s

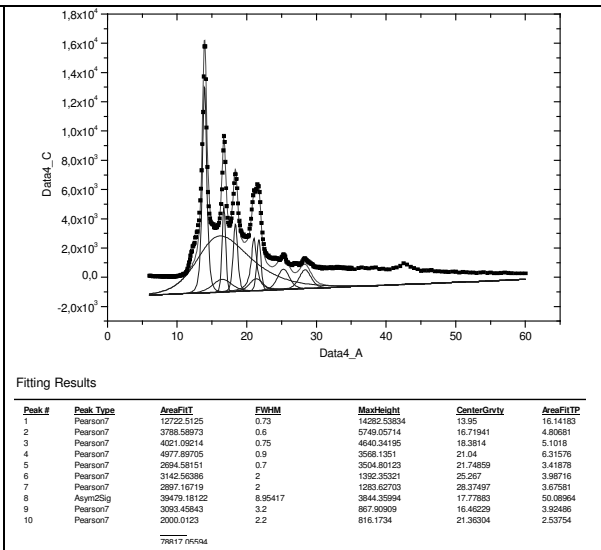


Fig. A2: iPP 4 K/s

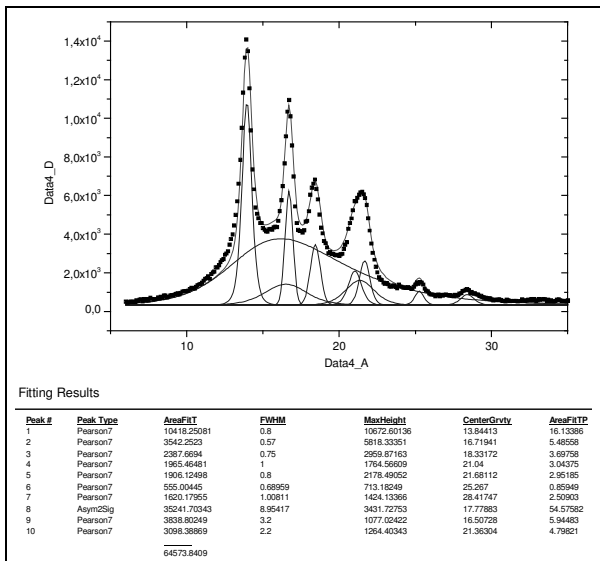


Fig. A3: iPP 9 K/s

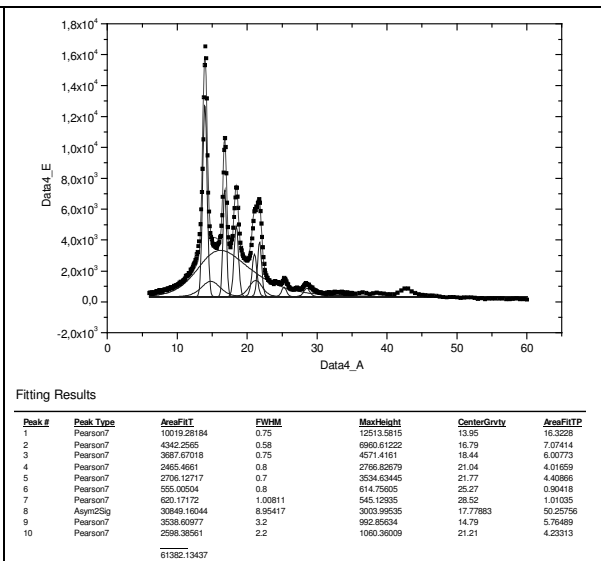
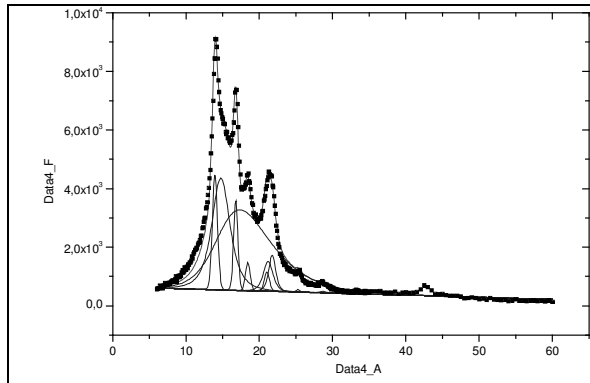


Fig. A4: iPP 12 K/s

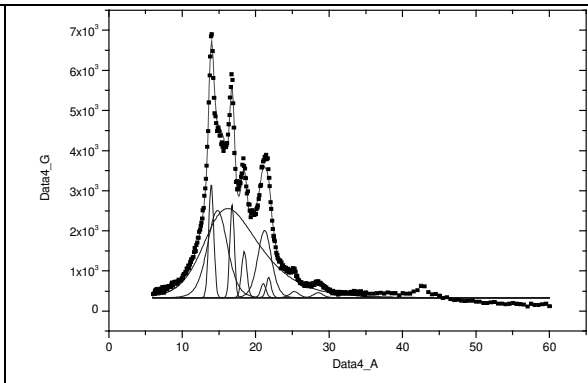
Appendix - 2



Fitting Results

Peak #	Peak Type	AreaFIT	FWHM	MaxHeight	CenterGrvty	AreaFITP
1	Pearson7	3519.26526	0.9	3692.9427	13.95	6.22044
2	Pearson7	2042.25403	0.7	2722.09416	16.79	3.60975
3	Pearson7	987.66856	0.75	1224.3822	18.44	1.74573
4	Pearson7	785.45749	0.8	859.02146	21.04	1.35297
5	Pearson7	895.12161	0.8	921.23025	21.77	1.42484
6	Pearson7	555.00578	1.5	327.8699	25.27	0.98099
7	Pearson7	420.17029	1.5	248.21578	28.52	0.74266
8	Asym2Sig	34143.56768	8.95417	3324.79448	17.77883	60.34978
9	Pearson7	9738.20154	3.2	2732.32591	14.79	17.21256
10	Pearson7	3598.39176	2.2	1468.44678	21.21	6.36027
		56676.12399				

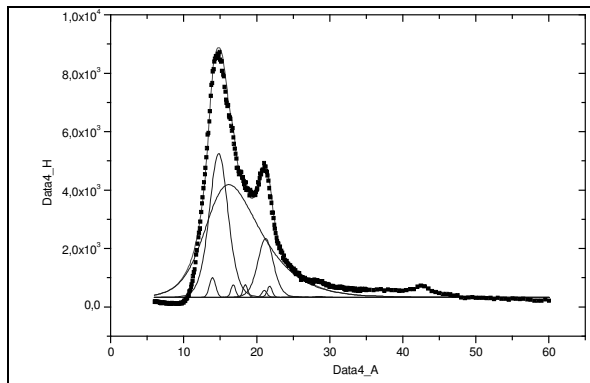
Fig. A5: iPP 30 K/s



Fitting Results

Peak #	Peak Type	AreaFIT	FWHM	MaxHeight	CenterGrvty	AreaFITP
1	Pearson7	2419.28584	0.8	2832.71894	13.95	5.5111
2	Pearson7	1742.25356	0.75	2171.18269	16.79	3.96883
3	Pearson7	850.66848	0.75	1054.5302	18.44	1.93781
4	Pearson7	315.45521	0.8	354.01417	21.04	0.7166
5	Pearson7	436.12048	0.8	498.43758	21.77	0.99348
6	Pearson7	455.00494	1.5	268.79437	25.27	1.03649
7	Pearson7	320.16948	1.5	189.14025	28.52	0.72534
8	Asym2Sig	26822.6827	8.95417	2611.90751	17.77883	61.10164
9	Pearson7	6438.41882	3.2	1806.4792	14.79	14.66663
10	Pearson7	4098.36483	2.2	1672.49013	21.21	9.33606
		43898.43433				

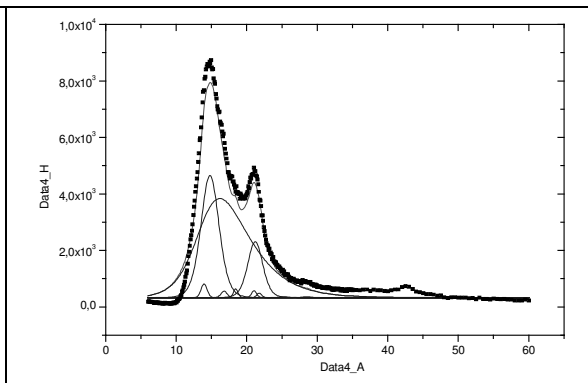
Fig. A6: iPP 40 K/s



Fitting Results

Peak #	Peak Type	AreaFIT	FWHM	MaxHeight	CenterGrvty	AreaFITP
1	Pearson7	719.28978	1	673.76484	13.95	1.12856
2	Pearson7	342.25384	0.75	426.51404	16.79	0.537
3	Pearson7	350.66818	0.75	434.70541	18.44	0.5502
4	Pearson7	215.4547	0.8	241.79032	21.04	0.33905
5	Pearson7	336.12017	0.8	384.14827	21.77	0.52737
6	Pearson7	50.00166	1.5	29.5385	25.27	0.07845
7	Pearson7	50.16728	1.5	29.63634	28.52	0.07871
8	Asym2Sig	39634.24642	8.95417	3859.45971	17.77883	62.18613
9	Pearson7	16438.25822	3	4919.54674	14.79	25.79163
10	Pearson7	5598.40372	2.5	2010.4658	21.21	8.7839
		63734.86192				

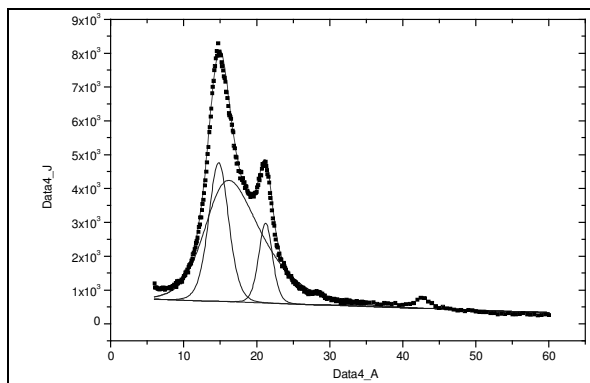
Fig. A7: iPP 76 K/s



Fitting Results

Peak #	Peak Type	AreaFIT	FWHM	MaxHeight	CenterGrvty	AreaFITP
1	Pearson7	719.28978	1	673.76484	13.95	1.12856
2	Pearson7	342.25384	0.75	426.51404	16.79	0.537
3	Pearson7	350.66818	0.75	434.70541	18.44	0.5502
4	Pearson7	215.4547	0.8	241.79032	21.04	0.33905
5	Pearson7	336.12017	0.8	384.14827	21.77	0.52737
6	Pearson7	50.00166	1.5	29.5385	25.27	0.07845
7	Pearson7	50.16728	1.5	29.63634	28.52	0.07871
8	Asym2Sig	39634.24642	8.95417	3859.45971	17.77883	62.18613
9	Pearson7	16438.25822	3	4919.54674	14.79	25.79163
10	Pearson7	5598.40372	2.5	2010.4658	21.21	8.7839
		63734.86192				

Fig. A8: iPP 93 K/s



Fitting Results

Peak #	Peak Type	AreaFIT	FWHM	MaxHeight	CenterGrvty	AreaFITP
1	Pearson7	14698.92431	3.2	4098.94463	14.79447	25.52673
2	Pearson7	5789.40865	2.2	2382.56614	21.21812	10.10734
3	Asym2Sig	36880.94628	8.95417	3591.3519	17.77883	64.38794
		57279.27925				

Fig. A9: iPP 986 K/s

WAXD fittings EOC

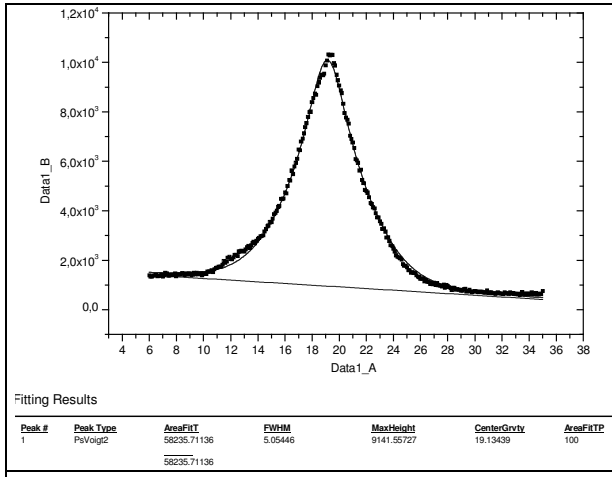


Fig. A10: EOC 0.12 K/s

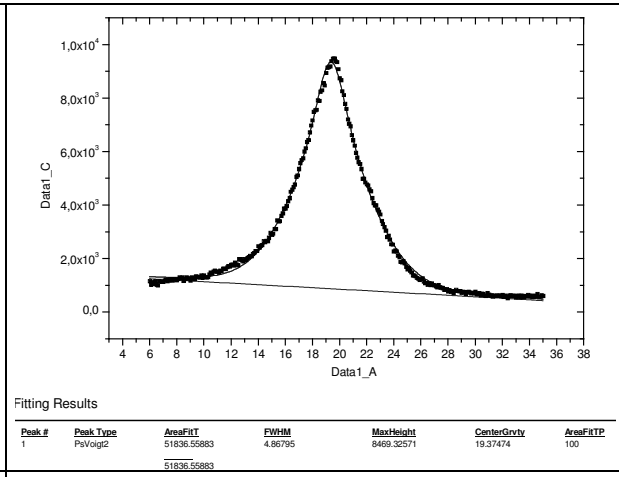


Fig. A11: EOC 24 K/s

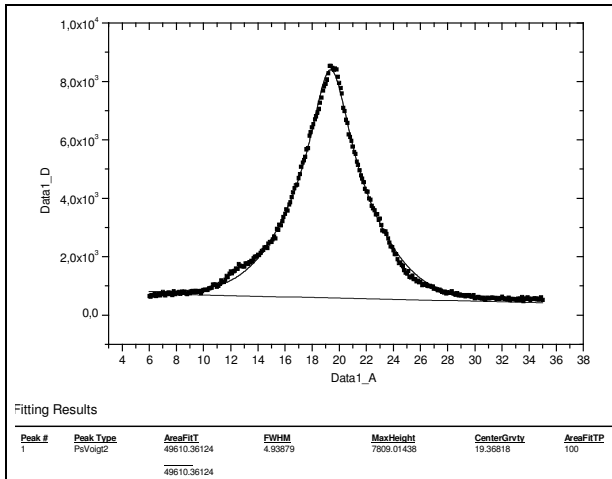


Fig. A12: EOC 171 K/s

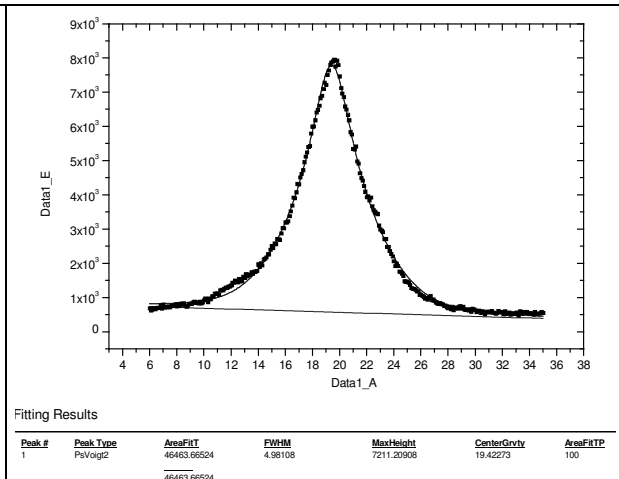


Fig. A13: EOC 200 K/s

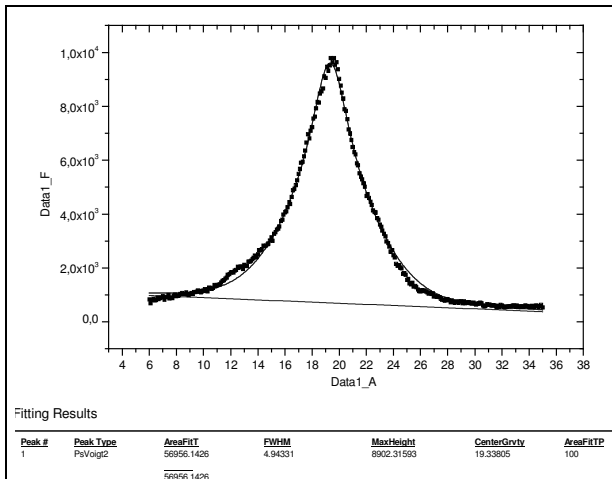


Fig. A14: EOC 600 K/s

WAXD fittings EPDM

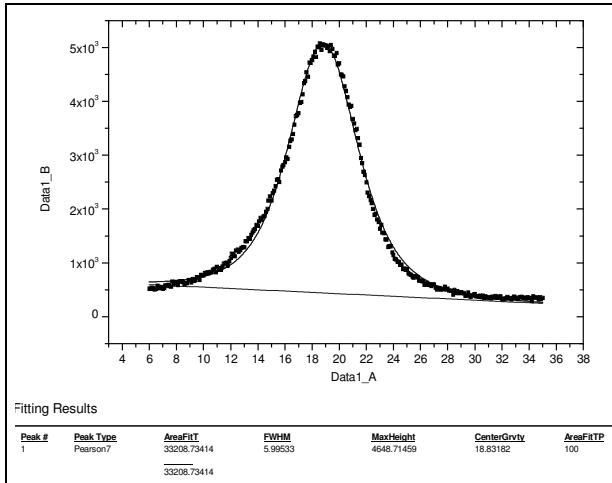


Fig. A15: EPDM 4 K/s

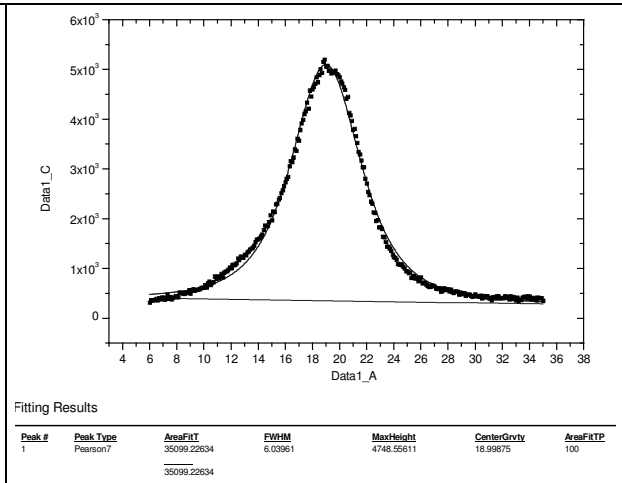


Fig. A16: EPDM 15 K/s

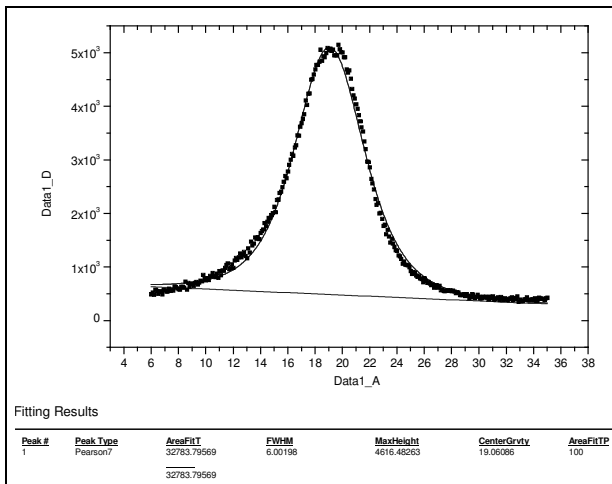


Fig. A17: EPDM 100 K/s

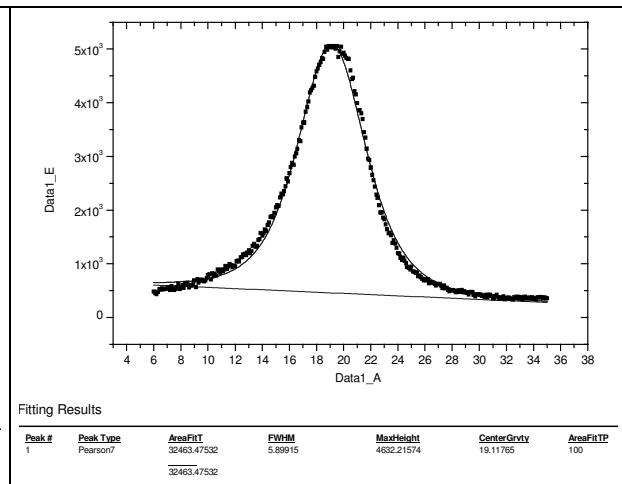


Fig. A18: EPDM 700 K/s

WAXD fittings PP/EOC 30/70p

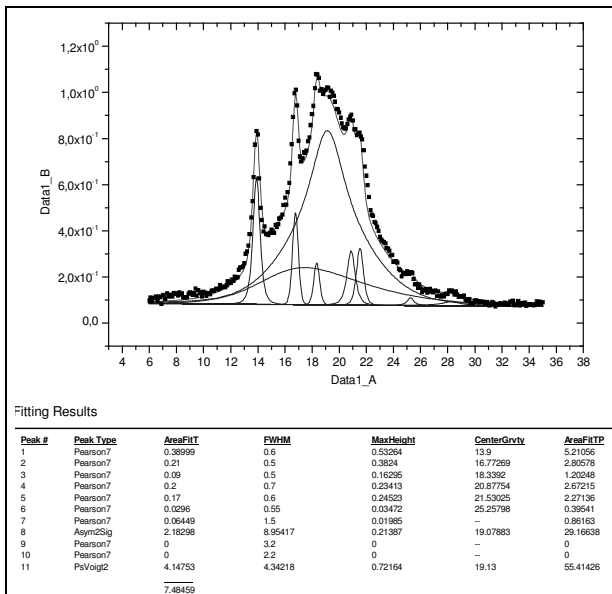


Fig. A19: PP/EOC 30/70p 0.57 K/s

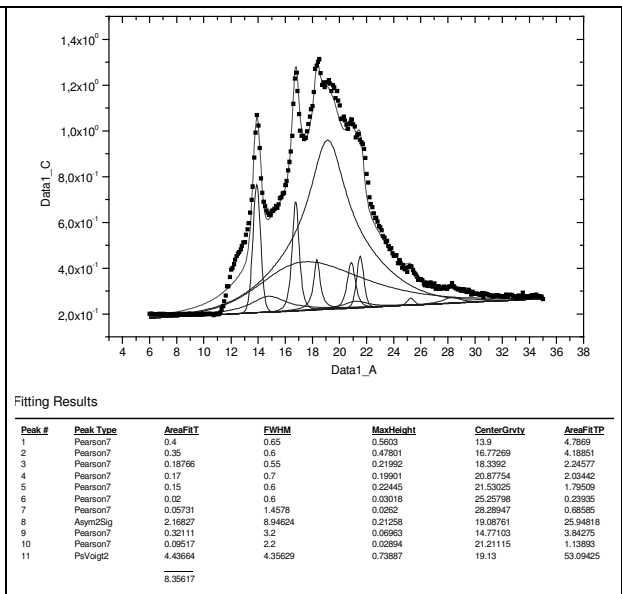


Fig. A20: PP/EOC 30/70p 1.9 K/s

Appendix - 5

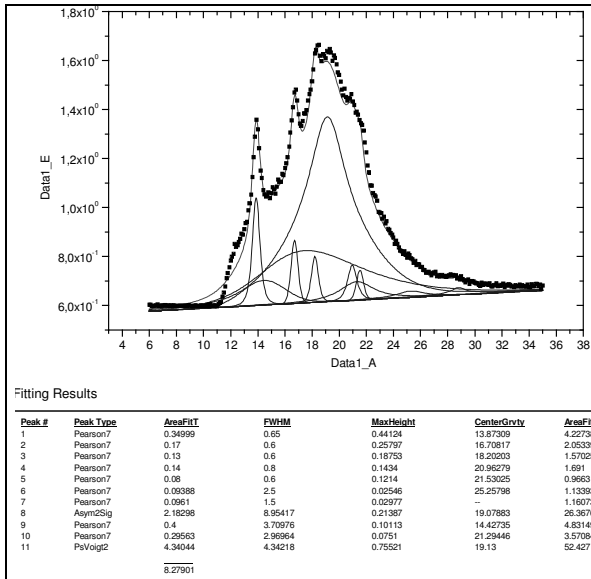


Fig. A21: PP/EOC 30/70p 8 K/s

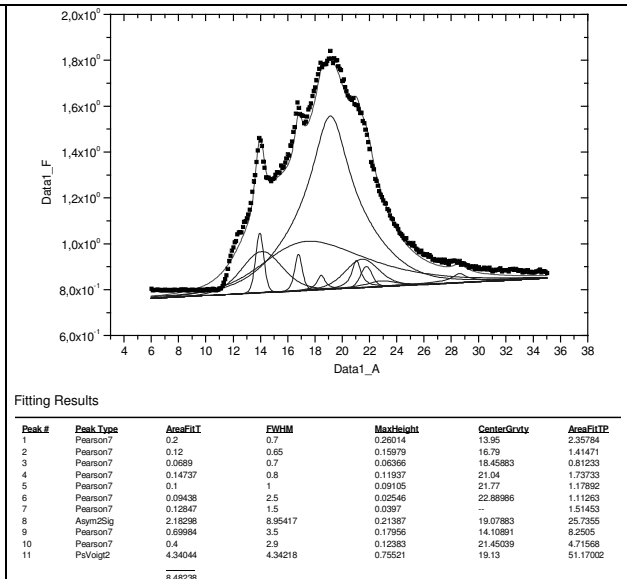


Fig. A22: PP/EOC 30/70p 17 K/s

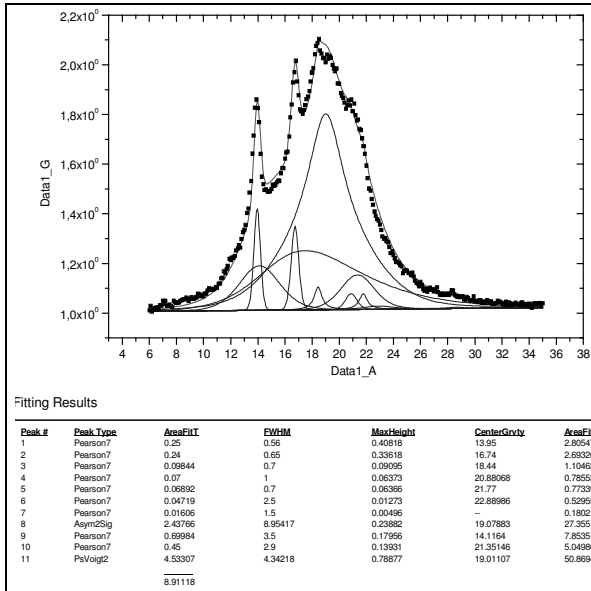


Fig. A23: PP/EOC 30/70p 55 K/s

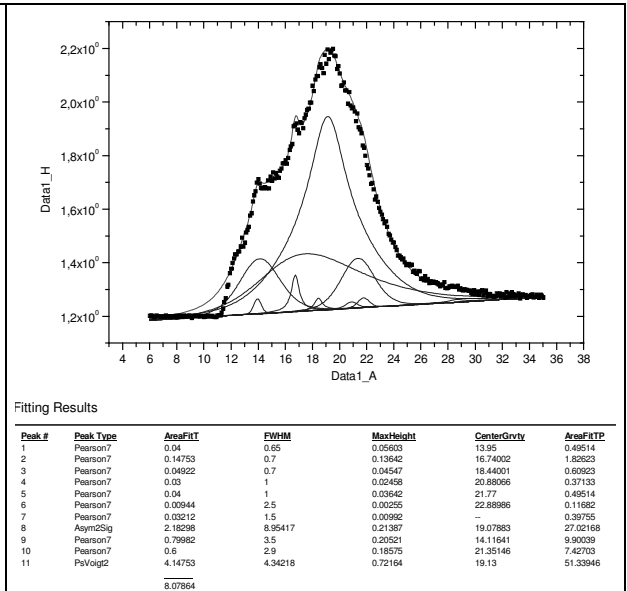


Fig. A24: PP/EOC 30/70p 72 K/s

Appendix - 6

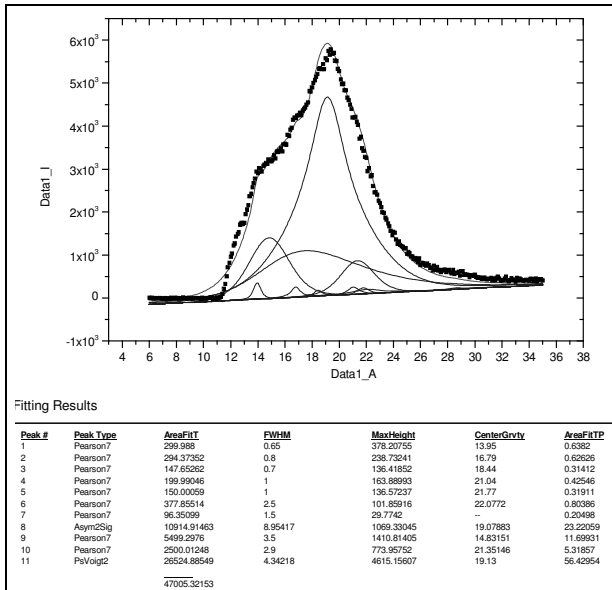


Fig. A25: PP/EOC 30/70p 80 K/s

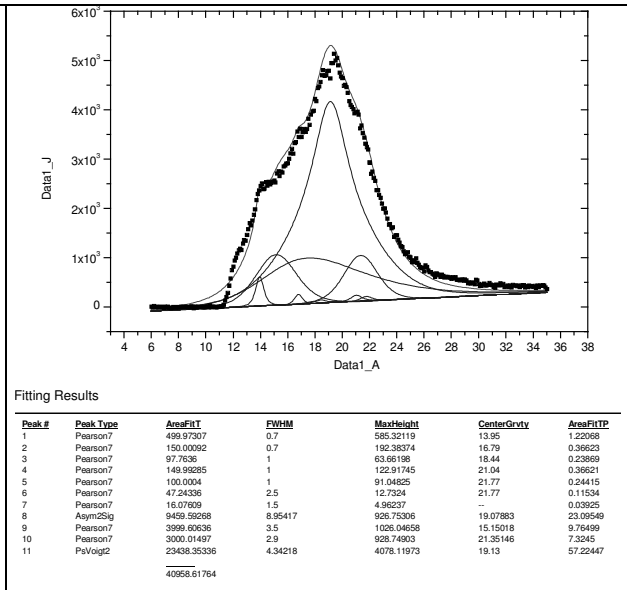


Fig. A26: PP/EOC 30/70p 120 K/s

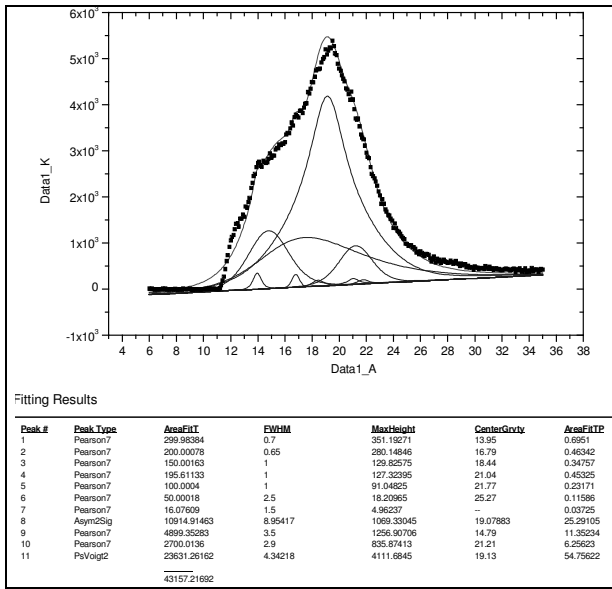


Fig. A27: PP/EOC 30/70p 192 K/s

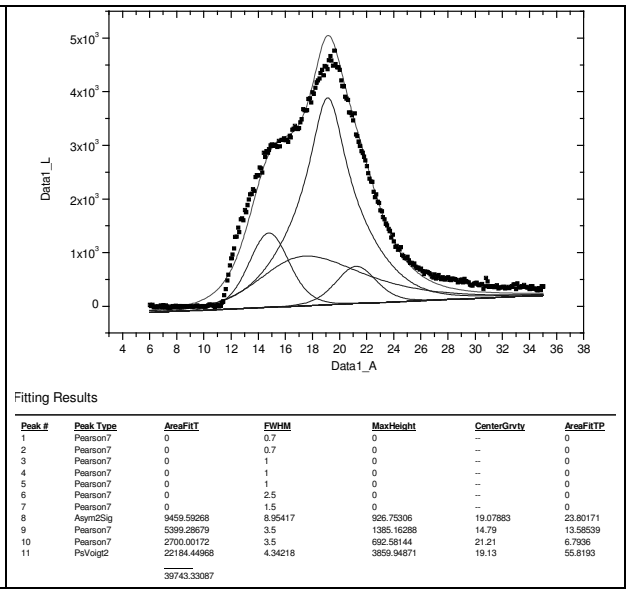


Fig. A28: PP/EOC 30/70p 860 K/s

WAXD fittings PP/EOC 70/30p

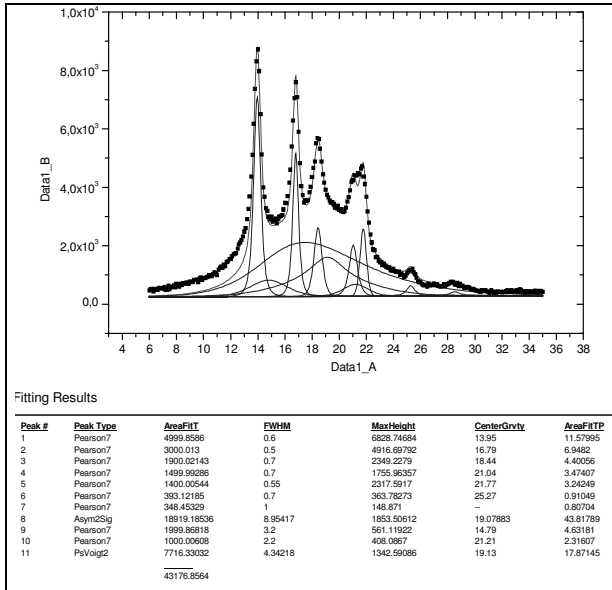


Fig. A29: PP/EOC 70/30p 7 K/s

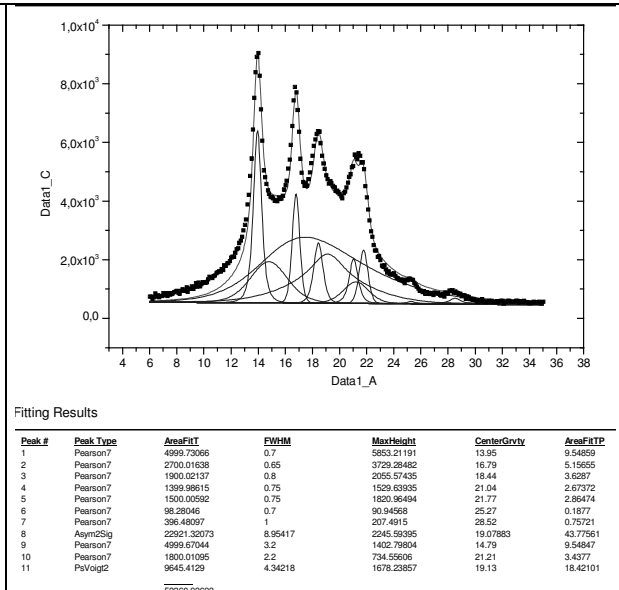


Fig. A30: PP/EOC 70/30p 16 K/s

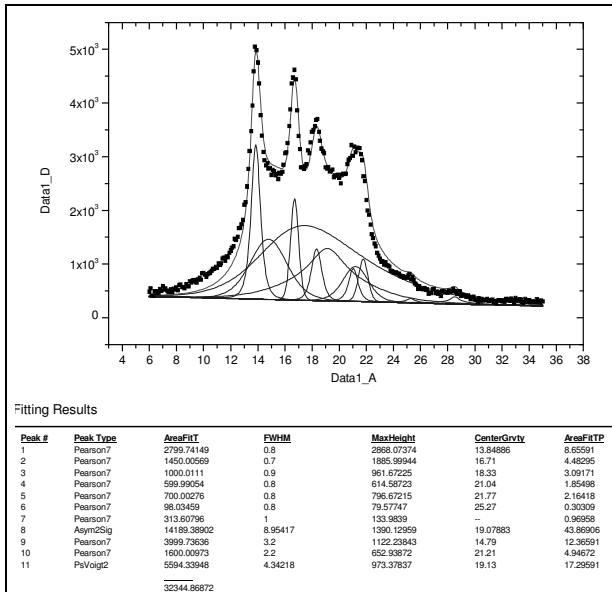


Fig. A31: PP/EOC 70/30p 50 K/s

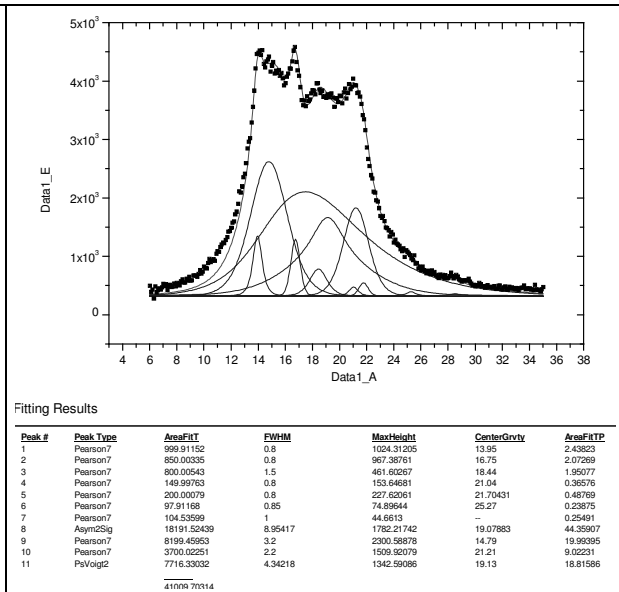


Fig. A32: PP/EOC 70/30p 80 K/s

Appendix - 8

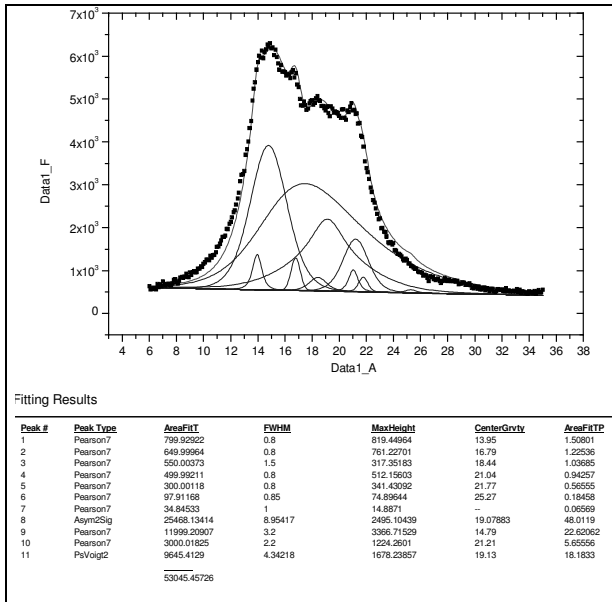


Fig. A33: PP/EOC 70/30p 90 K/s

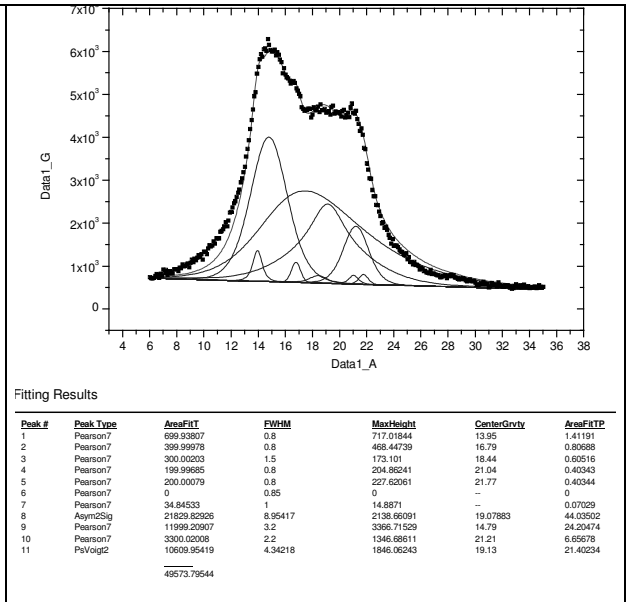


Fig. A34: PP/EOC 70/30p 123 K/s

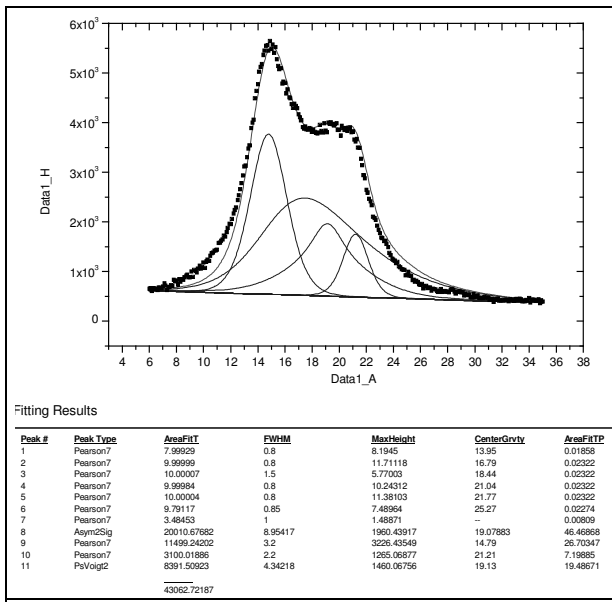


Fig. A35: PP/EOC 70/30p 931 K/s

WAXD fittings PP/EPDM 30/70p

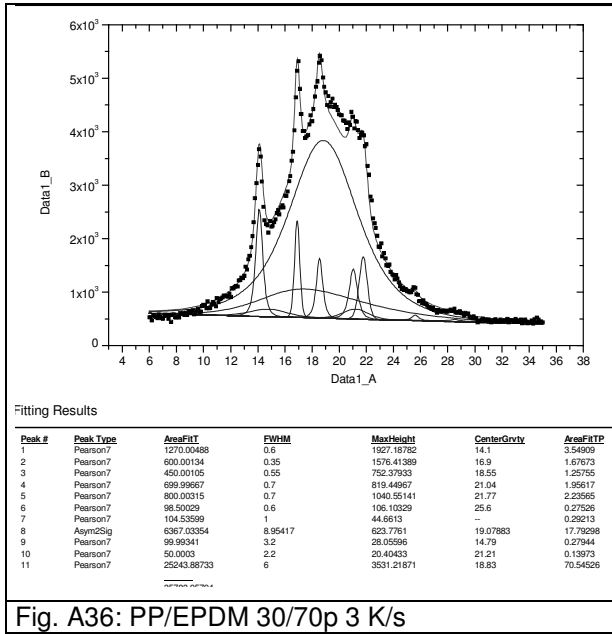


Fig. A36: PP/EPDM 30/70p 3 K/s

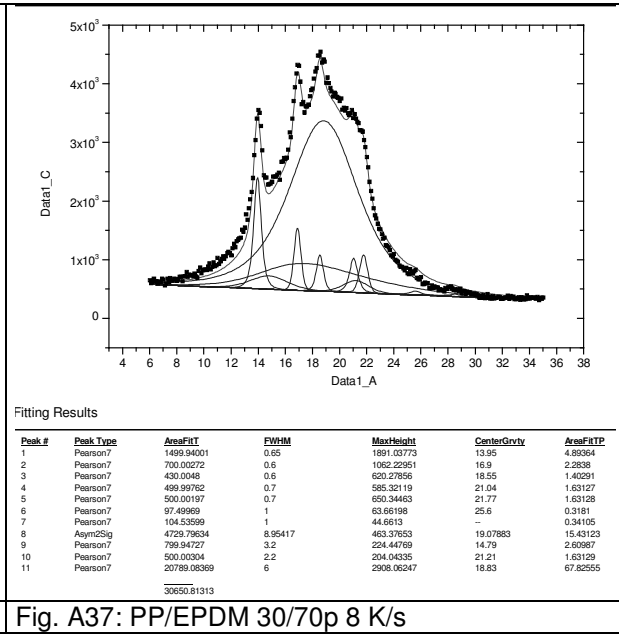


Fig. A37: PP/EPDM 30/70p 8 K/s

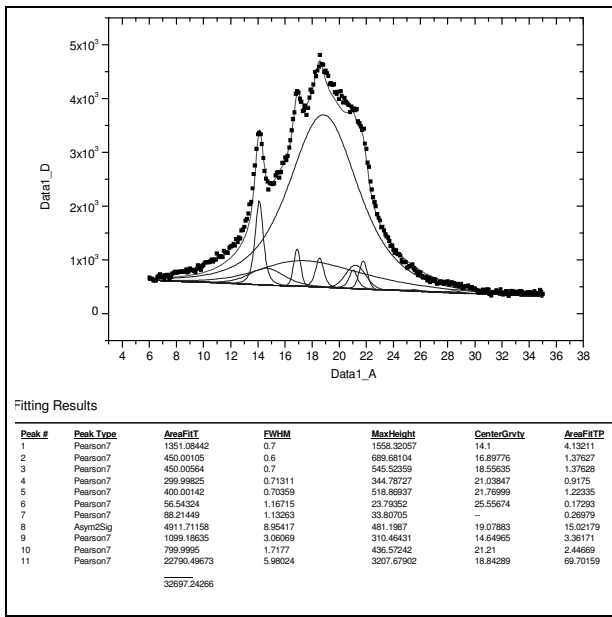


Fig. A38: PP/EPDM 30/70p 22 K/s

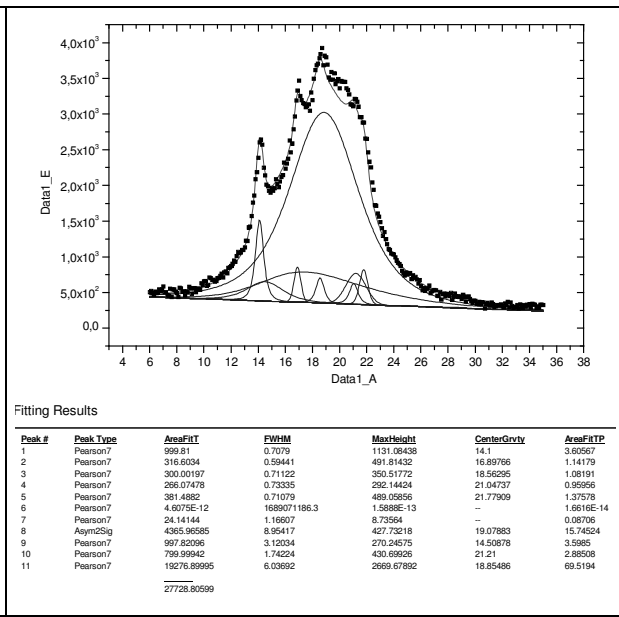


Fig. A39: PP/EPDM 30/70p 30 K/s

Appendix - 10

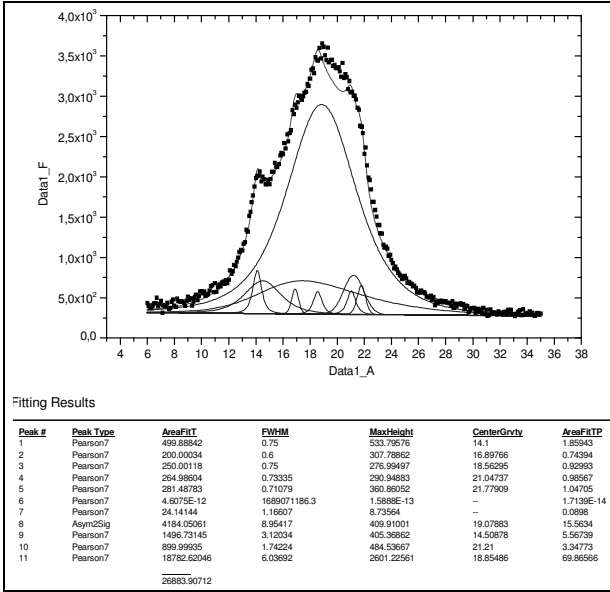


Fig. A40: PP/EPDM 30/70p 58 K/s

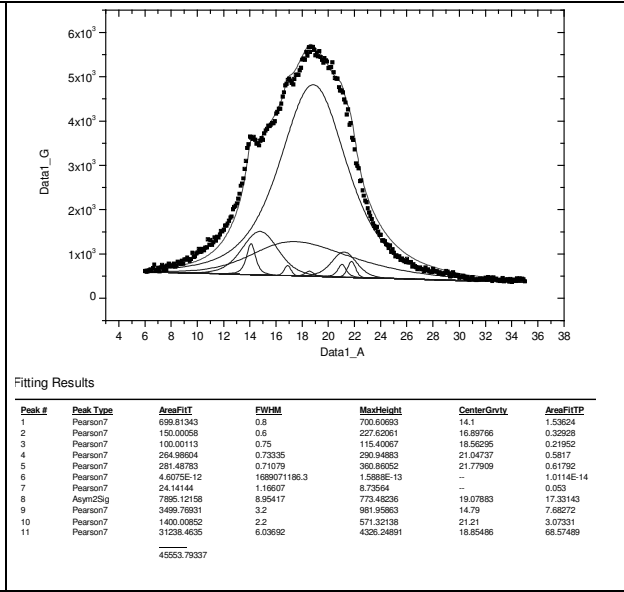


Fig. A41: PP/EPDM 30/70p 76 K/s

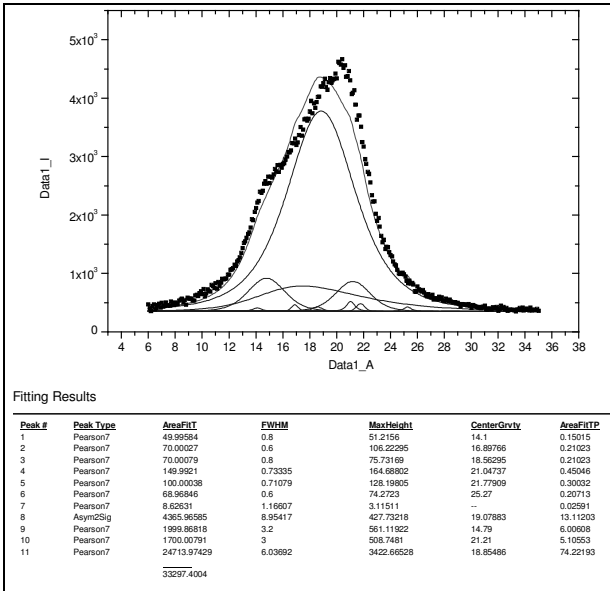


Fig. A42: PP/EPDM 30/70p 98 K/s

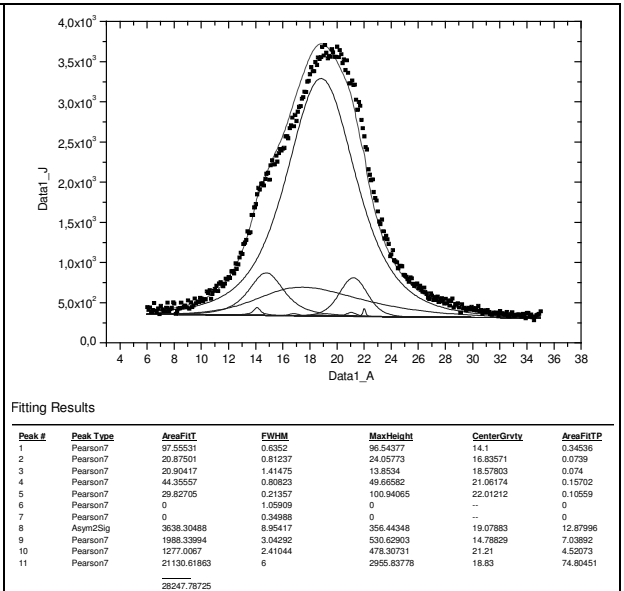


Fig. A43: PP/EPDM 30/70p 180 K/s

Appendix - 11

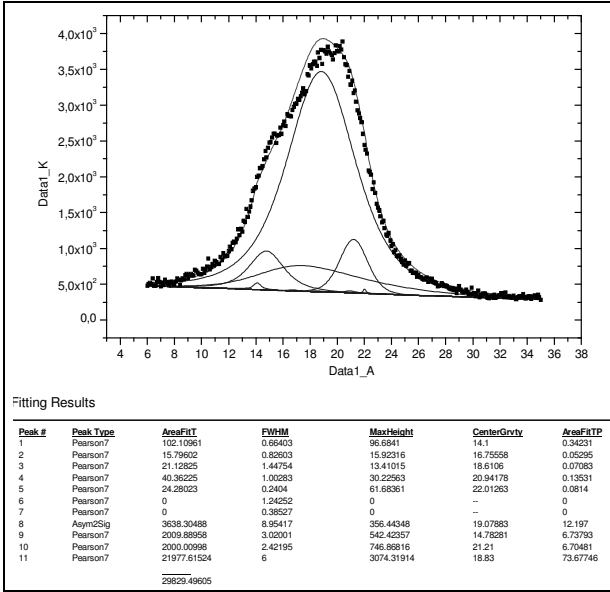


Fig. A44: PP/EPDM 30/70p 204 K/s

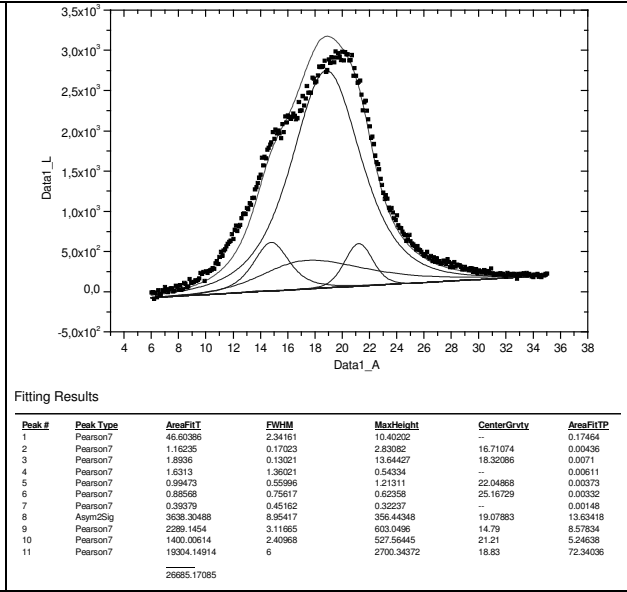


Fig. A45: PP/EPDM 30/70p 1025 K/s

WAXD fittings PP/EPDM 30/70r

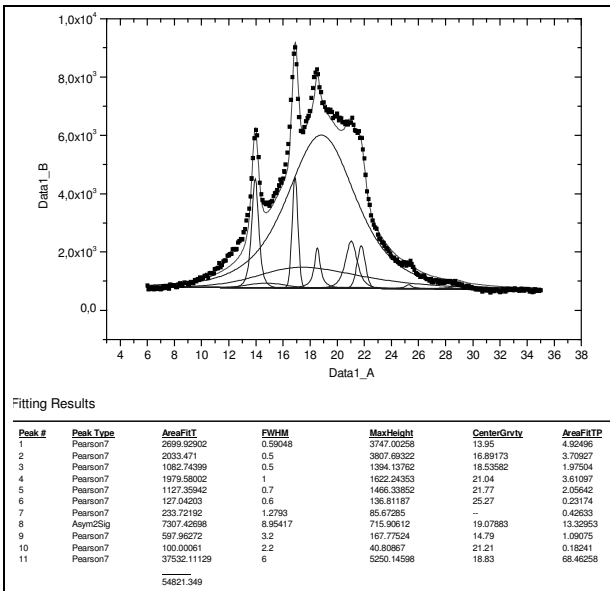


Fig. A46: PP/EPDM 30/70r 0.5 K/s

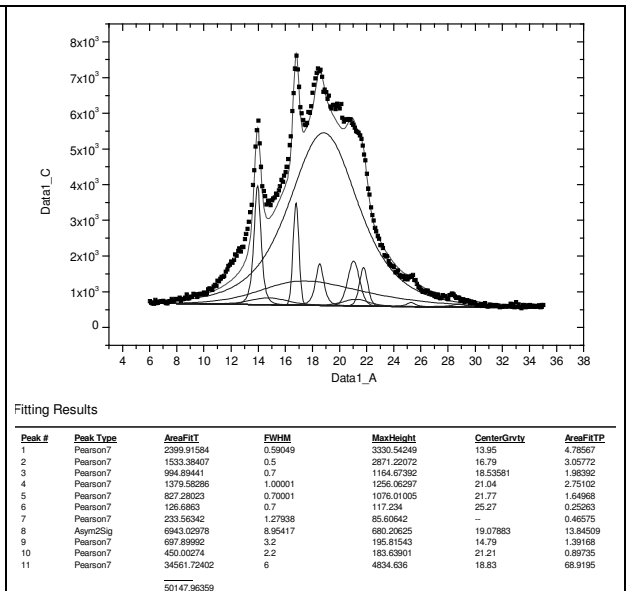


Fig. A47: PP/EPDM 30/70r 4 K/s

Appendix - 12

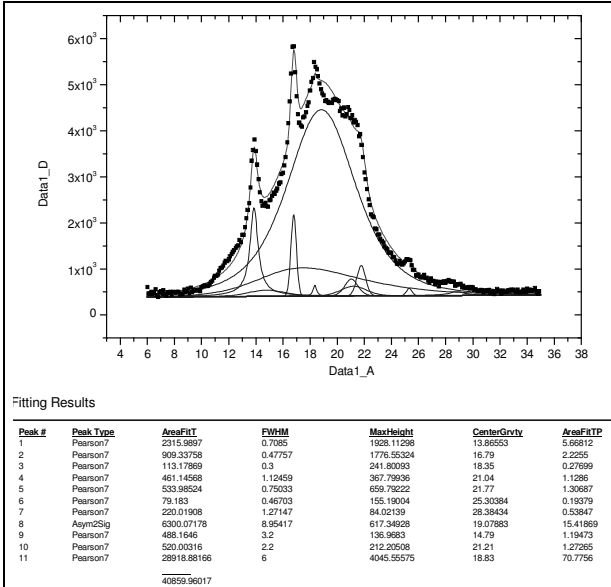


Fig. A48: PP/EPDM 30/70r 14 K/s

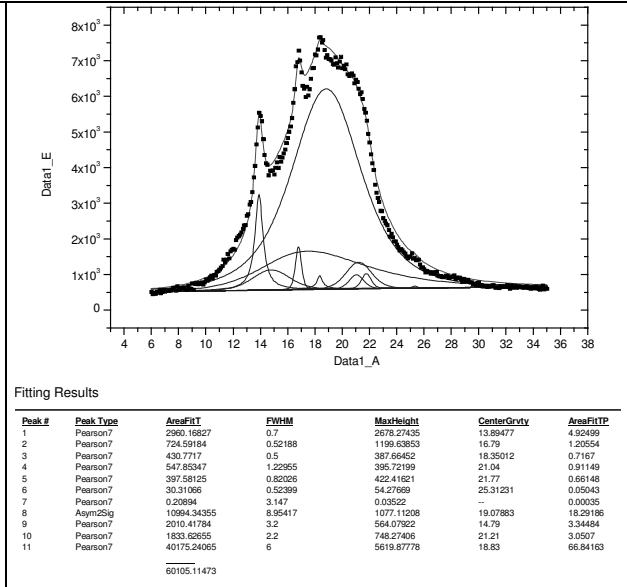


Fig. A49: PP/EPDM 30/70r 42 K/s

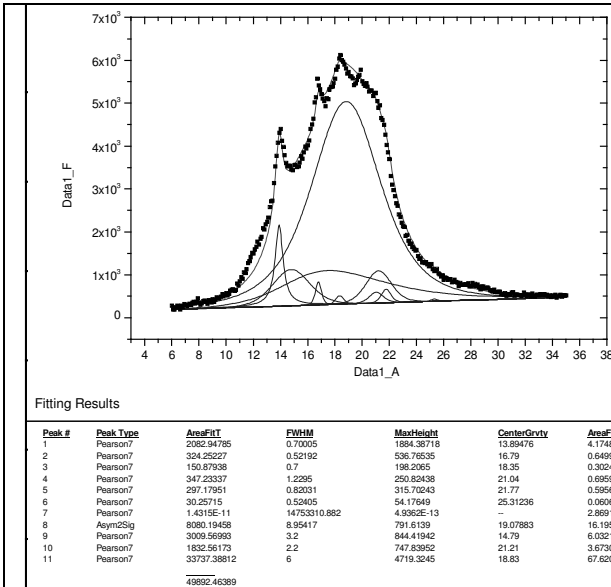


Fig. A50: PP/EPDM 30/70r 65 K/s

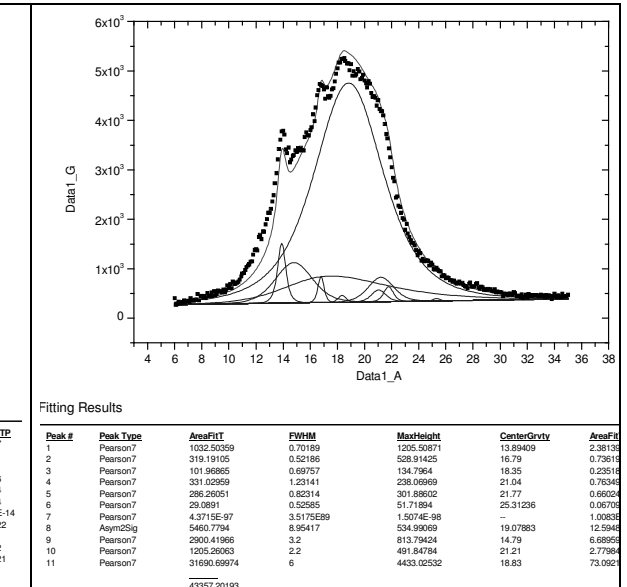


Fig. A51: PP/EPDM 30/70r 92 K/s

Appendix - 13

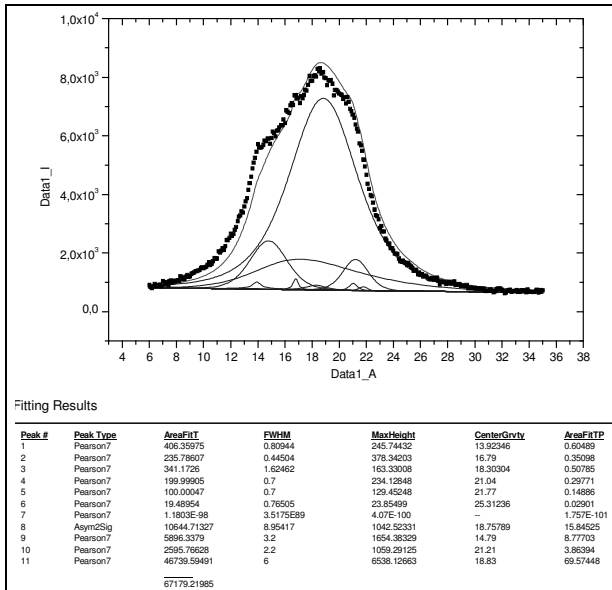


Fig. A52: PP/EPDM 30/70r 98 K/s

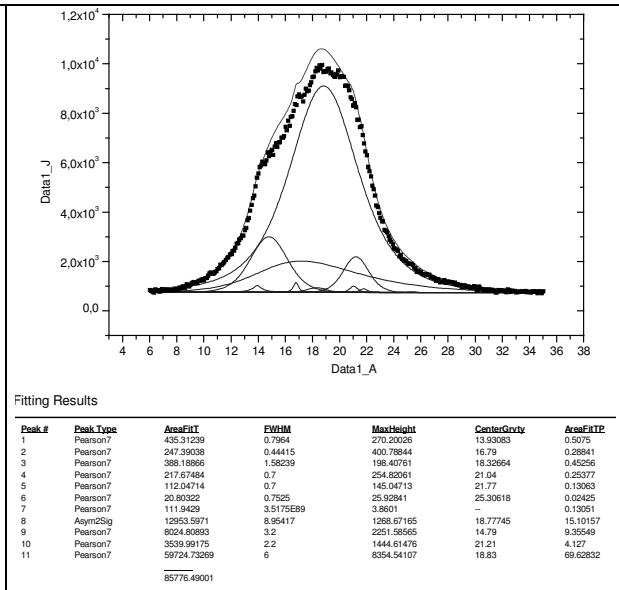


Fig. A53: PP/EPDM 30/70r 110 K/s

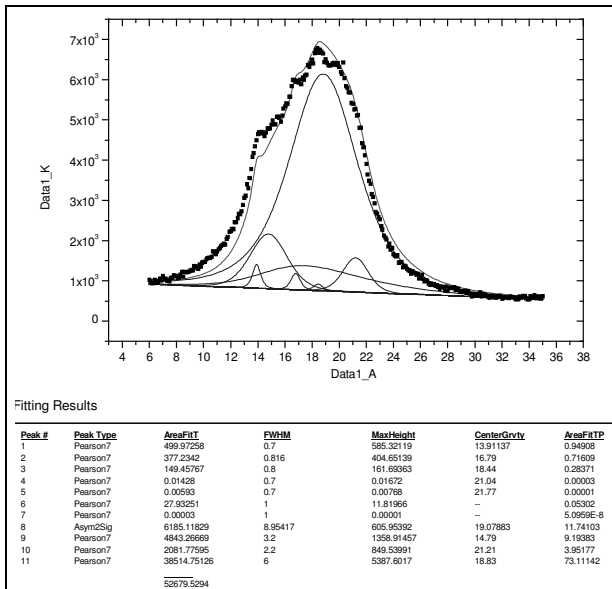


Fig. A54: PP/EPDM 30/70r 143 K/s

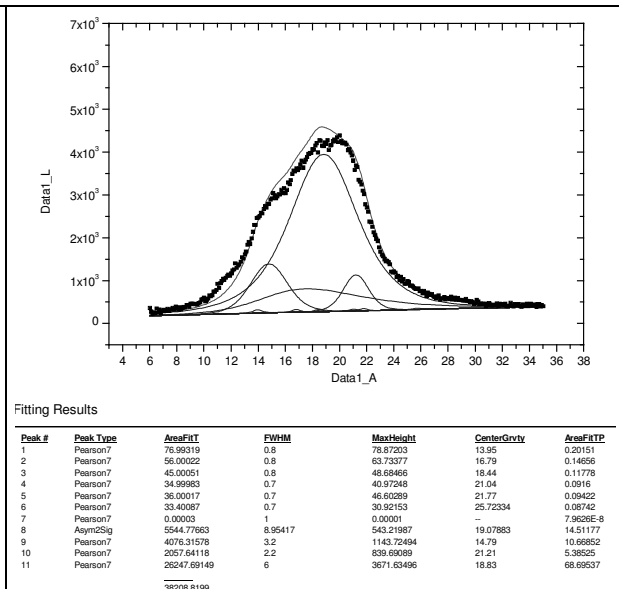


Fig. A55: PP/EPDM 30/70r 309 K/s

Appendix - 14

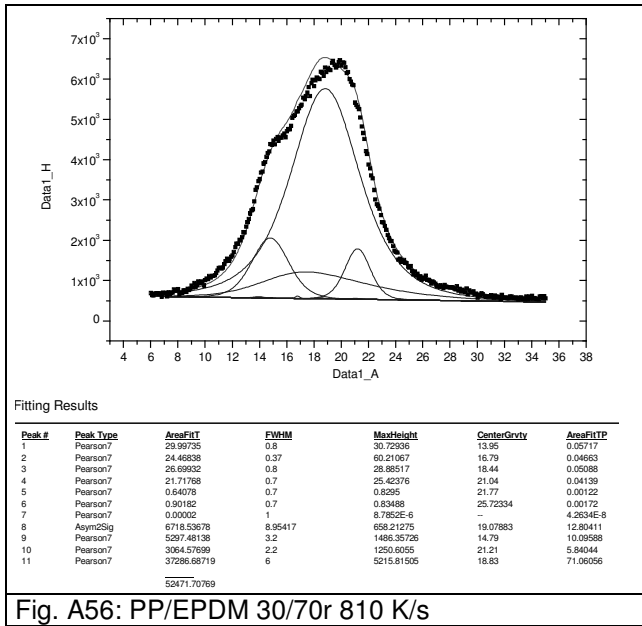


Fig. A56: PP/EPDM 30/70r 810 K/s

DSC Thermograms

iPP

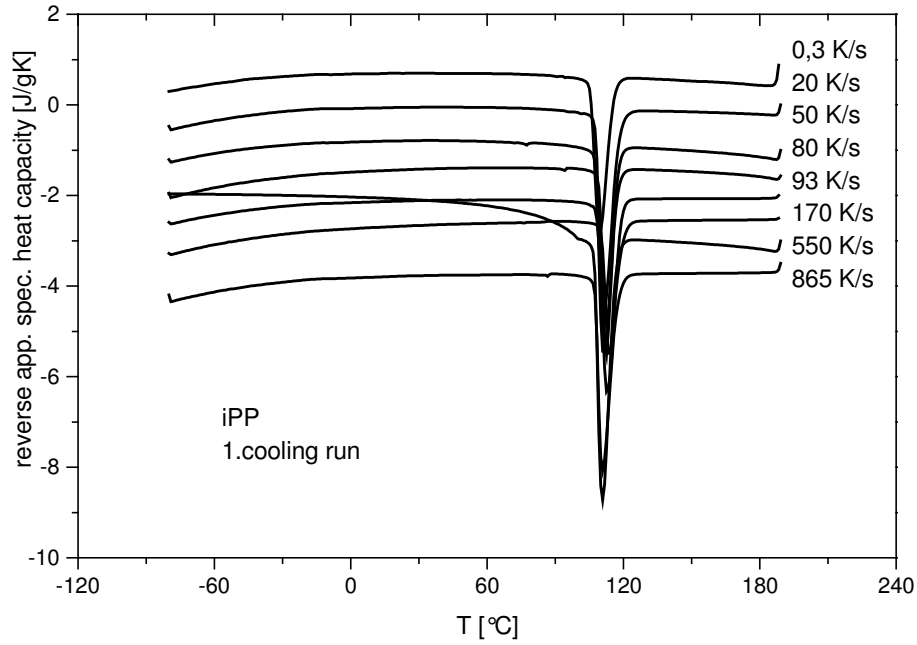


Fig. A57: 1st DSC cooling scan of iPP solidified with indicated cooling rates.

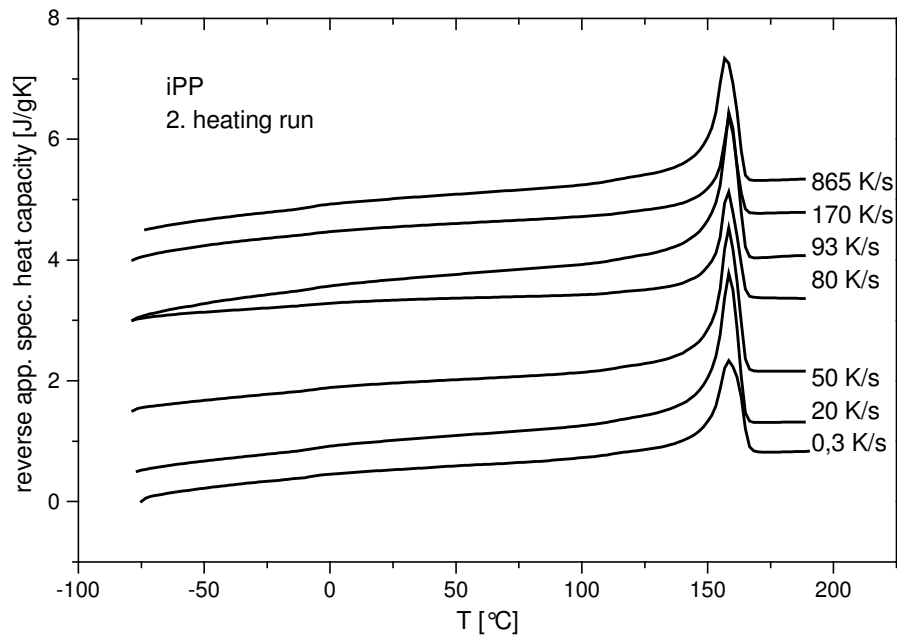


Fig. A58: 2nd DSC heating scan of iPP solidified with indicated cooling rates.

PP/EOC 30/70p

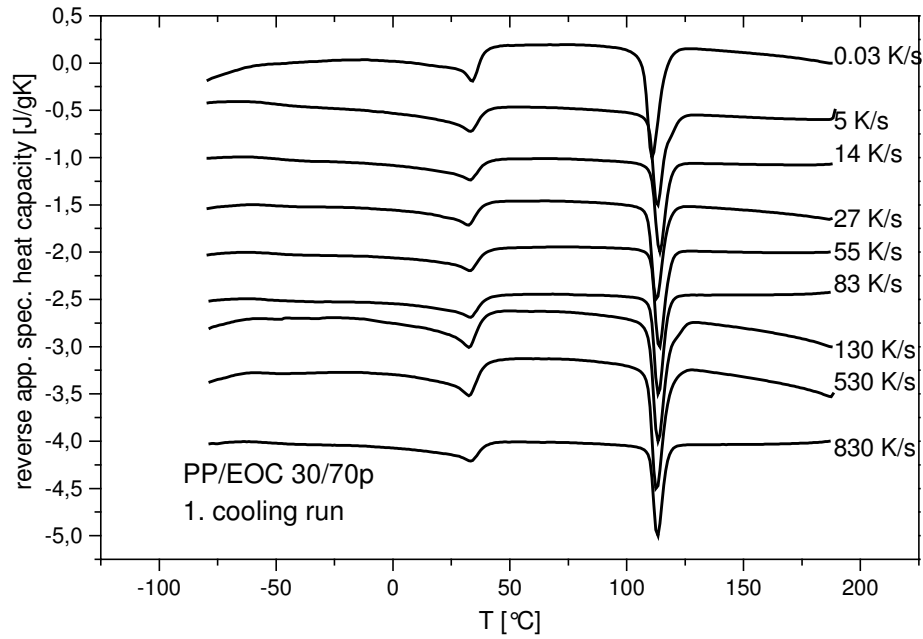


Fig. A59: 1st DSC cooling scan of PP/EOC 30/70p solidified with indicated cooling rates.

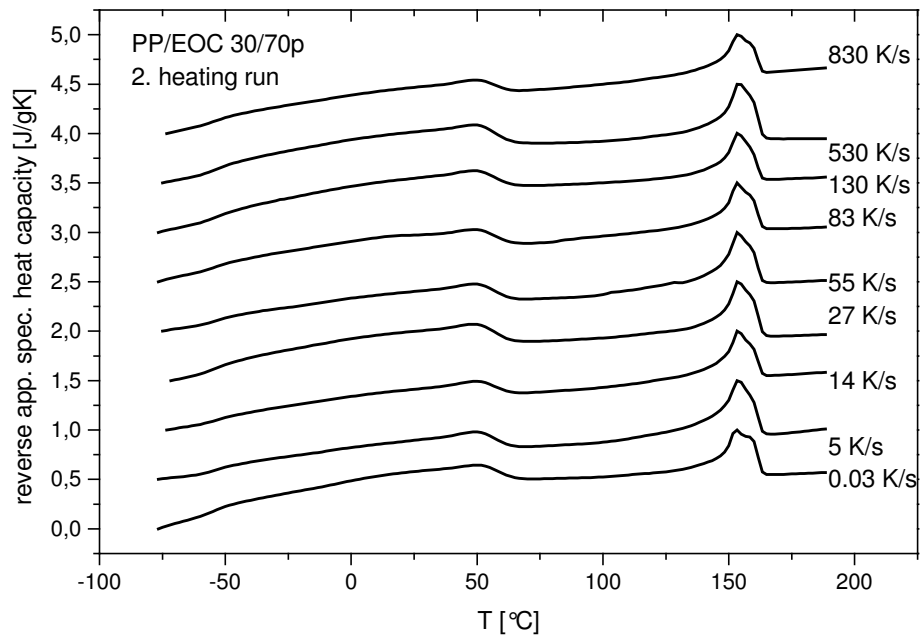


Fig. A60: 2nd DSC heating scan of PP/EOC 30/70p solidified with indicated cooling rates.

PP/EPDM 30/70p

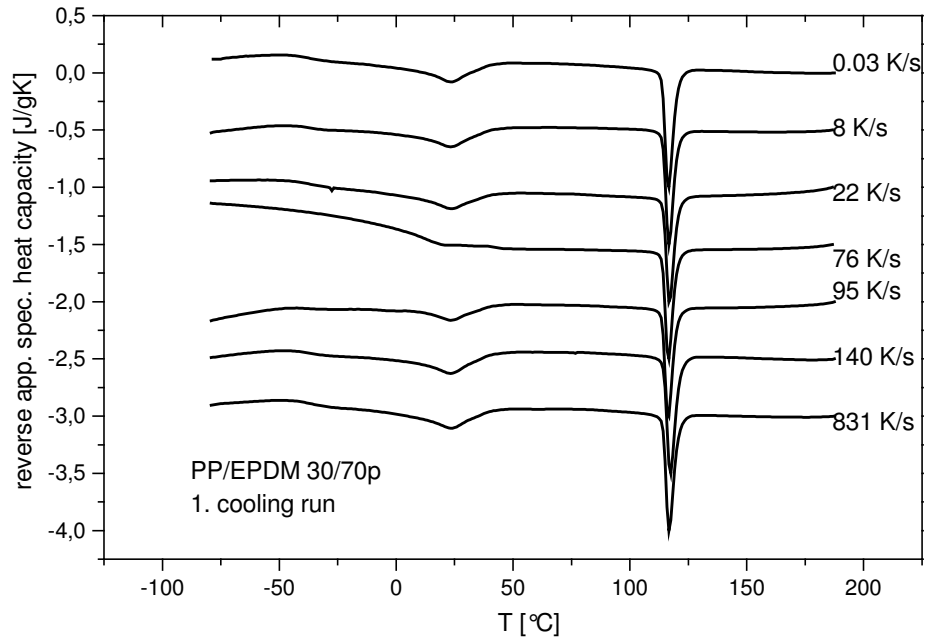


Fig. A61: 1st DSC cooling scan of PP/EPDM 30/70p solidified with indicated cooling rates.

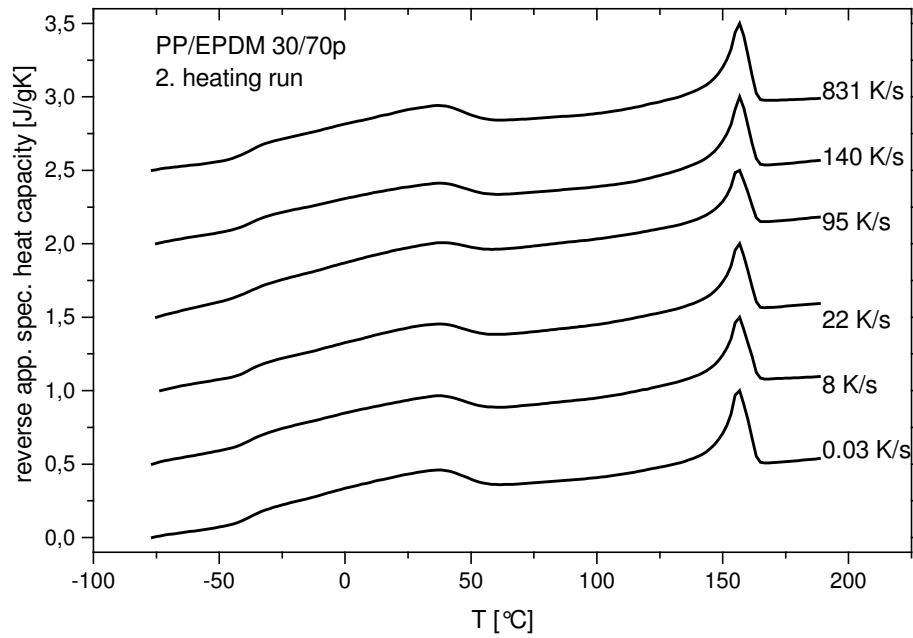


Fig. A62: 2nd DSC heating scan of PP/EPDM 30/70p solidified with indicated cooling rates.

PP/EPDM 30/70r

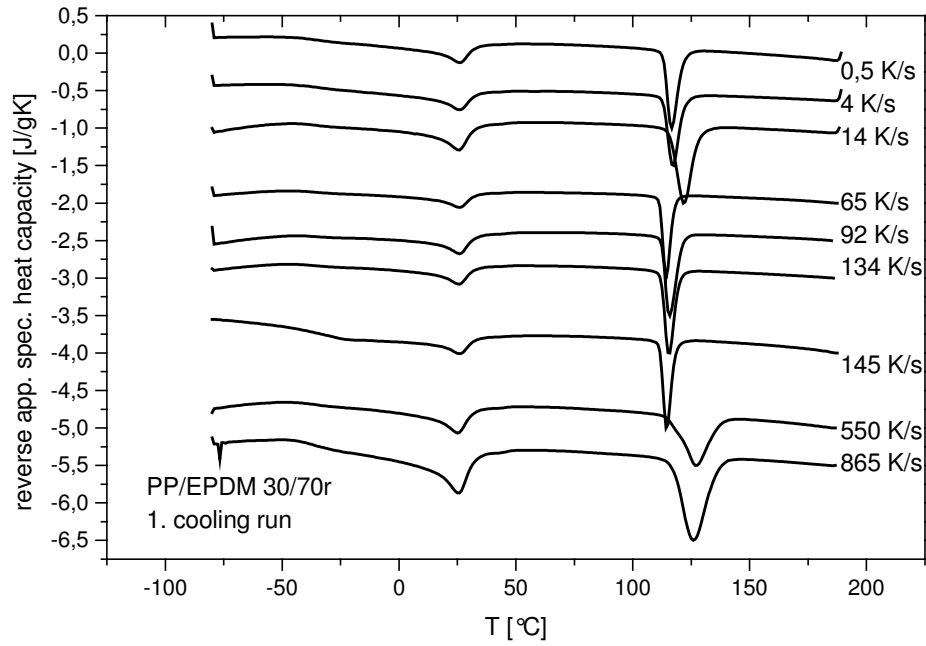


Fig. A63: 1st DSC cooling scan of PP/EPDM 30/70r solidified with indicated cooling rates.

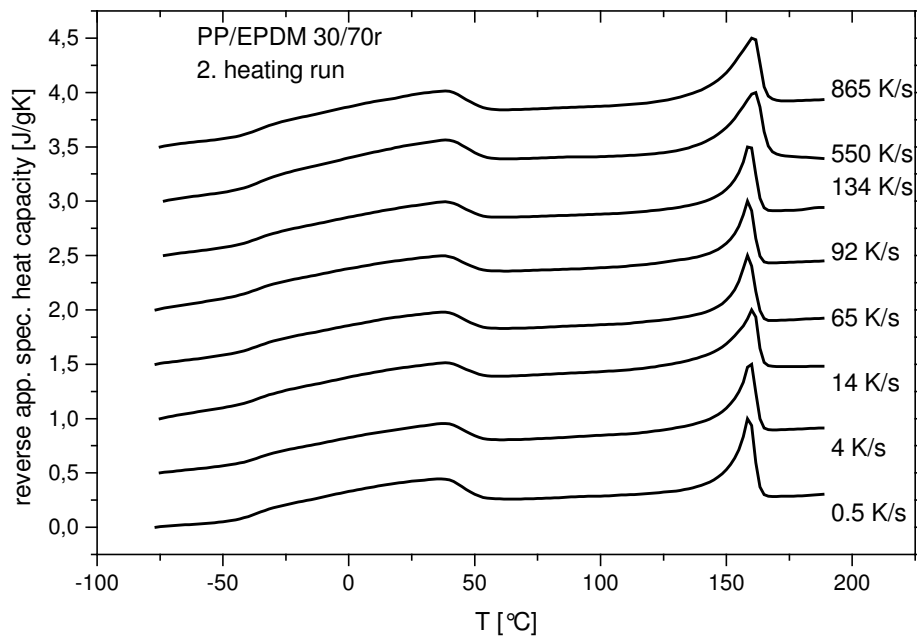


Fig. A64: 2nd DSC heating scan of PP/EPDM 30/70r solidified with indicated cooling rates.

Lebenslauf

Persönliche Daten

Nachname: Scharnowski
Vorname: Dörte
Geburtsdatum: 27.11.1974
Geburtsort: Brandenburg a.d. Havel
Nationalität: deutsch
Familienstand: verheiratet

Schulbildung

1981-1990 Grundsule in Halle/S.
1990-1991 Vorbereitungsjaar auf die Abiturstufe, Halle/S.
1991-1992 Internationaler Schüleraustausch Highschool in Capac, MI,
(USA)
1992-1994 Gymnasium Halle/S, Abitur 06/1994

Studium

1994-1999 Studium an der Martin-Luther-Universität Halle-Wittenberg
Abschluss als Diplom-Ingenieur im Studiengang
Werkstoffwissenschaft 12/1999
2000-2004 Promotion an der Martin-Luther-Universität Halle-Wittenberg,
Fachbereich Ingenieurwissenschaften

Beruf

seit 2002 Wissenschaftliche Mitarbeiterin an der Martin-Luther-
Universität Halle-Wittenberg, Fachbereich
Ingenieurwissenschaften, Kunststofftechnik